

# **Development of a multi-disciplinary toolkit to study time cells in the hippocampus**

A Thesis

Submitted to the  
Tata Institute of Fundamental Research,  
Mumbai  
for the degree of Doctor of Philosophy  
in Biology

by  
Kambadur Gundu Ananthamurthy

Tata Institute of Fundamental Research  
Mumbai  
July, 2023

## **DECLARATION**

This thesis is a presentation of my original research work. Wherever contributions of others are involved, every effort is made to indicate this clearly, with due reference to the literature, and acknowledgment of collaborative research and discussions.

The work was done under the guidance of Professor Upinder S. Bhalla, at the Tata Institute of Fundamental Research, Mumbai.



**Kambadur Gundu Ananthamurthy**

In my capacity as supervisor of the candidate's thesis, I certify that the above statements are true to the best of my knowledge.



**Prof. Upinder S. Bhalla**

Date: 28<sup>th</sup> July, 2023

# Acknowledgments

Projects like the ones described in this thesis cannot be accomplished without good, strong leadership. I thank Upi for the opportunity to learn and grow in his lab, and his patience to see me through tough moments.

I thank Shona and Mukund for advice and help over the past decade. I thank my seniors Mehrab, Ashesh, Partha, and Subha. I hope I can make them proud, someday.

I thank my colleagues Sahil, Dilawar, Oliver, and Aditya for helping me whenever I asked.

I thank Sriram, Manoj, Krishna, and Amit for everything I learnt in CIFF. I thank Mohini, Mugdha, Sebastien, Arnab, and Terence, for being my friends for as long as they could.

I thank Supriya, Harini, Anupratap, Sohail, and Prabahan, my well-wishers from Shona lab.

I thank KS Krishnan for help and advice, in the early days of the programme. His absence cannot be filled with anything else.

I thank Sanjay, Axel, Panic, Vatsala, Uma, Madan, and Jitu, for always bringing a breath of inspiration to my life and my work.

I thank Dr. Shane Heiney for showing me the way with trace eye-blink conditioning, and Dr. Daniel Dombeck for the chronic hippocampus preparation.

I'm indebted to the Animal Care and Resource Center (ACRC), the Central Imaging and Flow Facility (CIFF), Dorababu & the Electronics Workshop, Devakumar & the Mechanical Workshop, for anything and everything I have been able to make or create.

I thank Swarna and Nikhila for teaching me Tennis. I also thank the Football group, the Badminton group, the Music group, the Theater group, and the Improv group, for always giving me a chance to explore.

I thank Neha Panwar for being there in the end.

“Very little” is what I’d have achieved without my parents. I hope to be a good person and live up to the values they have taught me.

I thank the canteen, the sports facility and gym, hospitality, instrumentation, and admin, for helping me with everything else.

*for Archana && Bujju,*

# Index of Tables

<b>Table 1:</b> Summary table of behaviour protocols attempted and essential results.....	108
<b>Table 2:</b> Recipe for ready-to-use cortex buffer. The buffer is typically prepared and stored in aliquots to be used each week. The correct pH range of the buffer was often a crucial factor ensuring the success of the hippocampal preparation.....	118

# Table of Figures

<b>Figure 1:</b> A schematic representation of the Trisynaptic Pathway as observed with coronal slices, along the longitudinal axis of the hippocampus. Image adapted from the webpage for the Neural Circuits and Memory Lab, University of Wisconsin (Milwaukee) [ <a href="https://sites.lsa.umich.edu/diba-lab/neural-circuits-of-the-hippocampus/">https://sites.lsa.umich.edu/diba-lab/neural-circuits-of-the-hippocampus/</a> ] .....	33
<b>Figure 2:</b> Water delivery calibration to reward the animal consistently with the same volume of water.....	74
<b>Figure 3:</b> Optoisolator circuit to amplify +5V DC input to +12V DC output.....	76
<b>Figure 4:</b> Lick detector circuit based on a MOSFET design. Whenever the animal performed a lick, a +5V DC Output would be read out.....	77
<b>Figure 5:</b> Typical trial structure with the various phases. Each trial was followed by a randomized Inter-Trial Interval (ITI).....	79
<b>Figure 6:</b> Performance evaluation for two example mice trained to Protocol 1.1 and 1.2. Percentage of total licks in the various trial phases (Pre-Tone, Tone, CT, and ITI), across all sessions of training (coloured bar plots) for A) Mouse 3, and B) Mouse .....	80
<b>Figure 7:</b> Performance evaluation for two example mice trained to Protocol 2. Percentage of total licks in the various trial phases (Pre-Tone, Tone, CT, and ITI), across all sessions of training (coloured bar plots), for (A) Mouse S1, and (B) Mouse S2 .....	85
<b>Figure 8:</b> Schematic representation of the experimental setup for a simple detection task where the animal must perform a lick upon correctly detecting the presence of the conditioned stimulus (CS; from a range of modalities).....	88
<b>Figure 9:</b> Typical trial structure with the various phases and lick dependent relationships.....	89
<b>Figure 10:</b> (A) Performance traces for all the animals individually shown in dashed grey lines. Mean + SEM in black. (B) Mean Performance (%) and Mean Go Tone Lick Percentage (%) with Session for the Go/No-Go Task, plotted in black and green,	

respectively.....	90
<b>Figure 11:</b> The number of licks in the pre-tone (blue), no-go tone (red), and go tone (green) phases, in a representative animal, in a session with maximum Performance (%). .....	91
<b>Figure 12:</b> Schematic representation to showcase the two main subtypes of Classical Conditioning (Eye-Blink Conditioning, for our experiments) based on the relative timing and presentation of the CS and US. ....	94
<b>Figure 13:</b> Trial-by-trial (left) and trial-averaged running speed (right) for two example animals, (A) M2 Session 12, and (B) M5 Session 12. ....	97
<b>Figure 14:</b> Schematic representation of (A) the behaviour rig with 2-Photon imaging, to train head-fixed mice on a Trace Eye-Blink Conditioning (TEC) task, and (B) relative time intervals between the CS and US. ....	99
<b>Figure 15:</b> A picture of a head-fixed mouse clamped on the behaviour rig, with key components: 1) Red LED Illumination, 2) Blue LED CS, 3) Air-puff port directed to the left eye, and 4) Height-adjustable Treadmill. ....	100
<b>Figure 16:</b> Steps from behaviour video frame to Fraction of Eye-Closed (FEC) analysis .....	101
<b>Figure 17:</b> Conditioned Responses (CRs) are small amplitude eye-blanks triggered by the CS, and develop with multiple training sessions, while Unconditioned Responses (URs) are large eye-blanks to the US, typically consistent across sessions. (A,B) Trial-by-trial FEC traces for M11 (A) Session 2, and (B) Session 4. (C,D) Trial-averaged FEC traces for M11 (C) Session 2, and (D) Session 4, with paired (red) and probe (green) trials. ....	103
<b>Figure 18:</b> Performance in terms of the percentage of Hit Trials to total trials across sessions, including an ISI switch from 250 ms to 350 ms. Here, M2 is a strong learner (>60% hit trials/session) and M5 is a weak learner (30-60 % hit trials/session). M1, M3, and M4 did not learn the task.....	104
<b>Figure 19:</b> Conditioned Responses (CRs) are preserved for previously learnt ISIs, and switching the ISI to longer intervals results in Complex (multi-CR) eye-blink responses. (A,B) Trial-by-trial FEC scores for (A) 250 ms ISI (left) and (B) 500 ms ISI. (C,D) Trial-averaged FEC traces for (C) 250 ms ISI, and (D) 500 ms ISI, with paired (red) and probe (green) trials. ....	105
<b>Figure 20:</b> Conditioned Response (CR) onset timing is maintained across ISI switches. Representative examples from a short ISI switch from (A) 250 ms to (B) 350 ms (right). .....	106
<b>Figure 21:</b> Bar plots for Conditioned Response (CR) onset across	

multiple sessions of training after ISI switch from 250 ms to 350 ms, irrespective of how strongly the animals learnt the task. (A) red, strong learner, and (B) blue, weak learner.....	106
<b>Figure 22:</b> Representative example of mice trained to 550 ms ISI (Session 6) and 750 ms (Session 4). (A,B) Trial-by-trial FEC responses for (A) 550 ms ISI (M17 Session 6), and (B) 750 ms ISI (M22 Session 4). (C,D) Trial-averaged FEC responses for (C) 550 ms ISI (M17 Session 6), and (D) 750 ms ISI (M22 Session 4), with paired (red) and probe trials (green). .....	107
<b>Figure 23:</b> (A) A schematic of the rodent brain, showcasing the two hippocampi, one in each hemisphere. The hippocampi lie ~1 mm (mice) below the cortical surface. (B) The hippocampal preparation allows optical access to the deep lying hippocampal CA1 cells, relative to the skull/cortex. The CA1 cell bodies arrange in a laminar fashion as a tight cell body layer that can be visualized by fluorescence (using either OGB-1 or GCaMP). .....	115
<b>Figure 24:</b> Figure 24: Schematic representation for stereotaxic viral injection. ....	121
<b>Figure 25:</b> (A) Representative Two-Photon Calcium Image of a plane of Hippocampal CA1 cells, bolus loaded with Oregon Green Bapta-1 (OGB-1), at an instant in time. Example cells marked out post-hoc as pink, green, blue and red. Scale bar 20 $\mu$ m. (B) Representative dF/F (%) traces for the calcium activity. Recorded in a single 10s video for example cells – pink, green, blue, and red. Scale bar 1 sec; 10% dF/F. ....	123
<b>Figure 26:</b> Tissue Degradation over time. Representative Two-Photon Calcium images of a snapshot in time of the Hippocampal CA1 cell body layer on (A) Day 1 after the surgery and (B) Day 3, after the surgery. Scale bar 30 $\mu$ m. ....	125
<b>Figure 27:</b> Chronic calcium imaging of the same Hippocampal CA1 cells over weeks. Representative 2-Photon images from (A) Day 20, and (B) Day 21, after surgery. Landmarks have been marked and were used to confirm frame registration and identify cells. Scale bar 100 $\mu$ m. ....	126
<b>Figure 28:</b> (A) Representative Two-Photon Calcium Image of a plane of Hippocampal CA1 cells expressing GCaMP6f at an instant in time. Example cells marked out post-hoc in pink, blue, and green, with no-cell background in red. Scale bar 20 $\mu$ m. (B) Representative dF/F (%) traces for the calcium activity recorded in a single 10s video for example cells – pink, blue, and green, with no-cell background in red. Scale bar 2 sec; 10% dF/F. ....	127
<b>Figure 29:</b> (A) Correlation Coefficients for cell pairs from an example two-photon recording. (B) Meta-K Means clustering with cell pairs	

using the heuristic that within group pairs would be more similar than between group pairs. In this example, the cells were clustered into two groups, I (red) and II (yellow). (C) Two-Photon image of the field of view of cells; same as Figure 25A. (D) Spatial organization of correlated cell pair groups during spontaneous activity (Modi et al., 2014) .....	129
<b>Figure 30:</b> (A) Trial-averaged (25 trials) calcium activity from ~100 CA1 cells in trials where a 5000 Hz tone was presented (red bar). (B) Trial-averaged (18 trials) calcium activity from the same cells in trials where a 5 LPM air-puff to the ipsilateral whiskers was presented (red bar). Scale bar 1 sec (black bar) .....	130
<b>Figure 31:</b> (A) Correlation Coefficients for cell pairs from post whisker-puff stimulation periods. (B) Meta-K Means clustering with cell pairs using the heuristic that within group pairs would be more similar than between group pairs. In this example, the cells were clustered into three groups I (red), II (orange), and III (yellow). (D) No clear spatial organization of correlated cell pair groups post whisker stimulation. ....	131
<b>Figure 32:</b> (A) Correlation Coefficients for cell pairs from a trial-shuffle control dataset (B) Meta-K Means clustering revealed that there were no cell pair groups identified. ....	132
<b>Figure 33:</b> Example Time Cells visualized as event raster plots (A, B, C), along with the trial-summed activity profiles (D, E, F) suggesting ~50% hit trials, for cells 29 and 72 from Session 1 (session type 5) with mouse M26, and slightly lower reliability (~25% hit trials) from cell 105. The Conditioned Stimulus (CS; blue LED) is presented at time 0 ms. ....	136
<b>Figure 34:</b> Example Other Cells visualized as event raster plots (A, B, C), along with the trial-summed activity profiles (D, E, F) for cells 10, 25, and 120 from Session 1 (session type 5) with mouse M26. The Conditioned Stimulus (CS; blue LED) is presented at time 0 ms.....	137
<b>Figure 35:</b> Event Time Histograms or tuning curves for Identified Time-Locked Cells with trial-summed peaks in session 4 of training (session type 5) with mouse M26. (A) Unsorted list of Time cells. (B) Peak-sorted list of the same cells. Here, 1 bin = 3 frames = ~210 ms (sampling rate 14.5 Hz without binning; ~5 Hz with binning). As per the (legacy) session type 5 protocol, the CS (50 ms Blue LED flash) was presented in frame bin 39, followed by a stimulus-free trace interval during frame bins 40 and 41, and then the US (50 ms airpuff to ipsilateral eye) was presented in frame bin 42.....	138
<b>Figure 36:</b> Temporal Information (bits) vs Sorted time cell number from the analytically identified Time Cells in Session 4 (session type 5) with mouse M26. No clear trend was observed.....	139
<b>Figure 37:</b> More time cells observed to attain tuning as training	

sessions. Event Time Histograms of the identified set of time cells between A) Sessions 1 and (B) Session 2, with mouse M26 (session type 5). ....	141
<b>Figure 38:</b> Sorted Time Cells form Sequences that develop with learning. Trial-Averaged calcium activity traces for all recorded cells across A) Session 1, B) Session 2, and C) Session 4, with mouse M26 (sessiontype 5). Time 0 ms was aligned to the CS. The CS + Trace + US interval lasted from 0-600 ms, here.....	142
<b>Figure 39:</b> Same/similar tuning across session 1 and session 2 for this example time cell. Blue Event Time Histograms represent the tuning curve for the cell for session 1 (date: 20180508) and Red represent the same but for session 2 (date: 20180509). Pearson's correlation coefficient between the two session pairs was 0.7011. ....	143
Figure 40: Three example chronically tracked cell pairs with tuning peaks arriving earlier with training sessions (rows). Blue Event Time Histograms represent the tuning curve for any cell for session 1 (date: 20180508) and Red represent the same but for session 2 (date: 20180509). Pearson's correlation coefficient between the session pairs was 0.6.348, 0.5872 and 0.7027 for A) cell pair 1, B) cell pair 2, and C) cell pair3, respectively. ....	144
<b>Figure 41:</b> Example chronically tracked cell pair with de-tuning between session 1 and 4. Blue Event Time Histograms represent the tuning curve for the example cell for session 1 (date: 20180508) and Red represent the same but for session 4 (date: 20180514). Pearson's correlation coefficient between the two curves was -0.0606. ....	145
<b>Figure 42:</b> Comparing chronically tracked time cells across sessions for all matched cell pairs by (A) Correlation Analysis, and (B) Timing of peaks.....	146

## Table of Contents

<b>DECLARATION</b> .....	2
<b>Acknowledgments</b> .....	3
<b>Index of Tables</b> .....	6
<b>Table of Figures</b> .....	6
<b>Table of Contents</b> .....	10
<b>Abstract</b> .....	13
<b>Chapter 1 – Introduction</b> .....	15
Projects and overall goals .....	15

<b>A toolkit to study time cells: Thesis Objectives .....</b>	<b>16</b>
<b>Engrams associated with Learning and Memory .....</b>	<b>18</b>
<b>Dynamics in the neural code for engrams .....</b>	<b>20</b>
<b>Theories on the function of the hippocampus.....</b>	<b>24</b>
<b>A brief introduction to associative learning .....</b>	<b>29</b>
<b>Space and time in the hippocampus .....</b>	<b>32</b>
<b>“Single-cell, multi-trial” vs. “multi-cell, single-trial” approaches in Neuroscience .....</b>	<b>38</b>
<b>Dimensionality reduction in the analysis of physiology.....</b>	<b>41</b>
<b>Synthetic benchmarks for pre-hoc development of analytical procedures .....</b>	<b>42</b>
<b>Single-Unit Electrophysiology vs 2-Photon Calcium Imaging to study the Hippocampus .....</b>	<b>45</b>
<b>Calcium imaging by 2-Photon Microscopy .....</b>	<b>47</b>
<b>Automated ROI detection for large-scale Calcium Imaging datasets .....</b>	<b>51</b>
<b>Short Summaries of the 3 projects.....</b>	<b>51</b>
Project I - How do sensory representations transform with learning?.....	51
Project II - How does the timing of cellular activity adjust to behavioural task variables? .....	53
Project III - What is the best way to detect and score time-tuned cellular activity? ....	54
<b>Code Availability .....</b>	<b>56</b>
<b>Bibliography .....</b>	<b>56</b>
<b>Chapter 2 – Behaviour.....</b>	<b>70</b>
<b>Towards understanding brain activity in a reproducible context.....</b>	<b>70</b>
<b>Operant conditioning [Project I] .....</b>	<b>72</b>
Required features .....	72
Water delivery and calibration .....	74
Opto-isolator circuit for solenoid control .....	75
Lick detection circuit.....	76
Controlling task details and protocol information.....	77
Head-bar implant, Animal Handling, and Water deprivation .....	78
PROTOCOL 1.1: Stimulus Detection Task.....	78
PROTOCOL 1.2: Stimulus Detection Task with aversive punishment .....	79
Results – Protocols 1.1 and 1.2.....	81
Protocol 2: Stimulus Detection task with timeout box .....	81
Results – Protocol 2 .....	83
Protocol 3: Delayed Non-Match to Sample (DNMS).....	86
Results – Protocol 3 .....	87
Protocol 4: Go/No-Go Task .....	87
Results – Protocol 4 .....	89

Operant conditioning experiments failed to match behavioural requirements .....	92
<b>Trace Eye-Blink Conditioning [Project II] .....</b>	<b>93</b>
Tracking eye-blink responses.....	95
Treadmill and tracking running speed .....	96
Behaviour rig and protocol control - Software .....	98
Analysis - TEC .....	101
Results - TEC.....	102
<b>Bibliography .....</b>	<b>109</b>
<b>Chapter 3 – Imaging.....</b>	<b>111</b>
<b>Physiology in the hippocampus .....</b>	<b>112</b>
<b>Methodology – Acute and chronic imaging [Projects I &amp; II] .....</b>	<b>114</b>
<b>Preparation of Cortex Buffer .....</b>	<b>116</b>
<b>Oregon Green Bapta-1 injections for acute imaging.....</b>	<b>118</b>
<b>GCaMP and chronic imaging .....</b>	<b>120</b>
<b>Results - Imaging .....</b>	<b>122</b>
2-Photon calcium imaging of hippocampal CA1, <i>in vivo</i> .....	122
Acute Imaging of OGB-1 loaded hippocampal CA1, <i>in vivo</i> .....	122
Chronic imaging of hippocampal CA1 using GCaMP.....	124
Spontaneous activity during non-stimulus periods .....	127
Spatial organization of activity correlated cells during spontaneous activity.....	128
Stimulus evoked responses .....	129
Spatial organization of activity correlated cells post whisker-puff stimulation.....	131
Chronic imaging now possible for weeks with the same mouse .....	133
Preliminary analysis to identify time cells .....	134
Tuning, re-tuning, and de-tuning of time cells across sessions .....	140
<b>Bibliography .....</b>	<b>148</b>
<b>Chapter 4 – Analysis.....</b>	<b>152</b>
<b>Chapter 5 – Discussion .....</b>	<b>159</b>
<b>The study of hippocampal CA1 sequences .....</b>	<b>159</b>
<b>Standardizing combined behaviour and recording experiments.....</b>	<b>162</b>
<b>Mapping sequences to abstract variables .....</b>	<b>163</b>
<b>Better temporal resolution requires new techniques.....</b>	<b>165</b>
<b>Does the brain create or predict? .....</b>	<b>166</b>
<b>Bibliography .....</b>	<b>168</b>
<b>All Bibliography .....</b>	<b>171</b>

## Abstract

The mammalian Hippocampus is considered important for the formation of several kinds of memory, one of which is the association between stimuli occurring separately in time. Several studies have shown that small populations of Hippocampal CA1 cells fire in time-locked sequences, "bridging" the time gap in temporal tasks (B. Kraus et al., 2013; MacDonald et al., 2011, 2013; Pastalkova et al., 2008), including a single-session version of Trace Eye-Blink Conditioning or TEC (Modi et al., 2014). Such cells are commonly termed time cells (Eichenbaum, 2017; MacDonald et al., 2011).

The main goal of the Thesis was to be able to study time cells under a variety of behavioural tasks and conditions and elucidate several physiological properties. We standardised a multi-day Trace Eye-Blink Conditioning (TEC) protocol to train head-fixed C57Bl6 mice (Siegel et al., 2015). TEC involves an association between a previously neutral Conditioned Stimulus (CS) with an eye-blink inducing Unconditioned Stimulus (US), across an intervening, stimulus-free, Trace Interval. We were able to observe stable, adaptive learning with our protocol. We also standardized an *in vivo* imaging preparation to record calcium activity from Hippocampal CA1 cells, adapted from previously published methods (Dombeck et al., 2010; Modi et al., 2014). We used a custom-built two photon laser-scanning microscope and performed galvo-scans through the imaging window, during TEC acquisition. The behaviour and imaging was conducted simultaneously to record calcium activity as the animal learnt the task. Chronic Calcium Imaging allowed us to track and record the activity of the same cells, confirmed morphologically. We could then identify time cells across sessions, and

look for adaptations in tuning curves, along multiple sessions. Furthermore, numerous approaches have been developed to analyse time cells and neuronal activity sequences, but it is not clear if their classifications match, nor how sensitive they are to various sources of data variability. We provide two main contributions to address this: A resource of synthetic 2-photon calcium activity data, and a survey of several methods for analyzing time cell data using our synthetic data as ground truth. The synthetic dataset and its generation code are useful for profiling future methods, testing analysis tool-chains, and as input to computational and experimental models of sequence detection. We characterized strengths and weaknesses of several time-cell analysis methods. Finally, we benchmark how computational requirements scale with large datasets typical of recent recording technologies.

# Chapter 1 – Introduction

The vertebrate Central Nervous System (CNS), consisting primarily of the central ganglia (brain) and the spinal cord, samples and receives information from the external world offering top-down control over the activity of all parts of the body. Functions like exploration, food acquisition, and danger aversion, all involve complex coordination between,

- the Sensory Systems (that integrate information from the environment),
- the Memory Systems (that integrate sensory information with prior experience), and
- the Motor Systems (that integrate motor plans and execute movement).

## Projects and overall goals

The overall focus of the work and experiments described in this Thesis was to study Memory Systems, specifically, in terms of,

**Project I:** How do sensory representations transform with learning?

**Project II:** How does the timing of cellular activity adjust to behavioural task variables?

### **Project III:** What is the best way to detect and score time-tuned cellular activity?

Narrowing down, we as a lab were interested in the mammalian hippocampus, a brain structure which is important for consolidating information (from Sensory and other Memory Systems) to enable certain kinds of short-term memory and the translation of short-term memory to long-term.

## **A toolkit to study time cells: Thesis Objectives**

Ramón y Cajal, one of the pioneers of neuroscience around 1900, utilized Camillo Golgi's staining method to conclusively describe neurons in the brain as independent functional units connected to each other in intricate networks made up of many nodes ( $\sim 10^6 - 10^9$ ). These neurons have since been described not just anatomically, but also on the basis of genetics, development, and neurophysiology.

In the sub-discipline of Learning and Memory an often studied neuron type is the pyramidal neuron, an example of which is the hippocampal CA1 pyramidal neuron. It has been an important goal to study memory and the neural code in terms of finer temporal order, *viz.*, behavioural time scales (~ms to s). Combining

- stable, adaptable trace eye-blink conditioning behaviour, and,
- cellular resolution 2-photon calcium imaging of hippocampal CA1, *in vivo*,
- with the goal to study time cell physiology,

was the core objective of the toolkit and the thesis as a whole.

Development in circuit manipulation tools using light-mediated activation or suppression of neuronal excitability (Luo et al., 2018), afford experimenters the ability to control circuits at ms time scales. Concomitant progress in effective physiological models of network activity during bouts of recall of the learnt behavioural trace require standardized behaviour and recording. For us, this mandated the design of a relatively low-cost, end-to-end configurable, combined behavioural and recording technology, to reliably study the neural code at the ms time scale, *in vivo*.

This thesis describes a toolkit of techniques ranging in a wide, multi-disciplinary scope, assembled with standardized hardware and software routines studying animal behaviour, network neurophysiology, and statistical analyses. The aim of the toolkit was to support the experimental ability to study the hippocampal CA1 pyramidal neuron network, under strictly controlled behavioural contexts designed to train experimental mice on temporal or episodic memory tasks. Specifically, these tasks such as trace eye-blink conditioning (TEC) have previously been described to elicit hippocampal CA1 sequences (B. Kraus et al., 2013; B. J. Kraus et al., 2015; MacDonald et al., 2011, 2013; Modi et al., 2014; Pastalkova et al., 2008). This spatiotemporal network activity sequence is dynamic and built from individual hippocampal CA1 pyramidal neurons showcasing time tuned activity through spiking. These cells are called time cells (Eichenbaum, 2017; MacDonald et al., 2011).

More generally, sequential activity is hypothesized to be involved even in the retrieval of evidence from memory, during more complex behavioural decisions that are not directly informed by the sequences of stimuli presented (see Shadlen & Shohamy, 2016 for review). It is still uncertain if sequential activity comprehensively describes the dynamic, physiological substrate of the neural code for memory and learning, *i.e.* – the engram, at behavioural time scales, or that other mechanisms may also be applicable, depending on the requirements of the task. We now discuss engrams and the temporal limitations of identifying engram cells using activity based molecular techniques.

## **Engrams associated with Learning and Memory**

The term "engram" (coined by Richard Semon) refers to the physical substrate of memory in the organism, used for storing and recalling memories (Josselyn & Tonegawa, 2020). Donald Hebb's theory of Hebbian Plasticity (Hebb, 1949) postulated that memory formation was correlated to modulations in synaptic strength and connectivity. The theory critically emphasized that the pair of neurons connected through the synapse undergoing plasticity to strengthen efficacy, required the spiking activity of both neurons. In subsequent decades, research into the idea led to the theory of spike-timing-dependent plasticity (Caporale & Dan, 2008), a mechanism of synaptic plasticity based on the relative timing of activity of the neurons. It is still a matter of debate whether the biophysical manifestation of the engram is the synapse, the activity of the neurons, biophysical or chemical processes, but it is

likely that the engram is distributed across several computational scales in the brain.

An important first step in early neuroscience research attempted to identify specific functions for specific brain regions. Experimenters would train a variety of model systems to specific behavioural tasks and attempt to delineate specific brain regions crucial (or not) to the task using targeted lesion or ablation studies (see Vaidya et al., 2019 for review).

Eric Kandel's experiments with the Aplysia sensory neurons studied gill withdrawal - an aversive but stable, adaptive behaviour (Carew et al., 1971). The reliability of this learned response allowed the experiments to include crucial electrophysiological and neurochemical circuit dissections that ultimately lead to the discovery of the entire neural circuit orchestrating the task, even to the level of cellular signaling. This led to decades of research focused on the plasticity of synapses across nervous systems in the animal kingdom.

With the development of more sophisticated recording and molecular techniques, further details on mechanism within specific brain regions and circuits could be described. Specifically, technological advancements in molecular neuroscience led to the development of a number of fluorescent sensors, conditional tagging, activators and inhibitors that allowed cellular resolution tracing of the engram (Luo et al., 2018).

Experiments by Sheena Josselyn, Alcino Silva, and colleagues led to the discovery that the intrinsic excitability of a pyramidal neuron in any

network positively biased the probability of recruitment to the engram (Han et al., 2009; Rogerson et al., 2014; Silva et al., 2009; Yiu et al., 2014; Y. Zhou et al., 2009), *viz.*, the tagged set of cells were active when memory was learnt and recalled. The engram seemed to be described in terms of the cellular sub-population involved but the experiment could only identify the same over a relatively longer window of time (~mins.). This could lead to only a static list of cells which may even have included False Positives (Type I error). Importantly, any dynamics in the spatiotemporal patterns of activity of the pyramidal neurons were not amenable to study at shorter timescales (~ms.). On the other hand, physiological recordings could describe these dynamics at short timescales, but were rarely translated to chronic measurements of the activity of the same cells across days and sessions, given technical limitations at the time.

## Dynamics in the neural code for engrams

We first discuss some important results that help motivate the study of physiological recordings in the context of engrams, *i.e.*, the dynamical nature of the neural code (~ms to s). In later sections we will describe these dynamics in more detail.

Place cells and their role in spatial navigation have been studied in great detail through decades of research ever since they were first described by John O’Keefe (O’Keefe & Dostrovsky, 1971). We did not explicitly study place cells in this thesis but some key discoveries in literature require mention, with the goal to build a case for a theory of CA1 ensemble sequences (Modi et al., 2014). Briefly, place cells are

pyramidal neurons that showcased a higher than baseline probability of firing action potentials whenever animals navigating spatial environments visited specific locations. The tuning curves or firing fields for these cells often map to the real spatial trajectory of the animal and is thought to be an assimilation of both brain external stimuli such as visual cues, as well as brain internal variables such as motivation, goal orientation, memory, and experience(Ferbinteanu et al., 2011; Ferbinteanu & Shapiro, 2003; Foster, 2017; Frank et al., 2000; Wood et al., 2000).

As the animal enters these landmark locations in any spatial context, these place cells showcase Phase Precession, firing earlier in phase to cycles of Theta a network rhythm clocked at ~4-10 Hz, as the animal's position changes relative to the landmark. These navigation mapped place cell sequences are called Theta Sequences (Foster & Wilson, 2007), typically mapped to a few active neurons at a time.

In very specific contexts, these place cells express activity sequences synchronized to Sharp Wave Ripples, a different network activity phenomenon clocked at ~10-30 Hz, often not tied to the animal's location, called Replay Sequences (Csicsvari et al., 2007; Foster & Wilson, 2006). These sequences have been described to play out typically in reverse temporal order to models of place cell sequences describing known trajectories in space.

There is variability in the firing of place cells in any spatial context, and studies have mapped specific sequences to very specific trajectory goals (going towards or away from locations) with modulation by both egocentric and allocentric orientations cues(Davidson et al., 2009;

Ferbinteanu et al., 2011; Ferbinteanu & Shapiro, 2003; Frank et al., 2000; Wood et al., 2000) and movement speed based estimates of distance (Kropff et al., 2015).

Place cell and time cell sequences have many similarities and differences in descriptive neurophysiology, but may emerge from the same memory organization principles (Buzsáki & Llinás, 2017). It is argued that there is significance to the exact phrasing of the CA1 sequence in any given context. Furthermore, a very interesting feature observed is Time-stamping, *viz.*, time dependent overlap of ensemble responses to different contexts and behavioural parameters (Cai et al., 2016; Mau et al., 2018).

We developed and standardized a multi-session, adaptable Trace Eye-Blink Conditioning (TEC) paradigm in which head-fixed mice learn to form associations between neutral and high-valence stimuli. We describe associative learning in later sections as well in Chapter 2 – “Behaviour”. TEC has been previously observed to elicit CA1 activity sequences even in a single session of training (Modi et al., 2014). The functional involvement of the hippocampus in the acquisition of Conditioned Responses (CRs) has been studied and implicated by studying acquisition rates to multiple trace intervals. It was found that memory load, inferred in terms of task difficulty with longer trace intervals (300 ms vs 500 ms), was crucial to observing an effect of hippocampal lesions on the behavioural expression of CRs (Moyer et al., 1990).

Several stimulus modalities have been used as the Unconditioned Stimulus (US) such as periorbital air-puffs and electrical shocks (see

Disterhoft & Weiss, 2017 for review). Throughout all our TEC experiments, we chose to use the mildly aversive air-puff to elicit the Unconditioned Response (UR) to the US. Further, we use a flash of a blue LED as the Conditioned Stimulus (CS), expecting to observe reliable Conditioned Responses (CRs) to the CS within 3-7 days, for trace intervals of ~250 ms (Siegel et al., 2015). CRs are observed as a preemptive eye-blink response elicited reliably before the presentation of the US – a reproducible attempt to avoid the discomfort of the aversive air-puff. This is in accordance with the Rescorla-Wagner model of Classical Conditioning, which assumes that association of the CS and US based on repeated pairing depends on how well the presence of the CS predicts the future occurrence of the US, along with other variables such as the relative intensities and modalities of the presented stimuli (Rescorla & Wagner, 1972). Extensions to this model have suggested that there could be negative effects to the associative learning when other CS (CS1, CS2, etc.) are also paired together in within-compound-association tasks such as “backward blocking” (Hamme & Wasserman, 1993). For our experiments we used only one CS for any training session, typically a 50 ms flash of a blue LED. However, our behavioural setup allows for multiple CS types, e.g., CS1 = Blue LED flash and CS2 = auditory tone, to be presented based on the experiment.

Transient increases in CA1 excitability post acquisition of the task were described up to 4-5 days (Moyer et al., 1996) and could be important to the forging of the task specific spatiotemporal sequences during learning. In an *in vitro* assay, coronal sections of the hippocampus (Figure 1) were stimulated at the Perforant Path to the cells of the Dentate Gyrus in patterns that could be mnemonically mapped to

stereotypic, temporal sequences of Excitatory Postsynaptic Potentials (EPSPs) read out at the hilar mossy cell layer ~400-500 ms later (Hyde & Strowbridge, 2012). This suggested the presence of temporal sequences even at the Dentate Granule cell layer, many synapses before the hippocampal CA1.

On a longer timescale, hippocampal lesion-based experiments on mice have been used to describe the role of the hippocampus to within 4 weeks of TEC, with deficits in Conditioned Responses (CRs) as a readout of the effect of the lesion (Takehara et al., 2002). We aimed to examine the processes that underlie this time-dependent role of the hippocampus by chronically tracking the same cohort of hippocampal CA1 cells across the sessions of TEC, at cellular resolution, using galvo-scanning 2-photon calcium imaging. We were specifically interested in studying the emergence and long-term activity dynamics of time cells, touted to be the behavioural time scale ( $\sim 10\text{-}10^3$  ms) expression of the memory engram during associative learning, as described in later sections. Preliminary results and additional details on our TEC paradigm may be found in Chapter 2 – “Behaviour”.

## **Theories on the function of the hippocampus**

We now provide a very brief outline of the four main ideas of hippocampal function studied over the past few decades. These are,

- A) Response Inhibition - Studied mostly in the 1960's, this perspective described the Hippocampus as important to the ability of animals to inhibit their impulses and natural, habitual,

or dominant behavioral responses to stimuli, in order to select more appropriate responses. This perspective was justified by two observations with regard to animals with hippocampal damage - 1) these animals tended to be hyperactive, and 2) were unable to withhold previously learnt responses. British psychologist Jeffrey Alan Gray developed this perspective to link hippocampal activity with anxiety (McNaughton & Gray, 2000). Studies have now implicated the hippocampus in the facilitation of correct responses and inhibition of incorrect responses during contextual memory tasks, though not for visual discrimination of contexts (Kim & Lee, 2012). Response Inhibition is considered an executive function and the brain circuitry involved, also includes (other than the hippocampus) the prefrontal cortex, subthalamic nucleus, and caudate nucleus (Diamond, 2013). Inhibitory control is typically impaired in patients with drug addiction, attention deficit hyperactivity disorder (ADHD), obsessive compulsive disorder (OCD), and Tourette's syndrome, among many others, and is an active area of research (Diamond, 2013; Nestler et al., 2015). Typical neuropsychological tests used to measure inhibitory control include the Stroop task, Go/No-Go task, Simon task, Flanker task, anti-saccade tasks, delay of gratification tasks, and stop-signal tasks (Diamond, 2013).

- B) Episodic Memory – a form of declarative or explicit memory that refers to the ability and mechanistic paradigms that allow for the behavioural recall of a collection of past personal experiences, occurring at particular places and times to the subject. The term was coined by Endel Tulving in 1972 (see Clayton et al., 2007),

although the perspective was popularized many decades prior, by the psychological studies on Patient H. M. (Henry Molaison), who had been suffering from epileptic seizures and had to undergo extensive hippocampectomy (surgical destruction of the hippocampi), as treatment. American neurosurgeon William Beecher Scoville and British-Canadian neuropsychologist Brenda Milner were pioneers of this study and were able to describe severe anterograde and partial retrograde amnesia in the patient post surgery (Scoville & Milner, 1957). Since the late 2000's, the discovery and description of time cells (B. Kraus et al., 2013; B. J. Kraus et al., 2015; MacDonald et al., 2011, 2013; Modi et al., 2014; Pastalkova et al., 2008), has reinvigorated this perspective. Nine important, collective properties of episodic memory distinguish it from other types of memory (see Conway, 2009 for review) *viz.*, episodic memory

- i) is a summary record of sensory-perceptual-conceptual-affective processing,
- ii) retains patterns of activation/inhibition over long periods,
- iii) is often represented in the form of visual images,
- iv) is perspective centered (subjective),
- v) is a representation of short time slices of experience,
- vi) is represented on a temporal dimension roughly in order of occurrence,
- vii) subject to rapid forgetting (extinction),
- viii) helps make autobiographical remembering specific, and,
- ix) is recollectively experienced when accessed.

The study of episodic memory and time cells forms the core of this thesis, and further details, experiments, and preliminary results are discussed in subsequent sections and chapters.

C) Spatial Cognition – is the ability of experimental animals to locate and ascribe valence to points in space, during the navigation of environments (see Hartley et al., 2014 for review). Originally popularized by the remarkable work of American-British neuroscientist John O’Keefe and American psychologist Lynn Nadel, the link between hippocampal function and spatial navigation was solidified with the discovery and subsequent descriptions of place cells (Morris et al., 1982; O’Keefe & Dostrovsky, 1971; O’Keefe & Recce, 1993). This perspective is the most popular amongst the known and studied functions of the Hippocampus and has been the subject of a large body of work. Indeed, the Nobel Prize in Physiology or Medicine 2014 was awarded to John O’Keefe, May-Britt Moser, and Edvard I. Moser, for “The Brain’s Navigational Place and Grid Cell System”. Both egocentric as well as allocentric cues are assimilated in an individual’s ability to navigate space, creating a mental representation of the environment or cognitive map (see “Focus on Spatial Cognition,” 2017 for review). There is evidence that the hippocampus and striatal circuits process different aspects of the environment, using very different learning rules, *i.e.*, incidental learning and associative reinforcement, respectively (Burgess, 2008). Spatial Cognition and place cells will be discussed to a limited extent in subsequent sections though these topics were not explicitly studied in the experiments for this thesis.

D) Contextual Mapping – An emerging consensus in the field is that the hippocampus actually builds contextual maps of the

environment or perceived events, with expansions to the neural activity code along any relevant dimension of stimuli. Stimuli or events cuing any modality, e.g., spatial, temporal, frequency, etc., may be assimilated, along with more brain internal variables such as (but not limited to) motivation, expected reward status, prior experience in related tasks, and goal-orientation (task specific). Furthermore, this allows the hippocampus to make predictive models that bind new information streams to collectively update predictions (M. R. Cohen & Kohn, 2011; Eichenbaum, 2017; Miller et al., 2023; O'Keefe & Nadel, 1978). Pattern separation and conjunctive representation of the combined multi-modal experience in the hippocampus, has been implicated in reinforcement learning (Ballard et al., 2019). Contextual mapping considers the hippocampal-entorhinal circuit as a Tolman-Eichenbaum machine (TEM) with the medial entorhinal cortex (MEC) cells thought to describe important aspects of past experience and the hippocampal cells implicated in binding the current sensory experience with prior experience (Ballard et al., 2019; Eichenbaum, 2017), with the goal to develop a functional model of the subjective experience of animals and flexibly selecting appropriate responses. To complement studies on place and time cells, the mapping of auditory tone frequencies in a frequency sweep (a relatively abstract external concept) has also been reported in the hippocampus-entorhinal circuit (Aronov et al., 2017).

Episodic memory forms the central function of study for all the hippocampus related experiments described in the thesis. Trace Eye-

Blink Conditioning (TEC) is an example of a task used to study episodic recall (Thompson, 2004). The behavioural acquisition and expression of CRs correlate well with the neuronal expression of spatiotemporal sequences of time cells (Modi et al., 2014). Our experiments aimed to describe finer details such as how the animals assign valence to the neutral Conditioned Stimulus (CS) and how time cell population codes adapt to changes in the trace interval. Some characteristic features of the engram at behavioural time scales, *viz.*, time cell activation sequences, have been described as preliminary results (Chapter 3 – “Imaging”), under the behavioural context of TEC, an associative learning task.

## A brief introduction to associative learning

The ability to physiologically record cells is insufficient without placing the experimental animals in precisely defined, stable behavioural contexts. Only in this way can neural activity be checked for correlations or mapping to distinct changes in external behaviour variables and the decisions that the animal makes, accordingly. Combining behaviour and recording was considered an important guiding principle in all our experiments. Associative learning is the overall process by which animals develop behavioural valence to neutral stimuli that occur in temporal conjunction to other potent, behaviour eliciting stimuli. We wished to study the network level responses in the hippocampus, *in vivo*, especially during early learning of associated stimuli, *i.e.*, behavioural acquisition, combining stable, adaptable associative learning paradigms such as Trace Eye-Blink

Conditioning (TEC) with cellular resolution, behaviour time scale, high-yield recordings of neurophysiology.

Prior to the early 20th century, Structuralism was a dominant perspective in Psychology, insisting on introspection - the observation and report of one's own mind and thoughts. Experiments and discoveries by Ivan Pavlov at the Military Medical Academy in Petrograd (St. Petersburg), eventually led to a dramatic shift in perspective, with the birth of Classical Conditioning, a type of associative learning. Following the very same methodology advocated by Francis Bacon (early 17th century), quantitative data from carefully conducted animal experiments were recorded, with the idea to narrow down on a small number of hypotheses that could explain experimental observations.

Ivan Pavlov provided essential demonstrations of anticipation and made tremendous progress in understanding the circumstances on which anticipation depends, and this is why Classical Conditioning is also often referred to as Pavlovian Conditioning. Following Pavlov's studies (Pavlov, 1927), it was proposed that Classical Conditioning was a prototypical example of Association. While it does have caveats such as covert learning when observable behaviour may be blocked (Dickinson et al., 1983; Krupa & Thompson, 2003), Associative learning is rich with a variety of animals and association tasks that have been crucial to study memory and learning over the past century.

Typically, animals require no prior training to elicit a behavioural or motor movement to biologically potent stimulus (appetitive or aversive), called an Unconditioned Stimulus (US). Examples include food, water,

electrical shock, temperature shock, etc.. Without pairing with a US, a neutral stimulus elicits no observable response from an animal, and such a stimulus is called a Conditioned Stimulus (CS). Examples include simple auditory tones, flashes of light, among others.

Classical Conditioning is both the behavioural procedure as well as the learning process that results from the pairing of a previously neutral stimulus (CS) with a biologically potent stimulus (US). Repeated pairing allows animals to make implicit associations between the CS and US, and essentially anticipate the occurrence of the US, once the CS is observed. Animals report this forecasting feat by producing the same response that they would to a US, albeit often a milder version. Typical protocols for Classical Conditioning, follow the regime of Forward pairing, *viz.*, - the CS is presented before the US, and this temporal structure will be followed unanimously across all behaviour experiments described in this thesis.

The standardization of the behavioural task, physiological recording (imaging) preparation, as well as the custom analysis routines to look for various physiological features are described in this thesis. Combining these multi-disciplinary approaches allowed us to develop a toolkit to study time cells in the hippocampus, under strict behavioural contexts. It is important to note, however, that spatiotemporal sequences of activity as measured by calcium imaging based simultaneous recordings of a large number of cells, are not limited to the hippocampus, being studied even in the visual cortex (Pachitariu et al., 2017; Poort et al., 2015), somatosensory cortex (Petersen, 2019), entorhinal cortex (Heys et al., 2014), and even in the cerebellum (Giovannucci et al., 2017). Essentially, the analytical methods

developed (Ananthamurthy & Bhalla, 2023) can easily be adapted to other neuronal network recordings where time-tuning may be applicable. Experimental protocols for associative learning have been standardized for a variety of animals, in a variety of experimental conditions. The specific issue is of developing an experimental system that can run simultaneous TEC behaviour and 2-photon imaging, in concert, and provide the context for time cell physiology to be studied, *in vivo*. It was important to design both aspects of the experiments (behaviour and imaging) since these were the most suitable conditions for studies on time cells.

## **Space and time in the hippocampus**

Damage to the hippocampal system has been shown to cause the impairment of long-term memory or amnesia, in human patients, rodents, and non-human primates. Interestingly, such damage to the Hippocampus seems to have no observable effect on the capacity for acquisition and expression of skilled performance. These two results suggest the role of the Hippocampus in certain kinds of memory, but not all.

Anatomically, the hippocampal system receives input from, and in turn, projects to the neocortical brain regions that serve as the site to process higher order categories and modalities of information. The hippocampal circuit is anatomically  $>3-4$  synapses away from the peripheral nervous system, and information typically arrives after many layers of intervening processing and computation. It is thus suggested that the hippocampus holds a privileged position in the brain, receiving

the outcomes of the computation of the brain's various modules, and relating to them (Baudry & Lynch, 1981; Ekstrom & Ranganath, 2018; Moscovitch et al., 2016; Poppenk et al., 2013; Tao et al., 2021). A large majority of the cortical information is sent to the Hippocampus via the Entorhinal Cortex (EC). This information is processed in roughly three stereotactically and molecularly separable layers of cells in the following order: EC → Dentate Gyrus → CA3 → CA1. This pathway from the EC to the CA1 has three separate synaptic connections (across the layers) and is also known as the Trisynaptic Pathway (Figure 1). The output of the CA1 is then sent to other cortical areas.

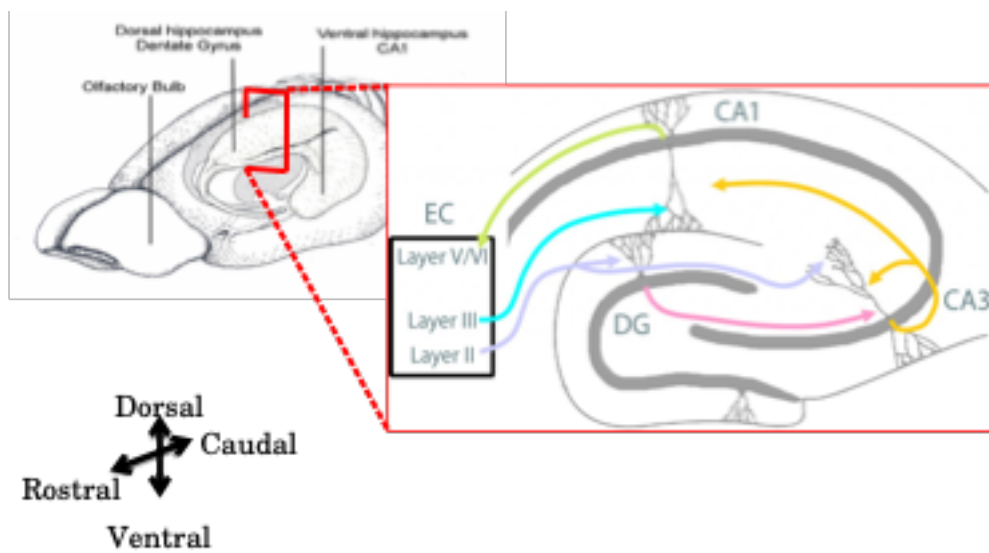


**Figure 1:** A schematic representation of the Trisynaptic Pathway as observed with coronal slices, along the longitudinal axis of the hippocampus. Image adapted from the webpage for the Neural Circuits and Memory Lab, University of Wisconsin (Milwaukee) [<https://sites.lsa.umich.edu/diba-lab/neural-circuits-of-the-hippocampus/>].

One of the most significant discoveries in the hippocampal system and surrounding brain structures was the role played in spatial cognition.

An enormous corpus of research has conclusively described,

- head-direction cells: with tuning curves tied to the direction that experimental animals were oriented to. These cells respond to egocentric vestibular cues as well as allocentric sensory cues (Ranck, 1973; Taube et al., 1990), in the dorsal presubiculum, retrosplenial cortex, entorhinal cortex, thalamus, and striatum, among others.
- grid cells: with multi-modal tuning curves at regular spatial positions as a lattice, across the environment being navigated. These cells assimilate information about location, distance, and direction, and are typically found in the entorhinal cortex (Fyhn et al., 2004; Hafting et al., 2005).
- boundary vector cells: with tuning curves to the edges of the environment being navigated. These cells are typically found in the subiculum, pre- and para-subiculum, and entorhinal cortex (Bjerknes et al., 2014; Lever et al., 2009; O'Keefe & Burgess, 1996; Savelli et al., 2008; Solstad et al., 2008).
- speed cells: with modulated firing rates based on the actual running or movement speed of the animals. These cells are typically found in the entorhinal cortex (Kropff et al., 2015).
- place cells: with tuning curves to specific locations in the environment (O'Keefe & Dostrovsky, 1971; O'Keefe & Recce, 1993). These cells may be found in several hippocampal sub-layers but often studied in the CA1.

The activity of neurons in the hippocampus of awake, behaving animals is modulated by significant stimuli or objects in the

environment as well as relationships between temporally discontiguous but relevant, paired stimuli. With the discovery of place cells, it was clear that the CA1 of animals navigating a spatial environment, showcased location specific firing fields. With the discovery of time cells, it was noted that the CA1 of animals could elicit spatiotemporal sequences of activity whenever the animal was required to make a link between stimuli or events, even with a stimulus-free period in between. Together, these results provided an important physiological parallel between the spatial learning and episode learning deficit seen with damage to the Hippocampus. Curiously, both place cells and time cells, as well as the sequences built up with them were non-topographically mapped, *i.e.*, they may be located anywhere in the hippocampus, with no obvious spatial order (Dombeck et al., 2010; Modi et al., 2014)(Dombeck et al., 2010; Modi et al., 2014), in contrast to results from the cortex (Dombeck et al., 2009; Ozden et al., 2008).

In an experiment published in 2008, Eva Pastalkova and colleagues from Gyorgy Buzsaki's lab had rats navigate a figure 8 maze, with the animal being rewarded with water, in between trials, if they managed to alternate between the left and right arms (Pastalkova et al., 2008). As an added nuance in the task, just before launching into the left or right arms, the animal had to spend a fixed amount of time running a treadmill, held in place. This would allow self-motion cues, but with the absence of any other external stimuli. Impressively, single-units recorded from the hippocampal CA1 cells revealed strong correlation with the time spent on the treadmill, despite the absence of external cues, and that different cells tuned to different time points, forming a spatiotemporal sequence of activation (Pastalkova et al., 2008). In a different experiment published in 2011, Christopher J. MacDonald and

colleagues from Howard Eichenbaum's lab had rats had to go around a maze and perform a olfactory task (MacDonald et al., 2011). The animals were first presented with an odour, then made to wait for a delay period in a cordoned off section of the maze, before being allowed to either dig for a reward or continue on the maze, depending on the odour presented. As trials progressed, Hippocampal CA1 cells were recorded (single-units) and found to not only be modulated by the decision to be taken, but also to the amount of time spent in the delay period. Experimentally, the delay period could be elongated or shortened, each having an effect on remapping of the tuning fields of the various CA1 cells, but to different extents (MacDonald et al., 2011).

In 2013, the Eichenbaum group published their findings with head-fixed rats (no movement in space) performing a Delayed Match-To Sample (DMS) task with pairs of odours, where again time tuned activity could be observed with a sequence of Hippocampal CA1 cell activations, that depended on the identity of the first odour (MacDonald et al., 2013). In 2014, Mehrab Modi, Ashesh Dhawale, and Upinder Bhalla published their results with head-fixed mice learning and performing a Trace Eye-Blink Conditioning (TEC), wherein it was observed that Hippocampal CA1 cell activity sequences emerged in close relation to the acquisition of behavioural performance, thus cementing the idea that sub-populations of Hippocampal CA1 cells could bridge temporal gaps between relevant, paired stimuli, and that they did so with the activity of time-tuned cells (Modi et al., 2014).

Finally, it was important to study if these apparently time-tuned cells were tuned to the actual duration of time in a delay period, or whether it was more important for these cells to track the distance run. In an

experiment published in 2013, Benjamin Kraus and colleagues from Howard Eichenbaum's lab again had their rats navigate a figure 8 maze, but with a motorized treadmill in the central arm, to experimentally regulate the running speed. With this setup, the study was successful at delineating that both time spent running and distance run were important features, and that different cells could tune to either of the features (B. Kraus et al., 2013; B. J. Kraus et al., 2015). Whenever hippocampal CA1 cells showcased time-tuned activity (as opposed to space/location-tuned activity), such cells were dubbed "Time Cells" (Eichenbaum, 2017; MacDonald et al., 2011).

Other interesting physiological parallels between the CA1 place cells and time cells are,

1. Phase Precession: In relation to theta oscillations (6-10 Hz) measured as local field potentials (LFP), individual cells tended to fire action potentials at progressively earlier phases with each successive cycle, described first for place cells (O'Keefe & Recce, 1993), and then also for time cells (Pastalkova et al., 2008).
2. Temporal Compression: Sequences of place or time cells could be elicited at significantly shorter time scales, with fidelity in the participating cells (Dragoi & Buzsáki, 2006; Foster, 2017). Indeed, with regard to the typically studied regime of ~100-200 ms or behaviour time scales, the same sequence may be elicited at ~10 ms as short segments during Sharp Wave Ripples (Dragoi et al., 1999; V. Itskov et al., 2008; Jadhav et al., 2012; O'Keefe & Recce, 1993; Valero et al., 2015) or even as the whole sequences during Replay (Csicsvari et al., 2007; Diba & Buzsáki, 2007; Foster, 2017; Foster & Wilson, 2006; Gupta et

- al., 2010; Pfeiffer & Foster, 2013) or Pre-play (Dragoi, 2013; Drgoi & Tonegawa, 2011).
3. Remapping: Systematic changes in the experimental paradigm, such as those to the size of the experimental arena or in the time interval between stimuli or events, would result in systematic changes in the firing fields of place (Muller & Kubie, 1989) and time cells (MacDonald et al., 2011).
  4. Variable Firing Fields: The width of the firing fields for a set of place or time cells, respectively, may be variable. However, an important distinction here is that there is as yet no clearly identified predictor of the widths for place cells to spatial directions, while time cells tuned to later time points in the inter-stimulus or delay periods usually exhibit a widening of firing fields (B. Kraus et al., 2013; B. J. Kraus et al., 2015; MacDonald et al., 2011, 2013; Mau et al., 2018; Pastalkova et al., 2008). The significance of firing field density and tuning widths is as yet an open line of inquiry.

Single-units recorded from the medial entorhinal cortex (MEC) as well as the hippocampal CA1 that were found tuned to specific frequency “landmarks” during frequency sweeps self-initiated by rats (Aronov et al., 2017), suggesting that the CA1 could tune to variables other than space and time. This added even more weight to “Contextual Mapping” as an important function of the hippocampus.

## **“Single-cell, multi-trial” vs. “multi-cell, single-trial” approaches in Neuroscience**

A dominant, early perspective in neurophysiology had been to record activity from a single cell, over many trials, under a variety of conditions (bath applications in slice physiology, different physiological conditions like stress and genetic background, etc.). For more than one recorded cell, the process would be repeated, till the dataset was complete.

An intermediate perspective was to record from multiple cells simultaneously, yet treat each cell independently for analysis towards correlation and mechanism studies, across many repeats of experimental conditions or trials (same as above).

An important and more modern perspective is to record from multiple cells simultaneously, and use this network or population activity to decode single-trial characteristics (position, time, stimulus presence, etc.) using very powerful numerical and mathematical algorithms involving (but not limited to) Bayesian Decoding and Information Theory. The essential idea is that the neuronal code of the brain is not defined just by the activity of single neurons since they may only encode very specific fractions of the experience, but rather that the population encodes the full experience, using a number of distributed and redundant strategies.

- Bayesian Decoding: Using the activity of multiple, simultaneously recorded neurons to develop a likelihood estimate of the evidence (firing rate combinations) to the experimental parameter (spatial position, relative time, etc.) and combine this with the experimentally determined prior (probability), to obtain estimates of the conditional or

posterior probability of a parameter value, given evidence.

Bayes' Rule describes

$$P(A|B) = P(B|A).P(A)/P(B)$$

... where,

A: Parameter value (position, time, etc.)

B: Evidence (cellular firing rate)

P(A): Prior Probability (experimentally defined)

P(B): Probability of evidence (Firing Rate)

P(A|B): Posterior probability of parameter value given evidence

P(B|A): Likelihood estimate of evidence given parameter value (based on recordings)

This methodology has been used to not only successfully predict specific time points in a trial from population activity, but has also been used to observe that the population activity from a session of recording is able to predict time points in trials conducted on subsequent sessions of recording, up unto 3-4 sessions (Mau et al., 2018).

- Information Theory: Using recorded cellular activity to estimate how much information this activity carries about experimental parameters (position, time, stimuli, etc.) in a trial-by-trial fashion. Three essential metrics have been used,
  1. Information per activity spike ( $I_{\text{spike}}$ ), in bits/spike
  2. Information per unit time ( $I_{\text{sec}}$ ), in bits/sec
  3. Mutual Information (MI) between evidence and parameter value, in bits

William Skaggs, Bruce McNaughton and colleagues published a series of experiments working out the value of Information Theory

based approaches to deciphering the hippocampal code, reviewed previously (Skaggs et al., 1996). This idea was later adapted strongly by the field but focus throughout, remained on place cells.

A major step forward with “multi-cell, single-trial” approaches is the benefit of resolving how each cell and inter-cell interactions contribute to stimulus representation, behavioural task variables, and other brain-intrinsic computation. Technological advances in large-scale neurophysiology recordings such as the increased density of tetrode drives, Neuropixels, Optical sectioning and microscopy, Resonant scanning, etc., have enabled the discovery of well coordinated sequences of cellular activity such as Sharp Wave Ripples (SWRs), Replay, and behavioural timescale spatio-temporal sequences, *in vivo*, among others. This is primarily due to a radical improvement in an experimenter’s ability to simultaneously record from multiple cells (Foster, 2017), going from yields of ~10 cells to even ~ $10^4$  cells, per animal.

## Dimensionality reduction in the analysis of physiology

Bayesian and Information theoretic approaches as well as methods like Principal Component Analysis (PCA) afford the experimenter a variety of mathematical procedures to examine dimensionality reduction, viz., the transformation of high-dimensional neurophysiological activity from recorded cells into low-dimensional representations that still retain meaningful properties of the original data (Pudil & Novovičová, 1998; van der Maaten et al., 2009). Such

pre-processing steps in analysis often help delineate the contributions of test variables to function. Claude Shannon is often credited with development of Information Theory (Shannon, 1948), yet the field has evolved to also describing how relevance is assigned to a signal, based on statistical associations between multiple signals or stimuli in a sensory experience (Bialek et al., 1996, 2001; Chigirev & Bialek, 2004; Tishby et al., 1999).

In the final version of the paper (Ananthamurthy & Bhalla, 2023; attached as Chapter 4 – “Analysis”), we reoriented focus on the most popular of the algorithms, and provide very well performing Python/C++ implementations, especially of the Ridge-to-background ratio (Mau et al., 2018) and Temporal Information (Mau et al., 2018) calculations, each of which consider cellular physiology and estimate a score for time cell-like behaviour.

## **Synthetic benchmarks for pre-hoc development of analytical procedures**

An interesting study published in 2018 used synthetic test datasets to go to the extent of estimating place cell detection algorithm performance on the basis of  $I_{\text{spike}}$ ,  $I_{\text{sec}}$  and MI (Souza et al., 2018). They found,

1. MI could outperform the other two in a variety of scenarios.
2.  $I_{\text{spike}}$  and  $I_{\text{sec}}$  may still be useful in identifying unique subpopulations of place cells.
3. Important algorithmic adjustments could be made to the calculations of  $I_{\text{spike}}$  and  $I_{\text{sec}}$ , to equalize performance between them and MI.

There is clear nuance in the population code that required such a perspective during analysis. Eichenbaum and colleagues popularized the use of such metrics in the context of time cells (Mau et al., 2018), yet a systematic approach to identifying the best algorithms for time cells was requisite. We resorted to the use of such surrogate synthetic datasets acting as a large cohort of user-configurable test datasets to benchmark and characterize the predictive performance of a variety of time cell detection algorithms (Ananthamurthy & Bhalla, 2023; attached as Chapter 4 – “Analysis”). Analysis on real physiology datasets where categorical labels must be assessed is expected to benefit from this comparative analysis. Our Python/C++ implementations were rigorously tested and developed to the extent of excellent predictive performance. These algorithmic procedures may be used to study the nuances of time cell sequences with more statistical confidence.

Correlation analysis between pairs of recorded cells is one of the most important analytical directions taken by neurophysiologists understanding brain function, and has been reviewed previously (M. R. Cohen & Kohn, 2011). However, such analysis can be subject to False Positives, without appropriate significance studies. Specifically, it is important to look at whether the activity profile or tuning curves for cells (in relation to task variables) is significant above chance or other clearly defined cutoffs, using a large number of randomized surrogates of the recorded activity, generated by adding random timing shifts or bootstraps. Multiple pairwise correlations may not be sufficient to identify synchronous sequential activity in the network, without looking at higher orders of correlation across recorded cells. Ultimately, such studies benefit from simultaneous high-yield recordings, updated analytical procedures utilizing surrogate data for significance analysis,

examining repetitions across trials (or trial-to-trial variability), and even the use of multiple analytical strategies, as reviewed previously (Foster, 2017; Grün, 2009).

Internally driven as opposed to externally driven network models of activity sequences have been proposed as the mechanism driving hippocampal CA1 sequences (Buzsáki & Llinás, 2017; Eichenbaum, 2017). The CA1 neurons participating in any sequence may represent physiologically mappable attractors in temporally specific contexts. Our 2-photon calcium recordings are expected to shed light on important correlations between task variables and the spatiotemporal sequence of activity, measured chronically, at cellular resolution.

Synfire chains (Abeles, 1982, 1991, 2004, 2009; Abeles et al., 2004) as sequential neuronal activity patterns or motifs have been described in cortical slices *in vitro* (Reyes, 2003), as well as *in vivo* (Ikegaya et al., 2004). The 2004 study described these sequences as songs (Ikegaya et al., 2004) that can incorporate new information as extensions of the motifs by combining multiple synfire chains (Bienenstock, 1995). However, an important consideration is that the original theoretical ideas behind synfire chains assumed feed-forward connections between layers of neurons, with recognition by subsequent neurons looking only at waves of synchrony, rather than specific individual neuronal identities (Abeles, 2004). Another important perspective is that these cortical sequences could be artifacts elicited just by chance, given the nature of membrane voltage fluctuations (McLelland & Paulsen, 2007; Mokeichev et al., 2007). There is thus some speculation over the significance of “cortical songs”, *in vivo*. The

use of properly developed and benchmarked analytical procedures, tested and verified on physiology-equivalent test datasets (synthetic), is expected to help alleviate potential doubts in published physiology results (real recordings). For proper testing of our time cell detection algorithms, we incorporated many important user-controllable parameters for the generation of synthetic datasets, such as (but not limited to) Noise, Event Widths, Hit Trial Ratio, Trial-pair Imprecision, and Background Activity. Furthermore, reported but not popularly accepted physiological sequences such as synfire chains (Ikegaya et al., 2004) and preplay (Dragoi & Tonegawa, 2011), may now be more rigorously tested using the time cell analysis and detection algorithms provided (Ananthamurthy & Bhalla, 2023; attached as Chapter 4 – “Analysis”).

## **Single-Unit Electrophysiology vs 2-Photon Calcium Imaging to study the Hippocampus**

The most well characterized and studied function of the hippocampus and surrounding tissue (Entorhinal Cortex, Parasubiculum, etc.) was the role these tissue systems played in Spatial Navigation and Coding. Single-Unit Electrophysiology was paramount to being able to isolate the activity from individual cells, and eventually was used to discover and describe properties of place cells (O’Keefe & Dostrovsky, 1971), grid cells (Fyhn et al., 2004; Hafting et al., 2005)(Fyhn et al., 2004; Hafting et al., 2005), head-direction cells (Taube et al., 1990), along with numerous other important physiological discoveries, as detailed previously. However, even with advances in the density of tetrode

recordings, the yield of recorded cells from any given animal was often limited to <50 cells. It was only with the invention of Neuropixels (Jun et al., 2017) that this yield could be expanded to ~1000 cells. We had opted to utilize calcium imaging by 2-Photon Microscopy (Denk et al., 1990; Stosiek et al., 2003). This methodology, allowed us to record ~100-150 cells per session with our mice, albeit with significant cost to the recording frame rate on account of the limitations of the technique. Electrical recordings may be sampled even >20 kHz, while imaging based techniques typically cannot be used to record wide fields of view, sampled at >100 Hz (1-2 orders of magnitude, comparing sampling rates). Many spike sorting algorithms (see Buccino et al., 2022 for review) as well as automated ROI detection (see Robbins et al., 2021 for review) have been suggested for automated cell source identification, yet challenges remain, such as,

- 1) scalability - more sources to identify from ever larger datasets force longer analysis runs.
- 2) reproducibility – pre-processing analytical steps require manual curation to clean up the raw datasets, and this often affects the final result. We discuss details of our technique along with challenges and preliminary results, in Chapter 3 – “Imaging”.

The hippocampi (one in each hemisphere) of the mouse brain lie ~1 mm below the most superficial layers of cortex (just inside the cranium), a barrier typically too wide for typical 1-photon fluorescence imaging systems (Confocal, Spinning Disk, etc.). This poses a very difficult challenge for imaging preparations since there are hardware and other technical limits to how long the working distance of microscope objectives can be made. The use of 2-photon microscopy combined with combinations of cortical excavations (to aid physical

access), microendoscopes, as well as prisms to guide emitted fluorescence, have all been used to achieve deep brain imaging based recordings at cellular resolution, in rodents (Andermann et al., 2013; Attardo et al., 2015; Barreto et al., 2009; Barreto & Schnitzer, 2012; Dombeck et al., 2010; Heys et al., 2014; Murray & Levene, 2012; Velasco & Levene, 2014; Ziv et al., 2013).

All imaging preparation standardizations described in this thesis invoke 2-Photon calcium imaging of hippocampal CA1 cells at cellular resolution (1 pix = ~1  $\mu$ m), following cortical excavations just above the left hippocampus (Dombeck et al., 2010).

## Calcium imaging by 2-Photon Microscopy

Typically, as cells become activated and elicit action potentials, there is often a large concomitant influx of  $\text{Ca}^{2+}$  ions through voltage gated calcium channels all around the perisomatic membrane, amongst other cellular compartments. Several organic dyes have been developed that reversibly bind  $\text{Ca}^{2+}$  ions in the cytosol and either become fluorescent or emit greater fluorescence (often with a red shift) when in this  $\text{Ca}^{2+}$ -bound state (Paredes et al., 2008). Additionally tremendous advances in molecular biology has seen the deployment of Genetically Encoded Calcium Indicators (GECIs) that may be exogenously incorporated into the genome of target cells. These GECIs serve the same function as organic calcium dyes, but may easily be replenished in the cytosol given the cell's natural machinery for transcription and translation, and whose Fluorescence properties can be engineered for brightness, responsivity,  $\text{Ca}^{2+}$  binding  $K_d$ , and fluorescence emission wavelengths.

The number of cells that may be recorded by fluorescence is often only limited to either the spread of the organic dye or the imaging magnification settings, allowing for yields of 100-1000 cells.

With any Imaging based neurophysiology, there is always a trade-off between yield (number of cells recorded simultaneously) and temporal resolution. Increasing the yield by recording over a larger area of tissue requires many more pixels per imaging frame, resulting in a loss of temporal resolution (frame rate). On the other hand, increasing the frame rate necessitates capturing fewer pixels per frame, decreasing yield. There is even a limitation of simply zooming out, since stable fluorescence intensity fluctuations can only be identified when each cell is defined at least by a certain number of pixels, to allow proper isolation.

Specifically with calcium imaging, the signal to be recorded corresponds to  $\text{Ca}^{2+}$  flux in the cytoplasm as measured by the change in emitted fluorescence of reporters such as GCaMP, with a  $\tau_{\text{rise}} = 10$ -100 ms and  $\tau_{\text{fall}} = 100$ -300 ms (Chen et al., 2013). This signal is one or two orders of magnitude slower than the action potential ( $\sim 2$ -5 ms). However, this may not necessarily be a limitation since a dominant idea in the field is to simply consider rate coding, or time-averaged spiking activity (Abeles, 2004), bringing down the effective temporal resolution of the electrical record.

Genetically Encoded Voltage Indicators (GEVIs) that fluoresce with higher emission during membrane voltage dynamics have also been developed. However, their localization onto the membrane of the cell, instead of the cytoplasm, diminishes the total emitted photon flux per

unit time, and requires longer bin times to achieve reasonable signal-to-noise, as reviewed previously (Mollinedo-Gajate et al., 2021). This unfortunately brings down the frame rate even more than what can be achieved with GECIs. We avoided GEVIs in the projects described in this thesis.

A major advancement in Fluorescence Imaging was the invention of Confocal and Multiphoton (typically 2-Photon) Microscopes, which allowed for unprecedented recording signal-to-noise by optical sectioning. 2-Photon Imaging itself was an important development for the neurophysiology of tissue greater than 300  $\mu\text{m}$  in thickness, typical of rodent brain tissue, because it avoids wasteful excitation of imaging planes that are not in focus (out-of-plane). The 2-Photon effect requires two photons of longer wavelength (lower energy per photon), to near instantaneously excite a fluorophore. The photon flux is highest at the focal plane (with an N-squared dependence) of the microscope so only the section of the tissue corresponding to the focal place is allowed to achieve fluorescence. Additionally, longer wavelengths of excitation light can more easily penetrate deeper layers of tissue, due to comparatively lower scattering or Rayleigh effect (Denk et al., 1990; Helmchen & Denk, 2005).

The hippocampus (specifically the hippocampal CA1) was the main brain structure of interest for all our physiology experiments, and lies under about 1 mm of cortical tissue for mice. This is a depth that is difficult to image even with 2-Photon Microscopy. The typical methodology employed in such cases is to perform a cortical excavation just above the Hippocampus filling the crevice with optically clearer agarose or silicone elastomer. Even so, the hippocampal CA1

cell body layer (*Stratum Pyramidale*) still lies about 150-300  $\mu\text{m}$  below the external capsule and corpus callosum fibers (left intact for chronic imaging). Accordingly, we combined cortical excavation with 2-Photon microscopy, using a long working distance objective with a wide field of view, imaging cytosolic  $\text{Ca}^{2+}$  activity with the help of either an organic dye (OGB-1; acute imaging) or a GECI (GCaMP6f; chronic imaging).

An important perspective that has motivated the use of Imaging based physiology recordings (as opposed to Electrophysiological methods) other than potential yield, is that imaging provides anatomical confirmation of any particular recorded cell, and this in turn allows for,

- A) Unambiguous isolation of the same cell across multiple imaging sessions (across days and weeks). Single-Units are ultimately only algorithmically resolved and this can be done only for cells that are active and are represented in multiple spatially separated electrodes. However, very recently, Ashesh Dhawale and colleagues from Bence Olveczky's lab have devised a solution to track the movement of electrodes in tissue over time and use this information to ensure chronic recording of the same units (Dhawale et al., 2017). This technique was not available at the time when experiments for this thesis were started.
- B) Unambiguous detection of the lack of activity in an otherwise recorded cell. Since the cell can be anatomically identified independent of activity, it is possible to observe the absence of  $\text{Ca}^{2+}$  activity. Automated cell ROI detection (Francis et al., 2012; Maruyama et al., 2014; Mukamel et al., 2009; Pachitariu et al., 2017; Pnevmatikakis et al., 2016) simplifies the pre-processing step of cell isolation even over large batch sizes. These

procedures inherently require the use of the calcium activity profiles of recorded cells, viz., inactive cells (though anatomically visible), may not be isolated.

## **Automated ROI detection for large-scale Calcium Imaging datasets**

A number of automated ROI detection algorithms have been cited in literature that require minimal user intervention, perform relatively fast identification for a large number of identified sources (putative cells).

Some popular algorithms include PCA/ICA (Mukamel et al., 2009), Suite2p (Pachitariu et al., 2017), and Non-Negative Matrix Factorization or NNMF (Pnevmatikakis et al., 2016), which all have been developed to the extent where comparable or oftentimes much better ROI detection is achieved than as compared to the more tedious hand-drawn ROIs which scales very poorly with orders of cells recorded.

We have strictly followed Suite2p (Pachitariu et al., 2017) for all physiological ROI (cell sources) described in this thesis.

## **Short Summaries of the 3 projects**

### **Project I - How do sensory representations transform with learning?**

Sensory Systems Neuroscience is a very popular field spanning studies looking at numerous brain regions and sub-regions in the

cortex and hippocampus, *in vivo* (R. A. Andersen et al., 1993; Fassihi et al., 2017; Khan et al., 2010; Meeks et al., 2010; Petersen, 2019; Poort et al., 2015; Voelcker et al., 2022), among several others. Many if not most of these studies describe neural activity in animals with expert levels of behavioural learning and performance to the presented stimuli. Lacunae still remain as to mechanisms deployed during active or online learning especially in the early stages of behavioural training. There are not many published physiological readouts from large CA1 populations, *in vivo*, under behavioural contexts for time cell activation, during the early, acquisition phases (Sessions 1-7, etc.) in associative learning. It is unclear what the spatiotemporal pattern of activity would reveal with a systematic, longitudinal survey.

We deployed our experiments with the intention to study how Calcium Imaging by 2-Photon could reveal finer population level details of network activity as the animals were tested on the learning of an operant conditioning or lick behaviour task. We were able to,

1. Prototype OGB-1 based calcium imaging *in vivo*, from head-fixed mice in a manner suited to combined behaviour and recording experiments, and
2. Study preliminary data from animals that correlation based functional activity clusters of recorded CA1 cells have spatial organization during bouts of spontaneous activity.

However, we were not satisfied with the level and rate of learning in our test animals eventually leading to a search for more stable behaviour paradigms in mice. Additionally, the use of OGB-1 as the Calcium Indicator also had to be abandoned since this fundamentally disallowed multi-day tracking of the same cells. We discuss our

prototyping efforts and preliminary data for this project in detail, in the first few sections each of Chapters 2 (“Behaviour”) and 3 (“Imaging”).

## **Project II - How does the timing of cellular activity adjust to behavioural task variables?**

Research on the cerebellum has made substantial progress in the elucidation of network mechanisms correlating well with external stimulus timing based variables, as animals learn Trace Eye-Blink Conditioning and Delay Conditioning (Kalmbach, Davis, et al., 2010; Kalmbach, Ohyama, et al., 2010; Medina et al., 2000; Ohyama et al., 2003; Siegel & Mauk, 2013). The preeminent studies on time cells in the hippocampus have focused on the context of appetitive reinforcing stimuli (Eichenbaum, 2004, 2017; B. Kraus et al., 2013; B. J. Kraus et al., 2015; MacDonald et al., 2011, 2013; Mau et al., 2018; Pastalkova et al., 2008). Time cells in the behavioural context of Trace Eye-Blink conditioning, an aversive learning paradigm, have been explored (Modi et al., 2014), but details such as correlations with rates of behavioural learning, tuning adaptability, and long-term stability (~weeks) of the time sequences are yet to be studied. The degree of variability in time cell responses under these conditions is likely to inform mechanistic models of spatiotemporal sequences as observed in the hippocampus.

We prototyped a GCaMP6f based *in vivo* hippocampal preparation that allowed for chronic, longitudinal recordings of hippocampal CA1, by 2-Photon Calcium Imaging (Dombeck et al., 2010) that could be

combined with a stable and adaptable learning protocols of Trace Eye-Blink Conditioning (Siegel et al., 2015).

From our preliminary set of recordings we were able to,

1. Detect time cells in our population recordings,
2. Observe signs of expansion of the time cell sub-population over early stages of learning, and
3. Observe shifts in the timing of peak for known, chronically tracked time cells, typically moving away from the US and towards the CS.

Technical difficulties prevented us from expanding our experimental recording datasets to the point where these results could be looked at more critically and the results may be sufficient for publication. We discuss our prototyping efforts and preliminary data for this project in detail, in the last few sections each of Chapters 2 (“Behaviour”) and 3 (“Imaging”).

### **Project III - What is the best way to detect and score time-tuned cellular activity?**

Given that we had collected a reasonable sample of multi-day tracked cells while head-fixed mice were being trained to a Trace Eye-Blink Conditioning (TEC) task, we wished to move forward to identifying time cells in the most reliable way, with the aim to drawing quality conclusions from the physiology recordings.

The paper entitled “Synthetic Data Resource and Benchmarks for Time Cell Analysis and Detection Algorithms” (Ananthamurthy & Bhalla, 2023) was a consolidation of our progress to analyse physiology data from real and synthetic cells expressed as calcium activity trials and sessions.

Here, we used a computational approach and developed categorically labelled, user definable, large scale synthetic datasets, as a test bed to compare and benchmark the predictions made by popular time cell detection algorithms. We were able to test the sensitivity of these computational algorithms across a wide array of experimental recording parameters, and could ultimately conclude the best operational regimes for each of them. All of the code base for this project is freely available online (<https://github.com/bhallalab/TimeCellAnalysis>) and is intended to be a resource to researchers.

The paper is attached as Chapter 4 (“Analysis”).

## Code Availability

All our code for Synthetic Data generation and time cell Analysis is available at <https://www.github.com/bhallalab/TimeCellAnalysis>.

All our code for conducting Trace Eye-Blink Conditioning (TEC) behaviour is available at  
<https://www.github.com/ananthamurthy/eyeBlinkBehaviour>.

Analysis scripts for evaluating TEC performance are available at  
<https://github.com/ananthamurthy/MATLAB/tree/master/TECAnalysis>.

## Bibliography

- Abeles, M. (1982). *Local Cortical Circuits: An Electrophysiological Study*. Springer-Verlag.  
<https://books.google.co.in/books?id=s25lwwEACAAJ>
- Abeles, M. (1991). *Corticonics: Neural Circuits of the Cerebral Cortex*. Cambridge University Press. <https://doi.org/DOI:10.1017/CBO9780511574566>
- Abeles, M. (2004). Time Is Precious. *Science*, 304(5670), 523–524.  
<https://doi.org/10.1126/science.1097725>
- Abeles, M. (2009). *Synfire Chains* (L. R. B. T.-E. of N. Squire, Ed.; pp. 829–832). Academic Press.  
<https://doi.org/https://doi.org/10.1016/B978-008045046-9.01437-6>
- Abeles, M., Hayon, G., & Lehmann, D. (2004). Modeling compositionality by dynamic binding of synfire chains. *Journal of Computational Neuroscience*, 17(2), 179–201.  
<https://doi.org/10.1023/B:JCNS.0000037682.18051.5f>
- Ananthamurthy, K. G., & Bhalla, U. S. (2023). Synthetic Data Resource and Benchmarks for Time Cell Analysis and Detection Algorithms. *ENeuro*, ENEURO.0007-22.2023.  
<https://doi.org/10.1523/ENEURO.0007-22.2023>
- Andermann, M. L., Gilfoy, N. B., Goldey, G. J., Sachdev, R. N. S., Wölfel, M., McCormick, D. A., Reid, R. C., & Levene, M. J. (2013). Chronic Cellular Imaging of Entire Cortical Columns in Awake

- Mice Using Microprisms. *Neuron*, 80(4), 900–913.  
<https://doi.org/10.1016/j.neuron.2013.07.052>
- Andersen, R. A., Snyder, L. H., Li, C.-S., & Stricanne, B. (1993). Coordinate transformations in the representation of spatial information. *Current Opinion in Neurobiology*, 3(2), 171–176.  
[https://doi.org/https://doi.org/10.1016/0959-4388\(93\)90206-E](https://doi.org/https://doi.org/10.1016/0959-4388(93)90206-E)
- Aronov, D., Nevers, R., & Tank, D. W. (2017). Mapping of a non-spatial dimension by the hippocampal-entorhinal circuit. *Nature*, 543(7647), 719–722. <https://doi.org/10.1038/nature21692>
- Attardo, A., Fitzgerald, J. E., & Schnitzer, M. J. (2015). Impermanence of dendritic spines in live adult CA1 hippocampus. *Nature*, 523(7562), 592–596. <https://doi.org/10.1038/nature14467>
- Ballard, I. C., Wagner, A. D., & McClure, S. M. (2019). Hippocampal pattern separation supports reinforcement learning. *Nature Communications*, 10(1), 1073. <https://doi.org/10.1038/s41467-019-10899-1>
- Barreto, R. P. J., Messerschmidt, B., & Schnitzer, M. J. (2009). In vivo fluorescence imaging with high-resolution microlenses. *Nature Methods*, 6(7), 511–512. <https://doi.org/10.1038/nmeth.1339>
- Barreto, R. P. J., & Schnitzer, M. J. (2012). In vivo optical microendoscopy for imaging cells lying deep within live tissue. *Cold Spring Harbor Protocols*, 2012(10), 1029–1034.  
<https://doi.org/10.1101/pdb.top071464>
- Baudry, M., & Lynch, G. (1981). Hippocampal glutamate receptors. *Molecular and Cellular Biochemistry*, 38(1), 5–18.  
<https://doi.org/10.1007/BF00235685>
- Bialek, W., Callan, C. G., & Strong, S. P. (1996). Field Theories for Learning Probability Distributions. *Physical Review Letters*, 77(23), 4693–4697. <https://doi.org/10.1103/physrevlett.77.4693>
- Bialek, W., Nemenman, I., & Tishby, N. (2001). Predictability, Complexity, and Learning. *Neural Comput.*, 13(11), 2409–2463.  
<https://doi.org/10.1162/089976601753195969>
- Bienenstock, E. (1995). A model of neocortex. *Network: Computation in Neural Systems*, 6(2), 179–224. [https://doi.org/10.1088/0954-898X\\_6\\_2\\_004](https://doi.org/10.1088/0954-898X_6_2_004)
- Bjerknes, T. L., Moser, E. I., & Moser, M.-B. (2014). Representation of Geometric Borders in the Developing Rat. *Neuron*, 82(1), 71–78.  
<https://doi.org/10.1016/j.neuron.2014.02.014>
- Buccino, A. P., Garcia, S., & Yger, P. (2022). Spike sorting: new trends and challenges of the era of high-density probes. *Progress in Biomedical Engineering*, 4(2), 022005.  
<https://doi.org/10.1088/2516-1091/ac6b96>
- Burgess, N. (2008). Spatial Cognition and the Brain. *Annals of the New*

- York Academy of Sciences*, 1124(1), 77–97.  
<https://doi.org/https://doi.org/10.1196/annals.1440.002>
- Buzsáki, G., & Llinás, R. (2017). Space and time in the brain. *Science (New York, N.Y.)*, 358(6362), 482–485.  
<https://doi.org/10.1126/science.aan8869>
- Cai, D. J., Aharoni, D., Shuman, T., Shobe, J., Biane, J., Song, W., Wei, B., Veshkini, M., La-Vu, M., Lou, J., Flores, S. E., Kim, I., Sano, Y., Zhou, M., Baumgaertel, K., Lavi, A., Kamata, M., Tuszyński, M., Mayford, M., ... Silva, A. J. (2016). A shared neural ensemble links distinct contextual memories encoded close in time. *Nature*, 534(7605), 115–118.  
<https://doi.org/10.1038/nature17955>
- Caporale, N., & Dan, Y. (2008). Spike timing-dependent plasticity: a Hebbian learning rule. *Annual Review of Neuroscience*, 31, 25–46. <https://doi.org/10.1146/annurev.neuro.31.060407.125639>
- Carew, T. J., Castellucci, V. F., & Kandel, E. R. (1971). An Analysis of Dishabituation and Sensitization of The Gill-Withdrawal Reflex In Aplysia. *International Journal of Neuroscience*, 2(2), 79–98.  
<https://doi.org/10.3109/00207457109146995>
- Chen, T.-W., Wardill, T. J., Sun, Y., Pulver, S. R., Renninger, S. L., Baohan, A., Schreiter, E. R., Kerr, R. A., Orger, M. B., Jayaraman, V., Looger, L. L., Svoboda, K., & Kim, D. S. (2013). Ultrasensitive fluorescent proteins for imaging neuronal activity. *Nature*, 499(7458), 295–300. <https://doi.org/10.1038/nature12354>
- Chigirev, D., & Bialek, W. (2004, January). Optimal manifold representation of data: An information theoretic approach. *Advances in Neural Information Processing Systems 16 - Proceedings of the 2003 Conference, NIPS 2003*.
- Clayton, N. S., Salwiczek, L. H., & Dickinson, A. (2007). Episodic memory. *Current Biology*, 17(6), R189–R191.  
<https://doi.org/10.1016/j.cub.2007.01.011>
- Cohen, M. R., & Kohn, A. (2011). Measuring and interpreting neuronal correlations. *Nature Neuroscience*, 14(7), 811–819.  
<https://doi.org/10.1038/nn.2842>
- Conway, M. A. (2009). Episodic memories. *Neuropsychologia*, 47(11), 2305–2313.  
<https://doi.org/https://doi.org/10.1016/j.neuropsychologia.2009.02.003>
- Csicsvari, J., O'Neill, J., Allen, K., & Senior, T. (2007). Place-selective firing contributes to the reverse-order reactivation of CA1 pyramidal cells during sharp waves in open-field exploration. *The European Journal of Neuroscience*, 26(3), 704–716.  
<https://doi.org/10.1111/j.1460-9568.2007.05684.x>

- Davidson, T. J., Kloosterman, F., & Wilson, M. A. (2009). Hippocampal replay of extended experience. *Neuron*, 63(4), 497–507.  
<https://doi.org/10.1016/j.neuron.2009.07.027>
- Denk, W., Strickler, J. H., & Webb, W. W. (1990). Two-photon laser scanning fluorescence microscopy. *Science (New York, N.Y.)*, 248(4951), 73–76. <https://doi.org/10.1126/science.2321027>
- Dhawale, A. K., Poddar, R., Wolff, S. B. E., Normand, V. A., Kopelowitz, E., & Ölveczky, B. P. (2017). Automated long-term recording and analysis of neural activity in behaving animals. *eLife*, 6, e27702. <https://doi.org/10.7554/eLife.27702>
- Diamond, A. (2013). Executive Functions. *Annual Review of Psychology*, 64(1), 135–168. <https://doi.org/10.1146/annurev-psych-113011-143750>
- Diba, K., & Buzsáki, G. (2007). Forward and reverse hippocampal place-cell sequences during ripples. *Nature Neuroscience*, 10(10), 1241–1242. <https://doi.org/10.1038/nn1961>
- Dickinson, A., Nicholas, D. J., & Mackintosh, N. J. (1983). A re-examination of one-trial blocking in conditioned suppression. *The Quarterly Journal of Experimental Psychology B: Comparative and Physiological Psychology*, 35, 67–79.  
<https://doi.org/10.1080/14640748308400914>
- Disterhoft, J. F., & Weiss, C. (2017). Eyeblink Conditioning – A Behavioral Model of Procedural and Declarative Learning. In J. H. Byrne (Ed.), *Learning and Memory: A Comprehensive Reference (Second Edition)* (pp. 327–355). Academic Press.  
<https://doi.org/https://doi.org/10.1016/B978-0-12-809324-5.21087-0>
- Dombeck, D. A., Graziano, M. S., & Tank, D. W. (2009). Functional Clustering of Neurons in Motor Cortex Determined by Cellular Resolution Imaging in Awake Behaving Mice. *The Journal of Neuroscience*, 29(44), 13751 LP – 13760.  
<https://doi.org/10.1523/JNEUROSCI.2985-09.2009>
- Dombeck, D. A., Harvey, C. D., Tian, L., Looger, L. L., & Tank, D. W. (2010). Functional imaging of hippocampal place cells at cellular resolution during virtual navigation. *Nature Neuroscience*, 13(11), 1433–1440. <https://doi.org/10.1038/nn.2648>
- Dragoi, G. (2013). Internal operations in the hippocampus: single cell and ensemble temporal coding. *Frontiers in Systems Neuroscience*, 7, 46. <https://doi.org/10.3389/fnsys.2013.00046>
- Dragoi, G., & Buzsáki, G. (2006). Temporal encoding of place sequences by hippocampal cell assemblies. *Neuron*, 50(1), 145–157. <https://doi.org/10.1016/j.neuron.2006.02.023>
- Dragoi, G., Carpi, D., Recce, M., Csicsvari, J., & Buzsáki, G. (1999).

- Interactions between hippocampus and medial septum during sharp waves and theta oscillation in the behaving rat. *The Journal of Neuroscience : The Official Journal of the Society for Neuroscience*, 19(14), 6191–6199.  
<http://www.ncbi.nlm.nih.gov/pubmed/10407055>
- Dragoi, G., & Tonegawa, S. (2011). Preplay of future place cell sequences by hippocampal cellular assemblies. *Nature*, 469(7330), 397–401. <https://doi.org/10.1038/nature09633>
- Eichenbaum, H. (2004). Hippocampus: Cognitive processes and neural representations that underlie declarative memory. *Neuron*, 44(1), 109–120. <https://doi.org/10.1016/j.neuron.2004.08.028>
- Eichenbaum, H. (2017). On the Integration of Space, Time, and Memory. *Neuron*, 95(5), 1007–1018.  
<https://doi.org/10.1016/j.neuron.2017.06.036>
- Ekstrom, A. D., & Ranganath, C. (2018). Space, time, and episodic memory: The hippocampus is all over the cognitive map. *Hippocampus*, 28(9), 680–687.  
<https://doi.org/https://doi.org/10.1002/hipo.22750>
- Fassihi, A., Akrami, A., Pulecchi, F., Schönfelder, V., & Diamond, M. E. (2017). Transformation of Perception from Sensory to Motor Cortex. *Current Biology : CB*, 27(11), 1585-1596.e6.  
<https://doi.org/10.1016/j.cub.2017.05.011>
- Ferbinteanu, J., & Shapiro, M. L. (2003). Prospective and retrospective memory coding in the hippocampus. *Neuron*, 40(6), 1227–1239.  
[https://doi.org/10.1016/s0896-6273\(03\)00752-9](https://doi.org/10.1016/s0896-6273(03)00752-9)
- Ferbinteanu, J., Shirvalkar, P., & Shapiro, M. L. (2011). Memory Modulates Journey-Dependent Coding in the Rat Hippocampus. *The Journal of Neuroscience*, 31(25), 9135 LP – 9146.  
<https://doi.org/10.1523/JNEUROSCI.1241-11.2011>
- Focus on spatial cognition. (2017). *Nature Neuroscience*, 20(11), 1431.  
<https://doi.org/10.1038/nn.4666>
- Foster, D. J. (2017). Replay Comes of Age. *Annual Review of Neuroscience*, 40, 581–602. <https://doi.org/10.1146/annurev-neuro-072116-031538>
- Foster, D. J., & Wilson, M. A. (2006). Reverse replay of behavioural sequences in hippocampal place cells during the awake state. *Nature*, 440(7084), 680–683. <https://doi.org/10.1038/nature04587>
- Foster, D. J., & Wilson, M. A. (2007). Hippocampal theta sequences. *Hippocampus*, 17(11), 1093–1099.  
<https://doi.org/10.1002/hipo.20345>
- Francis, M., Qian, X., Charbel, C., Ledoux, J., Parker, J. C., & Taylor, M. S. (2012). Automated region of interest analysis of dynamic Ca<sup>2+</sup> signals in image sequences. *American Journal of*

- Physiology. Cell Physiology*, 303(3), C236-43.  
<https://doi.org/10.1152/ajpcell.00016.2012>
- Frank, L. M., Brown, E. N., & Wilson, M. (2000). Trajectory encoding in the hippocampus and entorhinal cortex. *Neuron*, 27(1), 169–178.  
[https://doi.org/10.1016/s0896-6273\(00\)00018-0](https://doi.org/10.1016/s0896-6273(00)00018-0)
- Fyhn, M., Molden, S., Witter, M. P., Moser, E. I., & Moser, M.-B. (2004). Spatial representation in the entorhinal cortex. *Science (New York, N.Y.)*, 305(5688), 1258–1264.  
<https://doi.org/10.1126/science.1099901>
- Giovannucci, A., Badura, A., Deverett, B., Najafi, F., Pereira, T. D., Gao, Z., Ozden, I., Kloth, A. D., Pnevmatikakis, E., Paninski, L., De Zeeuw, C. I., Medina, J. F., & Wang, S. S.-H. (2017). Cerebellar granule cells acquire a widespread predictive feedback signal during motor learning. *Nature Neuroscience*, 20(5), 727–734. <https://doi.org/10.1038/nn.4531>
- Grün, S. (2009). Data-Driven Significance Estimation for Precise Spike Correlation. *Journal of Neurophysiology*, 101(3), 1126–1140.  
<https://doi.org/10.1152/jn.00093.2008>
- Gupta, A. S., van der Meer, M. A. A., Touretzky, D. S., & Redish, A. D. (2010). Hippocampal Replay Is Not a Simple Function of Experience. *Neuron*, 65(5), 695–705.  
<https://doi.org/https://doi.org/10.1016/j.neuron.2010.01.034>
- Hafting, T., Fyhn, M., Molden, S., Moser, M.-B., & Moser, E. I. (2005). Microstructure of a spatial map in the entorhinal cortex. *Nature*, 436(7052), 801–806. <https://doi.org/10.1038/nature03721>
- Hamme, L. J. Van, & Wasserman, E. A. (1993). Cue Competition in Causality Judgments: The Role of Manner of Information Presentation. *Bulletin of the Psychonomic Society*, 31(5), 457–460. <https://doi.org/10.3758/bf03334962>
- Han, J.-H., Kushner, S. A., Yiu, A. P., Hsiang, H.-L. L., Buch, T., Waisman, A., Bontempi, B., Neve, R. L., Frankland, P. W., & Josselyn, S. A. (2009). Selective erasure of a fear memory. *Science (New York, N.Y.)*, 323(5920), 1492–1496.  
<https://doi.org/10.1126/science.1164139>
- Hartley, T., Lever, C., Burgess, N., & O'Keefe, J. (2014). Space in the brain: how the hippocampal formation supports spatial cognition. *Philosophical Transactions of the Royal Society B: Biological Sciences*, 369(1635), 20120510.  
<https://doi.org/10.1098/rstb.2012.0510>
- Hebb, D. O. (1949). The organization of behavior; a neuropsychological theory. In *The organization of behavior; a neuropsychological theory*. Wiley.
- Helmchen, F., & Denk, W. (2005). *Deep tissue two-photon microscopy*.

- 2(12), 9. <https://doi.org/10.1038/nmeth818>
- Heys, J. G., Rangarajan, K. V., & Dombeck, D. A. (2014). The Functional Micro-organization of Grid Cells Revealed by Cellular-Resolution Imaging. *Neuron*, 84(5), 1079–1090.  
<https://doi.org/10.1016/j.neuron.2014.10.048>
- Hyde, R. A., & Strowbridge, B. W. (2012). Mnemonic representations of transient stimuli and temporal sequences in the rodent hippocampus in vitro. *Nature Neuroscience*, 15(10), 1430–1438.  
<https://doi.org/10.1038/nn.3208>
- Ikegaya, Y., Aaron, G., Cossart, R., Aronov, D., Lampl, I., Ferster, D., & Yuste, R. (2004). Synfire chains and cortical songs: temporal modules of cortical activity. *Science (New York, N.Y.)*, 304(5670), 559–564. <https://doi.org/10.1126/science.1093173>
- Itskov, V., Pastalkova, E., Mizuseki, K., Buzsaki, G., & Harris, K. D. (2008). Theta-mediated dynamics of spatial information in hippocampus. *The Journal of Neuroscience : The Official Journal of the Society for Neuroscience*, 28(23), 5959–5964.  
<https://doi.org/10.1523/JNEUROSCI.5262-07.2008>
- Jadhav, S. P., Kemere, C., German, P. W., & Frank, L. M. (2012). Awake hippocampal sharp-wave ripples support spatial memory. *Science (New York, N.Y.)*, 336(6087), 1454–1458.  
<https://doi.org/10.1126/science.1217230>
- Josselyn, S. A., & Tonegawa, S. (2020). Memory engrams: Recalling the past and imagining the future. *Science (New York, N.Y.)*, 367(6473). <https://doi.org/10.1126/science.aaw4325>
- Jun, J. J., Steinmetz, N. A., Siegle, J. H., Denman, D. J., Bauza, M., Barbarits, B., Lee, A. K., Anastassiou, C. A., Andrei, A., Aydin, Ç., Barbic, M., Blanche, T. J., Bonin, V., Couto, J., Dutta, B., Gratiy, S. L., Gutnisky, D. A., Häusser, M., Karsh, B., ... Harris, T. D. (2017). Fully integrated silicon probes for high-density recording of neural activity. *Nature*, 551(7679), 232–236.  
<https://doi.org/10.1038/nature24636>
- Kalmbach, B. E., Davis, T., Ohyama, T., Riusech, F., Nores, W. L., & Mauk, M. D. (2010). Cerebellar Cortex Contributions to the Expression and Timing of Conditioned Eyelid Responses. *Journal of Neurophysiology*, 103(4), 2039–2049.  
<https://doi.org/10.1152/jn.00033.2010>
- Kalmbach, B. E., Ohyama, T., & Mauk, M. D. (2010). Temporal Patterns of Inputs to Cerebellum Necessary and Sufficient for Trace Eyelid Conditioning. *Journal of Neurophysiology*, 104(2), 627–640. <https://doi.org/10.1152/jn.00169.2010>
- Khan, A. G., Parthasarathy, K., & Bhalla, U. S. (2010). Odor representations in the mammalian olfactory bulb. *Wiley*

- Interdisciplinary Reviews. Systems Biology and Medicine*, 2(5), 603–611. <https://doi.org/10.1002/wsbm.85>
- Kim, S., & Lee, I. (2012). The hippocampus is required for visually cued contextual response selection, but not for visual discrimination of contexts. *Frontiers in Behavioral Neuroscience*, 6. <https://doi.org/10.3389/fnbeh.2012.00066>
- Kraus, B. J., Brandon, M. P., Robinson, R. J., Connerney, M. A., Hasselmo, M. E., & Eichenbaum, H. (2015). During Running in Place, Grid Cells Integrate Elapsed Time and Distance Run. *Neuron*, 88(3), 578–589. <https://doi.org/10.1016/j.neuron.2015.09.031>
- Kraus, B., Robinson, R., White, J., Eichenbaum, H., & Hasselmo, M. (2013). Hippocampal “Time Cells”: Time versus Path Integration. *Neuron*, 78(6), 1090–1101. <https://doi.org/10.1016/j.neuron.2013.04.015>
- Kropff, E., Carmichael, J. E., Moser, M.-B., & Moser, E. I. (2015). Speed cells in the medial entorhinal cortex. *Nature*, 523(7561), 419–424. <https://doi.org/10.1038/nature14622>
- Krupa, D., & Thompson, R. (2003). Inhibiting the Expression of a Classically Conditioned Behavior Prevents Its Extinction. *The Journal of Neuroscience : The Official Journal of the Society for Neuroscience*, 23, 10577–10584. <https://doi.org/10.1523/JNEUROSCI.23-33-10577.2003>
- Lever, C., Burton, S., Jeewajee, A., O'Keefe, J., & Burgess, N. (2009). Boundary Vector Cells in the Subiculum of the Hippocampal Formation. *The Journal of Neuroscience*, 29(31), 9771 LP – 9777. <https://doi.org/10.1523/JNEUROSCI.1319-09.2009>
- Luo, L., Callaway, E. M., & Svoboda, K. (2018). Genetic Dissection of Neural Circuits: A Decade of Progress. *Neuron*, 98(2), 256–281. <https://doi.org/https://doi.org/10.1016/j.neuron.2018.03.040>
- MacDonald, C. J., Carrow, S., Place, R., & Eichenbaum, H. (2013). Distinct hippocampal time cell sequences represent odor memories in immobilized rats. *The Journal of Neuroscience : The Official Journal of the Society for Neuroscience*, 33(36), 14607–14616. <https://doi.org/10.1523/JNEUROSCI.1537-13.2013>
- MacDonald, C. J., Lepage, K. Q., Eden, U. T., & Eichenbaum, H. (2011). Hippocampal “time cells” bridge the gap in memory for discontiguous events. *Neuron*, 71(4), 737–749. <https://doi.org/10.1016/j.neuron.2011.07.012>
- Maruyama, R., Maeda, K., Moroda, H., Kato, I., Inoue, M., Miyakawa, H., & Aonishi, T. (2014). Detecting cells using non-negative matrix factorization on calcium imaging data. *Neural Networks : The*

- Official Journal of the International Neural Network Society*, 55, 11–19. <https://doi.org/10.1016/j.neunet.2014.03.007>
- Mau, W., Sullivan, D. W., Kinsky, N. R., Hasselmo, M. E., Howard, M. W., & Eichenbaum, H. (2018). The Same Hippocampal CA1 Population Simultaneously Codes Temporal Information over Multiple Timescales. *Current Biology*, 28(10), 1499–1508.e4. <https://doi.org/10.1016/j.cub.2018.03.051>
- McLelland, D., & Paulsen, O. (2007). Cortical Songs Revisited: A Lesson in Statistics. *Neuron*, 53(3), 319–321. <https://doi.org/https://doi.org/10.1016/j.neuron.2007.01.020>
- McNaughton, N., & Gray, J. A. (2000). Anxiolytic action on the behavioural inhibition system implies multiple types of arousal contribute to anxiety. *Journal of Affective Disorders*, 61(3), 161–176. [https://doi.org/10.1016/s0165-0327\(00\)00344-x](https://doi.org/10.1016/s0165-0327(00)00344-x)
- Medina, J. F., Garcia, K. S., Nores, W. L., Taylor, N. M., & Mauk, M. D. (2000). Timing mechanisms in the cerebellum: testing predictions of a large-scale computer simulation. *The Journal of Neuroscience : The Official Journal of the Society for Neuroscience*, 20(14), 5516–5525. <https://doi.org/10.1523/JNEUROSCI.20-14-05516.2000>
- Meeks, J. P., Arnson, H. A., & Holy, T. E. (2010). Representation and transformation of sensory information in the mouse accessory olfactory system. *Nature Neuroscience*, 13(6), 723–730. <https://doi.org/10.1038/nn.2546>
- Miller, A. M. P., Jacob, A. D., Ramsaran, A. I., De Snoo, M. L., Josselyn, S. A., & Frankland, P. W. (2023). Emergence of a predictive model in the hippocampus. *Neuron*. <https://doi.org/10.1016/j.neuron.2023.03.011>
- Modi, M. N., Dhawale, A. K., & Bhalla, U. S. (2014). CA1 cell activity sequences emerge after reorganization of network correlation structure during associative learning. *eLife*, 3, e01982–e01982. <https://doi.org/10.7554/eLife.01982>
- Mokeichev, A., Okun, M., Barak, O., Katz, Y., Ben-Shahar, O., & Lampl, I. (2007). Stochastic Emergence of Repeating Cortical Motifs in Spontaneous Membrane Potential Fluctuations In Vivo. *Neuron*, 53, 413–425. <https://doi.org/10.1016/j.neuron.2007.01.017>
- Mollinedo-Gajate, I., Song, C., & Knöpfel, T. (2021). Genetically Encoded Voltage Indicators. *Advances in Experimental Medicine and Biology*, 1293, 209–224. [https://doi.org/10.1007/978-981-15-8763-4\\_12](https://doi.org/10.1007/978-981-15-8763-4_12)
- Morris, R. G. M., Garrud, P., Rawlins, J. N. P., & O'Keefe, J. (1982). Place navigation impaired in rats with hippocampal lesions.

- Nature*, 297(5868), 681–683. <https://doi.org/10.1038/297681a0>
- Moscovitch, M., Cabeza, R., Winocur, G., & Nadel, L. (2016). Episodic Memory and Beyond: The Hippocampus and Neocortex in Transformation. *Annual Review of Psychology*, 67(1), 105–134. <https://doi.org/10.1146/annurev-psych-113011-143733>
- Moyer, J. R. J., Thompson, L. T., & Disterhoft, J. F. (1996). Trace eyeblink conditioning increases CA1 excitability in a transient and learning-specific manner. *The Journal of Neuroscience : The Official Journal of the Society for Neuroscience*, 16(17), 5536–5546. <https://doi.org/10.1523/JNEUROSCI.16-17-05536.1996>
- Mukamel, E. A., Nimmerjahn, A., & Schnitzer, M. J. (2009). Automated analysis of cellular signals from large-scale calcium imaging data. *Neuron*, 63(6), 747–760. <https://doi.org/10.1016/j.neuron.2009.08.009>
- Muller, R. U., & Kubie, J. L. (1989). The firing of hippocampal place cells predicts the future position of freely moving rats. *The Journal of Neuroscience : The Official Journal of the Society for Neuroscience*, 9(12), 4101–4110. <https://doi.org/10.1523/JNEUROSCI.09-12-04101.1989>
- Murray, T. A., & Levene, M. J. (2012). Singlet gradient index lens for deep in vivo multiphoton microscopy. *Journal of Biomedical Optics*, 17(2), 021106. <https://doi.org/10.1117/1.JBO.17.2.021106>
- Nestler, E. J., Hyman, S. E., Holtzman, D. M., & Malenka, R. C. (2015). Higher Cognitive Function and Behavioral Control. In *Molecular Neuropharmacology: A Foundation for Clinical Neuroscience*, 3e. McGraw-Hill Education. <neurology.mhmedical.com/content.aspx?aid=1105916482>
- Ohyama, T., Nores, W. L., Murphy, M., & Mauk, M. D. (2003). What the cerebellum computes. *Trends in Neurosciences*, 26(4), 222–227. [https://doi.org/10.1016/S0166-2236\(03\)00054-7](https://doi.org/10.1016/S0166-2236(03)00054-7)
- O'Keefe, J., & Burgess, N. (1996). Geometric determinants of the place fields of hippocampal neurons. *Nature*, 381(6581), 425–428. <https://doi.org/10.1038/381425a0>
- O'Keefe, J., & Dostrovsky, J. (1971). The hippocampus as a spatial map. Preliminary evidence from unit activity in the freely-moving rat. *Brain Research*, 34(1), 171–175. [https://doi.org/10.1016/0006-8993\(71\)90358-1](https://doi.org/10.1016/0006-8993(71)90358-1)
- O'Keefe, J., & Nadel, L. (1978). The Hippocampus as a Cognitive Map. In *Philosophical Studies* (Vol. 27). <https://doi.org/10.5840/philstudies19802725>
- O'Keefe, J., & Recce, M. L. (1993). Phase relationship between hippocampal place units and the EEG theta rhythm. *Hippocampus*, 3(3), 317–330.

- <https://doi.org/10.1002/hipo.450030307>
- Ozden, I., Lee, H. M., Sullivan, M. R., & Wang, S. S.-H. (2008). Identification and Clustering of Event Patterns From In Vivo Multiphoton Optical Recordings of Neuronal Ensembles. *Journal of Neurophysiology*, 100(1), 495–503.  
<https://doi.org/10.1152/jn.01310.2007>
- Pachitariu, M., Stringer, C., Dipoppa, M., Schröder, S., Rossi, L. F., Dalgleish, H., Carandini, M., & Harris, K. D. (2017). Suite2p: beyond 10,000 neurons with standard two-photon microscopy. *BioRxiv*, 61507. <https://doi.org/10.1101/061507>
- Paredes, R. M., Etzler, J. C., Watts, L. T., Zheng, W., & Lechleiter, J. D. (2008). Chemical calcium indicators. *Methods (San Diego, Calif.)*, 46(3), 143–151.  
<https://doi.org/10.1016/j.ymeth.2008.09.025>
- Pastalkova, E., Itskov, V., Amarasingham, A., & Buzsaki, G. (2008). Internally Generated Cell Assembly Sequences in the Rat Hippocampus. *Science*, 321(5894), 1322–1327.  
<https://doi.org/10.1126/science.1159775>
- Pavlov, I. P. (1927). Conditioned reflexes: an investigation of the physiological activity of the cerebral cortex. In *Conditioned reflexes: an investigation of the physiological activity of the cerebral cortex*. Oxford Univ. Press.
- Petersen, C. C. H. (2019). Sensorimotor processing in the rodent barrel cortex. *Nature Reviews. Neuroscience*, 20(9), 533–546.  
<https://doi.org/10.1038/s41583-019-0200-y>
- Pfeiffer, B. E., & Foster, D. J. (2013). Hippocampal place-cell sequences depict future paths to remembered goals. *Nature*, 497(7447), 74–79. <https://doi.org/10.1038/nature12112>
- Pnevmatikakis, E. A., Soudry, D., Gao, Y., Machado, T. A., Merel, J., Pfau, D., Reardon, T., Mu, Y., Lacefield, C., Yang, W., Ahrens, M., Bruno, R., Jessell, T. M., Peterka, D. S., Yuste, R., & Paninski, L. (2016). Simultaneous Denoising, Deconvolution, and Demixing of Calcium Imaging Data. *Neuron*, 89(2), 285–299.  
<https://doi.org/https://doi.org/10.1016/j.neuron.2015.11.037>
- Poort, J., Khan, A. G., Pachitariu, M., Nemri, A., Orsolic, I., Krupic, J., Bauza, M., Sahani, M., Keller, G. B., Mrsic-Flogel, T. D., & Hofer, S. B. (2015). Learning Enhances Sensory and Multiple Non-sensory Representations in Primary Visual Cortex. *Neuron*, 86(6), 1478–1490. <https://doi.org/10.1016/j.neuron.2015.05.037>
- Poppenk, J., Evensmoen, H. R., Moscovitch, M., & Nadel, L. (2013). Long-axis specialization of the human hippocampus. *Trends in Cognitive Sciences*, 17(5), 230–240.  
<https://doi.org/10.1016/j.tics.2013.03.005>

- Pudil, P., & Novovičová, J. (1998). Novel Methods for Feature Subset Selection with Respect to Problem Knowledge. In H. Liu & H. Motoda (Eds.), *Feature Extraction, Construction and Selection: A Data Mining Perspective* (pp. 101–116). Springer US.  
[https://doi.org/10.1007/978-1-4615-5725-8\\_7](https://doi.org/10.1007/978-1-4615-5725-8_7)
- Ranck, J. B. (1973). Studies on single neurons in dorsal hippocampal formation and septum in unrestrained rats: Part I. Behavioral correlates and firing repertoires. *Experimental Neurology*, 41(2), 462–531. [https://doi.org/https://doi.org/10.1016/0014-4886\(73\)90290-2](https://doi.org/10.1016/0014-4886(73)90290-2)
- Rescorla, R. A., & Wagner, A. (1972). A theory of Pavlovian conditioning: Variations in the effectiveness of reinforcement and nonreinforcement. In *Classical Conditioning II: Current Research and Theory: Vol. Vol. 2*.
- Reyes, A. D. (2003). Synchrony-dependent propagation of firing rate in iteratively constructed networks in vitro. *Nature Neuroscience*, 6(6), 593–599. <https://doi.org/10.1038/nn1056>
- Robbins, M., Christensen, C. N., Kaminski, C. F., & Zlatic, M. (2021). Calcium imaging analysis - how far have we come? *F1000Research*, 10, 258.
- Rogerson, T., Cai, D. J., Frank, A., Sano, Y., Shobe, J., Lopez-Aranda, M. F., & Silva, A. J. (2014). Synaptic tagging during memory allocation. *Nature Reviews Neuroscience*, 15(3), 157–169. <https://doi.org/10.1038/nrn3667>
- Savelli, F., Yoganarasimha, D., & Knierim, J. J. (2008). Influence of boundary removal on the spatial representations of the medial entorhinal cortex. *Hippocampus*, 18(12), 1270–1282. <https://doi.org/10.1002/hipo.20511>
- Scoville, W. B., & Milner, B. (1957). Loss of recent memory after bilateral hippocampal lesions. In *Journal of Neurology, Neurosurgery & Psychiatry* (Vol. 20, pp. 11–21). BMJ Publishing Group. <https://doi.org/10.1136/jnnp.20.1.11>
- Shadlen, M. N., & Shohamy, D. (2016). Decision making and sequential sampling from memory. *Neuron*, 90(5), 927–939.
- Shannon, C. E. (1948). A Mathematical Theory of Communication. *Bell System Technical Journal*, 27(3), 379–423. <https://doi.org/https://doi.org/10.1002/j.1538-7305.1948.tb01338.x>
- Siegel, J. J., & Mauk, M. D. (2013). Persistent Activity in Prefrontal Cortex during Trace Eyelid Conditioning: Dissociating Responses That Reflect Cerebellar Output from Those That Do Not. *The Journal of Neuroscience*, 33(38), 15272 LP – 15284. <https://doi.org/10.1523/JNEUROSCI.1238-13.2013>
- Siegel, J. J., Taylor, W., Gray, R., Kalmbach, B., Zemelman, B. V.,

- Desai, N. S., Johnston, D., & Chitwood, R. A. (2015). Trace Eyeblink Conditioning in Mice Is Dependent upon the Dorsal Medial Prefrontal Cortex, Cerebellum, and Amygdala: Behavioral Characterization and Functional Circuitry. *ENeuro*, 2(4), ENEURO.0051-14.2015. <https://doi.org/10.1523/ENEURO.0051-14.2015>
- Silva, A. J., Zhou, Y., Rogerson, T., Shobe, J., & Balaji, J. (2009). Molecular and cellular approaches to memory allocation in neural circuits. *Science (New York, N.Y.)*, 326(5951), 391–395. <https://doi.org/10.1126/science.1174519>
- Skaggs, W., McNaughton, B., Gothard, K., & Markus, E. (1996). An Information-Theoretic Approach to Deciphering the Hippocampal Code. *Neural Inf. Process Syst.*, 5.
- Solstad, T., Boccara, C. N., Kropff, E., Moser, M.-B., & Moser, E. I. (2008). Representation of Geometric Borders in the Entorhinal Cortex. *Science*, 322(5909), 1865–1868. <https://doi.org/10.1126/science.1166466>
- Souza, B. C., Pavão, R., Belchior, H., & Tort, A. B. L. (2018). On Information Metrics for Spatial Coding. *Neuroscience*, 375, 62–73. <https://doi.org/10.1016/j.neuroscience.2018.01.066>
- Stosiek, C., Garaschuk, O., Holthoff, K., & Konnerth, A. (2003). In vivo two-photon calcium imaging of neuronal networks. *Proceedings of the National Academy of Sciences of the United States of America*, 100(12), 7319–7324. <https://doi.org/10.1073/pnas.1232232100>
- Takehara, K., Kawahara, S., Takatsuki, K., & Kirino, Y. (2002). Time-limited role of the hippocampus in the memory for trace eyeblink conditioning in mice. *Brain Research*, 951(2), 183–190. [https://doi.org/10.1016/s0006-8993\(02\)03159-1](https://doi.org/10.1016/s0006-8993(02)03159-1)
- Tao, S., Wang, Y., Peng, J., Zhao, Y., He, X., Yu, X., Liu, Q., Jin, S., & Xu, F. (2021). Whole-Brain Mapping the Direct Inputs of Dorsal and Ventral CA1 Projection Neurons. *Frontiers in Neural Circuits*, 15. <https://doi.org/10.3389/fncir.2021.643230>
- Taube, J. S., Muller, R. U., & Ranck, J. B. J. (1990). Head-direction cells recorded from the postsubiculum in freely moving rats. I. Description and quantitative analysis. *The Journal of Neuroscience : The Official Journal of the Society for Neuroscience*, 10(2), 420–435. <https://doi.org/10.1523/JNEUROSCI.10-02-00420.1990>
- Thompson, R. F. (2004). In Search of Memory Traces. *Annual Review of Psychology*, 56(1), 1–23. <https://doi.org/10.1146/annurev.psych.56.091103.070239>
- Tishby, N., Pereira, F. C., & Bialek, W. (1999). The information

- bottleneck method. *Proc. of the 37-Th Annual Allerton Conference on Communication, Control and Computing*, 368–377.  
<https://arxiv.org/abs/physics/0004057>
- Vaidya, A. R., Pujara, M. S., Petrides, M., Murray, E. A., & Fellows, L. K. (2019). Lesion Studies in Contemporary Neuroscience. *Trends in Cognitive Sciences*, 23(8), 653–671.  
<https://doi.org/https://doi.org/10.1016/j.tics.2019.05.009>
- Valero, M., Cid, E., Averkin, R. G., Aguilar, J., Sanchez-Aguilera, A., Viney, T. J., Gomez-Dominguez, D., Bellistri, E., & de la Prida, L. M. (2015). Determinants of different deep and superficial CA1 pyramidal cell dynamics during sharp-wave ripples. *Nature Neuroscience*. <https://doi.org/10.1038/nn.4074>
- van der Maaten, L., Postma, E., & van den Herik, H. (2009). Dimensionality reduction: a comparative review. *Journal of Machine Learning Research*, 66–71.
- Velasco, M. G. M., & Levene, M. J. (2014). In vivo two-photon microscopy of the hippocampus using glass plugs. *Biomedical Optics Express*, 5(6), 1700–1708.  
<https://doi.org/10.1364/BOE.5.001700>
- Voelcker, B., Pancholi, R., & Peron, S. (2022). Transformation of primary sensory cortical representations from layer 4 to layer 2. *Nature Communications*, 13(1), 5484.  
<https://doi.org/10.1038/s41467-022-33249-1>
- Wood, E. R., Dudchenko, P. A., Robitsek, R. J., & Eichenbaum, H. (2000). Hippocampal Neurons Encode Information about Different Types of Memory Episodes Occurring in the Same Location. *Neuron*, 27(3), 623–633.  
[https://doi.org/https://doi.org/10.1016/S0896-6273\(00\)00071-4](https://doi.org/https://doi.org/10.1016/S0896-6273(00)00071-4)
- Yiu, A. P., Mercaldo, V., Yan, C., Richards, B., Rashid, A. J., Hsiang, H.-L. L., Pressey, J., Mahadevan, V., Tran, M. M., Kushner, S. A., Woodin, M. A., Frankland, P. W., & Josselyn, S. A. (2014). Neurons are recruited to a memory trace based on relative neuronal excitability immediately before training. *Neuron*, 83(3), 722–735. <https://doi.org/10.1016/j.neuron.2014.07.017>
- Zhou, Y., Won, J., Karlsson, M. G., Zhou, M., Rogerson, T., Balaji, J., Neve, R., Poirazi, P., & Silva, A. J. (2009). CREB regulates excitability and the allocation of memory to subsets of neurons in the amygdala. *Nature Neuroscience*, 12(11), 1438–1443.  
<https://doi.org/10.1038/nn.2405>
- Ziv, Y., Burns, L. D., Cocker, E. D., Hamel, E. O., Ghosh, K. K., Kitch, L. J., El Gamal, A., & Schnitzer, M. J. (2013). Long-term dynamics of CA1 hippocampal place codes. *Nature Neuroscience*, 16(3), 264–266. <https://doi.org/10.1038/nn.3329>

# **Chapter 2 – Behaviour**

## **Towards understanding brain activity in a reproducible context**

Our understanding of memory and learning depends upon the type of learning that is studied (Schreurs, 1989). Two important categories of memory and learning experiments are,

1. Non-associative (Habituation and Sensitization), and
2. Associative learning (Classical and Operant Conditioning).

Non-associative learning paradigms provide information about how an organism responds to repeated presentations of a single stimulus (Brown, 1998). However, it was of interest to us to study how animals responded to a number of events and stimuli being associated, and how the activity of the brain relates to this. Multi-modal stimulus integration is typical of the sensory experience. We felt it interesting to study how animals learnt to associate each stimulus modality, individually, given no clear *a priori* reason to assume that the physiological response would be identical for each. Hence, we chose to design our experiments to incorporate associative learning, which is a relatively permanent change in behaviour that results from the temporal conjunction of two or more events or stimuli.

Empirically, reproducible behaviour depends on strong associations between the events or stimuli being paired, and may often require

many repeated pairings or trials. Additionally, having the animal engage in the behavioural task and pay attention to the stimuli being presented, is crucial to look for important correlations between the experiment conditions (external) and brain activity (internal).

Anaesthetized animals have been previously used to study brain activity and led to important discoveries, e.g. - visual representation of moving bars in the visual cortex (Hubel & Wiesel, 1962), habituation in the Hippocampus (Deshmukh & Bhalla, 2003). However, it was clear that similar experiments repeated in awake animals did not result in the same observations. Indeed, animals needed to navigate a known environment before the discovery of place cells (O'Keefe & Dostrovsky, 1971), grid cells (Fyhn et al., 2004; Hafting et al., 2005), and head-direction cells (Ranck, 1973; Taube et al., 1990), among others, could be made. We chose to avoid anaesthetized animals for the experiments described in this thesis. It is unclear if deep states of anaesthesia are also conducive to time cell sequence activation. Additionally, even if some form of sequential activity may be in effect during anaesthetic states, it would be very difficult to implicate physiological relevance without appropriate experimental modulations in a behavioural context.

The reliability of the overt behavioural responses of the experiment animals then sets the conditions and parameter list to study physiology within the confines of reproducible behavioural contexts, and was considered an important mandate for the standardization of any of the behavioural tasks described in this chapter. Under the umbrella of associative learning, we began our experiments with various protocols related to operant conditioning wherein the reinforcing signal for

learning was a water reward to correctly timed licks. As will be discussed in the next few sections, we later switched to aversive conditioning with Trace Eye-Blink Conditioning.

## **Operant conditioning [Project I]**

Operant conditioning is both the procedure and a type of associative learning process through which the strength of a voluntarily performed behaviour is modified positively (appetitively) by reward (water, sucrose, food, etc.), or negatively (aversively) by punishment (air-puff to the eye, electrical shocks, etc.). For example, if the animal responds to a presented stimulus by performing a lick onto a water spout, then a water reward would strengthen the behaviour while Lithium Chloride solution (which is aversive) would weaken it.

We now describe our experiments and results with regard to operant conditioning, in more detail.

### **Required features**

For Project I, the goal was to study how the association of a neutral stimulus with a water reward modified the neurophysiological activity of the hippocampal CA1. We aimed to more systematically study time cells with the granularity of well-defined associative learning and ms resolution, high-yield (~100-150) CA1 recordings using 2-photon imaging. We believe this is why there is still insufficient clarity on the network level responses in the CA1, *in vivo*, especially during early

learning of associated stimuli, *i.e.*, behavioural acquisition. We outline our set of core objectives required as features for the behavioural task:

1. An assortment of different stimuli and modalities (light, tone, etc.) to be presented to the animal.
2. The animal must withhold any motor movement during the presentation of the stimuli, to study pure stimulus responses.
3. The animal must perform a lick for a water reward after the end of the stimulus presentation.
4. The animal must be able to make the association between stimuli and water reward within 7-14 days of training (given technical limitations of chronic recording from tissue).

The behavioural state of the animal, in terms of anxiety, motivation, attention, etc., may be variable when a naïve animal is presented with different stimuli. This may cause a large variability in the activity of cells, since the animal may not be paying attention to it. Also, if the animal were rewarded for performing the task it is expected that there would be motivation to pay attention to the stimuli presented. Finally, such a task would involve the animal associating the stimuli that it is trained to with a behavioural task and this would provide an apt context to study association related changes in stimulus responses.

In the following sections, we discuss some important protocols that we tried and tested and a list of the various kinds of behavioural tasks we employed for head-fixed mice.

For Project I, we tried several variations of operant conditioning including Stimulus Detection tasks, Delayed Non-Match to Sample (DNMS), as well as Go/No-Go tasks. Each of these tasks requires

animals to perform licks to the Conditioned Stimuli and for them to be rewarded (2-3  $\mu$ L water) or punished based on the task demands and protocol design.

### Water delivery and calibration

The lick port was made from a trimmed and smoothed 16 gauge syringe, connected to a water reservoir with small diameter tubing. A solenoid valve clamped onto this tubing, gated by a 12V DC signal. When this gate was opened, the volume of water could be regulated by the duration of the 12V DC signal. We calibrated the duration of gate opening to achieve ~2  $\mu$ L per pulse or spurt (Jaramillo & Zador, 2014). The weight of 100 spurts was measured and then divided by 100 to get the weight of 1 spurt. 65 ms was found corresponding to 2.5  $\mu$ L (this value is going to be used for behaviour). In the figure below (Figure 2), the measured volumes/weights are plotted as blue filled diamonds, error bars are presented as Standard Error and the linear trendline is shown in black.

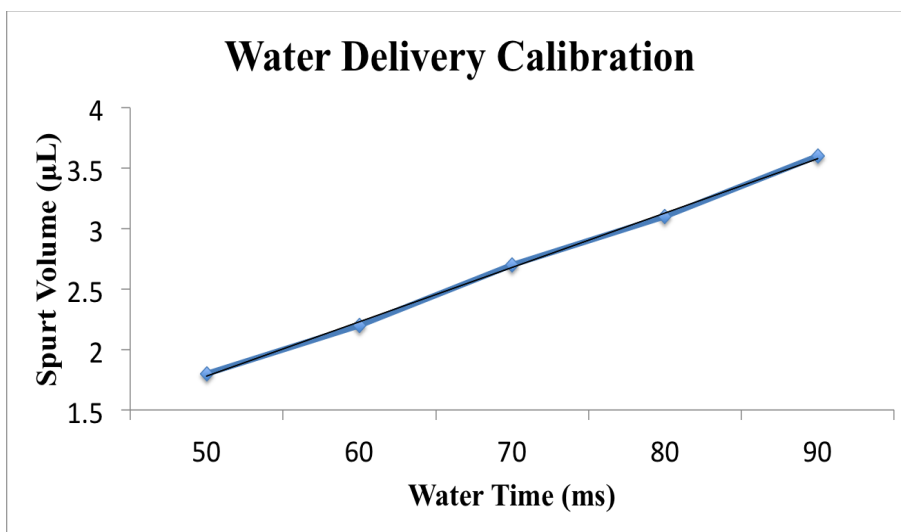


**Figure 2:** Water delivery calibration to reward the animal consistently with the same volume of water.

## **Opto-islator circuit for solenoid control**

To be able to programmatically control the 12V DC line to the solenoid valve, we used the following circuit (Figure 3), which accepted a 5V digital input from the DAQ (NI USB-6001) interfacing the lab computer to the behaviour rig.

### **Parts list**

1. 470 ohm resistor
2. 15 kohm resistor
3. MCT2e
4. ULN2003
5. Bases (adaptors for MCT2e and ULN2003)
6. +5V and +12V DC inputs from a Power Supply)
7. Source of +5V DC input (DAQ, etc.)
8. Connecting wires
9. Load Resistance (Solenoid, etc.)

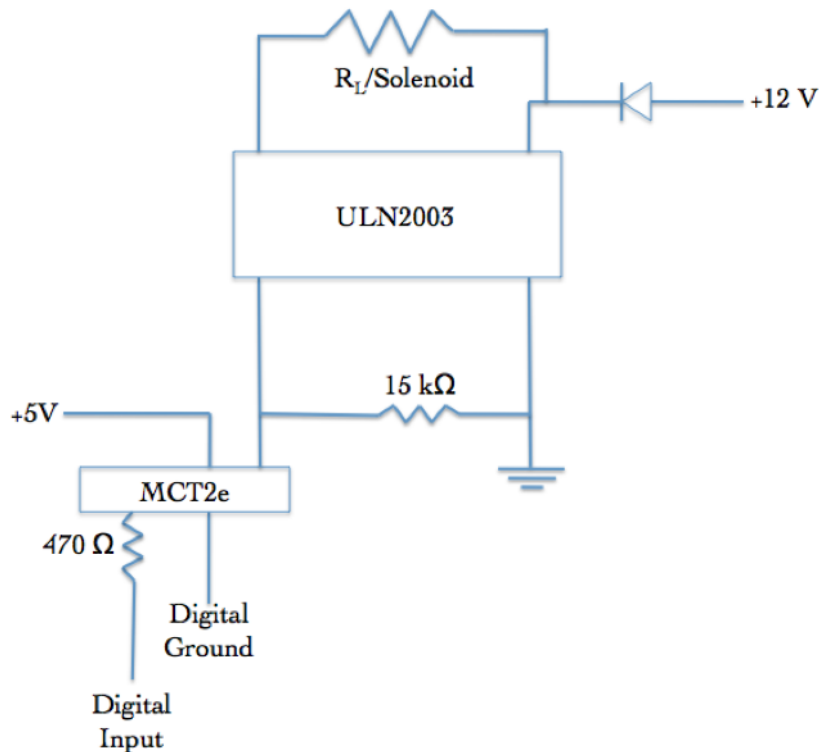


**Figure 3:** Optoisolator circuit to amplify +5V DC input to +12V DC output.

### Lick detection circuit

To be able to monitor the presence or absence of licks to the port, the conductive part (metal) of the lick port syringe was connected to a MOSFET such that a 5V DC voltage could be read out, whenever the animal would make contact with the port. This was designed as a readout to Stimulus Detection by the animal. The circuit diagram is shown below (Figure 4):

### Parts list

1. +5V Power Supply

2. 4.7 kohm resistor
3. 22 Mohm resistor
4. IN4007 Diode
5. NPN Transistor IRF540N (MOSFET)

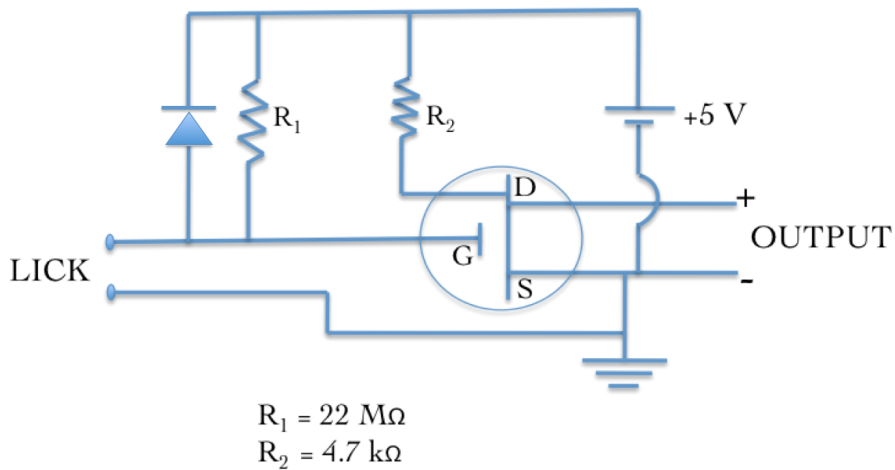


**Figure 4:** Lick detector circuit based on a MOSFET design. Whenever the animal performed a lick, a +5V DC Output would be read out.

## Controlling task details and protocol information

All protocols were controlled using custom scripts written in NI LabVIEW 8. These scripts were run on a lab desktop which interfaced with the DAQ (NI USB-6001) via USB. The DAQ,

1. Sent the 5V digital input to switch on the solenoid valve regulating water delivery, and
2. Received the 5V digital output of the lick detection circuit whenever a lick was produced by the animal.

## **Head-bar implant, Animal Handling, and Water deprivation**

All experiments were planned to be conducted on head-fixed C57Bl/6 mice, with the eventual intention to perform in vivo imaging on these animals. For this, we surgically implanted metal head-bars on the skull of the animals while they were maintained on 1-2% Isoflurane, above a heating pad (35°C). Surgeries would last no longer than 30 mins per animal.

After 1-7 days of recovery after surgery, we handled the animals gently for 2 days till the animals would appear comfortable with lifting and gentle collar grabbing. Next, for 3-4 days, we kept the animals head-clamped. We restricted our animals to ~1ml of water per day, keeping check that their body weight did not fall to below 80% of the weight on day 1.

## **PROTOCOL 1.1: Stimulus Detection Task**

We first tried the simplest version of the lick task wherein an auditory tone was followed by a water reward. The animal would have to withhold licking till the end of the stimulus presentation, and then perform the lick for the reward (Figure 5).

**Total number of trials:** 600/session; 1 session/day

**Trial phases:**

1. Stimulus free pre-tone (PT): 1 s

2. Tone: 5 kHz for 1 s
3. Critical timeout (CT): 100 ms
4. Inter-trial Interval (ITI): randomized between 2 s to 5



**Figure 5:** Typical trial structure with the various phases. Each trial was followed by a randomized Inter-Trial Interval (ITI).

Only licks during the critical timeout (CT) phase immediately after the Tone phase were rewarded while licks in other phases resulted in a phase restart. No aversive stimuli were presented in this particular protocol.

### **PROTOCOL 1.2: Stimulus Detection Task with aversive punishment**

**Total number of trials:** 600/session; 1 session/day

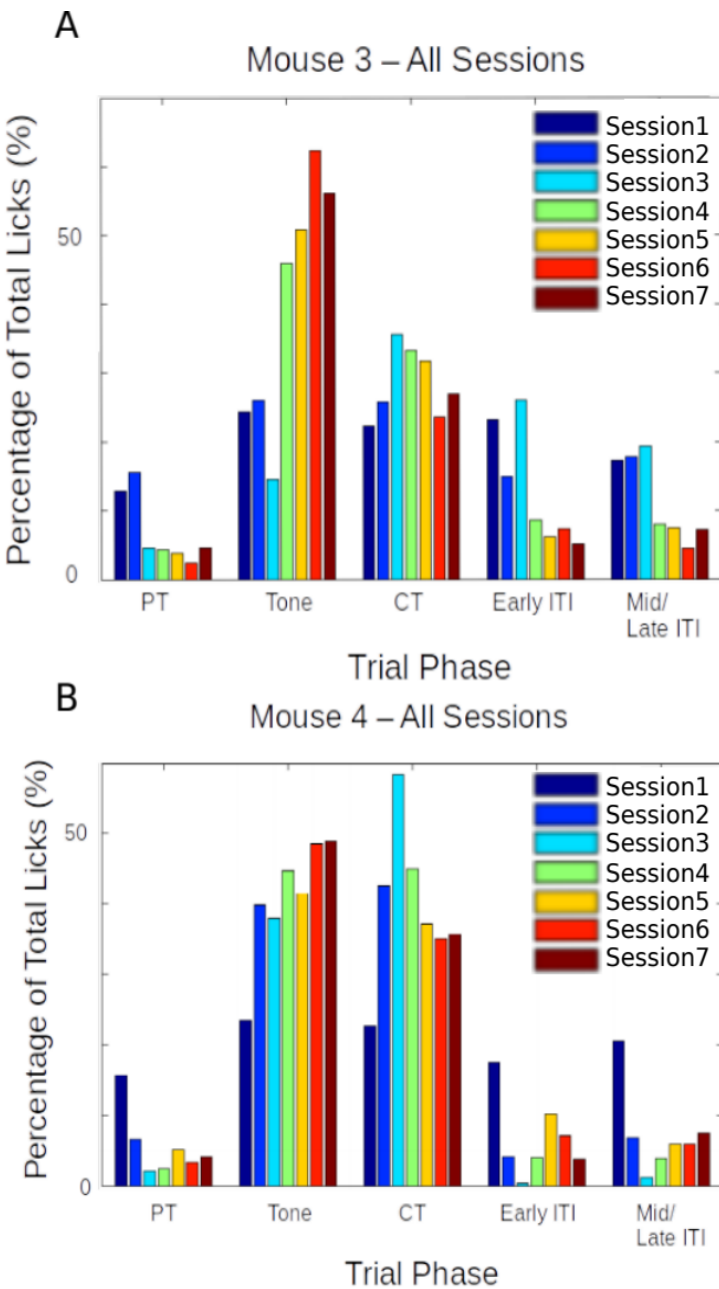


**Figure 6:** Performance evaluation for two example mice trained to Protocol 1.1 and 1.2. Percentage of total licks in the various trial phases (Pre-Tone, Tone, CT, and ITI), across all sessions of training (coloured bar plots) for A) Mouse 3, and B) Mouse 4.

Only licks during the critical timeout (CT) phase immediately after the Tone phase were rewarded while licks in other phases resulted in an aversive punishment, *viz.*, 100 ms air-puff to the body of the animal, before a phase restart. For Mouse 3 we started Protocol 1.2 from Session 3 while for Mouse 4 we started Protocol 1.2 from Session 2.

## **Results – Protocols 1.1 and 1.2**

The behavioural performance for each of the experiment animals was evaluated using custom analysis scripts written in MATLAB 2011. Here are the results from two mice trained based on Protocols 1.1 and 1.2 (Figure 6). In both the examples shown, animals would typically produce a great percentage of total licks even during the Tone period. Each animal was presented with 600 training trials/day (1 session/day). Protocols 1.1 and 1.2 were prototyping experiments by design. Given the nature of our results, we decided to abort these protocols in favour of more structured, less aversive protocols, as described in the next few sections. The inability of our mice to behaviourally discriminate or withhold incorrect or unrewarded licks even for 7-14 sessions was considered, and the task was ultimately deemed unsuccessful.

**Total animals trained:** 2

**Conclusion:** Aborted

## **Protocol 2: Stimulus Detection task with timeout box**

We also tried the same Stimulus Detection protocol, without an air-puff punishment, but with incorrect licks punished by a trial abort and a

stimulus-free timeout phase, which the animal could escape from if it withheld licking. We decided to train the animals in blocks, each with a specific goal that the animal had to achieve.

**Trial phases:**

- 1 Stimulus-free pre-tone (PT): 1 s
- 2 Tone: 5 kHz for a variable duration (based on Block)
- 3 Critical timeout (CT): 1000 ms
- 4 Inter-trial Interval (ITI): randomized between 2 s to 5 s

Only licks during the critical timeout (CT) phase immediately after the Tone phase were rewarded while licks in other phases resulted in a phase restart.

**Block 1:** Unconditional Water to get the animal to associate the tone

- ~20 trials
- 100 or 200 ms Tone duration
- Unconditional water provided at the end of the tone, irrespective of lick

**Block 2:** Conditional Water to get the animal to learn that licking with/after tone is going to be rewarded

- 100 or 200 ms Tone duration
- 1000 ms Reward phase
- Lick during/after tone (Reward phase) = reward
- No lick = no reward
- Lick during pre-tone = no reward/abortion of trial
- Lick during ITI = no reward/abortion of trial

- Animals graduate to the next Block of training only after achieving at least 70-80% success rates

**Block 3:** Training the animal to learn "when" to lick

- 1000 ms pre-tone, 100 or 200 ms Tone, 1000 ms Reward phase, 3-5 s randomized ITI
- Lick during Reward phase = reward
- Any lick during the pre-tone or the tone, aborts the trial and sends the program to a Timeout phase (lasting, 2-3 s)
- The timeout phase ends only when there is a 2-3 s (specified) interval of no licking
- If the timeout phase ends, a new trial begins
- Licks during ITI are also "punished" accordingly
- Animals graduate to the next Block of training only after achieving 70-80% success rates

**Block 4:** Same as Block 3, but with a gradually increasing tone duration in steps of 50/100 ms

- The tone duration is gradually increased, the increase being tailored to the performance of the animal
- It will be attempted to get the animals to learn to wait for 500-700 ms
- Animals graduate to the next Block of the experiment only after achieving 70-80% success rates

## Results – Protocol 2

The behavioural performance for each of the experiment animals was evaluated using custom analysis scripts written in MATLAB. Here are two representative examples of mice trained based on Protocol 2 – Block 3 (Figure 7).

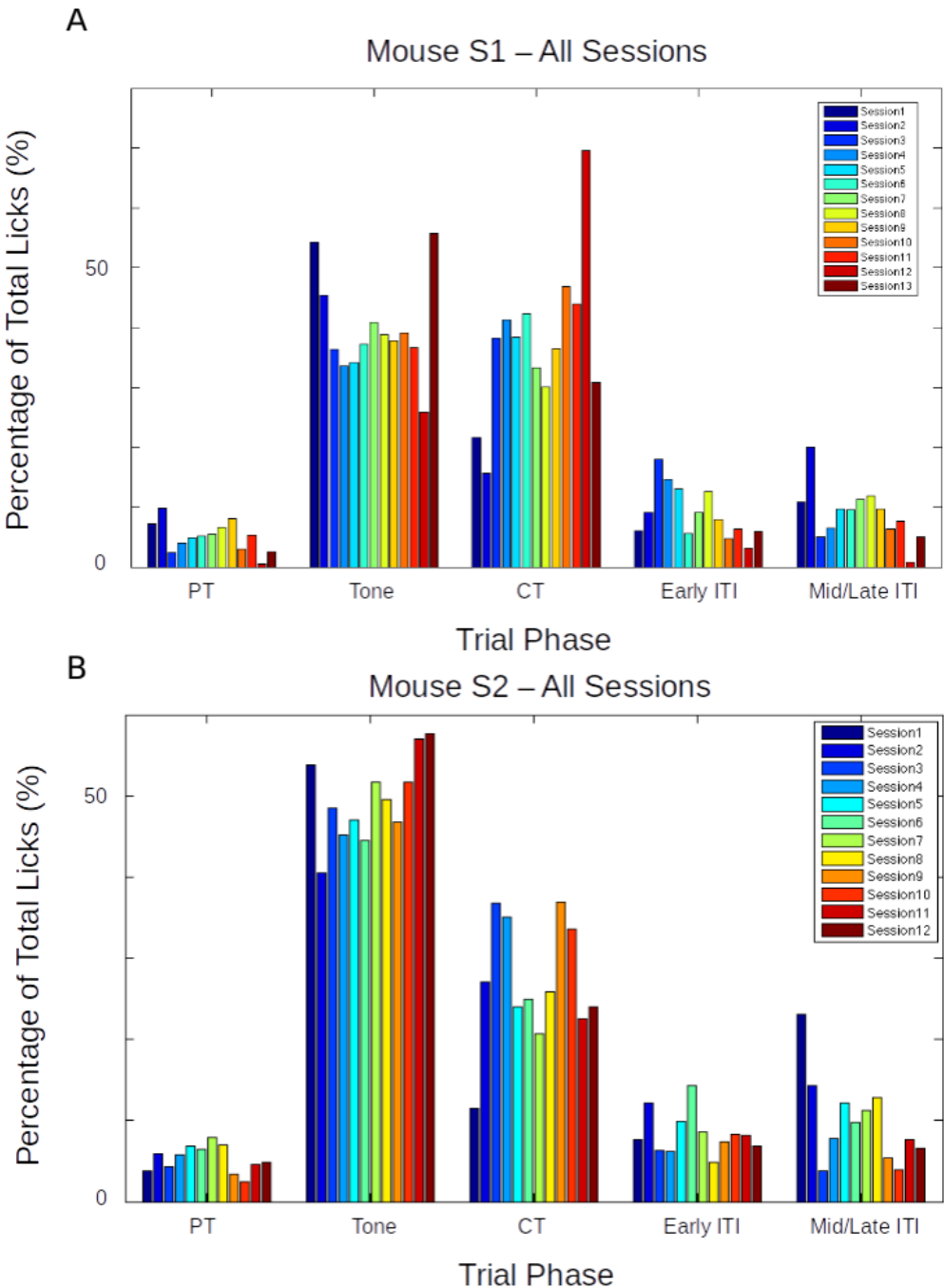


**Figure 7:** Performance evaluation for two example mice trained to Protocol 2. Percentage of total licks in the various trial phases (Pre-Tone, Tone, CT, and ITI), across all sessions of training (coloured bar plots), for (A) Mouse S1, and (B) Mouse S2.

Again, as is clear from the examples above, that while the mice eventually produced a decent percentage of total licks in the critical timeout (CT) phase to get a water reward, they did not learn to withhold licks during the Tone phase, even after >10 sessions. The task was ultimately unsuccessful.

**Total animals trained:** 4

**Conclusion:** Fail

### **Protocol 3: Delayed Non-Match to Sample (DNMS)**

Delayed Non-Match to Sample (DNMS) is a task that is ideally suited to study working memory and recognition (Chudasama, 2010), but we decided to try it. This task involves trial-by-trial presentation of two stimuli separated by a stimulus-free delay interval. For any given trial, if the two pseudorandomly chosen pairs of stimuli were identical, then licks would not be rewarded. However, if the pair of stimuli were different, then licks would be rewarded with 2  $\mu$ L water.

We referenced previously published protocols (Jaramillo & Zador, 2014) for their selection of auditory tone frequencies (3 kHz - 16.3 kHz) to select frequencies in the audible range. We had designed the experiment in such a way that the animal could behaviourally express a response to the perception of the various stimuli presented, as well as having learnt the overall task. We tried to incorporate more tones, in the hope that this may improve the chances of the animals focusing on the task specifics, instead of producing licks to just any stimulus.

**Tones used:** 6000 Hz, 8500 Hz, 10000 Hz, and 11500 Hz

**Trial phases:**

1. Pre-Tone duration (ms): 1000 ms
2. CS 1 duration (ms): 350 ms
3. Delay Interval duration (ms): 250 ms
4. CS 2 duration (ms): 350 ms (unless a correct lick is elicited)
5. ITI duration (s): randomized from 1 s to 3 s

**Punishment:** Timeout Box (minimum of 3s of no licks to escape)

**Reward:** 2  $\mu$ L of water

## **Results – Protocol 3**

>70-80% of the trials had to be aborted because the animals would not withhold licking after the 1st of the pair of tones was presented. This did not change even after 7 days (sessions) of training.

**Total animals trained:** 6

**Conclusion:** Fail

## **Protocol 4: Go/No-Go Task**

In an attempt to simplify the behavioural task, we decided to reconfigure the DNMS task to a simpler Go/No-Go task. Here, we would again present the animal with two stimuli, but with the only

condition being that the animal would have to lick after the second stimulus, and not before. This simplifies the behaviour to a certain extent, because the animals need only use the first stimulus as a cue for the second. Failure to perform this task could more easily then be attributed to a lack of attention in that trial. Only the data from the trials where the animal succeeds to do the task would be considered for analysis. Training related changes in actual stimulus representations would be carefully dissected out. Furthermore, such a task would control for the behavioural state of the animal and help provide important datasets.

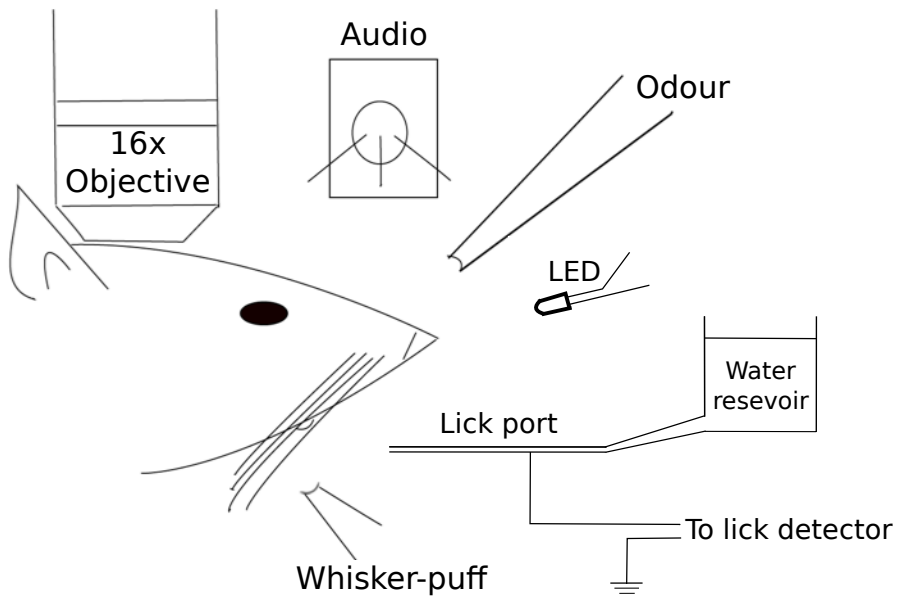


**Figure 8:** Schematic representation of the experimental setup for a simple detection task where the animal must perform a lick upon correctly detecting the presence of the conditioned stimulus (CS; from a range of modalities).

In terms of imaging, we hoped to use the no-go stimulus to record a clean stimulus response without the possible contamination of movement (licking behaviour), and the go stimulus to verify attention (Figure 8).

Trials were designed to go through the following phases and have the animal graduate to subsequent phases, only after correctly performing the behaviour:

1. Pre-tone: Stimulus-free period; no lick
2. No-go tone: 7kHz tone period; no lick
3. Go tone: 10kHz tone period; lick for reward

If the animal would perform an incorrect lick, the particular phase currently occurring was restarted. Only licks to the Go tone were rewarded (Figure 9).

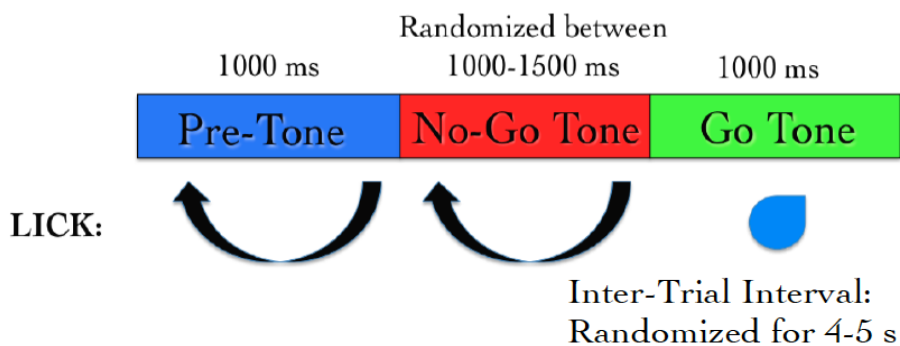


**Figure 9:** Typical trial structure with the various phases and lick dependent relationships.

## Results – Protocol 4

The behavioural performance improves only after ~3-4 sessions of training (Figure 10A). This is primarily due to an increase in the percentage of trials with a correct Go tone lick, as shown (Figure 10B).

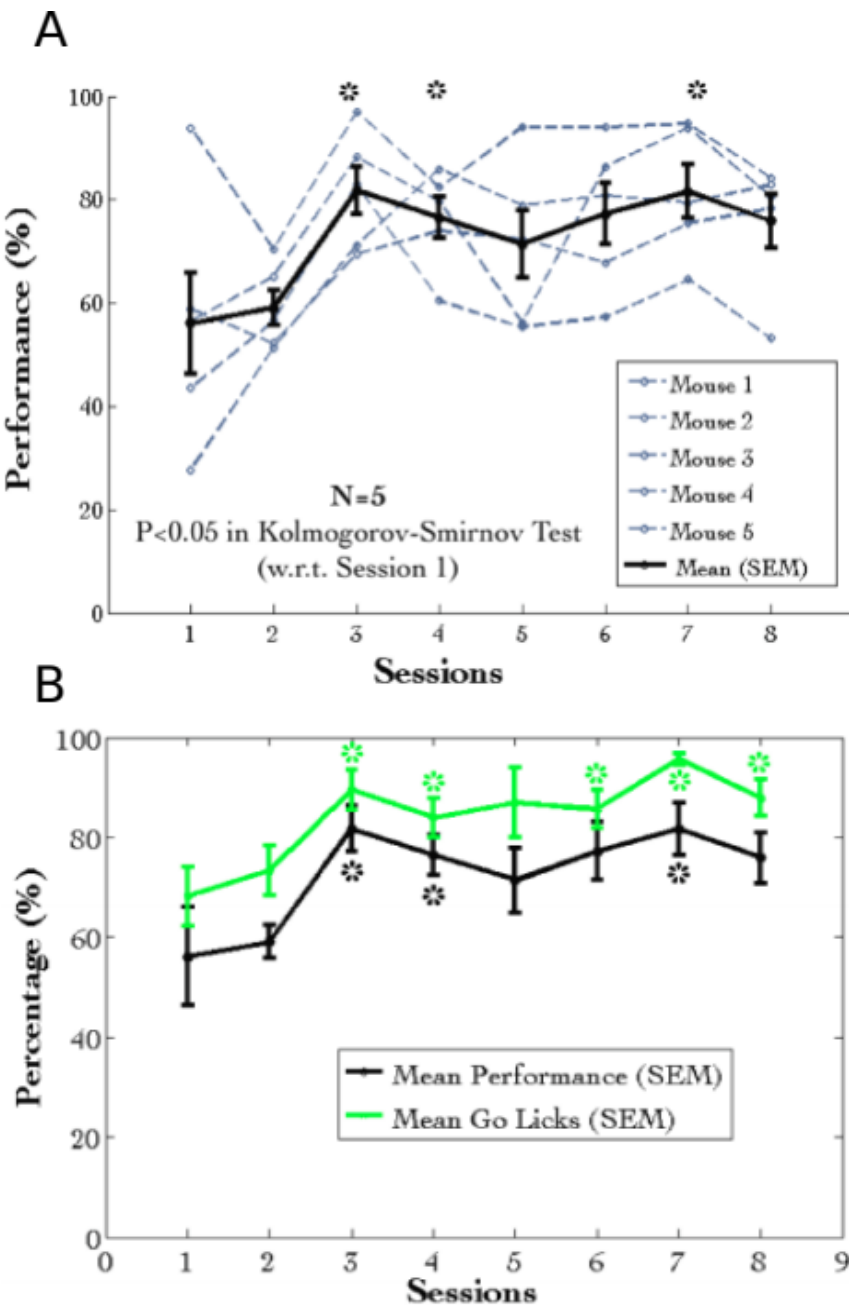


**Figure 10:** (A) Performance traces for all the animals individually shown in dashed grey lines. Mean + SEM in black. (B) Mean Performance (%) and Mean Go Tone Lick Percentage (%) with Session for the Go/No-Go Task, plotted in black and green, respectively.

A plot of the lick histogram for the various trial phases revealed that despite reaching the maximum success rate, the animals continued to lick during the no-go tone phase (incorrect lick) for a long duration of time (Figure 11). There was no difference in the amounts of time spent in the pre-tone or no-go tone phases. This suggested that the animals did not discriminate between the Go and no-go tones. Accordingly, the current protocol was not being learnt as expected.

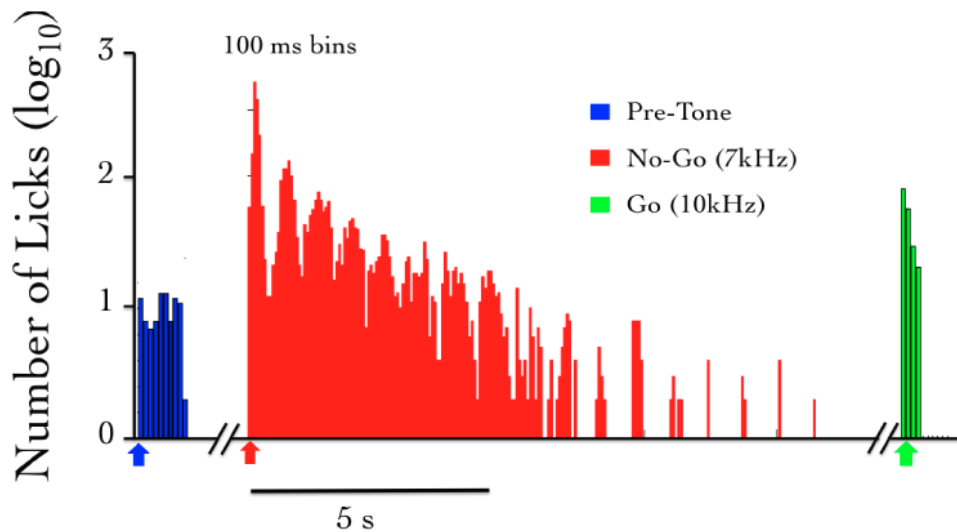


**Figure 11:** The number of licks in the pre-tone (blue), no-go tone (red), and go tone (green) phases, in a representative animal, in a session with maximum Performance (%).

We were not able to get discriminatory detection. Animals would resort to performing licks continuously and agnostically, to the go and no-go stimulus. In a study published many years later, it was determined that discriminatory tasks such as the one described above, could often require 3-4 weeks of training (Guo et al., 2014), since the animal was not punished with anything more than a delay or phase restart.

**Total animals trained:** 5

**Conclusion:** Fail

## **Operant conditioning experiments failed to match behavioural requirements**

Operant conditioning tasks have been extensively and successfully modeled in a variety of laboratories. For our specific experiments, we required a task that could be learnt within 1-2 weeks. This was because we were not confident on how many simultaneous days of chronic imaging, we could achieve with the *in vivo* chronic 2-photon calcium imaging preparation (see Chapter 3 – “Imaging”). Additionally, it typically takes 3-4 weeks for head-fixed rodents to acquire sufficient expertise in behavioural performance for Operant Conditioning tasks, *viz.*, behavioural discrimination - to lick to the rewarded stimulus and withhold licks for non-rewarded stimuli or incorrect trial phases (Guo et al., 2014). Some animals have been reported to learn such tasks within 1 week of training (Guo et al., 2014), but we did not observe this with our implemented protocols.

One alternative that we could have tried was to train the animals to expert levels of performance, and subsequently performed the hippocampus prep. The issue(s) with this is that,

- a) We wanted to study the hippocampal CA1 network during the learning or acquisition phase of behavioural training, as a distinct experiment from those published in literature.
- b) In such a protocol, we would require two separate surgeries, *viz.*, i) Head-bar implant, and, ii) hippocampus preparations. This, we believed would increase the technical difficulty of the overall experiment and could be more stressful for the experiment animals.

c) We suspected that there could be unknown effects on behavioural performance, post-surgery, complicating the analysis and insights we aimed to study.

Across all Operant Conditioning protocols attempted, we could not observe behavioural discrimination (not licking to incorrect phases) within 1-2 weeks of training. We considered the experiments as failures, in line with this reasoning.

Eventually, we had to abandon these experiments, to switch to an aversive conditioning task, *viz.*, Trace Eye-Blink Conditioning (TEC). With the change in the main behavioural task we also changed the project goals. The TEC task was standardized with the intention to work on Project II which is to study how animals make complex associations between different types of stimuli and how they adapt to changes to the inter-stimulus interval (ISI).

## **Trace Eye-Blink Conditioning [Project II]**

We have introduced the Trace Eye-Blink conditioning paradigm in Chapter 1 – “Introduction”, but some key definitions and results require mention. Eye-blink Conditioning is a class of Classical Conditioning and requires the presentation of a neutral stimulus (Conditioned Stimulus, CS) along with an eye-blink eliciting, mildly aversive stimulus (Unconditioned Stimulus, US). Depending on whether the CS presentation overlaps with the US presentation or if the two stimuli are separated by a stimulus free interval in between (Trace interval), the concomitant procedure is called Delay Conditioning or Trace

Conditioning, respectively (Figure 12). In either case, precise timing of the CS and US is mandated.

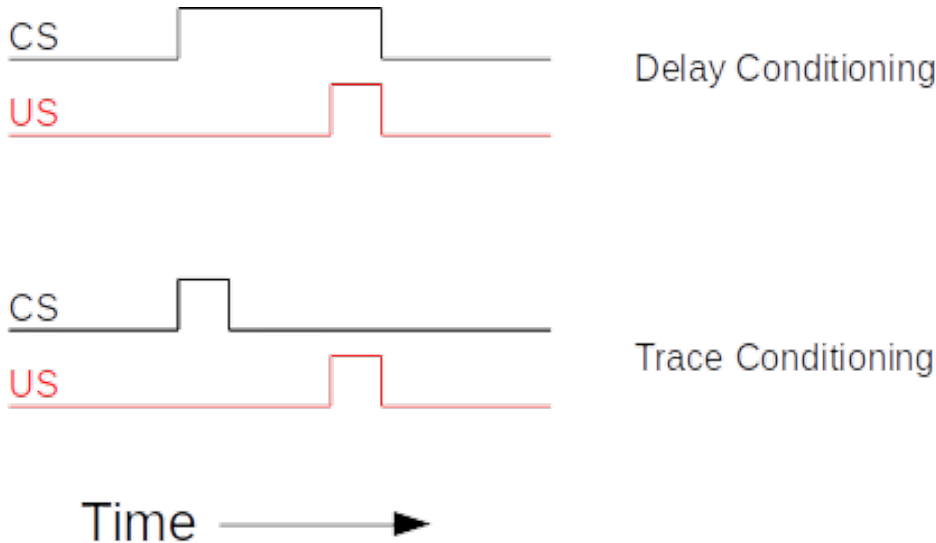


**Figure 12:** Schematic representation to showcase the two main subtypes of Classical Conditioning (Eye-Blink Conditioning, for our experiments) based on the relative timing and presentation of the CS and US.

The CS is usually an auditory tone or a visual stimulus (e.g.- LED Flash), while the US is typically a mild air-puff to the cornea, or a gentle electric shock to the eye-lid. Naive animals (rabbits, rodents, monkeys, etc.) produce a robust, reflexive eye-blink to the US (Unconditioned Response or UR) and ignore the CS, in early trials. However, with repeated pairing of CS and US, the animals are able to associate the two, and use the CS as a cue to predict the US, producing a partial, preemptive eye-blink just before the expected time of the US (Conditioned Response or CR). The CR develops in amplitude over multiple pairings or training sessions. In well trained animals, the CR begins at a time point closer and closer to the CS

onset, and usually merges with the UR. The animals produce this CR in an attempt to avoid the US.

Traditionally, Trace Eye-Blink Conditioning has been an important hippocampus-dependent behavioural task, and has been adapted to a variety of different species, spanning rabbits, rats, and mice.

Damage or inhibition of the hippocampus has been shown to limit task acquisition without affecting other non-hippocampus dependent tasks such as Delay Conditioning. In an experiment, Ibotenic Acid was used in a session dependent fashion, to observe both limitations in first acquiring the Trace Conditioning task, as well as detriments to behavioural recall, even after animals learn the task to a high degree of proficiency, suggesting the pivotal role that the hippocampus plays in temporal tasks of this nature (Tseng et al., 2004).

A single session of Trace Eye-Blink Conditioning, with strong stimuli (CS and US), has been previously employed (Modi et al., 2014), but with only up to 50% of the animals learning the task. Typically animals require around 3-7 sessions (~200-600 trials) to robustly learn the task. Accordingly, we designed and standardized a multi-session version of TEC, to allow more animals to learn and acquire the task, based on previously published work (Siegel et al., 2015).

## **Tracking eye-blink responses**

The most foolproof way to track eye-blink responses (especially with head-fixed animals) chronically (for multiple sessions across days), is

to use a video camera. We used a Point Grey Chameleon3 1.3 MP Monochrome USB3.0 camera) for this purpose. It is cost effective and with proper scaling of the resolution and field of view, can achieve recording rates of >200 frames per second (FPS). An important criteria for getting faster frame rates is to have better illumination, so that the camera may be set to lower exposure settings. We used a set of 5-10 Red colour LEDs as the light source, and these are run using a 12V DC line, with current limited resistors in series. Additionally, we used an IR-blocking filter to avoid capturing the 2-Photon excitation light (910-920 nm) when conduction behaviour and imaging experiments simultaneously. Finally, to focus the light from the eye of the animal onto the camera sensor, we used a Tamron M118FM16 lens (1/1.8, 16mm F/1.4).

## **Treadmill and tracking running speed**

Allowing the head-fixed animals to run on a treadmill was an important behaviour rig consideration, as this allows the animals to be more engaged and less stressed during experiments (Siegel et al., 2015). We considered treadmill tracking as a relevant variable to keep track of, despite the potential complications this could provide to imaging, viz., z-axis drift owing to relative motion between the brain tissue and microscope objective as the head-fixed animals run. We used a 6 inch cylindrical massage roller with a stainless steel axle running along the length. This axle had ball bearings on the two ends, to allow for free rotation against clamps. Additionally, we used linear actuators to be able to adjust the height of the treadmill relative to the head-fixing clamps.

On one side of the treadmill, we used a printed pattern of black squares (side length: 1 cm) along the circumference. This allowed an IR LED - Photodetector pair to catch the edges of the black printed squares. The number of edges detected per unit time, then gave us the run speed of the animals being trained. We followed previously published routines and protocols (Siegel et al., 2015) for setting up the treadmill and run speed tracking (Figure 13), over 50 ms sized bins, across each trial.

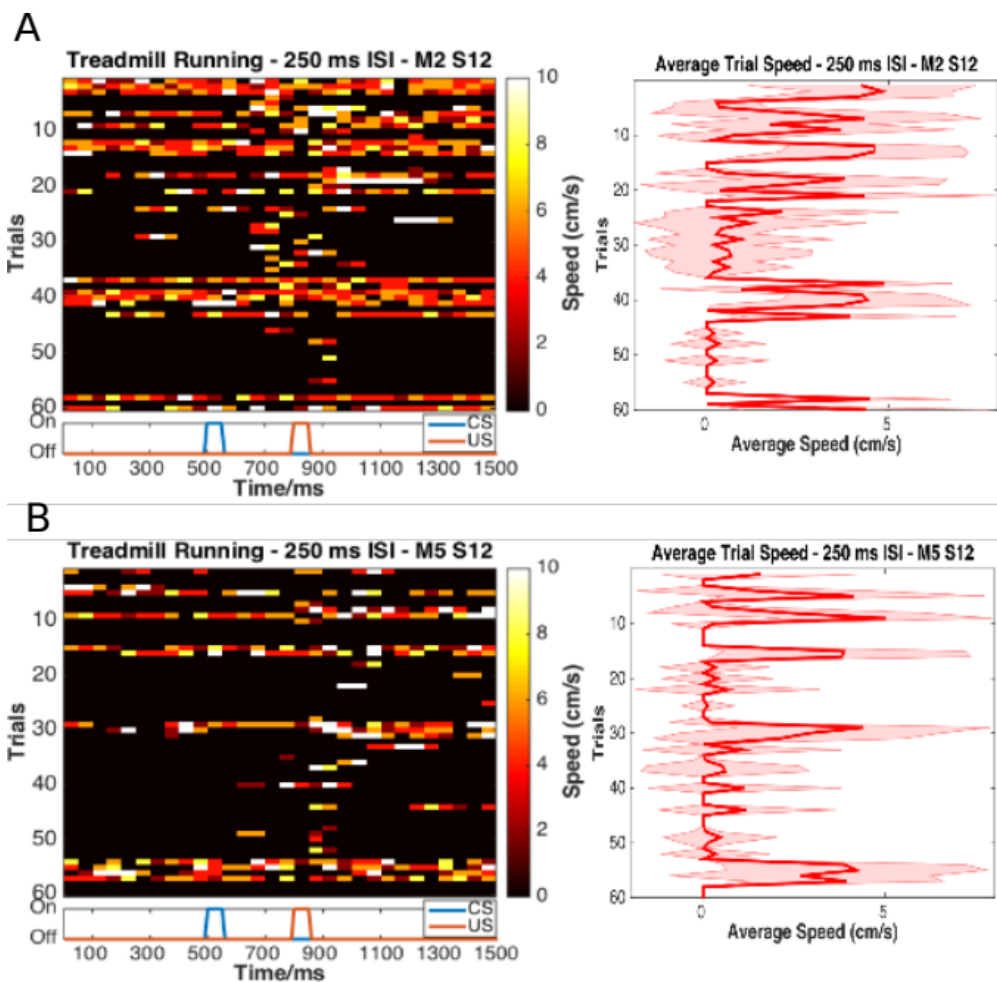


**Figure 13:** Trial-by-trial (left) and trial-averaged running speed (right) for two example animals, (A) M2 Session 12, and (B) M5 Session 12.

## **Behaviour rig and protocol control - Software**

For our initial experiments we used the open-source behaviour controlling software suite Bonsai (Windows version). Later on, we were able to implement our own custom codes that allowed integration of the video camera, Arduino for stimulus delivery and treadmill tracking, and the software side of the protocols. Dilawar S. Rajput was instrumental in setting up the camera pipeline and integrating it into the Arduino code. The Camera server was implemented in C++ with Spinnaker API (Point Grey) and this fetched frames from the camera. The camera client was written in Python, and this read the frames to produce a copy to monitor the video feed live, as well as write the video frames to disk as .tif files.

With this setup, the maximum memory usage was ~1.3 GB RAM, and the code (available at <https://github.com/BhallaLab/PointGreyCamera>) had the following dependencies:

- libopencv-dev, python-opencv
- cmake, g++, gnu-make
- libtiff-dev, python-tifffile, python-numpy
- python-gnuplotlib, gnuplot-x11

An important requirement for our behaviour experiment design was to be able to train the animals systematically under reproducible conditions, with the aim to have stable behavioural training and animal performance. We used a blue LED as the Conditioned Stimulus (CS, 50 ms flash) with an air-puff to the eye serving as the Unconditioned Stimulus (US, 50 ms pulse). We used an Arduino to orchestrate stimulus delivery and protocol design. All experiments were performed on head-fixed C57Bl6 mice, since we planned to use a stationary,

custom-built two-microscope to image hippocampal CA1 activity during task acquisition and recall (Figure 14; Figure 15).

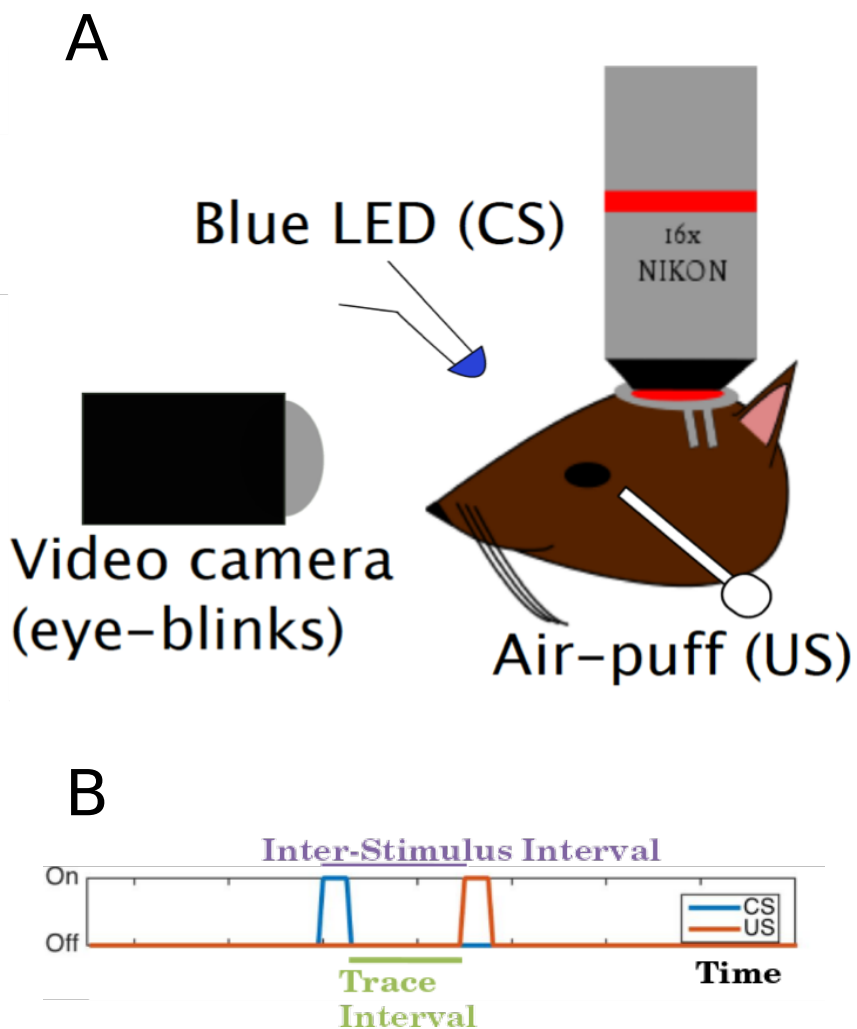


**Figure 14:** Schematic representation of (A) the behaviour rig with 2-Photon imaging, to train head-fixed mice on a Trace Eye-Blink Conditioning (TEC) task, and (B) relative time intervals between the CS and US.

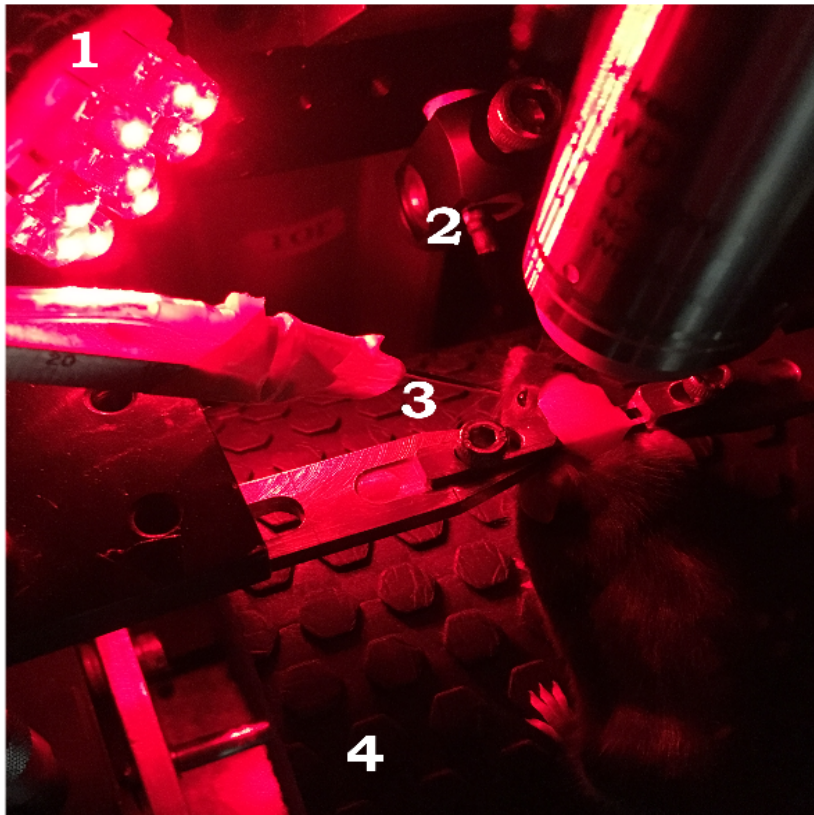


**Figure 15:** A picture of a head-fixed mouse clamped on the behaviour rig, with key components: 1) Red LED Illumination, 2) Blue LED CS, 3) Air-puff port directed to the left eye, and 4) Height-adjustable Treadmill.

## Analysis - TEC

Once the .tif movies of the eye of the animal being trained were saved, they were analyzed by a custom script written in MATLAB, wherein for every frame we (Figure 16),

- a) Adjust contrast (optional)
- b) Apply a median filter (optional)
- c) Crop out the pixels defining the eye and surrounding (identical number of pixels for all trials and animals)
- d) Binarize the image of the eye to get black pixels defining the visible (opened) portion of the eye
- e) Count the relative proportion of open vs closed eye pixels in the cropped image, and
- f) Assign each frame with a Fraction of Eye Closure (FEC) score.

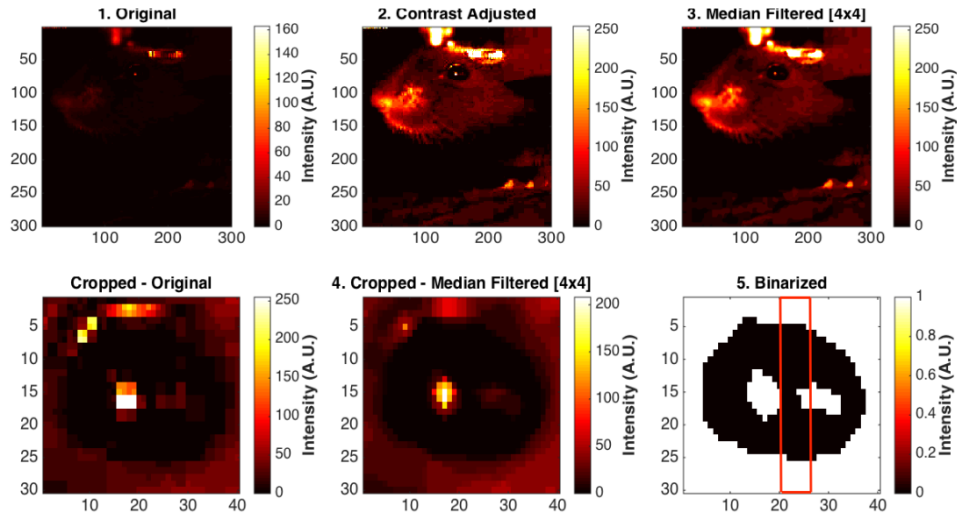


**Figure 16:** Steps from behaviour video frame to Fraction of Eye-Closed (FEC) analysis.

The FEC score then allowed us to analyse each trial's worth of frames for eye-blanks. There are many features of the eye-blink that could be

used to gauge the overall performance of the animal in terms of both the Conditioned Response (CR) as well as the Unconditioned Response (UR), but for our experiments, we chose to use Eye-Blink Amplitude (Siegel et al., 2015). Additionally, we studied whether the animals could produce CRs in the absence of the US, by pseudorandomly selecting 10% trials to skip the US (Probe Trials).

## **Results - TEC**

1. Animals showcase task acquisition by performing Conditioned Responses (CRs), observed as pre-emptive blinks timed to avoid the aversive US. The kinetics of the CR (timing, amplitude, etc.) are dependent on the amount of training, but are identical across paired and probe trials (Figure 17).

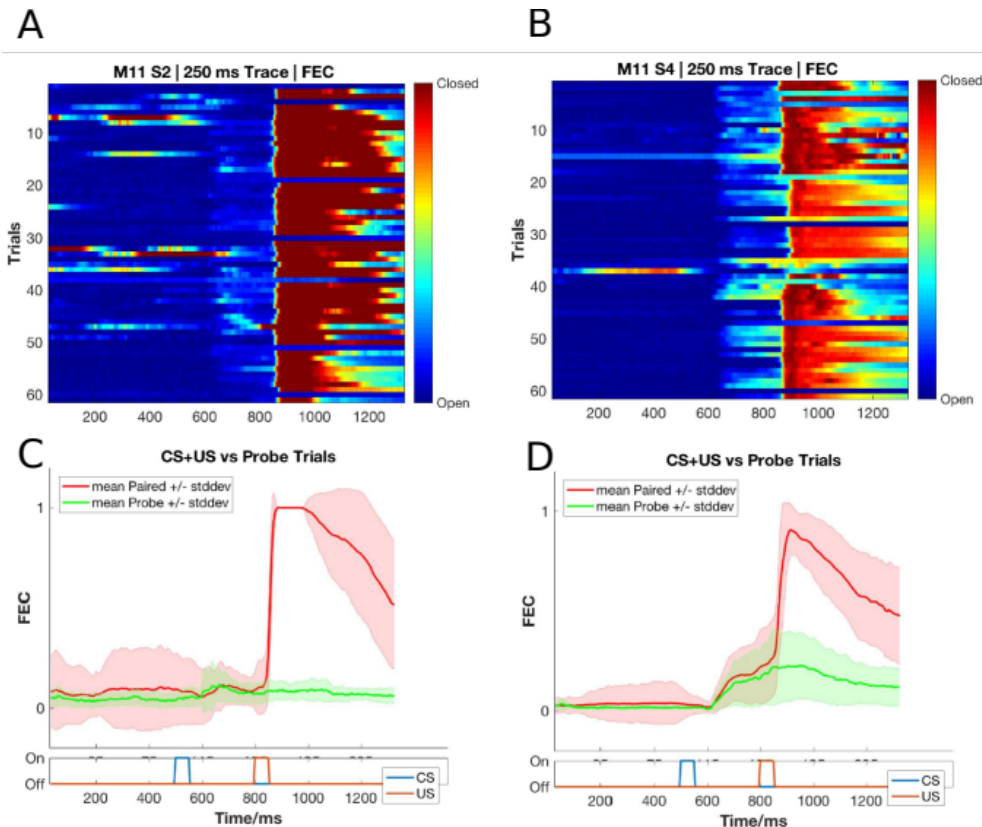


**Figure 17:** Conditioned Responses (CRs) are small amplitude eye-blanks triggered by the CS, and develop with multiple training sessions, while Unconditioned Responses (URs) are large eye-blanks to the US, typically consistent across sessions. (A,B) Trial-by-trial FEC traces for M11 (A) Session 2, and (B) Session 4. (C,D) Trial-averaged FEC traces for M11 (C) Session 2, and (D) Session 4, with paired (red) and probe (green) trials.

2. Most animals can pick up the task within 4-7 sessions (1 session/day, 60 trials/session), even if on water deprivation. Animals can also be subsequently trained to different inter-stimulus intervals. Using the Conditioned Response (CR) amplitude, each trial can be binarized to whether a CR was elicited (Hit Trial) or not (Miss Trial), by thresholding at mean trial FEC + 2\*Std. Dev.. Performance for the session is then

estimated as the ratio of Hit Trials to Total Trials (Figure 18). We additionally set a criterion that a performance of >70% be considered “strong learning”, 30-60% be considered “weak learning”, and “0-30%” be considered “non-learning”.

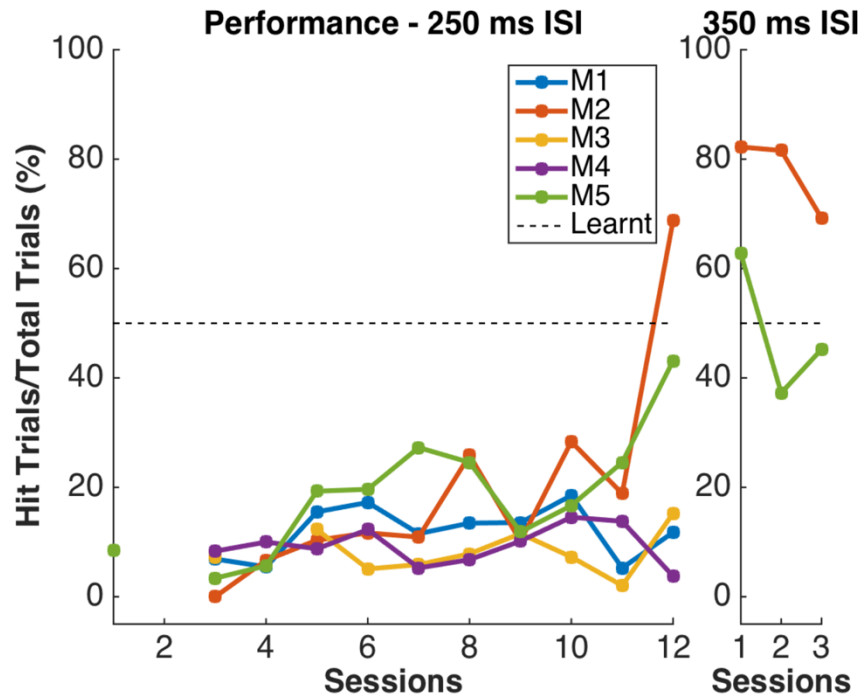


**Figure 18:** Performance in terms of the percentage of Hit Trials to total trials across sessions, including an ISI switch from 250 ms to 350 ms. Here, M2 is a strong learner (>60% hit trials/session) and M5 is a weak learner (30-60 % hit trials/session). M1, M3, and M4 did not learn the task.

3. Animals that learn multiple ISIs, especially when the second ISI is  $\geq 2x$  the first ISI, showcase complex eye-blinks without extinction of the previously learnt CRs. Once an animal showcases the ability to produce Conditioned Responses (CRs) to one inter-stimulus interval (ISI), this interval can be elongated. In the example shown below we first trained the

animal to a 250 ms ISI, and then switched to a 500 ms ISI (Figure 19).

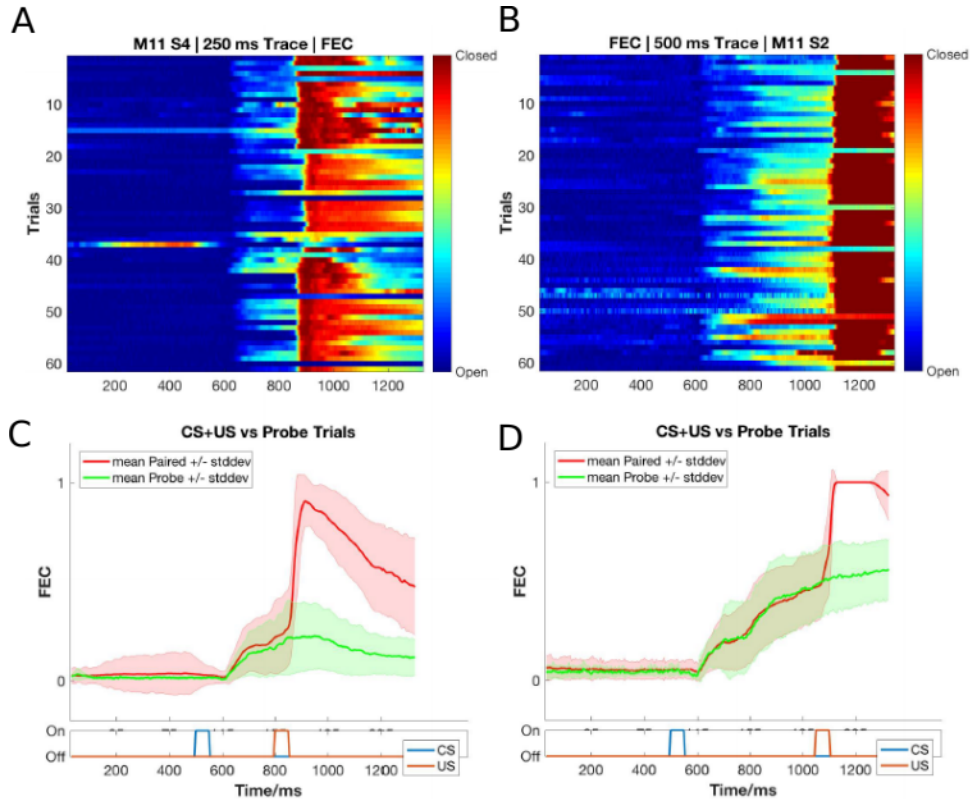


**Figure 19:** Conditioned Responses (CRs) are preserved for previously learnt ISIs, and switching the ISI to longer intervals results in Complex (multi-CR) eye-blink responses. (A,B) Trial-by-trial FEC scores for (A) 250 ms ISI (left) and (B) 500 ms ISI. (C,D) Trial-averaged FEC traces for (C) 250 ms ISI, and (D) 500 ms ISI, with paired (red) and probe (green) trials.

4. The onset of the Conditioned Response (CR) is not affected by the ISI switch, irrespective of how strongly the animals learn the task. CRs during paired and probe trials were near identical, showcasing that the animal (Figure 20; Figure 21).

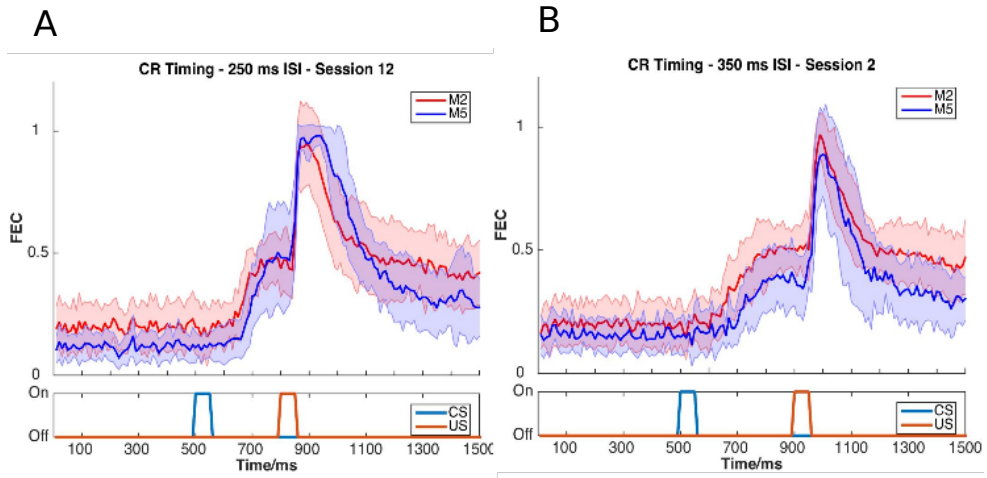


**Figure 20:** Conditioned Response (CR) onset timing is maintained across ISI switches. Representative examples from a short ISI switch from (A) 250 ms to (B) 350 ms (right).

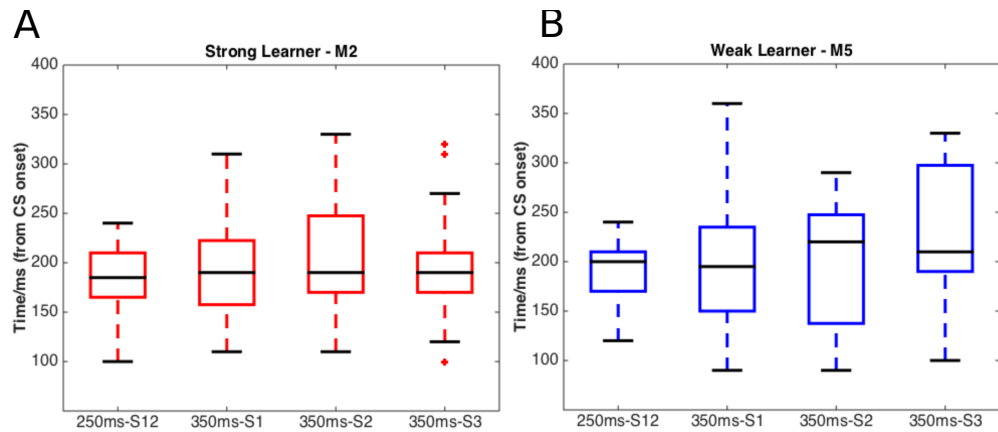


**Figure 21:** Bar plots for Conditioned Response (CR) onset across multiple sessions of training after ISI switch from 250 ms to 350 ms, irrespective of how strongly the animals learnt the task. (A) red, strong learner, and (B) blue, weak learner.

5. Animals can also be trained to very long ISIs from Session 1, with acquisition taking <10-14 days. Here we tried to train animals to either a 550 ms ISI or a 750 ms ISI. Note, however,

that unless multiple ISIs are taught to the same animal, the CR eye-blink is singular (Figure 22).

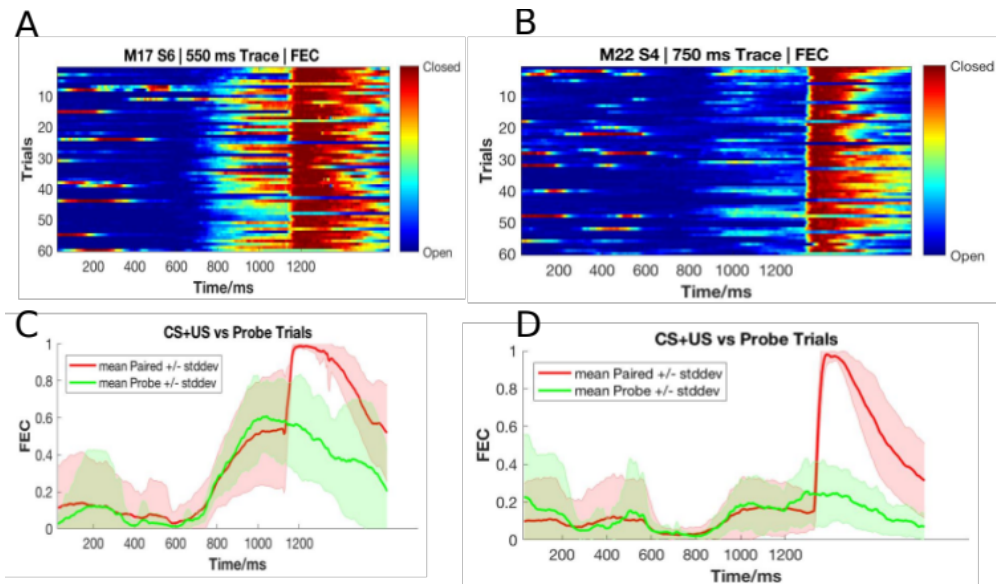


**Figure 22:** Representative example of mice trained to 550 ms ISI (Session 6) and 750 ms ISI (Session 4). (A,B) Trial-by-trial FEC responses for (A) 550 ms ISI (M17 Session 6), and (B) 750 ms ISI (M22 Session 4). (C,D) Trial-averaged FEC responses for (C) 550 ms ISI (M17 Session 6), and (D) 750 ms ISI (M22 Session 4), with paired (red) and probe trials (green).

**Total animals trained:** 18 [Conditioned Responses visible]

**Conclusion:** Success

Ultimately, we were satisfied with the Trace Eye-Blink Conditioning paradigm since we could observe stable conditioned responses that developed over a reasonably short period of training time (<1 week), and adaptable conditioned responses to behaviour parameter modulations, in head-fixed mice that could be subjected to simultaneous 2-Photon calcium imaging.

**Table 1:** Summary table of behaviour protocols attempted and essential results.

NAME	PUNISHMENT TYPE	REMARKS
Operant Protocol 1.1 (Stimulus Detection)	No water reward for incorrect licks	Lack of water reward for incorrect licks not enough for behavioural discrimination at <1 week of training
Operant Protocol 1.2 (Stimulus Detection)	Air-puff punishment for incorrect licks	Strong punishment for incorrect licks not enough for behavioural discrimination at <1-2 weeks of training.
Operant Protocol 2 (Stimulus Detection)	Timeout (3s) punishment for incorrect licks	Alternate or weaker punishment attempted but not enough for behavioural discrimination at <1 week of training.
Operant Protocol 3 (DNMS)	Timeout (3s) punishment for incorrect licks	Alternate punishment attempted but not enough for behavioural discrimination at <1 week of training No obvious effect of adding delay intervals between stimulus presentations
Operant Protocol 4 (Go/No-Go)	Trial base repeat punishment for incorrect licks	Alternate punishment attempted but not enough for behavioural discrimination at <1 week of training
Aversive Protocol (Trace Eye-Blink Conditioning)	No punishment	Animals learn the task and produce stable, adaptable Conditioned Responses (CRs) within 1 week of training

## Bibliography

- Brown, G. D. (1998). Nonassociative learning processes affecting swimming probability in the seashell Tritonia diomedea: habituation, sensitization and inhibition. *Behavioural Brain Research*, 95(2), 151–165.  
[https://doi.org/https://doi.org/10.1016/S0166-4328\(98\)00072-2](https://doi.org/https://doi.org/10.1016/S0166-4328(98)00072-2)
- Chudasama, Y. (2010). Delayed (Non)Match-to-Sample Task. In I. P. Stolerman (Ed.), *Encyclopedia of Psychopharmacology* (p. 372). Springer Berlin Heidelberg. [https://doi.org/10.1007/978-3-540-68706-1\\_1619](https://doi.org/10.1007/978-3-540-68706-1_1619)
- Deshmukh, S. S., & Bhalla, U. S. (2003). Representation of odor habituation and timing in the hippocampus. *The Journal of Neuroscience : The Official Journal of the Society for Neuroscience*, 23(5), 1903–1915.  
<https://doi.org/10.1523/JNEUROSCI.23-05-01903.2003>
- Fyhn, M., Molden, S., Witter, M. P., Moser, E. I., & Moser, M.-B. (2004). Spatial representation in the entorhinal cortex. *Science (New York, N.Y.)*, 305(5688), 1258–1264.  
<https://doi.org/10.1126/science.1099901>
- Guo, Z. V., Hires, S. A., Li, N., O'Connor, D. H., Komiyama, T., Ophir, E., Huber, D., Bonardi, C., Morandell, K., Gutnisky, D., Peron, S., Xu, N., Cox, J., & Svoboda, K. (2014). Procedures for Behavioral Experiments in Head-Fixed Mice. *PLOS ONE*, 9(2), e88678.  
<https://doi.org/10.1371/journal.pone.0088678>
- Hafting, T., Fyhn, M., Molden, S., Moser, M.-B., & Moser, E. I. (2005). Microstructure of a spatial map in the entorhinal cortex. *Nature*, 436(7052), 801–806. <https://doi.org/10.1038/nature03721>
- Hubel, D. H., & Wiesel, T. N. (1962). Receptive fields, binocular interaction and functional architecture in the cat's visual cortex. *The Journal of Physiology*, 160(1), 106–154.  
<https://doi.org/10.1113/jphysiol.1962.sp006837>
- Jaramillo, S., & Zador, A. M. (2014). Mice and rats achieve similar levels of performance in an adaptive decision-making task . In *Frontiers in Systems Neuroscience* (Vol. 8).  
<https://www.frontiersin.org/articles/10.3389/fnsys.2014.00173>
- Modi, M. N., Dhawale, A. K., & Bhalla, U. S. (2014). CA1 cell activity sequences emerge after reorganization of network correlation structure during associative learning. *eLife*, 3, e01982–e01982.  
<https://doi.org/10.7554/eLife.01982>
- O'Keefe, J., & Dostrovsky, J. (1971). The hippocampus as a spatial map. Preliminary evidence from unit activity in the freely-moving rat. *Brain Research*, 34(1), 171–175. [https://doi.org/10.1016/0006-8993\(71\)90358-1](https://doi.org/10.1016/0006-8993(71)90358-1)

- Ranck, J. B. (1973). Studies on single neurons in dorsal hippocampal formation and septum in unrestrained rats: Part I. Behavioral correlates and firing repertoires. *Experimental Neurology*, 41(2), 462–531. [https://doi.org/https://doi.org/10.1016/0014-4886\(73\)90290-2](https://doi.org/10.1016/0014-4886(73)90290-2)
- Schreurs, B. G. (1989). Classical conditioning of model systems: A behavioral review. *Psychobiology*, 17(2), 145–155. <https://doi.org/10.3758/BF03337830>
- Siegel, J. J., Taylor, W., Gray, R., Kalmbach, B., Zemelman, B. V., Desai, N. S., Johnston, D., & Chitwood, R. A. (2015). Trace Eyeblink Conditioning in Mice Is Dependent upon the Dorsal Medial Prefrontal Cortex, Cerebellum, and Amygdala: Behavioral Characterization and Functional Circuitry. *ENeuro*, 2(4), ENEURO.0051-14.2015. <https://doi.org/10.1523/ENEURO.0051-14.2015>
- Taube, J. S., Muller, R. U., & Ranck, J. B. J. (1990). Head-direction cells recorded from the postsubiculum in freely moving rats. I. Description and quantitative analysis. *The Journal of Neuroscience : The Official Journal of the Society for Neuroscience*, 10(2), 420–435. <https://doi.org/10.1523/JNEUROSCI.10-02-00420.1990>
- Tseng, W., Guan, R., Disterhoft, J. F., & Weiss, C. (2004). Trace eyeblink conditioning is hippocampally dependent in mice. *Hippocampus*, 14(1), 58–65. <https://doi.org/10.1002/hipo.10157>

## Chapter 3 – Imaging

The mammalian hippocampus is considered important in the formation of new memories about experienced events (episodic or autobiographical memory), general declarative memory (memories that can be explicitly verbalized), spatial memory and navigation, and associations between stimuli that are distinct in time, among other functions. To achieve this, the Hippocampus must integrate information from different areas of the cortex.

Much of the cortical information that enters the Hippocampus (at the Dentate Gyrus), comes through the Entorhinal Cortex, along the Perforant Path (Hjorth-Simonsen & Jeune, 1972). The Dentate Gyrus cell network then relays this information to the CA3 cell network through Mossy Fibers, which in turn relays the information to CA1 cells, through the Schaffer Collateral Fibers. This is popularly known as the Trisynaptic Circuit or Pathway (Figure 1 from Chapter 1 - "Introduction") and there is scope and evidence for computation and information processing at every step (MacDonald et al., 2011, 2013; Modi et al., 2014; Nakashiba et al., 2008; Suh et al., 2011). Finally, the CA1 cells have their outputs to other brain regions. It is important to note, however, that regions like the CA1 are known to have access to information directly from other brain regions, as well (P. Andersen et al., 2006).

Literature in the field suggests that naïve animals may have some sensory gating of “Neutral” stimuli at the level of the CA1 (Abe et al., 2014; Bellistri et al., 2013; Kamondi, 1998). The source of this inhibition (at least the step before the local interneurons) seems to be

the Medial Septum, through Fimbria-Fornix (Abe et al., 2014). Also, behavioural relevance allows the CA1 to elicit depolarizations that can be mapped to brain external stimuli (Dombeck et al., 2010; Harvey et al., 2009; P. M. Itskov et al., 2011; MacDonald et al., 2011, 2013; Modi et al., 2014; Pastalkova et al., 2008).

The Hippocampus consists of ventral and dorsal portions both of which are of similar composition but are parts of different neural circuits (Moser & Moser, 1998). The dorsal hippocampus performs primarily cognitive functions and in memory function, while the ventral hippocampus modulates emotional and affective processes (Fanselow & Dong, 2010).

## **Physiology in the hippocampus**

The Hippocampus is located deep in the medial temporal lobe of mammals and is defined by several sub-structures, including the Dentate Gyrus (one site for information input to the hippocampus) and the Hippocampus Proper constituted by the CA1, CA2, CA3 and CA4 cellular levels.

Using extracellular tungsten microelectrodes in naïve unanesthetized rabbits serially exposed to multimodal stimuli (Vinogradova, 2001), it was reported that in the CA1,

1. A major fraction the reactive neurons have unimodal responses (41-44%)

2. Multimodal neurons are modality-unspecific but have differentiated responses to stimuli of different modalities and even to various stimuli within a single modality
3. Many neurons respond by Phasic (evoked responses last for the duration and as long as the stimulus) and Specific (stimulus-specific pattern) responses
4. Neurons with inhibitory responses are encountered less frequently than those with various types of excitatory
5. Habituation (non-responsiveness to repeatedly presented stimuli) is present though not among all the responsive cells (71-75%) and is often gradual

Imaging based activity studies have the advantage of being able to capture many more cells (>100 from the same animal) during experiments (Dombeck et al., 2010; Pachitariu et al., 2017; Peron et al., 2015; Sofroniew et al., 2016) as compared to typical electrophysiological measurements. Imaging provides an unambiguous method to identify cells that are not active during a period of interest. Another advantage is that it provides anatomical confirmation to help track the same cell over multiple days of recording, without ambiguity, for longitudinal studies. Finally, imaging techniques have gained momentum in the study of the hippocampal CA1 various spatial scales, from cellular resolution somatic studies (Dombeck et al., 2010; Modi et al., 2014), to dendrites (Mizrahi, 2004; Sheffield & Dombeck, 2014), axonic boutons terminating on the CA1 interneuron populations (Kaifosh et al., 2013; Lovett-Barron et al., 2014), as well as spines (Attardo et al., 2015), *in vivo*.

We designed our imaging studies (for this thesis), with the aim to understand the network and cellular mechanisms of the hippocampal CA1 that corresponded with behavioral learning induced changes. We started by looking for CA1 responses to neutral stimuli in naive animals, *in vivo*. Subsequently, we planned to subject these animals to behavioural training and study if and how the same cells would respond.

Depending on the intended duration of the imaging experiments, *viz.*, a few hours (single session) or a few days and weeks (multiple sessions), we were able to standardize both an Acute as well as a Chronic *in vivo* hippocampal preparation. We now discuss the *in vivo* hippocampal preparation, physiology recordings, and a brief summary of the results. An important perspective for our experiments was to study how sensory stimulus responses of hippocampal CA1 develop with associative learning.

## **Methodology – Acute and chronic imaging [Projects I & II]**

The overall experiment deals with optically measuring the activity of the dorsal CA1 hippocampal neurons when different stimulus modalities are presented to a male C57BL/6 mouse. The thesis covers experiments conducted acutely (lasting <10 hours) using OGB-1 as a calcium sensor), as well as chronically (~7-21 days) using a genetically encoded calcium indicator, GCaMP6f).

The 2-Photon excitation wavelength for OGB-1 experiments was set to 810 nm (scattering coefficient:  $\sim 3$  rad $^2$ /mm) and the same for GCaMP6f was set to 910 nm (scattering coefficient:  $\sim 2$  rad $^2$ /mm) to image cell bodies (Min et al., 2017) in the CA1, *in vivo*. However, despite the relatively low scattering of longer wavelengths, the hippocampus cannot be imaged directly, through the cortex since the layer of cortex is too thick ( $\sim 1\text{-}1.5$  mm) to allow proper excitation of the sample. These infra-red (IR) photons are expected to be scattered almost completely, well before the imaging depth of the CA1 layer. These layers of cortex have to accordingly be carefully suctioned out to allow the microscope objective to have optical access to the exposed tissue (Figure 23).

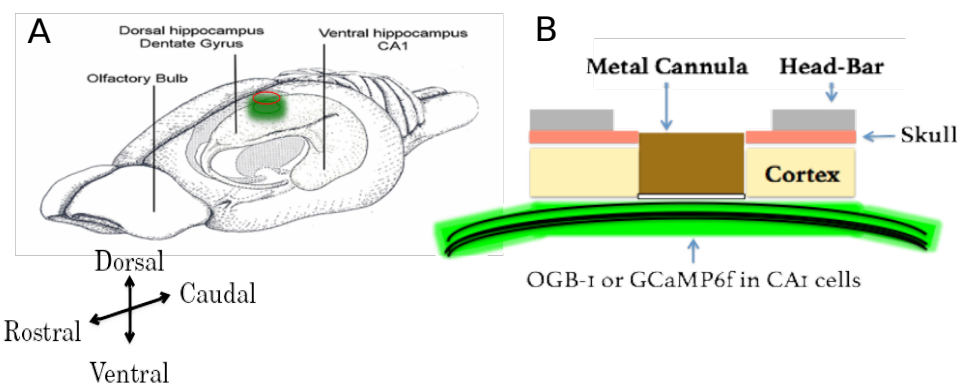


**Figure 23:** (A) A schematic of the rodent brain, showcasing the two hippocampi, one in each hemisphere. The hippocampi lie  $\sim 1$  mm (mice) below the cortical surface. (B) The hippocampal preparation allows optical access to the deep lying hippocampal CA1 cells, relative to the skull/cortex. The CA1 cell bodies arrange in a laminar fashion as a tight cell body layer that can be visualized by fluorescence (using either OGB-1 or GCaMP).

We first put the animal under anesthesia using a vapor chamber saturated with 3% isoflurane. Next, the animal was cheek-clamped and a light state of anesthesia was maintained using 1-2% isoflurane,

provided directly to the nozzle of the animal, keeping track of ~1 Hz breathing rate and a body temperature of 35-37 °C (with heating pad). The animal was given a haircut and a circular incision of ~5 cm circumference was made on the scalp, revealing the skull below. We then affixed head-bars and skull screws with the help of dental cement, to be able to clamp the animal post surgery on the 2-Photon Microscope.

The left, dorsal hippocampus was targeted with a 3-5 mm circular craniotomy aimed at 1.5 mm left and 2.0 mm behind bregma, tearing and peeling out the Dura to reveal the cortex. We then carefully aspirated out the cortex (part of the somatosensory cortex) under repeated washes of Cortex Buffer (see table 1 for recipe), until the horizontal CC fibre layer was visible. Finally, we added a drop of low gelling agarose and a 5 mm coverslip (for acute preps); Kwik-Sil and inserted a 3 mm metal cannula with a coverslip attached at the bottom (for chronic preps). We used different sensors depending on the requirement for the preparation, *viz.*, acute (OGB-1) or chronic imaging (GCaMP6f). We kept track of animals that showcased unusual gait or low/no mobility and avoided their use altogether for production datasets and experiments, in accordance with previously published protocols (Dombeck et al., 2010). We refer to this series of steps as the hippocampal preparation.

## Preparation of Cortex Buffer

We prepared cortex buffer by weighing out the required amount of the salts, NaCL, KCl, Glucose and HEPES (see table 2 for recipe) and

making up the volume of the solution with Milli Q Water to ~1000 ml. We then set the pH of the buffer using a calibrated pH meter to 7.35, using 1M NaOH<sub>(aq)</sub>. Next, we fill up the volume to 1000 ml and verify the pH (should not have changed). Finally, we filter the contents through a 0.22 um membrane using a vacuum filtration, and store at 6 °C.

Recipe for ready-to-use cortex buffer. The buffer is typically prepared and stored in aliquots to be used each week. The correct pH range of the buffer was often a crucial factor ensuring the success of the hippocampal preparation.

**Table 2:** Recipe for ready-to-use cortex buffer. The buffer is typically prepared and stored in aliquots to be used each week. The correct pH range of the buffer was often a crucial factor ensuring the success of the hippocampal preparation.

INGREDIENT	CONCENTRATION (mM)	AMOUNT (g or ml) for 1000 ml]
NaCl (s)	125	7.31 g
KCl (s)	5	0.373 g
Glucose (s)	10	1.8 g
HEPES (s)	10	2.38 g
CaCl <sub>2</sub> (aq)	2	1.6 ml of 1.25 M stock solution
MgCl <sub>2</sub> (aq)	2	1.5 ml of 1.3 M stock solution

## Oregon Green Bapta-1 injections for acute imaging

To prepare Oregon Green Bapta-1 (OGB-1) dye for microinjections, we first dissolve a 50 µg tube of OGB-1 in 5 µl of Pluronic Acid, and vortex the mix for 5 minutes. Separately, we dilute 20 µl of Phenol Red into 500 µl of cortex buffer, and transfer 45 µl of this solution to the OGB-1 mix. Next, we sonicate the 50 µl solution for 20 mins., followed by centrifugation at 10000 RPM for 5 seconds. The remaining supernatant is split into 7 aliquots (7 µl), and stored at -20 C for a maximum of one week (7 days).

For acute/single-day experiments, we injected OGB-1 using pulled, dye loaded micropipettes (~2 MΩ resistance, ~2 µm diameter) at a depth of 100-150 µm (Figure 23) from the topmost layer of exposed tissue, till a slow but detectable pulse of dye (visualized as a red/pink solution) may be visible just below the tissue surface. This allows the dye to be soaked up by the basal dendrites of the CA1 and takes 30-60 mins for incorporation into the cytoplasm. We typically allow the animal 1-2 hours of respite before the subsequent imaging session. High pressure ejection of the dye into the tissue may damage the neuropil, while very low pressures or clogs in the pipette affect the spread of the dye across the tissue. We aimed to image ~100 x 100 µm<sup>2</sup> of the tissue in any particular ROI, and achieved this with 5 minute injections with each micropipette aiming to load the dye at 2-3, well separated positions spread across the entire exposed dorsal surface. We estimated that the dye volume was <1000 nl/injection. After the injection cycle with any micropipette, we left the tissue undisturbed for at least 5-10 mins before pulling the micropipette out of the tissue. Once all the injections were complete, the exposure was sealed using 5% low gelling agarose making sure the temperature was cool enough to avoid heat-related tissue damage.

OGB-1 is eventually cleared from the cytoplasm but allows for a limited window for imaging studies (Stosiek et al., 2003). Reopening the agarose seal and re-injections were never attempted to prevent unnecessary damage to the underlying tissue. Additionally, the agarose plug itself was found to be unstable beyond 1-3 days. This resulted in the imaging possibility being limited to the same day as the surgery (acute imaging).

## **GCaMP and chronic imaging**

For chronic/multi-day experiments, we standardized a stereotaxic viral injection step, where we inject the gene for GCaMP5 or GCaMP6f into the dorsal hippocampus at -1.5 mm lateral, 2 mm posterior, and 1.3 mm dorsal from bregma on the skull surface (Figure 24).

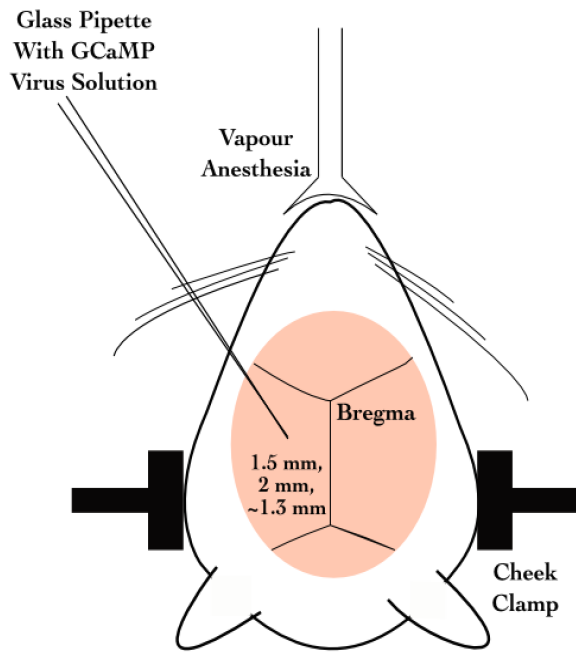


**Figure 24:** Schematic representation for stereotaxic viral injection.

Later on, we switched to directly using GCaMP6f transgenic mice (background: C56BL/6) which express GCaMP6f in the Hippocampus [Tg(Thy1-GCaMP6f)GP5.17Dkim JAX stock #025393]. This helped us circumvent the dye loading or viral injection steps, aiding in the potential success of the preparations, by way of tissue health and recording quality.

## **Results - Imaging**

### **2-Photon calcium imaging of hippocampal CA1, *in vivo***

The CA1 cell body layer is ~200 µm deep, in through the hippocampal surface. At these depths, scattering of excitation as well as emission light is significant. However, we are able to image at these depths with Two-Photon Imaging LASER Scanning Imaging (810 nm for OGB-1 and 910 nm for GCaMP5/GCaMP6f), where a high intensity pulsed LASER allows for two photons to near instantaneously excite fluorophores in a thin z-slice plane which is the focal plane of the Objective. Our LASER, the Coherent Chameleon Ultra II emits ~3 W at 810 nm, and ~2 W at 910 nm. At these depths, there is scattering of emitted photons. However, since only the focal plane is excited any and all emitted photons that we capture are part of the signal. We use a Nikon 16x water immersion, 0.8 NA, 3 mm working distance Objective (N16XLWD-PF), to get a large field of view.

### **Acute Imaging of OGB-1 loaded hippocampal CA1, *in vivo***

We injected OGB-1 dye into brain tissue for our acute imaging experiments (see Methodology for details). OGB-1 spreads throughout the cytoplasm and neuropil, and infiltrates the cell nucleus, giving the cells the appearance of solid circles (cells). The cell body (soma)

ranges from 10-15  $\mu\text{m}$  depending on the orientation of the imaging layer in 3D tissue space (Figure 25A).

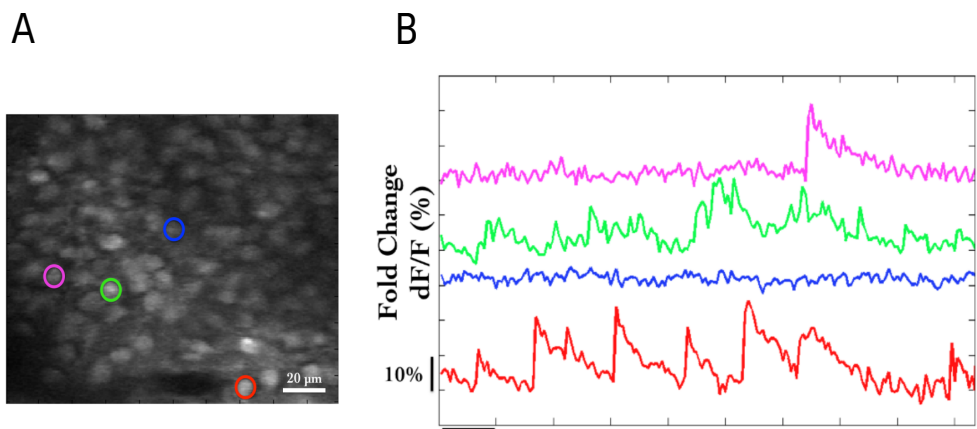


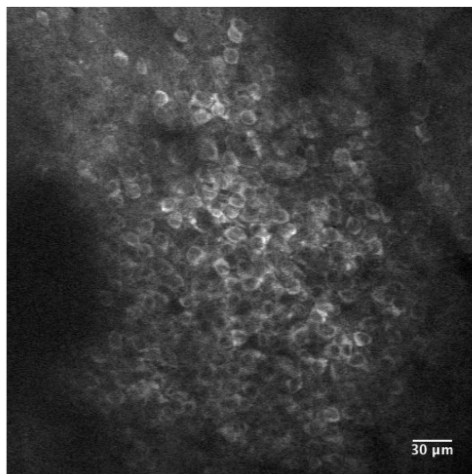
**Figure 25:** (A) Representative Two-Photon Calcium Image of a plane of Hippocampal CA1 cells, bolus loaded with Oregon Green Bapta-1 (OGB-1), at an instant in time. Example cells marked out post-hoc as pink, green, blue and red. Scale bar 20  $\mu\text{m}$ . (B) Representative  $dF/F$  (%) traces for the calcium activity. Recorded in a single 10s video for example cells – pink, green, blue, and red. Scale bar 1 sec; 10%  $dF/F$ .

Each cell in the recorded region of interest (ROI), is identified, marked out (in pixel identity), based on local activity of correlated pixels in the time series movies. The average intensity of the pixels corresponding to each cell for each frame in each recording video, is saved as the raw calcium fluorescence trace. Next, these raw calcium traces are baseline normalized to equate the baselines for each cell at 0, and describe the dynamic range of the intensity values as 0 to 1, or 1 to 100%. The corresponding time series of baseline normalized  $dF/F$  for the representative example cells are shown (Figure 25B; Figure 28B).

## **Chronic imaging of hippocampal CA1 using GCaMP**

For chronic imaging, tissue health was of paramount concern since it could easily degrade in time (Figure 26). With practice and standardization, we were able to get the preparations to survive for 2-4 weeks at very good signal-to-noise. Preparations that resulted in very poor signal-to-noise were often recorded but have been filtered out of the data showcased in this thesis. While preparations can sometimes last even months, typically it is crucial to consider if the ROI for recording could provide >20 cells, to continue the experiment. GCaMP is typically designed to be cytosolic and does not typically cross into the cell nucleus. GCaMP labeled cell bodies appear as doughnuts in the imaging slice (Figure 26A; Figure 27).

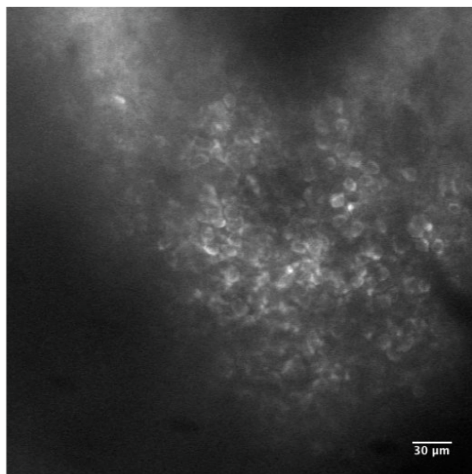
A



DAY 1

Laser Power (at 890 nm): ~50-60 mW  
Supply Voltage to PMT: 13.5 V  
Control Voltage to PMT: 0.5 V  
Preamplifier Sensitivity: 200 nA/V

B



DAY 3

Laser Power (at 890 nm): ~150 mW (!!)  
Supply Voltage to PMT: 12-13 V  
Control Voltage to PMT: 0.5 V  
Preamplifier Sensitivity: 200 nA/V

**Figure 26:** Tissue Degradation over time. Representative Two-Photon Calcium images of a snapshot in time of the Hippocampal CA1 cell body layer on (A) Day 1 after the surgery and (B) Day 3, after the surgery. Scale bar 30 μm.

Recordings with very good signal-to-noise, where the same chronically labeled CA1 cells could be anatomically identified on subsequent days even >2-3 weeks post surgery (Figure 27) were eventually acquired, and are featured in the data presented in Chapter 4.

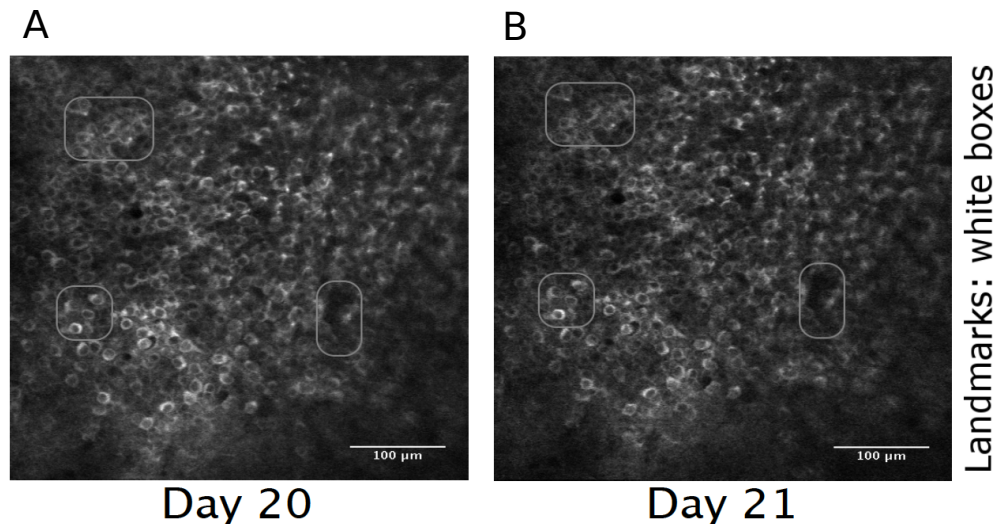


**Figure 27:** Chronic calcium imaging of the same Hippocampal CA1 cells over weeks. Representative 2-Photon images from (A) Day 20, and (B) Day 21, after surgery. Landmarks have been marked and were used to confirm frame registration and identify cells. Scale bar 100  $\mu\text{m}$ .

The magnification and resolution of the field of view are important parameters to consider when balancing magnification for the resolution and the maximization of the number of cells being simultaneously recorded from (Figure 25A; Figure 28A).

While recording at high frame rates for live imaging, we captured a relatively large number of cells ( $\sim 100$ ) in time-series imaging frames, at frame rates of around 10-15 frames per second (FPS). Subsequently, we subjected the animal to various stimuli across trials and saved these images for analysis.

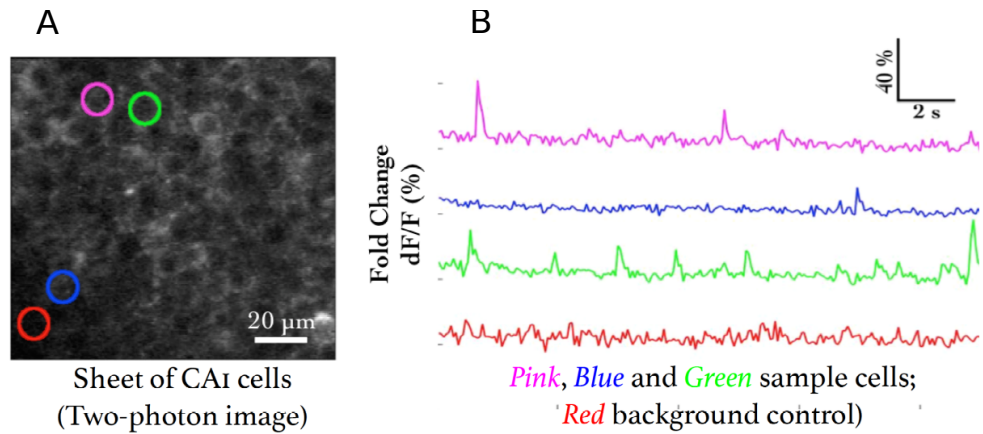


**Figure 28:** (A) Representative Two-Photon Calcium Image of a plane of Hippocampal CA1 cells expressing GCaMP6f at an instant in time. Example cells marked out post-hoc in pink, blue, and green, with no-cell background in red. Scale bar 20  $\mu$ m. (B) Representative dF/F (%) traces for the calcium activity recorded in a single 10s video for example cells – pink, blue, and green, with no-cell background in red. Scale bar 2 sec; 10% dF/F.

### Spontaneous activity during non-stimulus periods

We recorded the calcium activity from a large number of hippocampal CA1 cell bodies, while presenting various neutral and conditioning stimuli, including fairly large periods of time before and after stimulus presentation. Activity of cells, typically observed *in vivo*, in these periods is termed spontaneous activity. Cells may showcase variable rate (number of calcium events per sec) and timing. Given proper signal isolation for identified cells in an ROI, each source or “cell” may be considered independent, *i.e.* - there is minimized cross talk between the fluorescence emitted by each cell body.

## **Spatial organization of activity correlated cells during spontaneous activity**

As part of our Acute Imaging experiments using OGB-1, we studied the Pearson's Correlation Coefficient for the activity traces across all cell pairs, during bouts of spontaneous activity, viz., all frames from the beginning of the trial till the presentation of the stimulus, across all trials. Cell pairs showcased a range of correlation coefficients (Figure 29) and we were able to cluster cells based on activity using Meta-K Means (unpublished data from Dhawale, 2013; Modi et al., 2014). We set the initial seed to  $k = 3$ , with 1000 bootstrap iterations (see Modi et al., 2014 for sensitivity analysis), distance as specified by pair-wise correlation coefficient (Figure 29A; Figure 31A; Figure 32A), and a threshold of 80% to bundle meta-groups.

Correlations were calculated for all frames post the whisker-puff (stimulus), which corresponds to ~8 s of network activity. It is across this period that the clustering was performed.

The correlation analysis was performed to check for consistency across previous recordings in the lab (Modi et al., 2014; Ashesh Dhawale's Thesis). The idea here is to be able to provide proof-of-principle results to confirm if the technique was working. Additionally, although the results are from 1 animal, the session consists of 60 trials for each of the >100 cells recorded. This very preliminary result has been studied and described in detail, previously (Modi et al., 2014).

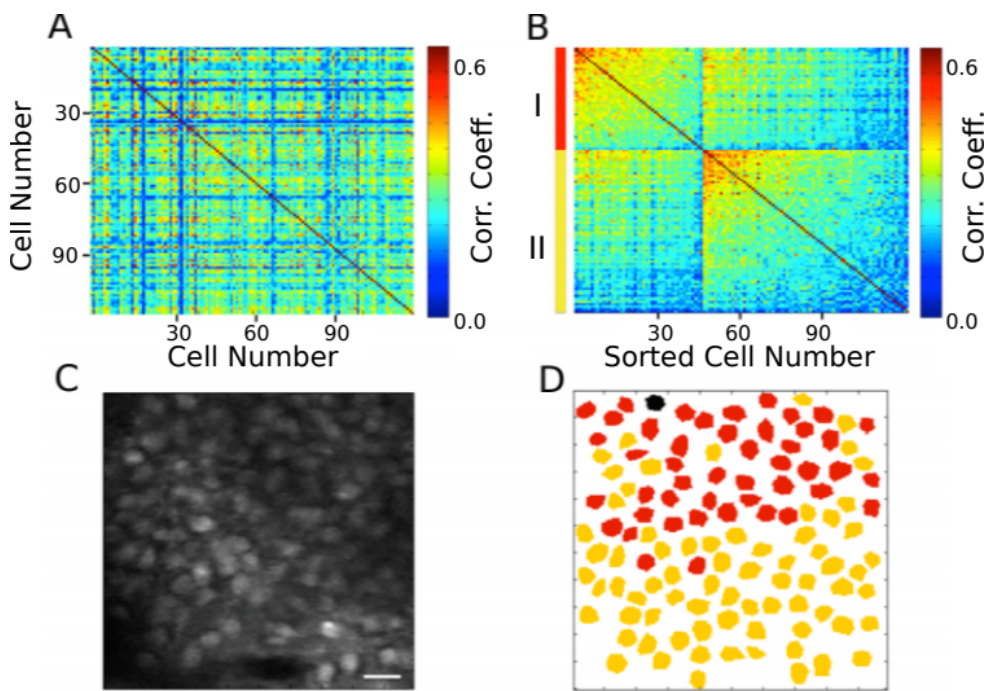


**Figure 29:** (A) Correlation Coefficients for cell pairs from an example two-photon recording. (B) Meta-K Means clustering with cell pairs using the heuristic that within group pairs would be more similar than between group pairs. In this example, the cells were clustered into two groups, I (red) and II (yellow). (C) Two-Photon image of the field of view of cells; same as Figure 25A. (D) Spatial organization of correlated cell pair groups during spontaneous activity (Modi et al., 2014).

## Stimulus evoked responses

We also recorded calcium activity from the same cells during presentation of various neutral stimuli to the animals. Here are the results of the auditory (tone) and somatosensory (whisker) stimulus experiments.

A neutral auditory tone at 5000 Hz (for 1 sec) was presented to the animals N= 6 animals; 25 trials). We observed no clear signs of cell activity modulation by neutral tones. Below, we show an example animal with trial-averaged calcium traces as dF/F (%), across all recorded cells with a 1 sec tone presentation (Figure 30A). We also presented animals to whisker stimulation by playing a 1s long air-puff (5 LPM) to the ipsilateral (left) whisker (N = 5 animals; 25 trials). In this case, we observed whisker-stimulation based cell activity modulation. Below, we show the trial-averaged calcium traces as dF/F (%) of the same example animal as above, presented with a 1 sec whisker-puff (Figure 30B).

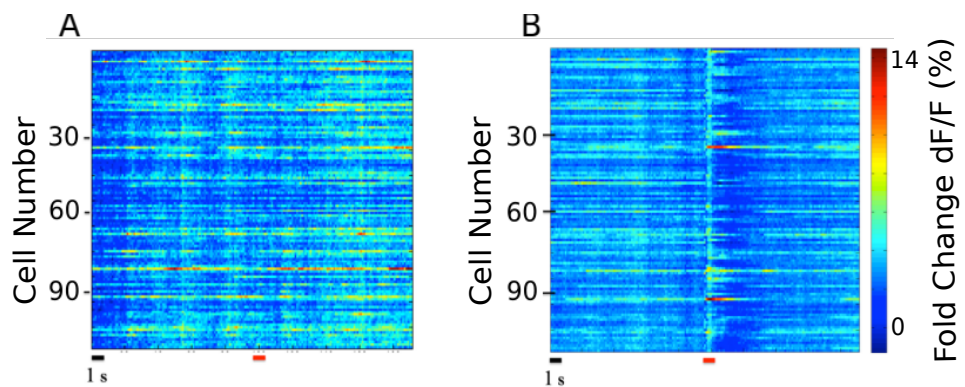


**Figure 30:** (A) Trial-averaged (25 trials) calcium activity from ~100 CA1 cells in trials where a 5000 Hz tone was presented (red bar). (B) Trial-averaged (18 trials) calcium activity from the same cells in trials where a 5 LPM air-puff to the ipsilateral whiskers was presented (red bar). Scale bar 1 sec (black bar).

The damage inflicted to the somatosensory cortex was only on one hemisphere. We presented somatosensory cortex to the ipsilateral whiskers, information that is expected to be processed on the contralateral hemisphere. In any case, we observed responses at the CA1 timed to the presentation of the whisker-puff, unlike trials with tone. We describe tuning modulations across days for the chronically

tracked time cells in the last section of Chapter 3 – “Imaging”. It is very difficult to isolate and therefore comment on the effect of tissue recovery, since we did not directly measure this variable.

### **Spatial organization of activity correlated cells post whisker-puff stimulation**

We attempted the same clustering analysis using Meta-K-Means on the activity profiles of all the cells post presentation of the whisker-puff till the end of the trial, across all trials (~8 s). These functionally correlated cell pair groups were found distributed across the imaging plane with no clear sign of spatial clustering (Figure 31).

Comparing Figure 29D and Figure 31C, we observe that the whisker-puff stimulation results in a change in the spatial map of correlated activity, in the same network of cells.

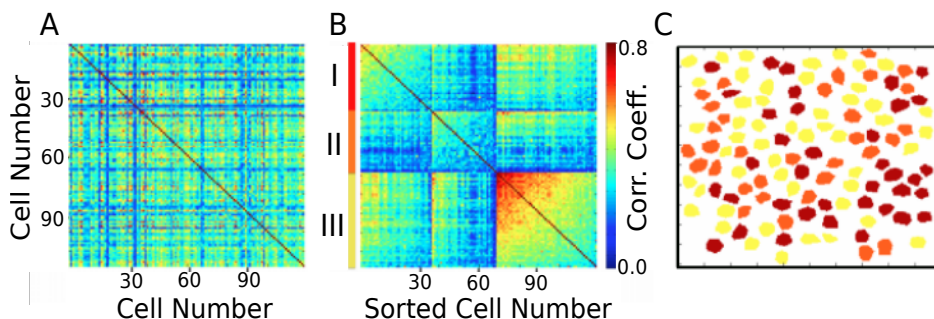


**Figure 31:** (A) Correlation Coefficients for cell pairs from post whisker-puff stimulation periods. (B) Meta-K Means clustering with cell pairs using the heuristic that within group pairs would be more similar than between group pairs. In this example, the cells were clustered into three groups I (red), II (orange), and III (yellow). (D) No clear spatial organization of correlated cell pair groups post whisker stimulation.

We did not have clear values for the exact duration of the persistence of the *in vivo*, hippocampal network state post US. This is actually a very interesting potential experiment, but we did not sub-divide the post-US period for this analysis. At the time, we only wished to see if our results were consistent with those previously published (Modi et al., 2014; Ashesh Dhawale's Thesis), as proof-of-principle for technique standardization.

As a control, we shuffled the trial time points for each cell pseudorandomly, to artificially break activity correlations. When we attempted the Meta-K-Means clustering on this surrogate dataset, we did not observe functional clustering (Figure 32).

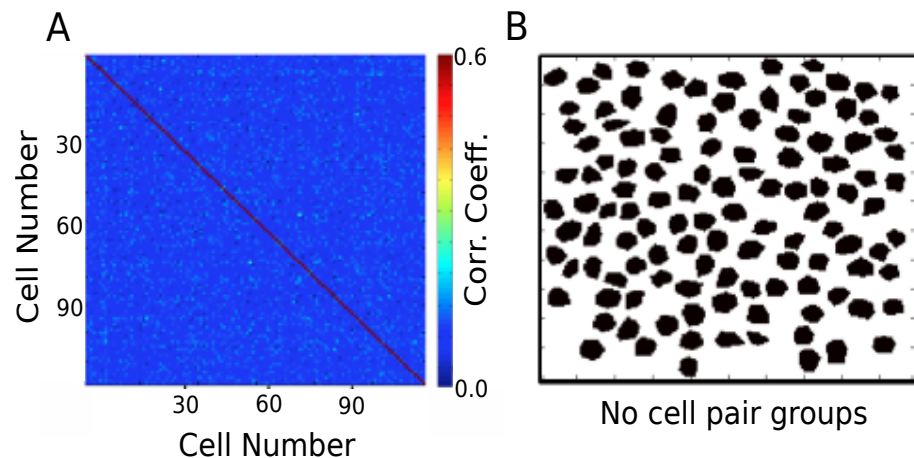


**Figure 32:** (A) Correlation Coefficients for cell pairs from a trial-shuffle control dataset (B) Meta-K Means clustering revealed that there were no cell pair groups identified.

## **Chronic imaging now possible for weeks with the same mouse**

The need for multi-day tracking was mandated for recordings through behavioural training, since the animals typically only learn Trace Eye-Blink Conditioning (TEC; Chapter 2) over the course of 3-7 days (Siegel et al., 2015). A different experiment design would have been to train animals and then perform the hippocampal preparation to record CA1 neural activity while the animal(s) exhibit learnt Conditioned Responses (CRs). However, we argued against this experimental design, on account of the following.

1. The actual cellular and network mechanisms that allow for the animal to learn the behavioural task would be very difficult to study given that the learning period would have passed.
2. The success rate of the hippocampal preparation is typically very low (estimated at ~33-50% based on the last 200 attempts), given potential sources of failures such as tissue decay, bleeding into the imaging window from damaged parts of the hippocampus, implant instability especially with stressed or unsettled experiment animals, and photobleaching from the 2-P excitation LASER over multiple imaging sessions. TEC is typically learnt by >50% animals (Modi et al., 2014; Siegel et al., 2015). We had argued for exposing the hippocampus for imaging before behavioural training since any successful preparations could then be subjected to the relatively more consistent behavioural training.
3. Having the preparation performed before training minimizes the number of times the animal would be subjected to surgery (to just the once), improving chances of animal health through the experiment.

Next, we discuss some preliminary results from the chronic imaging datasets. A non-overlapping set of results that feature in “Chapter 4 - Analysis” of this thesis, have been skipped here for brevity.

## Preliminary analysis to identify time cells

The analysis algorithm pertaining only to the results presented here in “Chapter 3 - Imaging”, was adapted from William Mau’s Temporal Information method (Mau et al., 2018; Chapter 4 – “Analysis”). This version of the algorithm is expected to be subject to some degree of Type I (false positives) and Type II (false negative) errors.

Subsequently, the algorithm was developed to the extent of the Python/C++ implementation featured in “Chapter 4 – Analysis”, with much superior prediction performance.

1. We applied a filter to select for cells that had activity in >25% of trials (irrespective of tuning)
2. We then develop Peri-stimulus Time Histograms (PSTH), using Area Under the Curve for a binsize of 3 frames, centering the “0 ms” to the onset of the Conditioned Stimulus for visualization.
3. Next, we estimate Temporal Information (TI), using

$$TI = 1/\lambda * \sum_j \lambda_j \log_2 (\lambda_j / \lambda) P_j$$

where,

$\lambda$ : Average Transient rate for each cell

$\lambda_j$ : Average transient rate for each cell in bin “j”

$P_j$ : Probability that the mouse was in time bin “j”

For every trial, we also random shuffled the frame points to develop a random activity model (1000 times) and ensure that  $\lambda > \lambda_{\text{rand}}$  in more than 99% of the models. Filtering for cells active in >25% trials with a  $\lambda > \lambda_{\text{rand}}$  in >99% shuffles along with the estimation of TI, provided us a handle on reliability.

We define time cells as cells with a higher probability of eliciting activation (tuning fields) to specific temporal landmarks across trials, rather than uniformly over the whole trial. For the results described in this chapter (Chapter 3 – “Imaging”), our temporal information calculation was used as a functional definition for time cells.

### Time Cells

During the experience of temporally organized events or stimuli, in this case post training to Trace Eye-Blink Conditioning, a rough contingent of ~20% of the total cells recorded, were observed to showcase time-locked calcium activity mapping the Blue LED or Conditioned Stimulus (CS) to the air-puff or Unconditioned Stimulus (US). These cells were classified as time cells. Here are some example time cells (Figure 33).

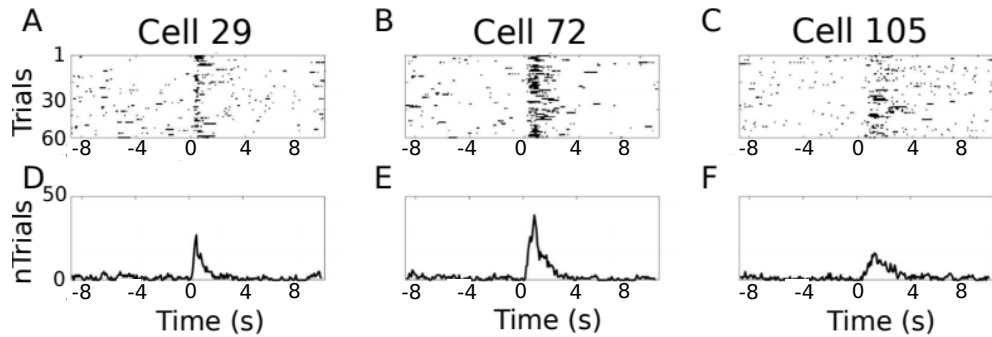


**Figure 33:** Example Time Cells visualized as event raster plots (A, B, C), along with the trial-summed activity profiles (D, E, F) suggesting ~50% hit trials, for cells 29 and 72 from Session 1 (session type 5) with mouse M26, and slightly lower reliability (~25% hit trials) from cell 105. **The Conditioned Stimulus (CS; blue LED) is presented at time 0 ms.**

## Other Cells

On the other hand, most cells did not clear our analysis algorithm checkpoints and were classified as other cells. Here are some example Other Cells (Figure 34) from the same session with mouse M26 (Session 1; session type 5).

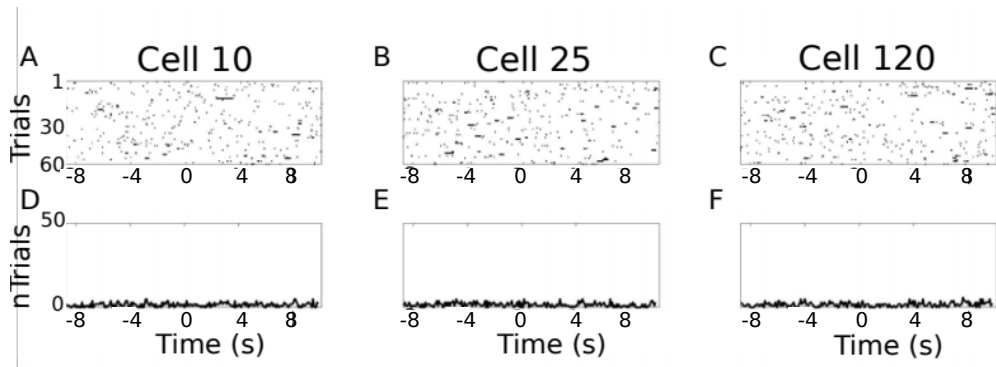


**Figure 34:** Example Other Cells visualized as event raster plots (A, B, C), along with the trial-summed activity profiles (D, E, F) for cells 10, 25, and 120 from Session 1 (session type 5) with mouse M26. **The Conditioned Stimulus (CS; blue LED) is presented at time 0 ms.**

Considering only the classified time cells, we sorted cells based on the time of the peak of the trial-average activity and a spatiotemporal sequence was visualized (Figure 35; also see “Chapter 4 - Analysis Figure 7H”). Peri-stimulus time histograms (PSTH) or event time histograms (ETH) were developed by summing the number of threshold crossing activity events per bin (bin size = 3 frames/bin or ~200 ms/bin at 14.5 Hz) across trials. Different cells showcase different widths for ETH or tuning curves (Figure 35A; Figure 35B).

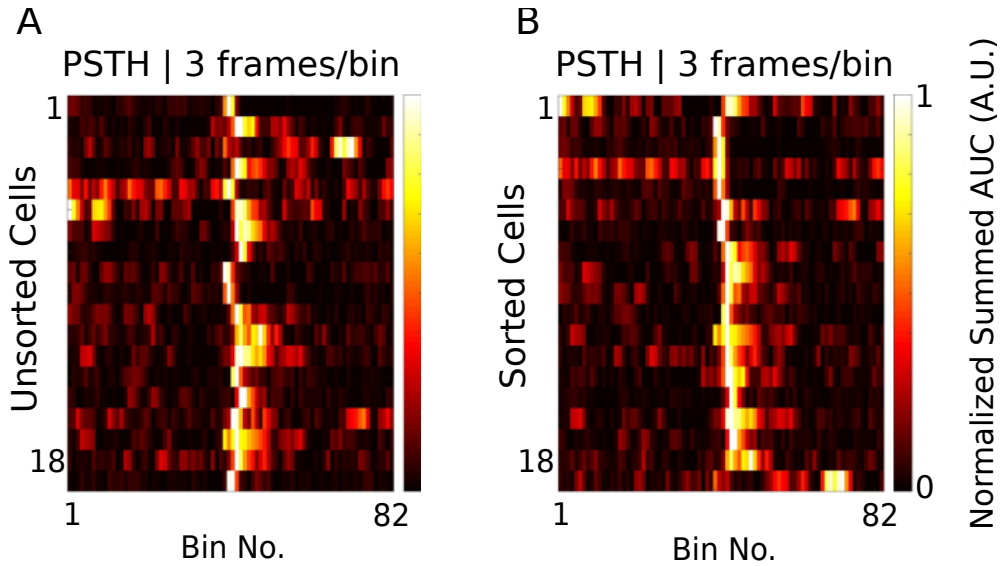


**Figure 35:** Event Time Histograms or tuning curves for Identified Time-Locked Cells with trial-summed peaks in session 4 of training (session type 5) with mouse M26. (A) Unsorted list of Time cells. (B) Peak-sorted list of the same cells. Here, 1 bin = 3 frames =  $\sim 210$  ms (sampling rate 14.5 Hz without binning;  $\sim 5$  Hz with binning). As per the (legacy) session type 5 protocol, the CS (50 ms Blue LED flash) was presented in frame bin 39, followed by a stimulus-free trace interval during frame bins 40 and 41, and then the US (50 ms airpuff to ipsilateral eye) was presented in frame bin 42.

We did not observe any obvious trend in the temporal information of time cells with peak times. For the same cells (as in Figure 35), we now look at the actual Temporal Information estimates plotted against sorted time cells (Figure 36).

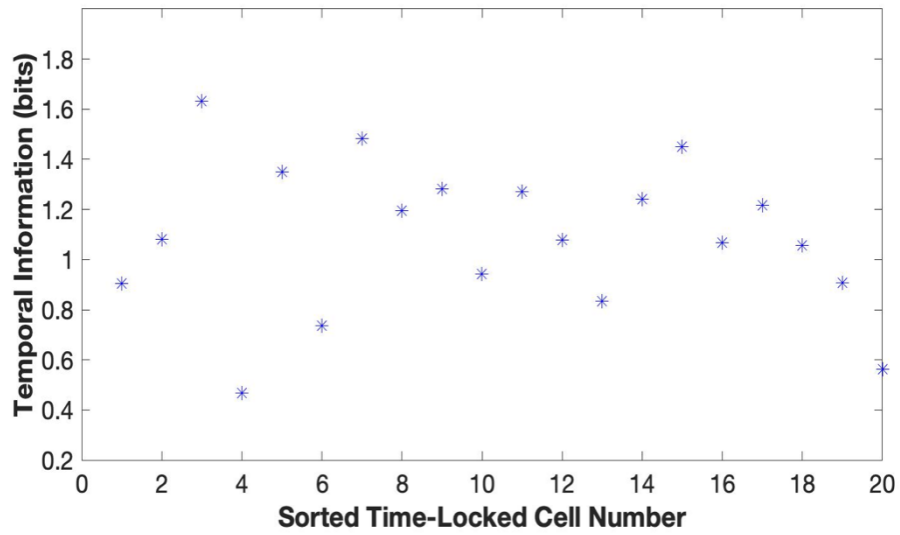


**Figure 36:** Temporal Information (bits) vs Sorted time cell number from the analytically identified Time Cells in Session 4 (session type 5) with mouse M26. No clear trend was observed.

It has been observed in time cell literature as well as in our real physiology recordings that time cells with tuning to later time points in a trial, tend to have wider tuning curves (B. J. Kraus et al., 2015; MacDonald et al., 2011, 2013; Mau et al., 2018; Pastalkova et al., 2008). This is why no obvious trend in a graph of Temporal Information vs time of peak sorted time cells, seemed curious enough to mention in the thesis. However, while we report the observation, we made no attempts to delineate further detail, given a limited number of observations. This legacy adaptation of the temporal information calculation had not been benchmarked and thus the result was not certain, at the time. Subsequently, we have observed similar results in other lab colleague's recordings, and avoided further discussion, with regard to the scope of this thesis.

## **Tuning, re-tuning, and de-tuning of time cells across sessions**

A crucial advantage of the chronic preparation was that many anatomically aligned and classified cells (as cell ROIs), could be recorded from over several days and sessions, to look for possible changes in calcium activity profiles across sessions in the same set of cells.

We noticed some evidence for an expansion of the set of identified time cells with sessions, up to a reliable pool of ~20% time cells. Altogether, from the pool of chronically aligned cells (across sessions), there was an increase from 7.7% to 23.1% of time cells. Considering the full cohort cells (irrespective of tracking across multiple training sessions) the increase was from 7.2% to 21.1% time cells. Here are

the classified time cells between two independent recording sessions, early in training (Figure 37).

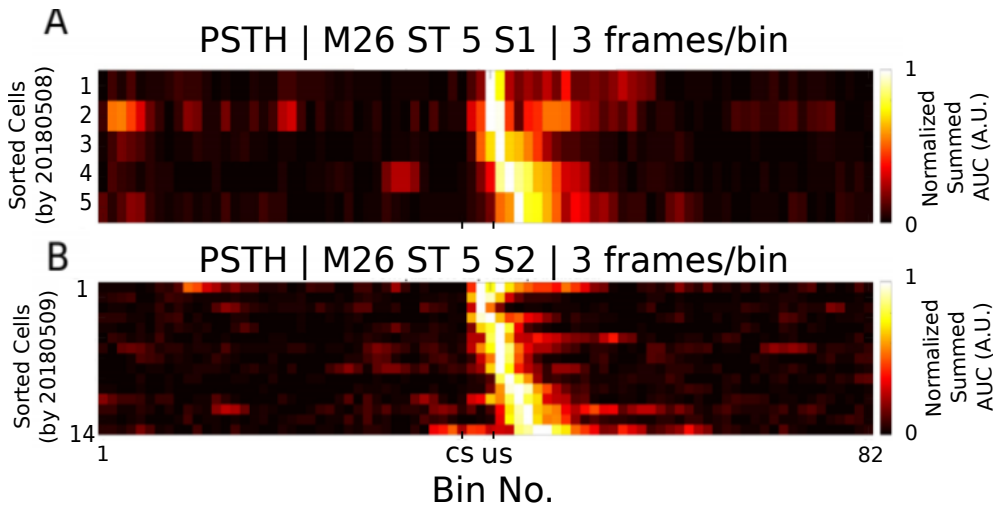


**Figure 37:** More time cells observed to attain tuning as training sessions. Event Time Histograms of the identified set of time cells between A) Sessions 1 and (B) Session 2, with mouse M26 (session type 5).

The same may also be visualized as trial-averaged calcium activity profiles for all recorded cells across independent recording sessions (Figure 38).

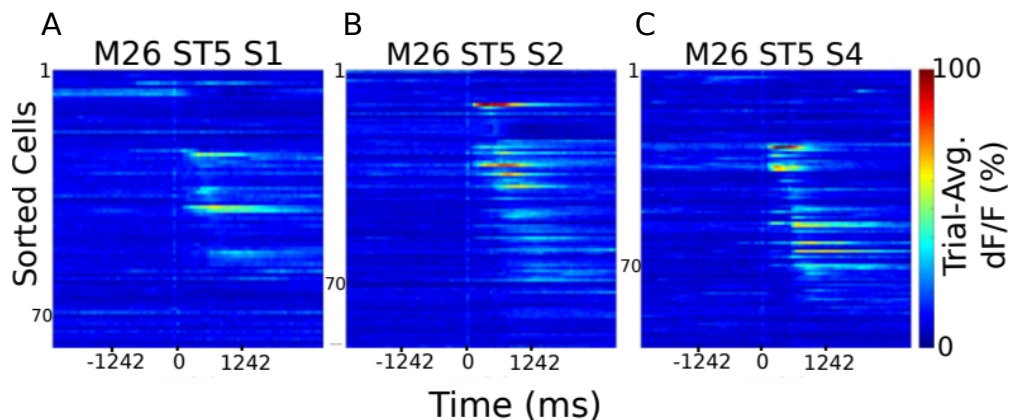


**Figure 38:** Sorted Time Cells form Sequences that develop with learning. Trial-Averaged calcium activity traces for all recorded cells across A) Session 1, B) Session 2, and C) Session 4, with mouse M26 (sessiontype 5). Time 0 ms was aligned to the CS. The CS + Trace + US interval lasted from 0-600 ms, here.

Chronically tracked time cells that showed reliable tuning across sessions were then compared to look for any shifts in the peak tuning bin. We observed examples of cells that maintained their tuning across pairs of sessions (Figure 39).

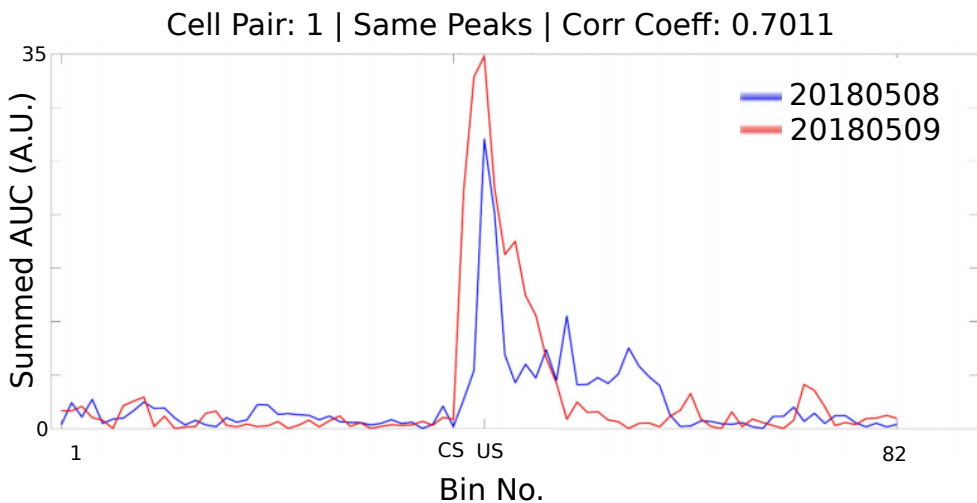


**Figure 39:** Same/similar tuning across session 1 and session 2 for this example time cell. Blue Event Time Histograms represent the tuning curve for the cell for session 1 (date: 20180508) and Red represent the same but for session 2 (date: 20180509). Pearson's correlation coefficient between the two session pairs was 0.7011.

Here are examples wherein the tuning curve peaks shift to earlier time points, across sessions (Figure 40) for Mouse M26, session type 5, session 1 vs 2.

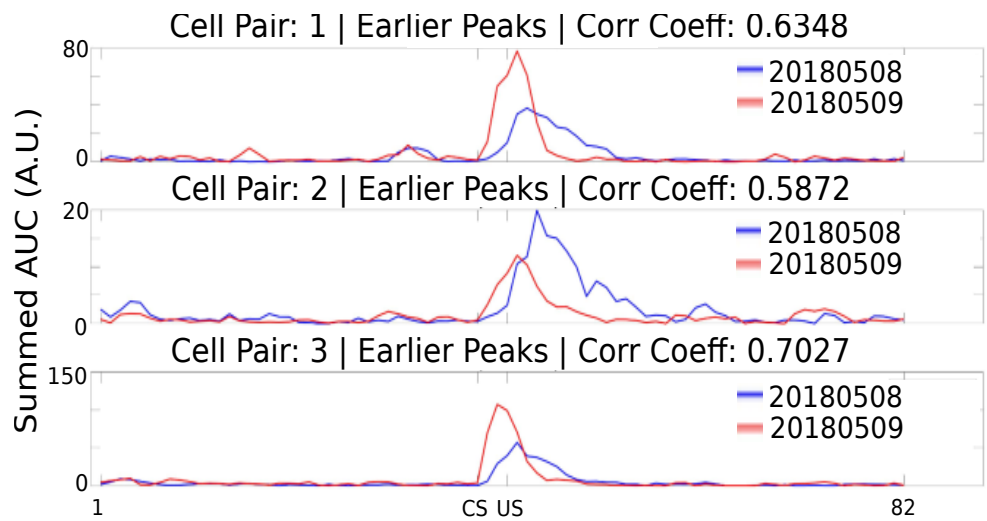


**Figure 40:** Three example chronically tracked cell pairs with tuning peaks arriving earlier with training sessions (rows). Blue Event Time Histograms represent the tuning curve for any cell for session 1 (date: 20180508) and Red represent the same but for session 2 (date: 20180509). Pearson's correlation coefficient between the session pairs was 0.6348, 0.5872 and 0.7027 for A) cell pair 1, B) cell pair 2, and C) cell pair 3, respectively.

Here is an example of a cell showcasing de-tuning for the CS-US interval, across sessions (Figure 41), potentially with a new, delayed peak almost 100 frames later.

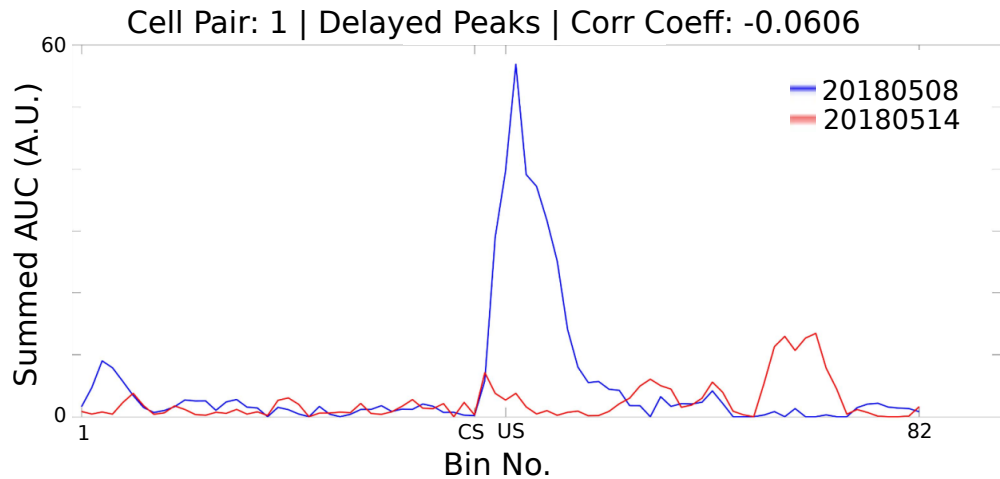


**Figure 41:** Example chronically tracked cell pair with de-tuning between session 1 and 4. Blue Event Time Histograms represent the tuning curve for the example cell for session 1 (date: 20180508) and Red represent the same but for session 4 (date: 20180514). Pearson's correlation coefficient between the two curves was -0.0606.

A full summary of the correlation based peak timing analysis for chronically identified time cells with mouse M26 is shown (Figure 42). Across all same cell pairs (~60% of all session-wise cells tracked; ~80 cells), there was positive correlation ( $>0.2$ ) in 71% of Time Cells (Figure 42A). Typically, we observed only at best a correlation coefficient of  $\sim 0.6\text{-}0.8$  across cell pairs (see Figures 29 and 31). We chose 0.2 as the threshold, accordingly.

Also a comparison of the tuning curve peaks between the same time cell pairs (Figure 42B) revealed that a majority of the re-tuned peaks occurred earlier in time, going across sessions (71%), with an equal

proportion of cells without much re-tuning (14%) or de-tuning to later time points (14%).

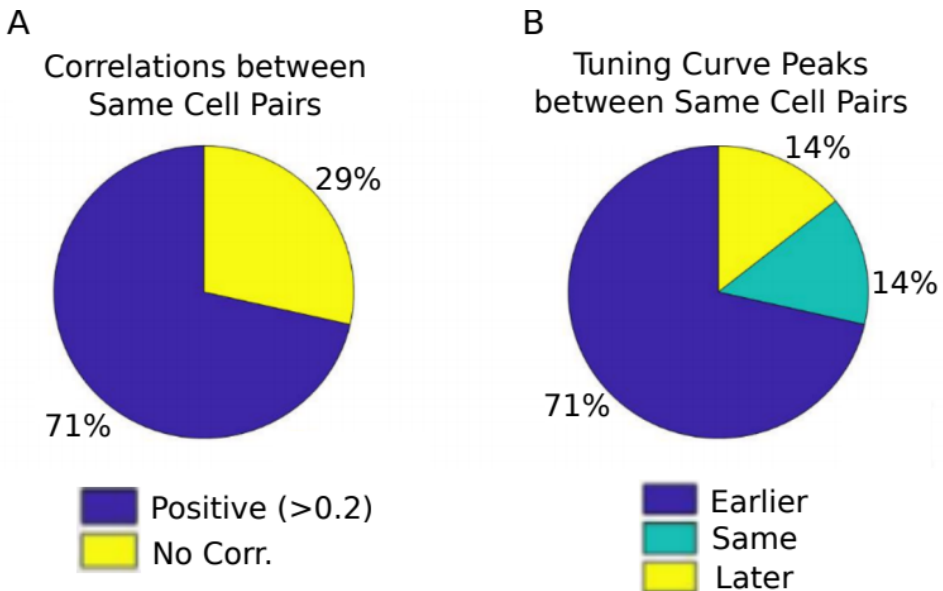


**Figure 42:** Comparing chronically tracked time cells across sessions for all matched cell pairs by (A) Correlation Analysis, and (B) Timing of peaks.

A summary of the key preliminary results observed using real physiology data is as follows.

1. Time cell tuning curve peaks typically began only after the presentation of the CS.
2. The width of the tuning curve peaks for time cells increased with tuning to later frame bins. This was consistent with the recordings presented in literature under physiological conditions (B. Kraus et al., 2013; B. J. Kraus et al., 2015; MacDonald et al., 2011, 2013; Mau et al., 2018; Pastalkova et al., 2008).
3. Pairwise time cell tuning curves for different time cells may have some overlap in timing, but peaks were observed in all frame bins between the CS and the US. This particular observation is confounded

by the short number of Trace period frames recorded and the requirement to consider 3 recording frames to every bin (Mau et al., 2018), decreasing the effective sampling rate even further (14.5 Hz without binning, to ~5 Hz with binning). However, the observation is still consistent with previous literature (B. Kraus et al., 2013; B. J. Kraus et al., 2015; MacDonald et al., 2011, 2013; Mau et al., 2018; Modi et al., 2014; Pastalkova et al., 2008).

4. A surprisingly large number of time cells could be identified with tuning peaks for frame bins occurring after the termination of the US. Single cell measurements tend to define responses up to 200-1000 ms post US. Our own correlation-based clustering analysis was across the whole post US phase (vs pre-stim phase), which corresponded to ~8s. It was surprising to us, that such a wide window post-US period could still reveal distinctly different spatial clustering to a comparable ~8s window pre-CS.

5. Considering all chronically tracked cells, the classified and sorted time cells formed sequences that were dynamic across learning sessions. Many time cells developed tuning curves with sessions while some time cells lost their tuning.

6. For the majority of time cells, re-tuning occurred with initial tuning to the timing of the US in earlier sessions, followed by a shift to earlier time points for the tuning peak, as training progressed through sessions.

Our preliminary imaging and behaviour results describe neuronal sequence activations based on the emergence or re-tuning dynamics of temporal tuning by time cells, during early phases of behavioural acquisition, in a chronically tracked fashion. Future directions to be explored in the lab include studying the reliability of a larger pool of

chronically tracked cells with switches in the inter-stimulus interval (ISI) between the CS and the US as well as with a larger palette of different stimuli testing out a battery of Conditioned Stimuli (CS1, CS2, etc.) and Unconditioned Stimuli (US1, US2, etc.). The goal is to understand how well the internal neural spatiotemporal CA1 sequence maps to the external behavioural protocol parameters, *in vivo*.

## Bibliography

- Abe, R., Sakaguchi, T., Matsumoto, N., Matsuki, N., & Ikegaya, Y. (2014). Sound-induced hyperpolarization of hippocampal neurons. *Neuroreport*, 25(13), 1013–1017.  
<https://doi.org/10.1097/WNR.0000000000000206>
- Andersen, P., Morris, R., Amaral, D., Bliss, T., & O'Keefe, J. (Eds.). (2006). *The Hippocampus Book*. Oxford University Press.  
<https://doi.org/10.1093/acprof:oso/9780195100273.001.0001>
- Attardo, A., Fitzgerald, J. E., & Schnitzer, M. J. (2015). Impermanence of dendritic spines in live adult CA1 hippocampus. *Nature*, 523(7562), 592–596. <https://doi.org/10.1038/nature14467>
- Bellistri, E., Aguilar, J., Brotons-Mas, J. R., Foffani, G., & de la Prida, L. M. (2013). Basic properties of somatosensory-evoked responses in the dorsal hippocampus of the rat. *The Journal of Physiology*, 591(10), 2667–2686. <https://doi.org/10.1113/jphysiol.2013.251892>
- Dhawale, A. K. (2013). *Temporal and spatial features of sensory coding in the olfactory bulb and hippocampus*. Tata Institute of Fundamental Research.
- Dombeck, D. A., Harvey, C. D., Tian, L., Looger, L. L., & Tank, D. W. (2010). Functional imaging of hippocampal place cells at cellular resolution during virtual navigation. *Nature Neuroscience*, 13(11), 1433–1440. <https://doi.org/10.1038/nn.2648>
- Fanselow, M. S., & Dong, H.-W. (2010). Are the dorsal and ventral hippocampus functionally distinct structures? *Neuron*, 65(1), 7–19. <https://doi.org/10.1016/j.neuron.2009.11.031>
- Harvey, C. D., Collman, F., Dombeck, D. A., & Tank, D. W. (2009). Intracellular dynamics of hippocampal place cells during virtual navigation. *Nature*, 461(7266), 941–946. <https://doi.org/10.1038/nature08499>
- Hjorth-Simonsen, A., & Jeune, B. (1972). Origin and termination of the hippocampal perforant path in the rat studied by silver

- impregnation. *The Journal of Comparative Neurology*, 144(2), 215–232. <https://doi.org/10.1002/cne.901440206>
- Itskov, P. M., Vinnik, E., & Diamond, M. E. (2011). Hippocampal representation of touch-guided behavior in rats: persistent and independent traces of stimulus and reward location. *PloS One*, 6(1), e16462. <https://doi.org/10.1371/journal.pone.0016462>
- Kaifosh, P., Lovett-Barron, M., Turi, G. F., Reardon, T. R., & Losonczy, A. (2013). Septo-hippocampal GABAergic signaling across multiple modalities in awake mice. *Nature Neuroscience*, 16(9), 1182–1184. <https://doi.org/10.1038/nn.3482>
- Kamondi, A. (1998). *Theta Oscillations in Somata and Dendrites of Hippocampal Pyramidal Cells In Vivo: Activity-Dependent Phase-Precession of Action Potentials*. 261(March), 244–261.
- Kraus, B. J., Brandon, M. P., Robinson, R. J., Connerney, M. A., Hasselmo, M. E., & Eichenbaum, H. (2015). During Running in Place, Grid Cells Integrate Elapsed Time and Distance Run. *Neuron*, 88(3), 578–589.  
<https://doi.org/10.1016/j.neuron.2015.09.031>
- Kraus, B., Robinson, R., White, J., Eichenbaum, H., & Hasselmo, M. (2013). Hippocampal “Time Cells”: Time versus Path Integration. *Neuron*, 78(6), 1090–1101.  
<https://doi.org/10.1016/j.neuron.2013.04.015>
- Lovett-Barron, M., Kaifosh, P., Kheirbek, M. A., Danielson, N., Zaremba, J. D., Reardon, T. R., Turi, G. F., Hen, R., Zemelman, B. V, & Losonczy, A. (2014). Dendritic inhibition in the hippocampus supports fear learning. *Science (New York, N.Y.)*, 343(6173), 857–863. <https://doi.org/10.1126/science.1247485>
- MacDonald, C. J., Carrow, S., Place, R., & Eichenbaum, H. (2013). Distinct hippocampal time cell sequences represent odor memories in immobilized rats. *The Journal of Neuroscience : The Official Journal of the Society for Neuroscience*, 33(36), 14607–14616. <https://doi.org/10.1523/JNEUROSCI.1537-13.2013>
- MacDonald, C. J., Lepage, K. Q., Eden, U. T., & Eichenbaum, H. (2011). Hippocampal “time cells” bridge the gap in memory for discontiguous events. *Neuron*, 71(4), 737–749.  
<https://doi.org/10.1016/j.neuron.2011.07.012>
- Mau, W., Sullivan, D. W., Kinsky, N. R., Hasselmo, M. E., Howard, M. W., & Eichenbaum, H. (2018). The Same Hippocampal CA1 Population Simultaneously Codes Temporal Information over Multiple Timescales. *Current Biology*, 28(10), 1499-1508.e4.  
<https://doi.org/10.1016/j.cub.2018.03.051>
- Modi, M. N., Dhawale, A. K., & Bhalla, U. S. (2014). CA1 cell activity sequences emerge after reorganization of network correlation

- structure during associative learning. *eLife*, 3, e01982–e01982.  
<https://doi.org/10.7554/eLife.01982>
- Moser, M.-B., & Moser, E. I. (1998). Distributed encoding and retrieval of spatial memory in the hippocampus. In *The Journal of Neuroscience* (Vol. 18, pp. 7535–7542). Society for Neuroscience.
- Nakashiba, T., Young, J. Z., McHugh, T. J., Buhl, D. L., & Tonegawa, S. (2008). Transgenic inhibition of synaptic transmission reveals role of CA3 output in hippocampal learning. *Science (New York, N.Y.)*, 319(5867), 1260–1264.  
<https://doi.org/10.1126/science.1151120>
- Pachitariu, M., Stringer, C., Dipoppa, M., Schröder, S., Rossi, L. F., Dalgleish, H., Carandini, M., & Harris, K. D. (2017). Suite2p: beyond 10,000 neurons with standard two-photon microscopy. *BioRxiv*, 61507. <https://doi.org/10.1101/061507>
- Pastalkova, E., Itskov, V., Amarasingham, A., & Buzsaki, G. (2008). Internally Generated Cell Assembly Sequences in the Rat Hippocampus. *Science*, 321(5894), 1322–1327.  
<https://doi.org/10.1126/science.1159775>
- Peron, S. P., Freeman, J., Iyer, V., Guo, C., & Svoboda, K. (2015). A Cellular Resolution Map of Barrel Cortex Activity during Tactile Behavior. *Neuron*, 86(3), 783–799.  
<https://doi.org/10.1016/j.neuron.2015.03.027>
- Siegel, J. J., Taylor, W., Gray, R., Kalmbach, B., Zemelman, B. V., Desai, N. S., Johnston, D., & Chitwood, R. A. (2015). Trace Eyeblink Conditioning in Mice Is Dependent upon the Dorsal Medial Prefrontal Cortex, Cerebellum, and Amygdala: Behavioral Characterization and Functional Circuitry. *ENeuro*, 2(4), ENEURO.0051-14.2015. <https://doi.org/10.1523/ENEURO.0051-14.2015>
- Sofroniew, N. J., Flickinger, D., King, J., & Svoboda, K. (2016). A large field of view two-photon mesoscope with subcellular resolution for in vivo imaging. *eLife*, 5(JUN2016), 1–20.  
<https://doi.org/10.7554/eLife.14472>
- Stosiek, C., Garaschuk, O., Holthoff, K., & Konnerth, A. (2003). In vivo two-photon calcium imaging of neuronal networks. *Proceedings of the National Academy of Sciences of the United States of America*, 100(12), 7319–7324.  
<https://doi.org/10.1073/pnas.1232232100>
- Suh, J., Rivest, A. J., Nakashiba, T., Tominaga, T., & Tonegawa, S. (2011). Entorhinal cortex layer III input to the hippocampus is crucial for temporal association memory. *Science (New York, N.Y.)*, 334(6061), 1415–1420.  
<https://doi.org/10.1126/science.1210125>

Vinogradova, O. S. (2001). Hippocampus as comparator: Role of the two input and two output systems of the hippocampus in selection and registration of information. *Hippocampus*, 11(5), 578–598.  
<https://doi.org/https://doi.org/10.1002/hipo.1073>

## **Chapter 4 – Analysis**

Our efforts to identify the best use cases for the various implemented time cell analysis algorithms on the basis of a testbed of user-defined, categorically labeled synthetic data with known ground truth (Project III), have been consolidated into a publication. The early access version of our paper (along with supplementary figures) has been attached.

## Novel Tools and Methods

# Synthetic Data Resource and Benchmarks for Time Cell Analysis and Detection Algorithms

Kambadur G. Ananthamurthy and Upinder S. Bhalla

<https://doi.org/10.1523/ENEURO.0007-22.2023>

National Centre for Biological Sciences - Tata Institute of Fundamental Research, Bellary Road, Bengaluru - 560065, Karnataka, India

## Abstract

Hippocampal CA1 cells take part in reliable, time-locked activity sequences in tasks that involve an association between temporally separated stimuli, in a manner that tiles the interval between the stimuli. Such cells have been termed time cells. Here, we adopt a first-principles approach to comparing diverse analysis and detection algorithms for identifying time cells. We generated synthetic activity datasets using calcium signals recorded *in vivo* from the mouse hippocampus using two-photon (2-P) imaging, as template response waveforms. We assigned known, ground truth values to perturbations applied to perfect activity signals, including noise, calcium event width, timing imprecision, hit trial ratio and background (untuned) activity. We tested a range of published and new algorithms and their variants on this dataset. We find that most algorithms correctly classify over 80% of cells, but have different balances between true and false positives, and different sensitivity to the five categories of perturbation. Reassuringly, most methods are reasonably robust to perturbations, including background activity, and show good concordance in classification of time cells. The same algorithms were also used to analyze and identify time cells in experimental physiology datasets recorded *in vivo* and most show good concordance.

## Significance Statement

Numerous approaches have been developed to analyze time cells and neuronal activity sequences, but it is not clear whether their classifications match, nor how sensitive they are to various sources of data variability. We provide two main contributions to address this: (1) a resource to generate ground truth labeled synthetic two-photon (2-P) calcium activity data with defined distributions for confounds such as noise and background activity, and (2) a survey of several methods for analyzing time cell data using our synthetic data as ground truth. As a further resource, we provide a library of efficient C++ implementations of several algorithms with a Python interface. The synthetic dataset and its generation code are useful for profiling future methods, testing analysis toolchains, and as input to computational and experimental models of sequence detection.

## Introduction

The mammalian hippocampus is important for the formation of several kinds of memory, one of which is the association between stimuli occurring separately in time. Time cells were originally described using tuning curves from single-unit recordings of cellular activity when rats ran on a running wheel in between behavioral decisions (Pastalkova et al., 2008). These cells exhibited time tuning of the order of seconds. Several further studies have shown that small populations of hippocampal CA1 cells

fire in time-locked sequences, “bridging” the time gap between stimulus and response in temporal delay tasks lasting several seconds (Pastalkova et al., 2008; MacDonald et al., 2011, 2013; Kraus et al., 2013). Cellular calcium imaging studies have also been used to report time cells, albeit at slower sampling rate (Modi et al., 2014; Mau et al., 2018). For example, similar interval tiling properties of hippocampal CA1 neurons were observed on much shorter, 500 ms timescales in a Trace Eyeblink Conditioning (TEC) task (Modi et al., 2014). Spontaneous sequential activity

Received January 2, 2022; accepted February 9, 2023; First published February 23, 2023.

The authors declare no competing financial interests.

Author contributions: K.G.A. and U.S.B. designed research; K.G.A. performed research; K.G.A. and U.S.B. analyzed data; K.G.A. and U.S.B. wrote the paper.

has also been reported in free-running animals (Villette et al., 2015). Such cells with a well-defined temporal firing field are commonly termed time cells (MacDonald et al., 2011; Eichenbaum, 2017). However, there is a wide diversity of methods used to detect and characterize time cells, and it is not clear how consistent these methods are in classifying cells as time cells. It is also unclear how sensitive each method may be to a range of physiological sources of variability and noise. A consistent set of benchmarks of classification performance is necessary to draw accurate and comparable conclusions from real physiology data across different methods and different laboratories. Our approach in the current study is not prescriptive, but pragmatic: we ask how existing methods work when we already know exactly which cells are time cells, and we determine how well each method deals with imperfect data.

The major approaches used to identifying time cells are tuning curves (peristimulus time histograms), temporal information (TI), principal component analysis with time offset, support vector machines, and bootstrap analysis of activity peaks. Several studies have used a temporal delay task lasting several seconds, in which a rat runs on a treadmill during the delay period. A temporal information metric (Mau et al., 2018) has been used to find individual time cells in such tasks. A distinct task involves monitoring recurrent sequences of activity during free-running treadmill recordings. Such datasets have been analyzed using offset principal component analysis (Kaifosh et al., 2013; Villette et al., 2015; Malvache et al., 2016), to first denoise two-photon (2-P) data, establish correlation coefficients, and detect hippocampal CA1 sequences. Time cells have also been reported for much shorter duration tasks (~500 ms) such as hippocampus-dependent trace conditioning (Tseng et al., 2004; Modi et al., 2014). Time cells in these 2-P datasets were identified using yet another method, in which bootstrapping was used to determine whether peak activity at a given time was different from chance. This method was termed ratio of ridge/background (Modi et al., 2014). Yet other methods have utilized support vector machines to categorize time cells (Ahmed et al., 2020). Additionally, while the applicability of a variety of algorithms for place cell detection has been previously compared (Souza et al., 2018), we have

K.G.A. and the experiments received support from the Department of Biotechnology Grant BT/PR12255/MED/122/8/2016 (to U.S.B.). National Centre for Biological Sciences-Tata Institute of Fundamental Research (NCBS-TIFR) provided resources for analysis equipment and support to U.S.B. through intramural funds supported by the Department of Atomic Energy, Government of India, Project Identification No. TRI 4006.

Acknowledgments: We thank Daniel Dombeck for help with the chronic preparation for physiological 2-P calcium recording of hippocampal CA1 cells and William Mau for his Temporal Information calculation code. We also thank Vinu Varghese and Bhanu Priya Somashekhar for helpful comments on this manuscript.

Correspondence should be addressed to Upinder S. Bhalla at [bhalla@ncbs.res.in](mailto:bhalla@ncbs.res.in).

<https://doi.org/10.1523/ENEURO.0007-22.2023>

Copyright © 2023 Ananthamurthy and Bhalla

This is an open-access article distributed under the terms of the Creative Commons Attribution 4.0 International license, which permits unrestricted use, distribution and reproduction in any medium provided that the original work is properly attributed.

focused on methods which are fully automatable and which scale well to large datasets, specifically comparing algorithms to detect time cells.

Time cell detection is closely related to sequence detection, which has been fraught with statistical challenges. For example, detection of synfire chains has been the subject of some debate (Ikegaya et al., 2004; Lee and Wilson, 2004; Mokeichev et al., 2007; Schrader et al., 2008). Time cell detection is usually easier, in that in most experiments there is a well-defined initiating stimulus and a known delay or trace phase (however, see Villette et al., 2015). For any cell identified as a time cell, it is desirable to define a score to measure quality or reliability along with decodable time. Hence it is also valuable to be able to compare the score of a time cell across recordings and even between groups, using well defined, analog measures. Each algorithm currently used in the literature implements a different scoring method and it is as yet unclear whether comparable results would be observed with other metrics.

In the current study, we compare these diverse methods by estimating their performance on synthetic test datasets where we controlled all features of the data, including the identity and timing of each time cell. The development of a synthetic dataset serves two purposes. First, it facilitates principled comparison of different methods, since the ground truth is known. Second, it facilitates an analysis over many dimensions of input variance, corresponding to very different experimental and neural circuit contexts. Richness in variety of input data allows for better sampling of the performance of the analyses under many potential conditions. We have explored variance along the key dimensions of noise, timing imprecision, signal widths, frequency of occurrence, as well as several others. To strengthen the applicability of this synthetic data resource to real data, our generated output uses sampled experimental data.

Our experimental data, synthetic dataset, and code base are intended to be a resource for algorithm testing and optimization.

## Materials and Methods

### Animals, chronic implants, and behavioral training

All animal procedures were performed in accordance with the National Centre for 114 Biological Sciences Institutional Animal Ethics Committee (project ID NCBS115 IAE-2016/20(M)), in accordance with the guidelines of the Government of India (Animal Facility CPCSEA registration number 109/1999/CPCSEA) and equivalent guidelines of the Society for Neuroscience.

To chronically monitor the activity of the same population of hippocampal CA1 cells, we implanted two- to four-month-old male and female GCaMP6f mice [Tg(Thy1-GCaMP6f)GP5.17Dkim JAX stock #025393] with an optical window and head-bar using a protocol adapted from previously published methods (Dombeck et al., 2010). Briefly, anesthesia was induced with 2–3% isoflurane in a chamber, and subsequently maintained (breathing rate of ~1 Hz) with 1–2% isoflurane, directly to the mouse's nose using an inverted pipette tip. Surgery was performed on a

temperature-controlled table, maintained at 36.5°C, while the anaesthetized animal was cheek-clamped. After a haircut, a ~5 cm piece of scalp was cut open to reveal the skull. A ~3 mm circular craniotomy was then performed at a position 2 mm caudal and ~1.5 mm lateral to bregma, on the left hemisphere. After gently tearing off the dura, the underlying cortex was carefully aspirated till the corpus callosum (CC) layer, clearing out any blood using repeated washes of cortex buffer (Modi et al., 2014). A small thickness of corpus callosum fibers were then carefully aspirated till horizontal CC fibers were sparse but visible. The cortex buffer was then carefully suctioned out to dry the exposure till tacky. The exposure was then quickly sealed using a thin layer of Kwik-Sil and a coverslip attached to the bottom of a 3 mm steel cannula. This preparation left the CA1 cell body layer ~200 μm below the most exposed tissue. Finally, an imaging head-bar was surgically implanted and fixed to the scalp, using dental cement and skull screws, before the animal was brought out of anesthesia.

The animals were allowed to recover for 1–5 d after implantation, with a further 3–4 d of habituation to the rig. Following this simultaneous behavioral training and 2-P *in vivo* imaging was conducted.

### Trace Eyeblink Conditioning (TEC)

We standardized a multi-session Trace Eyeblink Conditioning (TEC) paradigm to train head-fixed mice, based on previous literature (Siegel et al., 2015). TEC involves an association between a previously neutral conditioned stimulus (CS) with an eyeblink inducing unconditioned stimulus (US), across an intervening, stimulus-free, trace interval. Training involved 60 trials per session, one session a day, for approximately two weeks. The CS was a 50 ms blue LED flash while the US was a 50 ms air-puff to the left eye. The stimulus-free trace interval was 250–750 ms long, depending on the session. Additionally, a pseudorandom 10% of the trials were CS-only probe trials (no US) to test for learning. All behavior routines were controlled by programmed Arduinos. Eyeblinks were measured for every trial, by video camera (Point Gray Chameleon3 1.3 MP Monochrome USB3.0) based detection.

The conditioned response (CR) is observed as a preemptive blink before the US is delivered, in animals that learn the task. The analysis of the behavioral data was performed using custom written MATLAB scripts. In brief, each frame for every trial was:

1. Cropped to get the eye;
2. Binarized to get the pixels defining just the eye, and finally;
3. Given an FEC score from 0 to 1 (see below).

Every trial was then scored as a hit or miss, using the result of a two-sample Kolmogorov-Smirnov test between the FEC during the trace and pre-CS period (1% significance). The performance of an animal for a session was then established as the percentage of hit trials/total trials.

Definitions:

FEC: The fraction of eye-closed is estimated by counting the pixels defining the eye in every image of a time series, normalized by the maximum number of pixels defining the eye, in that session. Thus, every frame was given an analog score from 0 to 1, where,

- 0: fully opened eye
- 1: fully closed eye

CR: The conditioned response is the eye-closing transition during the trace period.

UR: The unconditioned response is the eye-closing transition when the US is delivered.

Performance: Percentage of hit trials/total trials. This allowed us to observe how the animals perform during and across sessions.

### Two-photon imaging

We used a custom-built two photon laser-scanning microscope (Modi et al., 2014) to record calcium activity from 100–150 hippocampal CA1 cell bodies *in vivo*, at cellular resolution. We performed galvo-scans through the imaging window, over a field of view of ~100 × 100 μm<sup>2</sup>, at 14.5 Hz, during TEC (Fig. 1A). An Arduino microcontroller was used to control the behavior routines, and it additionally sent a TTL trigger to initiate the imaging trials. The behavior and imaging were conducted simultaneously to record calcium activity when the animal was learning the task.

Time-series fluorescence data for various cells was extracted using Suite2P (Pachitariu et al., 2017). All further analysis and code development was done on MATLAB R2017b and batch analysis runs were performed on MATLAB R2021a. The average of the fluorescence values for cell specific pixels is then converted into the fold change relative to the baseline (dF/F<sub>0</sub>; F<sub>0</sub> as 10th percentile), for every marked cell, in every trial (Fig. 1B). These dF/F traces were used for the rest of the analysis.

### Curating a library of calcium events

For all synthetic data experiments, we used one good quality 2-P recording session's worth of data from one animal. We mapped our imaging dataset into a matrix of dF/F values for all cells, trials, and frames. We then identified calcium events as signal deviations that were above a threshold (mean ± 2\*SD) for more than four consecutive frames (frame rate: 14.5 Hz or ~70 ms per frame). Once identified, we curated a library for each event by a cell, and saved the respective start indices and widths. Using this library, we generated synthetic data by inserting experimental calcium events into the time series for each simulated cell. This approach just uses a time series of signal bins and amplitudes, hence is signal-agnostic and could be applied to other imaging and recording modalities. In the interests of data integrity, our synthetic datasets were watermarked to be distinguishable from real physiology datasets.

### Generating synthetic data

Synthetic data were generated using a custom-written MATLAB function script “generateSyntheticData()” in the provided code repository. We preallocated and set up a 3-D matrix of zeros (as cells, trials, frames), and added

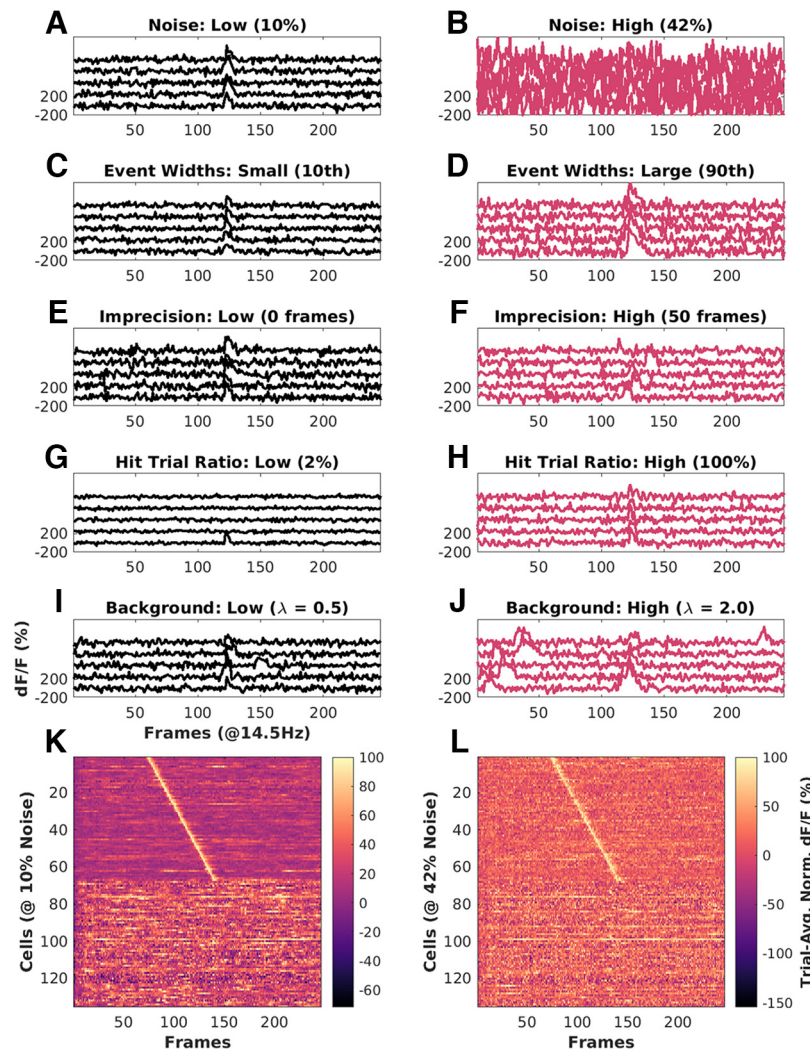


**Figure 1.** Key features of synthetic datasets. Left, Black panels, Low range of features. Right, Red panels, High range of features. **A**, Noise = 10%. **B**, Noise = 42%. **C**, Event width: 10th percentile  $\pm 1$  SD. **D**, Event width 90th percentile  $\pm 1$  SD. **E**, Imprecision at 0 frames FWHM. **F**, Imprecision at 50 frames FWHM. **G**, Hit trial ratio from 0% to 2%. **H**, Hit trial ratio from 0% to 100%. **I**, **J**, Background activity with the number of background spikes per background sampled from a Poisson distribution for with mean ( $\lambda$ ), for **I**:  $\lambda = 0.5$  (low), and **J**:  $\lambda = 2.0$  (high). **K**, **L**, Trial-averaged Calcium traces from example synthetic datasets of 135 neurons, displayed as heatmap sorted by time of peak Ca signal. **K**, Baseline physiology synthetic data trial-average with 10% noise (low) and high background activity ( $\lambda = 2$  to 3 events/trial). **L**, Same as **K** with 42% noise (high) and comparable background activity ( $\lambda = 2$  to 3 events/trial). In both cases, 50% of the cells (top 67) are time cells and the remainder are not. Extended Data Figure 1-1 describes the most important parameters modulated for datasets in each of the three parameter regimes, “Unphysiological,” “Canonical,” and “Physiological,” along with the false positives and false negatives, for each of the 10 implemented algorithms.

calcium events sampled from the Calcium Event Library at frames (time) determined by the synthesis algorithm. The input parameters to this algorithm included timing, noise, imprecision, event width selection, hit trial ratio, background activity, and several others. We aimed to cover the most likely conditions to affect timing and other experiment design properties. In more detail, we generated synthetic datasets using the following control parameters:

- Time cell percent

Value: Number between 0 and 100. This sets the number of cells that are assigned tuned calcium activity as a

percentage of total cells, and controls the number of positive and negative class cells in the dataset.

- Cell order

Value: ‘basic’ or ‘random.’ In ‘basic’ mode, time cells are indexed lower than other cells. In ‘random’ mode, the indices of time cells and other cells are randomly selected. This should have no impact on algorithm detection but is useful for visualization.

- Max hit trial percent

Value: Number between 0 and 100. This sets the maximum possible fraction of total trials, during which a Time Cell will exhibit tuned calcium activity.

- Hit trial percent assignment

Value: ‘fixed’ or ‘random.’ In ‘fixed’ mode, the number of hit trials is set as defined by max hit trial percent. In ‘random’ mode, the number of hit trials is calculated by randomly picking a value from a range ( $\frac{1}{2} \times \text{max hit trials}$ , max hit trials).

- Trial order

Value: ‘basic’ or ‘random.’ In ‘basic’ mode, the hit trials are indexed lower than miss trials. In ‘random’ mode, the indices of hit and miss trials are randomly selected. Specific patterns of hit and miss trials for a session have not been reported in physiology, so this feature is not implemented.

- Event width

Value: {0–100 percentile value, Integer N}. For each cell, this defines the selection of events based on width in frames. The percentile value is estimated from the histogram of all event widths. The variance of this selection is set by “N,” which adds  $N^*SD$  to the selection. All synthetic cells exhibit a range of different calcium events. This is considered an important parameter.

- Event amplification factor

Value: Number from 0 to  $+\infty$ . This allows additional control to multiplicatively amplify any chosen calcium event, before incorporation. Our library was curated from physiologically recorded signals. The default value is 1.

- Event timing

Value: ‘sequential’ or ‘random.’ In ‘sequential’ mode, the time of peak calcium activity is reflected by the indexing of the time cells. In ‘random’ mode, the time of peak calcium activity is randomly dispersed over the trial frame points.

- Start frame

Value: Number from 0 to total number of frames. This sets the timing of the first cell in a time cell sequence.

- End frame

Value: Number from 0 to total number of frames. This sets the timing of the last cell in a time cell sequence.

- Imprecision full width at half max (FWHM)

Value: Number from 0 to total number of frames. This sets the lower and upper bounds for the difference in timing of calcium activity across trial pairs for a time cell. We use this parameter to model trial to trial variability and is considered an important parameter to test.

- Imprecision type

Value: ‘none,’ ‘uniform,’ or ‘normal.’ In ‘uniform’ and ‘normal’ modes, the trial pair Imprecision is picked from a normal and uniform distribution, respectively. In ‘none’ mode, the trial pair Imprecision defaults to 0.

- Noise

Value: ‘Gaussian’ or ‘none.’ In ‘Gaussian’ mode, the noise is sampled as a time-series vector with points from

a Gaussian distribution. In ‘none’ mode, the noise percent defaults to 0.

- Noise percent

Value: Number from 0 to 100. This allows scaling for any sample noise point, based on the max signal value for any cell.

- Add background spikes for time cells

Value: Boolean 0 or 1. This switch controls the incorporation of background (untuned) activity for putative time cells.

- Add background spikes for other cells

Value: Boolean 0 or 1. This switch controls the incorporation of background (untuned) activity for other (nontime) cells.

- Background distribution mean

Value: Number from 0 to  $+\infty$ . This sets the mean ( $\lambda$ ) of the Poisson distribution to sample from when selecting how many background events to add per trial, for any given cell.

### Implementation of a reference quality measure, Q

In order to compare the readouts from the various time-cell detection methods, we implemented a reference measure of quality (Q) of synthetic time cells that used the known inputs to the generation algorithm.

Based on preliminary analysis, we selected following five parameters as the most likely to affect the behavior and detection of time cells:

1. Noise
2. Event width
3. Imprecision
4. Hit trial ratio
5. Background activity

Accordingly, we were able to calculate a reference quality measure, using the following equation:

$$\text{RefQ} = \text{HTR} \times \exp\left(-\{\alpha \times \text{MNP}/100 \times \text{EAF} + \beta \times \text{std. dev. EW}/\text{meanEW} + \gamma \times \text{std. dev. Imp}/\text{Stim Win}\}\right), \quad (1)$$

where HTR: hit trial ratio

MNP: max noise percent (%)

EAF: event amplification factor

EW: event widths (frames)

Imp: imprecision (frames)

Stim Win: stimulus window (frames)

$\alpha$ : 1

$\beta$ : 1

$\gamma$ : 10

The values of  $\alpha$ ,  $\beta$ , and  $\gamma$ , were set to have comparable effects of each of the terms inside the exponent. This reference Q was useful for debugging code and was the basis for a further metric for time cell classification discussed below. A representative synthetic activity trace for ‘low’ and ‘high’ values of each of these five parameters is shown in Figure 1.

All modulations for the datasets in this study along with the estimates for false positives and false negatives, across all algorithms are shown in Extended Data Figure 1-1.

### Separate analysis modules were developed for three categories of analysis

We implemented three analysis modules: *ti*, *r2b*, and *peq*, shorthand for temporal information, ridge-to-background, and parametric equations. The *ti* module implements three algorithms from Mau et al. (2018). The *r2b* module implements two algorithms from Modi et al. (2014). The *peq* module computes estimates for noise, hit trial ratio, event width and imprecision, and estimates a Q score as above. All three methods were implemented in C++ with a PyBind11 interface to Python. This combination is fast and efficient in memory use, and also has the ease-of-use of Python. Thanks to the native MATLAB interface to Python, all three methods can also be called from MATLAB.

### Synthetic datasets generated and analyzed in batch mode

We generated datasets pertaining to parameter sensitivity analysis by modulating one of the four main parameters and setting the others to noninterference levels. In this manner, we devised 99 cases to study in which one of the main parameters was varied. Note that in these cases the resultant activity was in an unphysiological regime because other sources of variation were kept to low levels so as not to interfere with the parameter of interest. With three randomized shuffles, we generated 297 unique datasets.

We wanted to use more realistic datasets, where we would modulate one of the four parameters while keeping the others to ranges typical of physiological data. We devised 12 canonical cases. With 10 randomized shuffles each, we generated 120 additional unique datasets in the canonical regime. Finally, we devised 12 physiological regime cases, identical to those in the canonical regime, with the addition of background (untuned) activity. This yielded another 150 datasets, with randomization.

Altogether, we had 567 unique datasets for our tests, each with 135 cells (total: 76,545 cells), 60 trials, and 246 frames/trial. Except when the percent time cells were modulated, all datasets featured 50% time cells.

We next implemented an analysis pipeline to run all the datasets through the time cell detection algorithms, yielding scores and predictions for each case. Finally, all the scores and predictions were collated for comparison and benchmarks as shown in the schematic (Fig. 2).

### Metrics for time cell classification performance

Recall is inversely proportional to the number of false negatives (Type II error) and is the fraction of true positive class predictions over all positive class ground labels.

$$\text{Recall} = \text{TPR}/(\text{TPR} + \text{FNR}) \quad (2)$$

Precision is inversely proportional to the number of false positives (Type I error) and is the fraction of true positive class predictions over all positive class predictions.

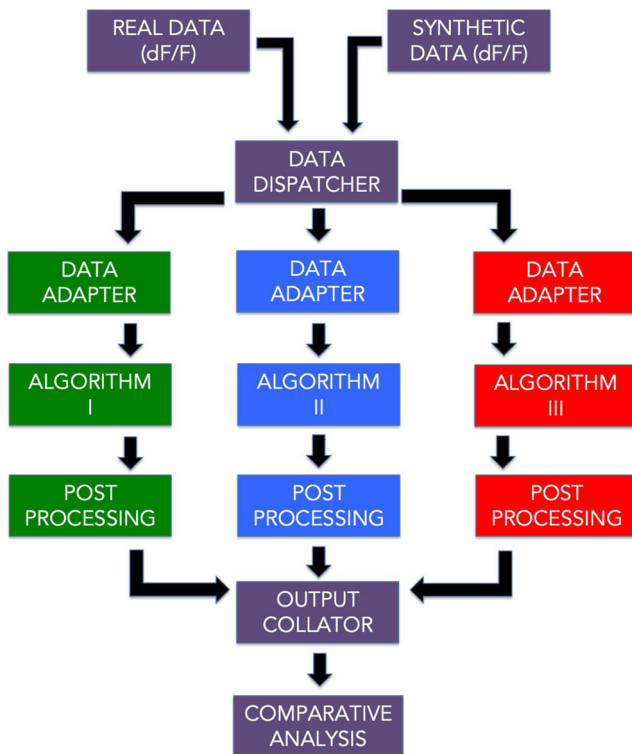


**Figure 2.** A schematic representation of the analysis pipeline. Physiology data as well as synthetic data were analyzed by 10 different implemented algorithms and the output was collated for comparative benchmarks.

$$\text{Precision} = \text{TPR}/(\text{TPR} + \text{FPR}). \quad (3)$$

F1 Score is the harmonic mean of recall and precision.

$$\text{F1 Score} = 2 * \text{Precision} * \text{Recall}/(\text{Precision} + \text{Recall}), \quad (4)$$

where

TPR: true positive rate

FNR: false negative rate

FPR: false positive rate

Here are the definitions for predictive/classification performance evaluation (Table 1).

Here are the important functions provided in the code base (Table 2).

Here are the MATLAB scripts running the comparative analysis and figure generation (Table 3).

### Code and resource availability

The code/software described in the paper is freely available online at <https://github.com/BhallaLab/TimeCellAnalysis>. The code is available as Extended Data 1.

## Results

We developed a pipeline (Fig. 2) with 10 different algorithm implementations for time cell detection, which involve scoring and then classifying cells.

Here, we describe the implementation of each of the methods.

**Table 1: Definitions for predictive/classification performance evaluation**

Ground truth	Prediction/classification	Remark
0/false/other cell	0/false	True negative (TN)
0/false/other cell	1/true	False positive (FP)
1/true/time cell	0/false	False negative (FN)
1/true/time cell	1/true	True positive (TP)

For each detection algorithm, the classification results were compared with known ground truth values to get the total number of true positive (TP), true negative (TN), false positive (FP), and false negative (FN) cases.

### Time cell scoring methods and classification

Temporal information: *tiBoot*, *tiMean*, *tiBoth*, *tiMean-O*, *tiBase-O* (Mau et al., 2018)

Here, we used the algorithm from Mau et al. (2018) as follows. There was an initial criterion of cells to have activity in at least 25% of trials. Their activity was summed into event time histograms with a bin size of three frames. The temporal information (TI) was estimated using Equation 5,

$$TI = 1 \times \lambda_j \times \log_2 \lambda_j \times P_j, \quad (5)$$

where,  $\lambda$  is the average transient rate for each cell;

$\lambda_j$  is the average transient rate for each cell in bin “j”;  $P_j$  is the probability that the mouse was in time bin “j.”

Bootstrapping was used to determine whether each cell had a TI greater than chance. We circularly randomized the frame points to develop a random activity model (1000 iterations) and classified cells as time cells if  $\lambda > \lambda_{rand}$  in >99% of the models for at least two consecutive bins. We implemented the activity filter from Mau et al. (2018); by considering the trial-averaged peak of the calcium traces for each of the cells, and testing for significance using bootstrapping (*tiMean*). A logical AND operation between the prediction lists for *tiBoot* and *tiMean*, provided us with the full Mau et al., 2018 Temporal Information based detection algorithm (*tiBoth*).

Additionally, we used Otsu’s threshold (Otsu, 1979) on the temporal information scores as well as the trial-averaged peaks to get *tiBase-O* and *tiMean-O* using the MATLAB function “graythresh()” (<https://in.mathworks.com/help/images/ref/graythresh.html>). The purpose of adding the Otsu’s threshold-based classification step was to study how well the scores could be classified with a fast thresholding method, rather than the computationally expensive bootstrap.

**Table 2: List of important functions provided in the code base**

Name	Description	Command line	Location	Language
synthesisDemo.m	Command line demo, output to file: “synthData-demo.mat”. Generates a synthetic 2-P time cell dataset file	\$ cd TimeCellAnalysis/rho-matlab/demos && matlab -nodisplay -nosplash -r “synthesisDemo; quit”	rho-matlab/demos	MATLAB
ti_demo.py	Command-line demo, output to console.	\$ python TcPy(ti_demo.py sampleData/sample_synth_data.mat	TcPy	Python interface and C++ numerics
r2b_demo.py	Command-line demo, output to console. Runs Ridge-to-Background analysis from Modi et al. (2014). Reports R2B Mean and R2B Bootstrap classifications	\$ python TcPy(r2b_demo.py sampleData/sample_synth_data.mat	TcPy	Python interface and C++ numerics
peq_demo.py	Command-line demo, output to console. Runs parametric equation analysis from current study. Reports PEQ threshold classification, and estimates for noise, event width, imprecision, and hit trial ratio for dataset	\$ python TcPy(peq_demo.py sampleData/sample_synth_data.mat	TcPy	Python interface and C++ numerics
ground_truth_check.py	Command-line demo, output to console. Uses synthetic data files to assess accuracy of classification by the various Mau and Modi algorithms	\$ python TcPy/ground-truth_check.py sampleData/sample_synth_data.mat	TcPy	Python interface and C++ numerics
Benchmark.py	Command-line demo, output to console. Simple time and memory benchmarks for the Mau, Modi, or PEQ algorithms	\$ python TcPy/run_batch_analysis.py sampleData/sample_synth_data.mat	TcPy	Python interface and C++ numerics
run_batch_analysis.py	Command-line production script, output to CSV files. Runs a batch analysis using all methods on a data file. Generates .csv files for TI, R2B, PEQ, and ground truth classifications	\$ python TcPy(ti_demo.py sampleData/sample_synth_data.mat	TcPy	Python interface and C++ numerics
pyBindMap.py	Provides an interface for MATLAB programmers, to the python/C__ fuctions using two wrapper functions: runTlanalysis and runR2Banalysis	Utility function, not run from command line	TcPy	Python
dodFbF.m	Utility function to convert experimental raw 2p calcium activity data from Suite2P to df/F form.	Utility function, not run from command line	rho-matlab/CustomFunctions	MATLAB

All these functions should be run from the cloned repository, TimeCellAnalysis.

**Table 3: List of paper figure generating scripts**

Name	Description	Command line
paperFigures	Plots all figures estimating algorithm performance for synthetic data analysis (paper Figs. 1, 4–6, and 8)	\$ matlab -r "paperFiguresSynth"
Synth.m		
paperFigures	Plots all figures estimating algorithm performance for real physiology data analysis (paper Fig. 7)	\$ matlab -r "paperFiguresReal"
Real.m		
paperFigures	For diagnostics; plots figures estimating algorithm performance over all the regimes (unphysiological, canonical, and physiologic)	\$ cd ../src && matlab -r "paperFiguresSplits"
Splits.m		

All these functions should be run from the cloned repository, TimeCellAnalysis/*p*-matlab/paperFigures.

### Ratio of ridge/background, *r2bMean*, *r2bBoot*, *r2bBase-O* (Modi et al., 2014)

Here, we re-implemented the algorithm from Modi et al., 2014. The time of peak response for each cell was identified in averaged, nonoverlapping trials' worth of  $\Delta F/F$  traces, in the CS-onset to US-onset period, or as specified. The rest of the trials were averaged and the summed area under the time of peak was estimated. The ridge was then defined to be a 200 ms window centered at the peak. Next, we calculated the summed area in the ridge window as well as the background (non-ridge frames) to get the ridge to background ratio. As a control condition, these traces were given random time-offsets and then averaged. An independent time of peak was identified for each random-offset, averaged trace and ridge to background ratio calculated for it. This bootstrapping was repeated 1000 times for each cell's data and averaged. The reliability score was then calculated individually, for each cell, as the ratio of the ridge to background ratio for aligned traces to the mean of that of the random-offset traces (*r2bMean*).

We also studied the significance of each cell's raw *r2b* values by comparing them to each of the *r2b* values of the randomized datasets, thresholding significance at the 99th percentile (*r2bBoot*). Finally, the raw *r2b* values were also thresholding using Otsu's Thresholding (*r2bBase-O*; Otsu 1979).

### Parametric equations, *peqBase* and *peqBase-O* (in-house)

We developed this method to score cells in a manner similar to the reference quality, which uses the known ground truth of the input parameters given to the generator functions for the synthetic dataset. Rather than using the known inputs, this method computes the corresponding parameters read out or estimated from the dataset, whether synthetic or real. It is applicable to labeled or unlabeled datasets. It is defined as:

$$Q = \text{HTR} \times \exp - \{\alpha \times N/S + \beta \times \text{std. dev. EW} / \text{mean EW} + \gamma \times \text{std. dev. Imp/Stim Win}\}, \quad (6)$$

where HTR: hit trial ratio

N/S: estimated noise/signal

EW: read out event widths (frames)

Imp: estimated imprecision (frames)

Stim Wind: stimulus window (frames)

$\alpha$ : 10

$\beta$ : 1

$\gamma$ : 10

While  $10 \times \alpha$  was required,  $\beta$ , and  $\gamma$ , were inspired by the same used for reference Q. Classification was then performed using Bootstrapping (as described above) as well as Otsu's threshold.

All of these implemented algorithms can handle unlabeled (real) or ground truth labeled (synthetic) data.

A schematic to describe the steps involved in each algorithm is shown (Fig. 3). We were then able to run all our synthetically generated datasets through each of the 10 implemented algorithms and perform comparative benchmarks.

### Good predictive power in time cell quality scores despite different distributions

We ran each of the analysis methods on our synthetic datasets to assess how they scored the (known) time cells. There were four methods that provided a scoring function for time-cell classification: *tIMean*, *tIBase*, *r2bBase*, and *peqBase* (Fig. 4A–D). By inspection, these methods appeared to have distinct distributions. Below we describe how we compare the distributions using correlation analysis. In subsequent sections we describe other methods in our study that used these scores to generate a categorization through thresholding or bootstrap.

In these synthetic experiments, time cells were generated with a single calcium event per hit trial. Event insertions into the synthetic datasets were subject to noise, variable selection of event widths, trial-pair or timing imprecision, and hit trial ratio. We generated 99 unique unphysiological combinations (3  $\times$  randomized shuffles) 12 unique canonical regime combinations (10  $\times$  randomized shuffles), as well as 15 unique physiological regime combinations featuring background activity (10  $\times$  randomized shuffles). In all, we performed our comparative analysis studies using 567 datasets, each with 135 cells, 60 trials/session, and 246 frames/trial at 14.5 Hz). We found that only *tIMean* and *tIBase* had a correlation coefficient of  $\sim 0.6$ , whereas other pairs were correlated below 0.4 (Fig. 4E).

Generalized linear regression (GLM) models were generated to look for the ideal thresholding value for the best classification predictions by each method. We used the MATLAB implementation of GLMs (*fitglm*); <https://in.mathworks.com/help/stats/fitglm.html>). This is a linear model assuming a binomial distribution of categories (0 or 1, i.e., other cell or time cell; Collett, 2002). We obtained good predictive power for the four methods that provided a scoring function for time-cell classification. We generated Receiver Operating Characteristic (ROC) curves by going over the full range of thresholds for the range of scores for each method

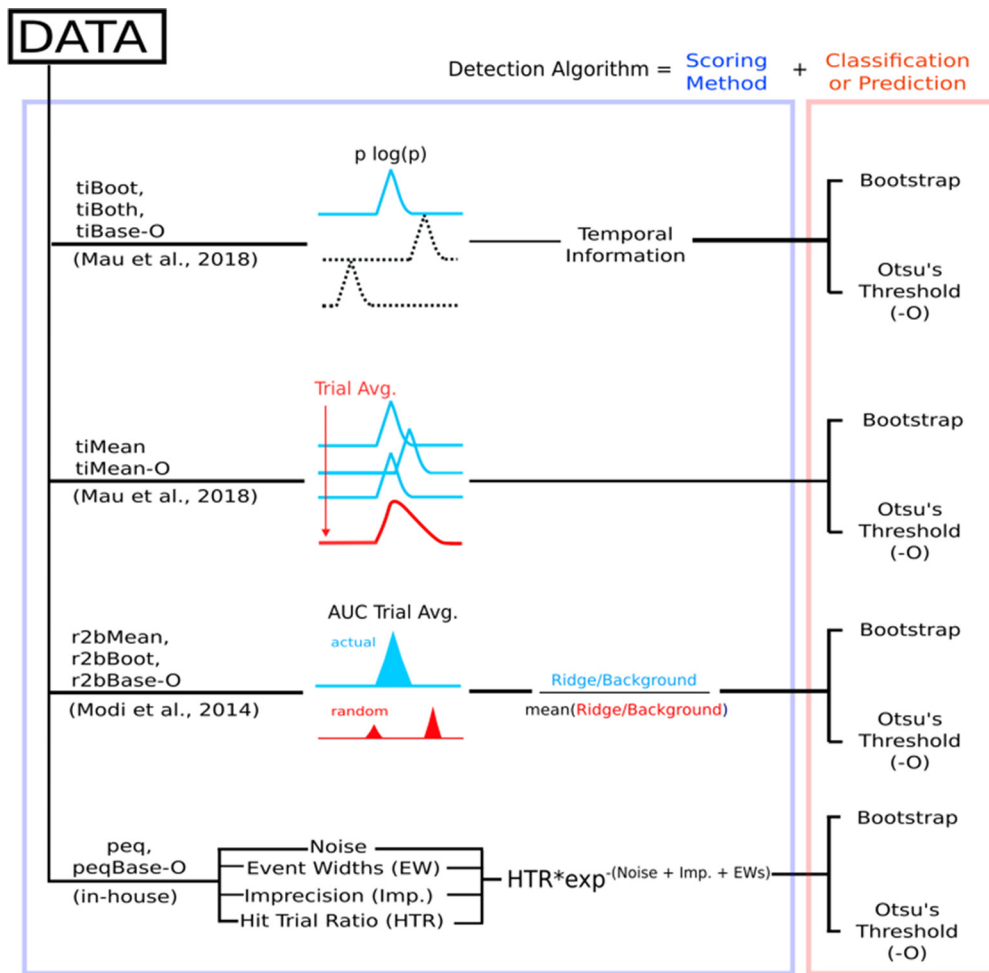


**Figure 3.** Schematic representation of the implemented algorithms, involving four different scoring methods followed by a classification step (bootstrapping or Otsu's automatic threshold) to have 10 complete time cell detection algorithms.

(ROC curves; Fig. 4F). We found that each distribution of scores had good predictive power, since ideal thresholds could be found to maximize TPR/FPR in all cases. We used the *tiBoth* categorization to distinguish time cells (Fig. 4G) from other cells (Fig. 4H), and plotted trial-averaged calcium traces to visually assess quality of classification as seen from raw data. Overall, each of our methods had distinct distributions of their base scores, but all had good predictive power for classification. The outcome of the classification steps is described in the next sections.

#### All algorithms exhibit near perfect precision with good recall

Next, we used the scores to classify the cells in our synthetic datasets, compared the predictions to ground truth, and established summaries for true and false cases. Confusion matrices were estimated to compare the predictions (classifications) for each algorithm, with reference to ground truth, and are shown (Fig. 5A,B). All methods exhibit very good precision (true positive classifications over the sum of all positive classifications), suggesting low false positive rates (Type I error; Fig. 5C). Most algorithms also generate good values for recall (true positive

classifications over ground-truth positives). We observed F1 scores (harmonic mean of recall and precision)  $>0.75$ , all the way to 1 (perfect score), for most of the algorithms, as shown (Fig. 5C), suggesting overall usability.

We noticed moderate to strong correlation ( $>0.8$ ) between the Boolean prediction lists for *tiMean*, *tiBoot*, *tiBoth*, *r2bMean*, and *r2bBoot* (Fig. 5D), but only weak to moderate correlation ( $<0.6$ ) between the other pairs of predictions. The *tiMean-O* method does slightly better (correlation  $\sim 0.7$  with the first five methods).

#### Algorithms differ in memory use and speed

Hardware and runtime requirements are a secondary, but practical concern when designing analysis of large datasets, and are specially relevant for experiment designs that require online analysis. We therefore looked at how memory use and runtime scaled on a per dataset basis when considering 67 or 135 cells per dataset ( $2\times$ ).

We ran the memory usage and runtime experiments on a gaming laptop (Lenovo Ideapad 3 Gaming) with a 6 core AMD Ryzen 5 4600H, 16 GB DDR4 RAM (3200 MHz) running MATLAB R2021a on Ubuntu 20.04. Note, however, that we have implemented all the time cell algorithms in

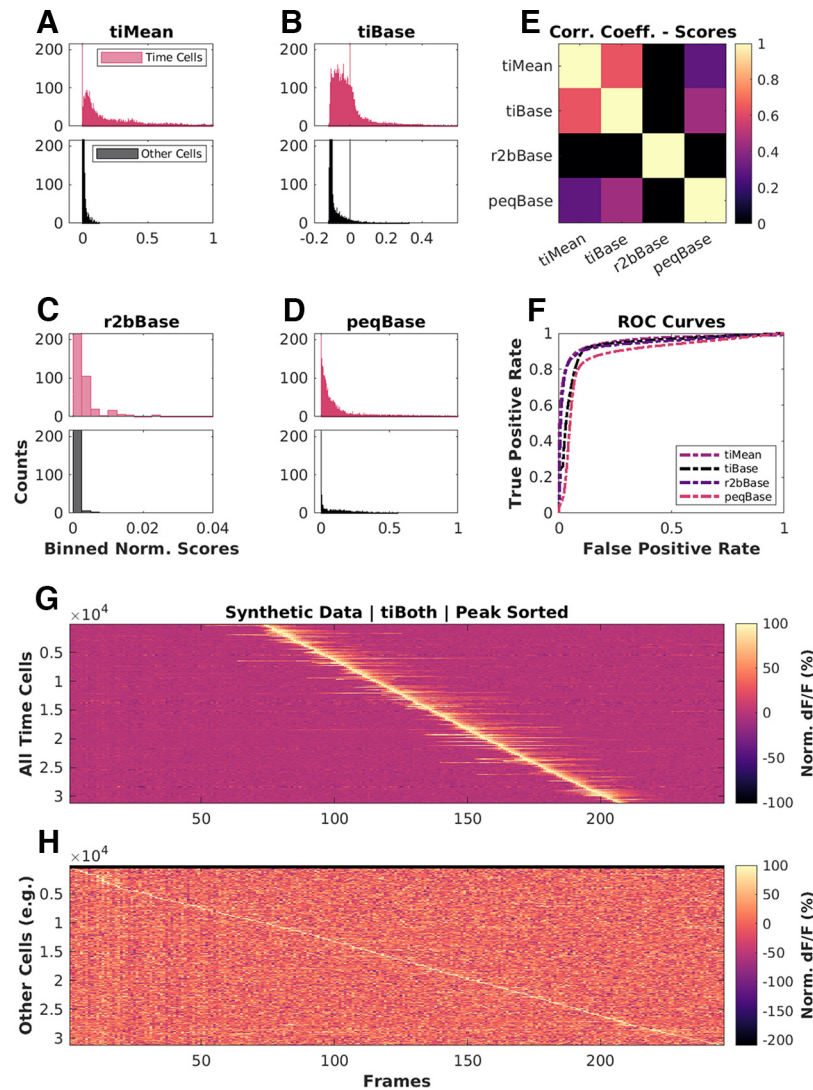


**Figure 4.** Base scores for different methods differ in their distributions but all have good predictive power. Scores for top (blue): time cells; bottom (red): other cells, across **A**, **tiMean**; **B**, **tiBase**; **C**, **r2bBase**; **D**, **peqBase**. **E**, Pairwise correlation coefficients between the distributions of analog scores (pooling time cells and other cells) by each of the four scoring methods. **F**, Receiver-operator characteristic (ROC) curves after generalized linear regression using the respective distributions of scores and comparisons with known ground truth. **G**, **H**, Trial-averaged calcium activity traces for cells classified as **G**, time cells; **H**, other cells.

serial and these do not use the additional cores. We found that most algorithms ran to completion requiring  $\sim$ 15 MB/dataset at a rate of  $\sim$ 1–4 s/dataset (135 cells/dataset). With 67 cells/dataset, the memory requirement and runtimes are approximately halved, suggesting that computational costs in memory and time were roughly linear with dataset size. We note that the analysis algorithms work independently for each cell. Thus, in principle, the analysis could be run in an embarrassingly parallel manner and should scale well on multicore architectures.

The synthesis of the main benchmarking datasets ( $N=567$  datasets or 76,545 total cells) required a more powerful analysis machine, running a 6 core AMD Ryzen 5 3600, 32GB of DDR4 RAM, running MATLAB R2021a on Ubuntu 20.04. Dataset batches up to  $\sim$ 30 datasets ( $N=40,500$  cells), however, could be easily handled by a less powerful laptop. The memory usage and runtime for

135 cells per dataset were accordingly,  $\sim$ 30 MB/dataset requiring  $\sim$ 1 s to complete. Thus, the methods scale readily to handle large datasets on modern hardware.

#### Physiologic range tests show sensitivity to noise but not to other features of the dataset

We next set out to see how these methods would work in estimated physiological ranges of signal confounds. Given our categorical labels on the synthetic data, we were able to split the datasets to look for the effects of the five main parameters: noise, event widths, imprecision, hit trial ratio, and background activity. We first computed the baseline physiology readouts keeping noise to 10%, event widths to the 60th percentile ( $\pm 1$  SD), imprecision to 0 frames, hit trial ratios to a range of 33–66%, and background activity to 0.9–1.2 events/trial for time cells

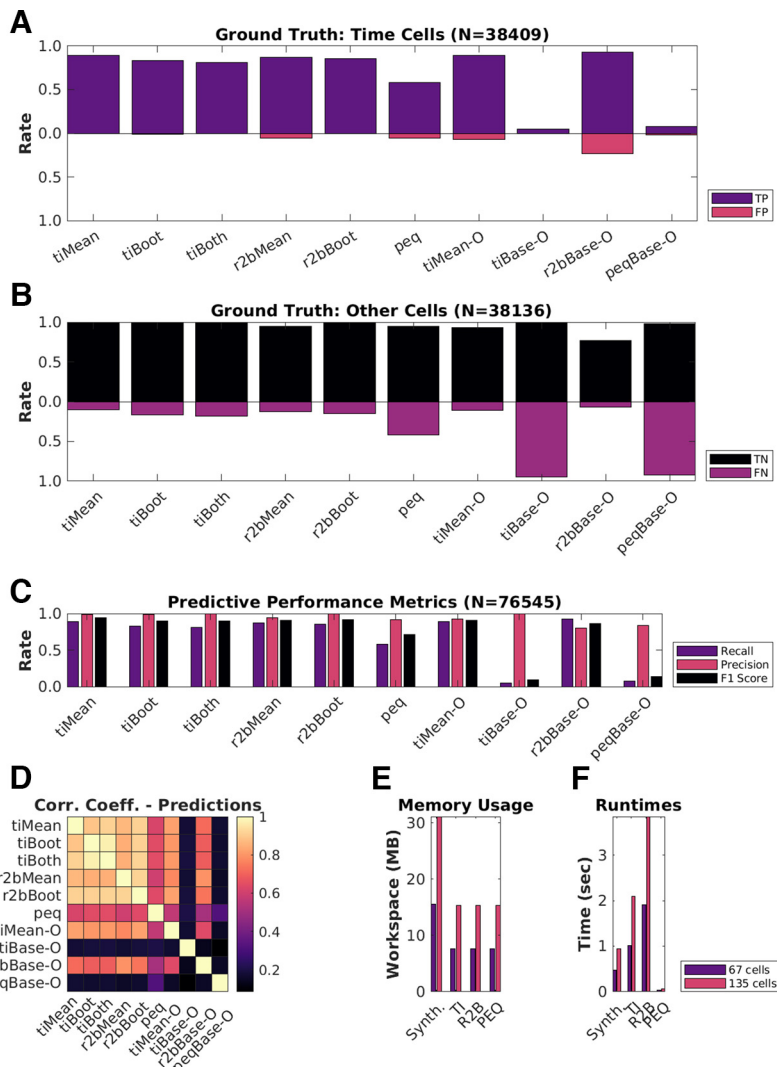


**Figure 5.** Good predictive performance by all algorithms. **A, B,** Classification performance of each of the 10 implemented detection algorithms. **A,** True positives (TP; purple), false positives (FP; red). **B,** True negatives (TN; black), false negatives (FN; purple). **C,** Predictive performance metrics [Recall = TP/(TP + FN), Precision = TP/(TP + FP), and F1 Score = Harmonic mean of Recall and Precision] to consolidate the confusion matrices. **D,** Pairwise correlation coefficients between the Boolean prediction lists by each of the 10 detection algorithms. Note that the first six methods correlate strongly. **E,** Average memory usage per dataset by the implemented algorithms on datasets with either 67 cells (purple) or 135 cells (red). **F,** Average runtimes per dataset by the implemented algorithms on datasets with either 67 cells (purple) or 135 cells (red).

(~50% of all synthetically generated cells,  $N=50$  baseline datasets, 135 cells/dataset, 60 trials/dataset). Next, we established dependency slopes for each of the algorithms, based on their predictions ( $N=10$  randomized shuffles for each case; Fig. 6B–F; Extended Data Figs. 6-1, 6-2).

Most methods exhibited a negative dependence of noise (range: 10% to 70%) on prediction F1 score (Fig. 6B). Although many methods are designed with some form of denoising strategy (trial-averaging, etc.), as expected all algorithms ran into classification difficulties at higher Noise levels. This reinforces the value of relatively high signal-to-noise recordings.

The relative insensitivity to event widths (Fig. 6C) is potentially useful for calcium imaging datasets where events may be slow, and in cases where slower tuning curves are

expected. However, this criterion may need to be stringent for analyses that need to precisely identify fine differences in cell responses.

We observed that most algorithms were insensitive to how frequently time cells were active across trials in a session (HTR). This is possibly the reason for the potential confusion among physiologists with regard to how many time cells were expected in a recorded dataset.

We found that the first six algorithms (tiMean, tiBoot, tiBoth, r2bMean, r2bBoot, and peq) gave equivalent predictions in ~66% of cases (Extended Data Fig. 6-1A). Next, we considered the various prediction lists across these top six algorithms and looked for consensus in time cell predictions from the most lenient threshold (“ $\geq 1$ ” algorithm), incrementally through the most stringent threshold (“ $=10$ ” algorithms). We thus established a

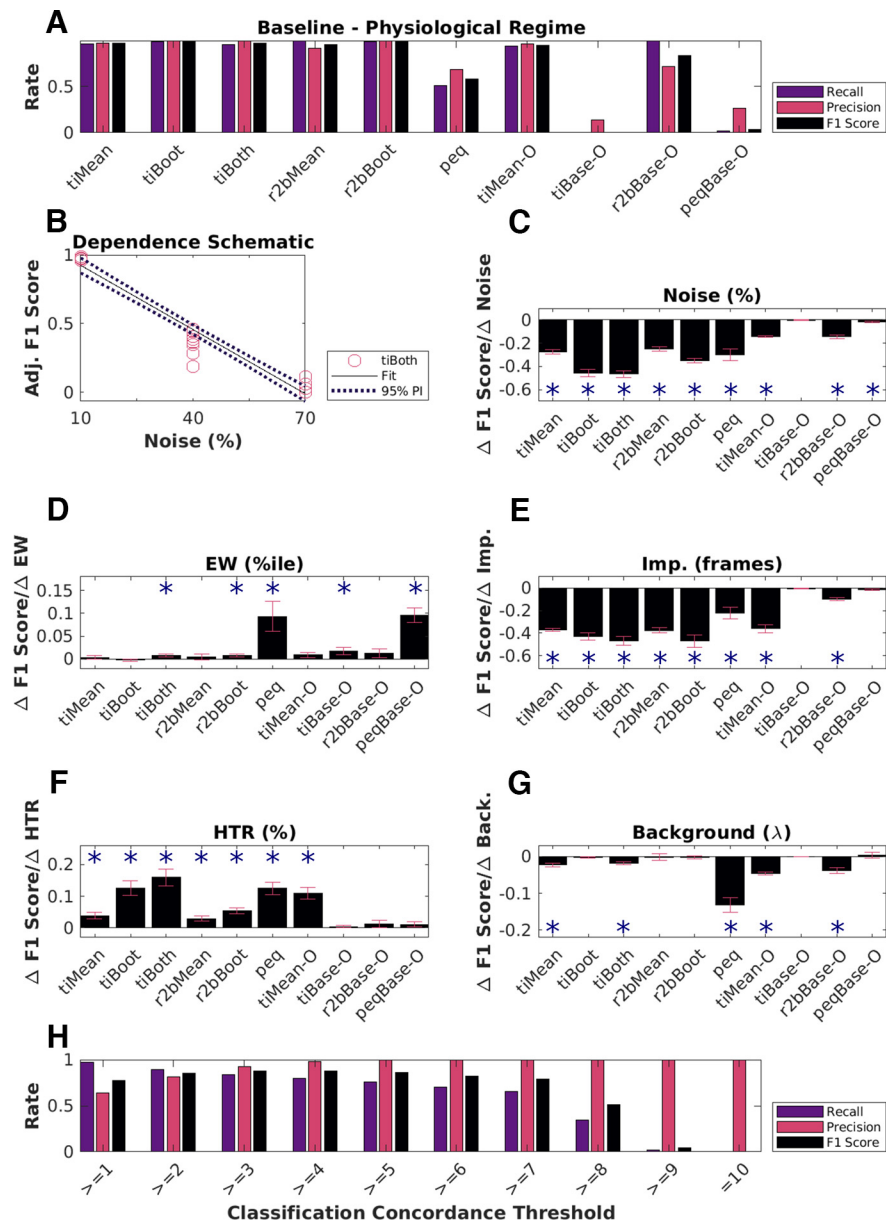


**Figure 6.** Physiological sensitivity analysis and concordance. **A**, Classification performance scores for all algorithms with the baseline physiology synthetic datasets ( $N=6750$  cells). The first five methods perform well. Peq does poorly by all measures when confronted with physiology-range activity variability. Otsu's threshold method for score classification also does not work well for any method under physiological conditions. **B**, Dependence of F1 score on noise as a schematic. This has an overall negative slope (dashed line) which was used for panel **C**, TI-both. A similar calculation was performed for each method. Panels **C–G**, Parameters were systematically modulated one at a time with respect to baseline and the impact on classification score for each algorithm was estimated by computing the slope, using repeats over 10 datasets each with an independent random seed. Significant dependence on the perturbing parameter was determined by testing whether the slope differed from 0 at  $p < 0.01$ , indicated by asterisks using the MATLAB function `coeffTest()`. Plotted here are bar graphs with mean and error as RMSE normalized by the square root of  $N$  ( $N=10$  datasets). **C**, Dependence on noise %. **D**, Dependence on event width percentiles. **E**, Dependence on imprecision frames. **F**, Dependence on hit trial ratio (HTR; %). **G**, Background activity (Poisson distribution mean,  $\lambda$ ). **H**, Classification performance using concordance for a range of classification thresholds. Extended Data Figure 6-1 describes the three-point line plot dependency curves for the F1 score for each of the implemented algorithms against each of the five main parameters modulated, as the mean of  $N=10$  datasets for each case, with error bars as SD. Extended Data Figure 6-2 showcases the linear regression fits for the same, with 95% prediction intervals (PIs), used to estimate the slopes of the various dependency curves.

Concordance based metric for time cell classification. We tested the predictive power of this Concordance based metric, which considers time cells based on consensus among the predictions from all the 10 implemented algorithms.

We identified differences in the classification performance, across the full range of concordance thresholds (Fig. 6H). With lower threshold values (“ $>=4$ ” and below), we notice a slight drop in the Precision, indicating an

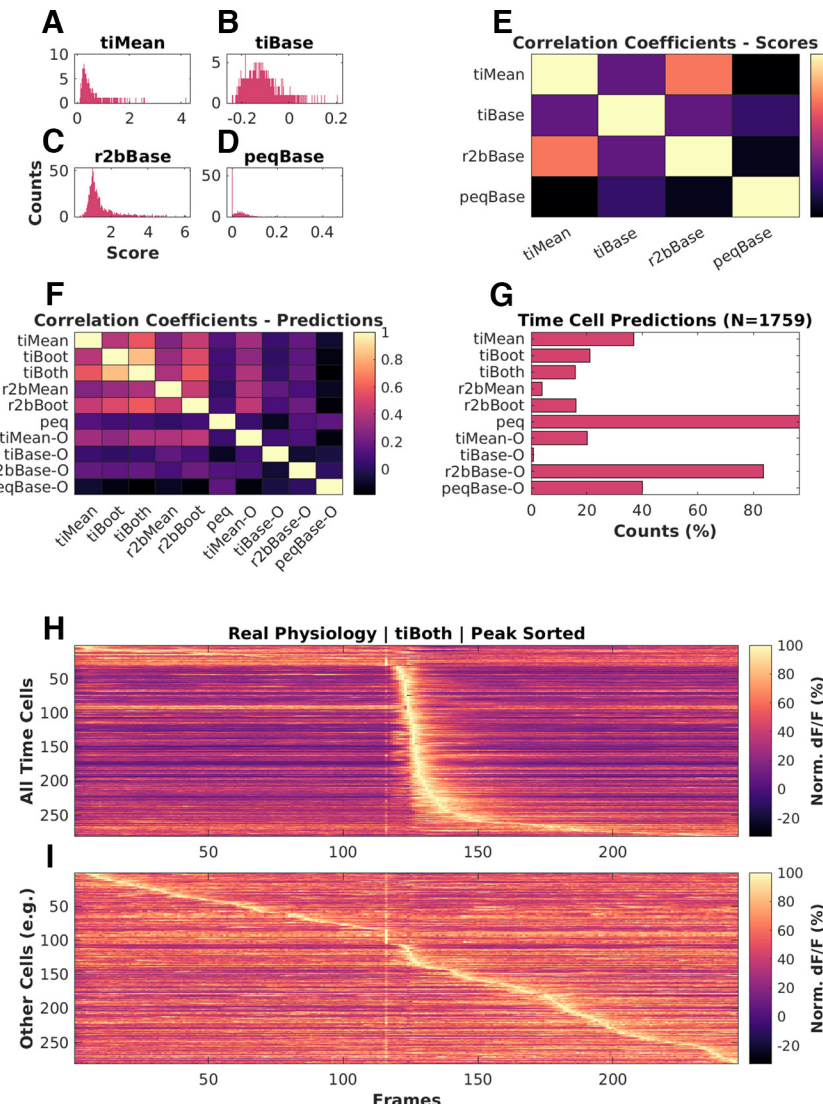


**Figure 7.** Analysis of experimental 2-P recordings of  $\text{Ca}^{2+}$  signals. **A–D**, Histograms of scores for physiologically recorded *in vivo* calcium activity from hippocampal CA1 cells (total  $N = 1759$ ), by (A) tiMean, (B) tiBase, (C) r2bBase, and (D) peqBase. **E**, Pairwise correlation coefficients between the distributions of analog scores by the four scoring methods. **F**, Pairwise correlation coefficients between the Boolean prediction lists by the 10 detection algorithms. **G**, Numbers of positive class (time cell) predictions by each of the detection algorithms. **H, I**, Trial-averaged calcium activity traces for (H) time cells and (I) other cells. LED conditioned stimulus (CS) is presented at frame number 116, as seen by the bright band of the stimulus artifact. Most cells classified as time cells are active just after the stimulus. There is a characteristic broadening of the activity peak for classified time cells at longer intervals after the stimulus. Some of the cells at the top of panel **H** may be false positives because their tuning curve is very wide or because of picking up the stimulus transient. Similarly, some of the cells in the middle of panel **I** may be false negatives because of stringent cutoffs, although they appear to be responsive to the stimulus.

increase in false positive rate (Type I error). On the other hand, with increasing threshold values it is the Recall that drops, suggesting a higher false negative rate (Type II error). We find that a concordance threshold of “ $>=4$ ” achieves the best recall, precision, and F1 scores, for time cell prediction (Fig. 6F). The utility of this approach is subject to the availability of resources to apply multiple algorithms to each dataset.

#### Time cells identified in real physiology recordings

We used the 10 different implemented algorithms on *in vivo* 2-P calcium recordings ( $N = 13$  datasets, namely,

1759 isolated cells from three animals across chronically recorded datasets), to compare time cell classification between the algorithms. As we observed for the synthetic data, experimental 2-P Ca traces also yielded different base scores from the four different methods (Fig. 7A–D). Again, consistent with the synthetic data, the pairwise correlation was weak to moderate (Fig. 7E). When we consider the boolean prediction lists (Fig. 7F), we observed moderate pairwise correlation between tiMean, tiBoot, tiBoth, r2bMean, and r2bBoot ( $>0.5$ ), and low or weak correlation between the other pairs ( $<0.5$ ). This was consistent with observations for the synthetic data but the correlations were overall slightly

weaker. The total number of time cells predicted were also different across the implemented algorithms (Fig. 7G). Algorithms such as *r2bBase-O* and *peq*, which had more false positives (Fig. 5B) also had more cells classified as time cells. The converse was not true. *r2bMean*, which had moderate false negatives as well as false positives on the synthetic dataset, classified very few of the experimental set as time cells. The trial-averaged activity of the detected time cells (Fig. 7H; including false positives) and other cells (Fig. 7I), based on the predictions by *tiBoth*, are shown. The experimentally recorded time cells exhibited a characteristic widening of tuning curves (Pastalkova et al., 2008; MacDonald et al., 2011, 2013; Kraus et al., 2013; Mau et al., 2018) with tuning to later time points (Fig. 7H).

Overall, four of the algorithms from the literature seemed consistent in their classifications as well as having reasonable numbers of classified time cells. These were the three algorithms from Mau et al. (2018; *tiMean*, *tiBoot*, and *tiBoth*), and the *r2bBoot* method derived from Modi et al. (2014). This is broadly in agreement with their performance on the synthetic datasets.

## Discussion

We have developed a full pipeline for comparing time cell detection algorithms. This starts with synthetic datasets for benchmarking, in which we program in the ground truth of cell identity and timed activity, and a range of perturbations characteristic of experiments. These include noise, event widths, trial-pair timing imprecision, hit trial ratio, and background activity. This resource is, in itself, a key outcome of the current study, and though it is designed for 2-P calcium imaging data it can be extended to rate-averaged single-unit recordings. We built a pipeline for running and comparing the outcome from five methods derived from two previous studies, and one from the current work. These algorithms were applied to synthetic and experimental datasets and compared against each other and, where possible, against ground truth. We observed that most algorithms perform well and substantially agree in their time cell classification, but there were different degrees of sensitivity to different forms of signal variability, notably noise and imprecision.

### The value of synthetic data in experimental science

Synthetic neural activity datasets are valuable in at least two main ways: evaluating algorithms for detection of important activity features, and for delivering stimuli to *in vitro* and simulated neurons, so as to provide a more physiological context in which to study input-output properties (Abbasi et al., 2020). While we have deployed our synthetic dataset for the specific purpose of comparing time cell detection algorithms, we suggest that it could also be useful for evaluating sequence analysis algorithms (Ikegaya et al., 2004; Foster and Wilson, 2006; Villette et al., 2015). Beyond the domain of neuronal data analysis, such synthetic datasets act as a test-bed for critique and development of analysis algorithms meant for deployment on real-world or typical use case data. They have been used previously to benchmark unsupervised outlier detection

(Steinbuss and Bohm, 2020), explainable machine learning (Liu et al., 2021), intrusion detection systems (Iannucci et al., 2017), 3D reconstruction algorithms (Koch et al., 2021), among several others. We report the first use of synthetic data pertaining to cellular physiology in the context of identifying time cells from network recordings. Moreover, our experiments study important operational differences across several previously published and new detection algorithms.

Our dataset may also be valuable for the second use case, stimulus delivery. There is a growing body of work on network detection of sequences (Ikegaya et al., 2004; Foster and Wilson, 2006; Csicsvari et al., 2007; Jadhav et al., 2012; Villette et al., 2015; Malvache et al., 2016) or even single-neuron sequence selectivity (Branco et al., 2010; Bhalla, 2017). More realistic input activity patterns with a range of physiological perturbations may be useful probes for such experimental and theoretical studies. Further, experimenter-defined neural activity inputs through optogenetic stimulation has already begun to use more complex temporal patterns than static or periodic illumination (Schrader et al., 2008; Dhawale et al., 2010; Bhatia et al., 2021). Our approaches to synthetic sequential neuronal activity generation may be useful to add more physiological dimensions to the sequential activity employed in such studies.

### Further dimensions of time cell modulation

Our experiments allowed us to probe for parametric dependence systematically across published and new algorithms. We observed little or no dependence of the predictive performance (F1 score) of the various algorithms to event widths, hit trial ratios, and background activity. We did observe the F1 scores for most algorithms to be negatively dependent on noise and imprecision. On the one hand, this is a useful outcome in that different methods yield similar time-cell classification. It is a limitation, however, if the network uses such response features for coding, since it means that these methods are insensitive to relevant response changes. Further potential coding dimensions were not explored. Thus, several potential behavioral correlates of tuned cells (Ranck, 1973), could not be studied in our experiments. Such correlates include but are not limited to measurements of spatial navigation (O'Keefe and Dostrovsky, 1971; O'Keefe and Nadel, 1978; Wilson and McNaughton, 1993) and decision-making (Foster and Wilson, 2006; Csicsvari et al., 2007; Diba and Buzsáki, 2007; Davidson et al., 2009; Karlsson and Frank, 2009; Gupta et al., 2010; MacDonald et al., 2013; Villette et al., 2015), as well as navigation across tone frequencies (Aronov and Tank, 2014). While each of these further inputs would be interesting to incorporate into synthetic datasets, this requires that the time cell generation algorithm itself incorporate some form of simulation of the neural context. This is beyond the scope of the current study.

A specific limitation of our dataset is that it assumes that time is encoded by individual neurons. This leaves out population encoding schemes in which no one cell responds with the level of precision or consistency that would clear the criteria we use. For example, many of the same studies that use the methods tested here also use

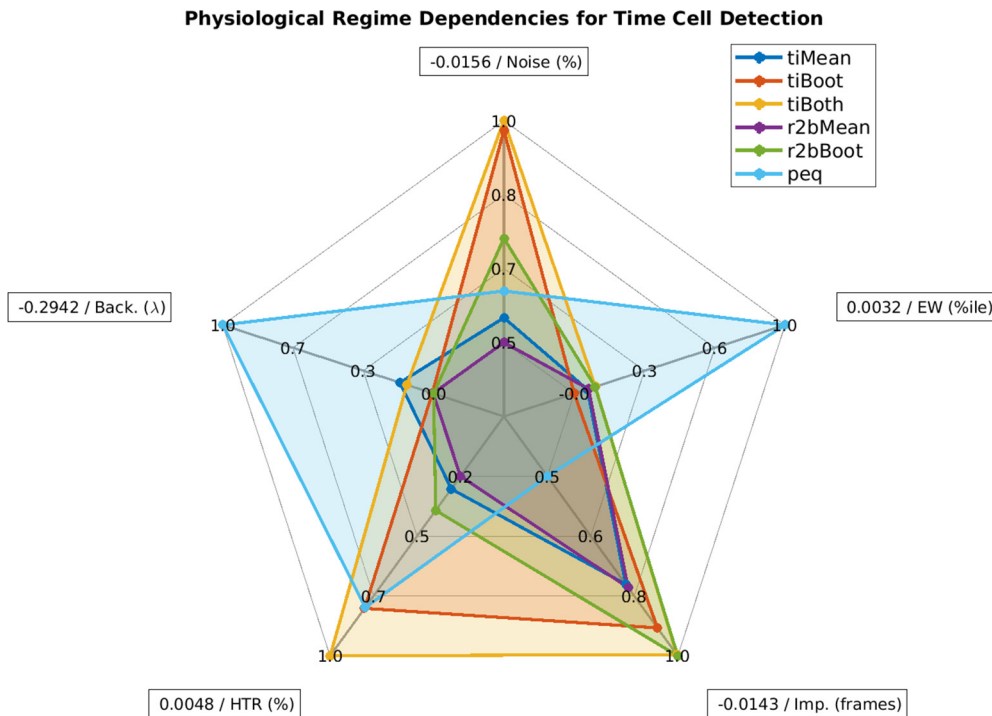


**Figure 8.** Spider plot summary. Relative sensitivity of the six best detection algorithms (*tiMean*, *tiBoot*, *tiBoth*, *r2bMean*, *r2bBoth*, and *peq*) to the five main parameters for data variability, noise (%), event widths (%ile), imprecision (frames), hit trial ratio (%), and background activity ( $\lambda$ ). A perfect algorithm would have very small values (i.e., low sensitivity) for each of the parameters and, thus, occupy only the smallest pentagon in the middle. Note that even the maximal absolute value of sensitivity for most parameters (outer perimeter) is quite small, indicated in boxes at the points of the spider plot.

neural network decoders to report time (Mau et al., 2018). Such decoders might detect time encoding without time cells. A similar situation of individual versus network coding appears for the closely related problem of sequence representation. Place cell replay sequences have been shown to be modulated by the prevalence of location specific aversive (Wu et al., 2017) as well as appetitive stimuli (Bhattarai et al., 2020). Such physiological findings have been the subject of theoretical models of behavior planning (Foster, 2017; Mattar and Daw, 2018), and have been reported to improve performance on multiple Atari games by artificial neural networks (Mnih et al., 2015) featuring salience detection and experience mapping. We suggest that synthetic data for such higher-order encoding schemes might be a useful tool, and could draw on the approaches in the current study.

#### Comparative analysis benchmarks and concordance

A particularly challenging time cell classification problem is when the same cells may play different timing roles, such as forward and reverse replay. This is made more difficult because of the relative rarity of forward replay sequences over the more typical reverse replay (Diba and Buzsáki, 2007; Foster, 2017). Preplay is also a topic of some debate (Dragoi and Tonegawa, 2013; Foster, 2017). At least one possible problem in such debates is the degree of consistency between time cell or sequence classifiers. Our pipeline allows for (1) error correction in case of nonconcordant classifications, (2) suggest candidate algorithms

with a dependence on dataset features like event widths, imprecision, and hit trial ratio, as well as (3) the possibility to expand the detection regime in more realistic physiological datasets using concordance.

#### Which algorithms to use?

We did not set out to rank algorithms, but our analysis does yield suggestions for possible use domains based on sensitivity to experimental perturbations (Fig. 8). In cases where runtime and compute resource use is a concern, we recommend using the temporal information method with Bootstrap along with the activity filter (*tiBoth*). Combinations of *tiBoth* with *r2bBoth* may be useful where there are rare and potentially multimodally tuned time cells (Pastalkova et al., 2008; Villette et al., 2015), either to combine their classification for stringent time cell identification, or to pool their classified cells. While it is tempting to use Otsu's threshold as a very fast alternative to bootstrapping, we found that none of the Otsu variants of these methods did a good job of classification. Ultimately, five of our algorithms *tiMean*, *tiBoot*, *tiBoth*, *r2bMean*, and *r2bBoth*: all based on either Mau et al. (2018) or Modi et al. (2014), have very good Precision, and classify with very few false positives (low Type I error). Many methods are susceptible to classification errors if the dataset has high noise.

Here we also implemented the parametric equation (*peq*) algorithm. It is not very good for time cell classification per se, as it is prone to false positives and is susceptible to noise and low hit trial ratios. However, it generates useful

additional estimates of the four key parameters of real data, namely, noise, hit trial ratio, event width and imprecision. This is useful for a first-pass characterization of the properties of the dataset.

### Sequence detection in large-scale recordings and scaling of analysis runs

The discovery of replay over the past two decades, has benefitted from the technological advances made in increasing the cellular yield of network recordings and has been reviewed previously (Foster, 2017). Further advances such as with the large scale recordings of  $\sim 10^3$  single units by electrical recording using Neuropixels (Jun et al., 2017), fast volumetric fluorescence scanning with up to  $\sim 10^4$  cells using resonant electro-optic imaging (Poort et al., 2015; Pachitariu et al., 2017; Bowman and Kasevich, 2021),  $\sim 10^3$  mesoscopes (Sofroniew et al., 2016), as well as advances in automated cell region of interest (ROI) detection, denoising, and neuropil subtraction (Pachitariu et al., 2017; Pnevmatikakis et al., 2016) only increase the scale and size of datasets, likely leading to longer analysis runtimes. In addition to our recommendations above for the temporal information/boot method for scalable time-cell analysis, our C++/Python implementations may also be useful in further optimizing these methods. Our implementations allow for relatively fast analysis of the same datasets with multiple algorithms.

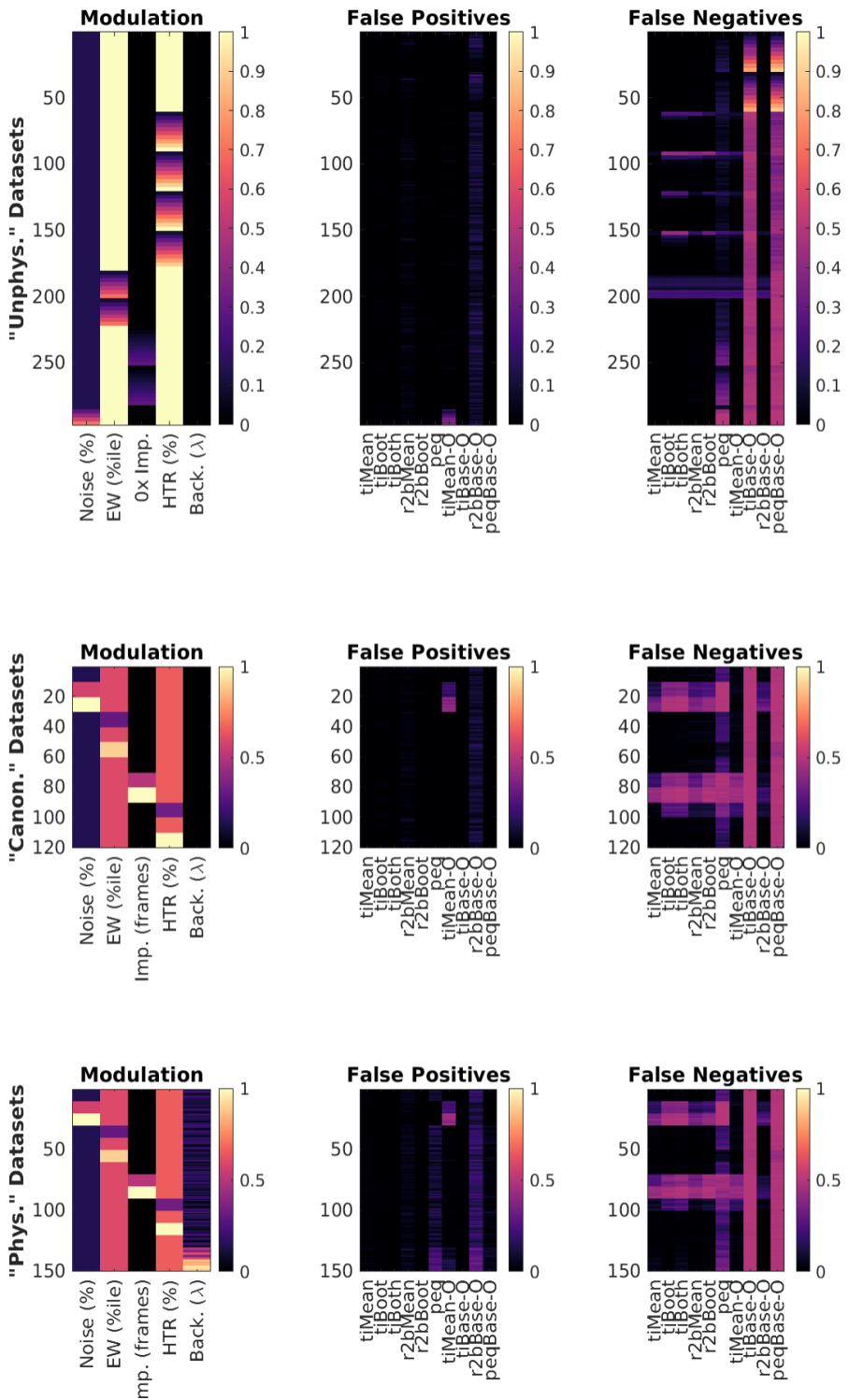
## References

- Abbasi S, Maran S, Jaeger D (2020) A general method to generate artificial spike train populations matching recorded neurons. *J Comput Neurosci* 48:47–63.
- Ahmed MS, Priestley JB, Castro A, Stefanini F, Solis Canales AS, Balough EM, Lavoie E, Mazzucato L, Fusi S, Losonczy A (2020) Hippocampal network reorganization underlies the formation of a temporal association memory. *Neuron* 107:283–291.e6.
- Aronov D, Tank DW (2014) Engagement of neural circuits underlying 2D spatial navigation in a rodent virtual reality system. *Neuron* 84:442–456.
- Bhalla US (2017) Synaptic input sequence discrimination on behavioral timescales mediated by reaction-diffusion chemistry in dendrites. *Elife* 6:e25827.
- Bhatia A, Moza S, Bhalla US (2021) Patterned optogenetic stimulation using a DMD projector. *Methods Mol Biol* 2191:173–188.
- Bhattarai B, Lee JW, Jung MW (2020) Distinct effects of reward and navigation history on hippocampal forward and reverse replays. *Proc Natl Acad Sci U S A* 117:689–697.
- Bowman AJ, Kasevich MA (2021) Resonant electro-optic imaging for microscopy at nanosecond resolution. *ACS Nano* 15:16043–16054.
- Branco T, Clark BA, Häusser M (2010) Dendritic discrimination of temporal input sequences in cortical neurons. *Science* 329:1671–1675.
- Collett D (2002) Modeling binary data. London: Chapman and Hall.
- Csicsvari J, O'Neill J, Allen K, Senior T (2007) Place-selective firing contributes to the reverse-order reactivation of CA1 pyramidal cells during sharp waves in open-field exploration. *Eur J Neurosci* 26:704–716.
- Davidson TJ, Kloosterman F, Wilson MA (2009) Hippocampal replay of extended experience. *Neuron* 63:497–507.
- Dhawale AK, Hagiwara A, Bhalla US, Murthy VN, Albeau DF (2010) Non-redundant odor coding by sister mitral cells revealed by light addressable glomeruli in the mouse. *Nat Neurosci* 13:1404–1412.
- Diba K, Buzsáki G (2007) Forward and reverse hippocampal place-cell sequences during ripples. *Nat Neurosci* 10:1241–1242.
- Dombeck DA, Harvey CD, Tian L, Looger LL, Tank DW (2010) Functional imaging of hippocampal place cells at cellular resolution during virtual navigation. *Nat Neurosci* 13:1433–1440.
- Dragoi G, Tonegawa S (2013) Distinct preplay of multiple novel spatial experiences in the rat. *Proc Natl Acad Sci U S A* 110:9100–9105.
- Eichenbaum H (2017) On the integration of space, time, and memory. *Neuron* 95:1007–1018.
- Foster DJ (2017) Replay comes of age. *Annu Rev Neurosci* 40:581–602.
- Foster DJ, Wilson MA (2006) Reverse replay of behavioural sequences in hippocampal place cells during the awake state. *Nature* 440:680–683.
- Gupta AS, van der Meer MAA, Touretzky DS, Redish AD (2010) Hippocampal replay is not a simple function of experience. *Neuron* 65:695–705.
- Iannucci S, Kholidy HA, Ghimire AD, Jia R, Abdelwahed S, Banicescu I (2017) A comparison of graph-based synthetic data generators for benchmarking next-generation intrusion detection systems. 2017 IEEE International Conference on Cluster Computing (CLUSTER), Honolulu, HI, pp. 278–289, <https://doi.org/10.1109/CLUSTER.2017.54>.
- Ikegaya Y, Aaron G, Cossart R, Aronov D, Lampl I, Ferster D, Yuste R (2004) Synfire chains and cortical songs: temporal modules of cortical activity. *Science* 304:559–564.
- Jadhav SP, Kemere C, German PW, Frank LM (2012) Awake hippocampal sharp-wave ripples support spatial memory. *Science* 336:1454–1458.
- Jun JJ, et al. (2017) Fully integrated silicon probes for high-density recording of neural activity. *Nature* 551:232–236.
- Kaifosh P, Lovett-Barron M, Turi GF, Reardon TR, Losonczy A (2013) Septo-hippocampal GABAergic signaling across multiple modalities in awake mice. *Nat Neurosci* 16:1182–1184.
- Karlsson MP, Frank LM (2009) Awake replay of remote experiences in the hippocampus. *Nat Neurosci* 12:913–918.
- Koch S, Worcel M, Silva C, Alexa M (2021) Hardware Design and Accurate Simulation of Structured-Light Scanning for Benchmarking of 3D Reconstruction Algorithms (Vol. 2021). Proceedings of the Neural Information Processing Systems Track on Datasets and Benchmarks 1 (NeurIPS Datasets and Benchmarks 2021). Retrieved from <https://openreview.net/forum?id=bNL5VfTe3p>.
- Kraus B, Robinson R, White J, Eichenbaum H, Hasselmo M (2013) Hippocampal “time cells”: time versus path integration. *Neuron* 78:1090–1101.
- Lee AK, Wilson MA (2004) A combinatorial method for analyzing sequential firing patterns involving an arbitrary number of neurons based on relative time order. *J Neurophysiol* 92:2555–2573.
- Liu Y, Khandagale S, White C, Neiswanger W (2021) Synthetic benchmarks for scientific research in explainable machine learning. <https://github.com/abacusai/xai-bench>.
- MacDonald CJ, Lepage KQ, Eden UT, Eichenbaum H (2011) Hippocampal “time cells” bridge the gap in memory for discontinuous events. *Neuron* 71:737–749.
- MacDonald CJ, Carrow S, Place R, Eichenbaum H (2013) Distinct hippocampal time cell sequences represent odor memories in immobilized rats. *J Neurosci* 33:14607–14616.
- Malvache A, Reichinnek S, Villette V, Haimerl C (2016) Awake hippocampal reactivations project onto orthogonal neuronal assemblies. *353:1280–1283*.
- Mattar MG, Daw ND (2018) Prioritized memory access explains planning and hippocampal replay. *Nat Neurosci* 21:1609–1617.
- Mau W, Sullivan DW, Kinsky NR, Hasselmo ME, Howard MW, Eichenbaum H (2018) The same hippocampal CA1 population simultaneously codes temporal information over multiple time-scales. *Curr Biol* 28:1499–1508.e4.
- Mnih V, Kavukcuoglu K, Silver D, Rusu AA, Veness J, Bellemare MG, Graves A, Riedmiller M, Fidjeland AK, Ostrovski G, Petersen S, Beattie C, Sadik A, Antonoglou I, King H, Kumaran D, Wierstra D,

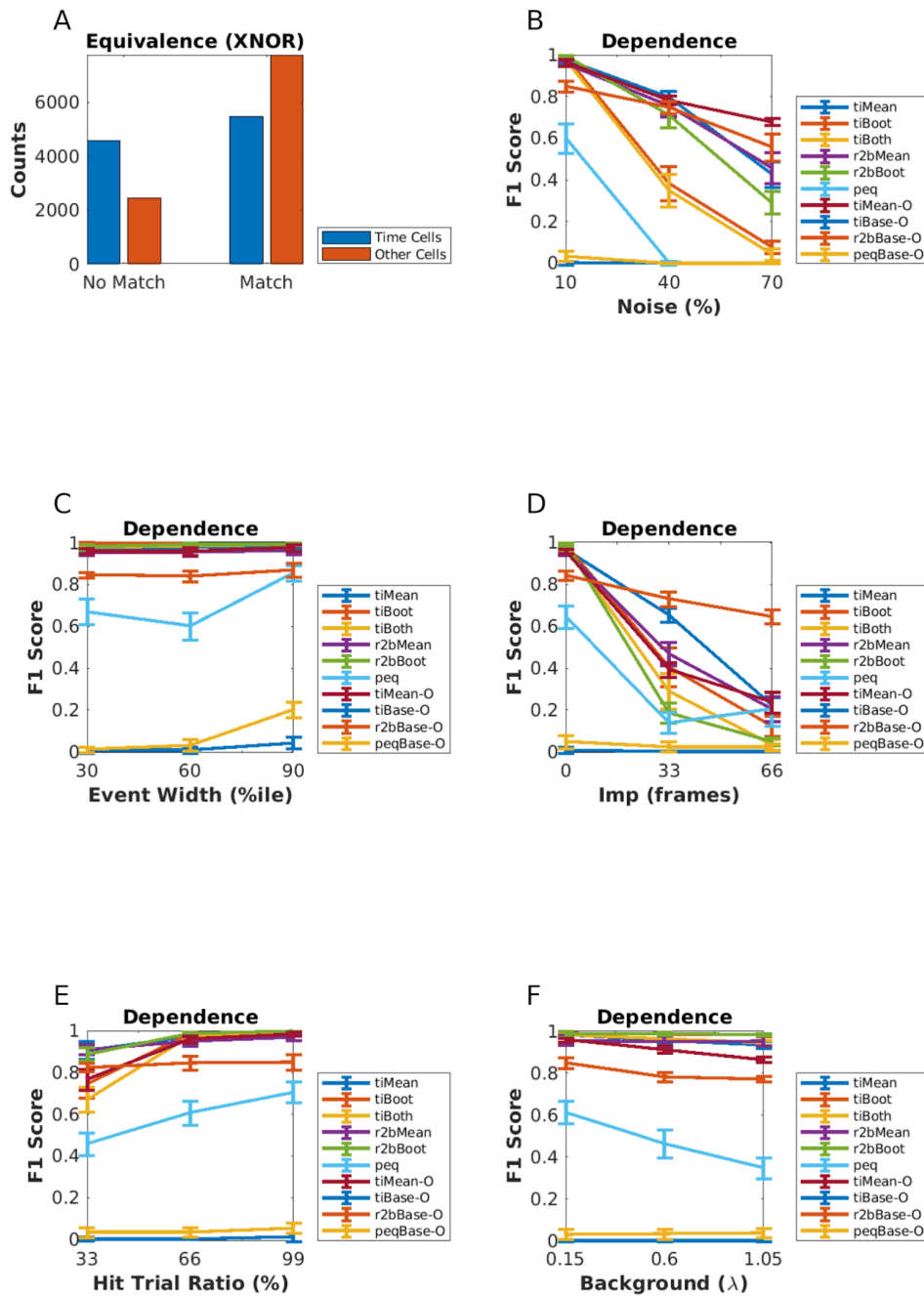
- Legg S, Hassabis D (2015) Human-level control through deep reinforcement learning. *Nature* 518:529–533.
- Modi MN, Dhawale AK, Bhalla US (2014) CA1 cell activity sequences emerge after reorganization of network correlation structure during associative learning. *Elife* 3:e01982.
- Mokeichev A, Okun M, Barak O, Katz Y, Ben-Shahar O, Lampl I (2007) Stochastic emergence of repeating cortical motifs in spontaneous membrane potential fluctuations in vivo. *Neuron* 53:413–425.
- O'Keefe J, Dostrovsky J (1971) The hippocampus as a spatial map. Preliminary evidence from unit activity in the freely-moving rat. *Brain Res* 34:171–175.
- O'Keefe J, Nadel L (1978) The hippocampus as a cognitive map. Oxford: Clarendon Press.
- Otsu N (1979) A threshold selection method from gray level histograms. *IEEE Trans Syst Man Cyber* 9:62–66.
- Pachitariu M, Stringer C, Dipoppa M, Schröder S, Rossi LF (2017) Suite2p: beyond 10,000 neurons with standard two-photon microscopy. *BioRxiv* 061507. <https://doi.org/https://doi.org/10.1101/061507>.
- Pastalkova E, Itskov V, Amarasingham A, Buzsáki G (2008) Internally generated cell assembly sequences in the rat hippocampus. *Science* 321:1322–1327.
- Pnevmatikakis EA, Soudry D, Gao Y, Machado TA, Merel J, Pfau D, Reardon T, Mu Y, Lacefield C, Yang W, Ahrens M, Bruno R, Jessell TM, Peterka DS, Yuste R, Paninski L (2016) Simultaneous denoising, deconvolution, and demixing of calcium imaging data. *Neuron* 89:285–299.
- Poort J, Khan AG, Pachitariu M, Nemri A, Orsolic I, Krupic J, Bauza M, Sahani M, Keller GB, Mrsic-Flogel TD, Hofer SB (2015) Learning enhances sensory and multiple non-sensory representations in primary visual cortex. *Neuron* 86:1478–1490.
- Ranck JB, J (1973) Studies on single neurons in dorsal hippocampal formation and septum in unrestrained rats. I. Behavioral correlates and firing repertoires. *Exp Neurol* 41:461–531.
- Schrader S, Grün S, Diesmann M, Gerstein GL (2008) Detecting synfire chain activity using massively parallel spike train recording. *J Neurophysiol* 100:2165–2176.
- Siegel JJ, Taylor W, Gray R, Kalmbach B, Zemelman BV, Desai NS, Johnston D, Chitwood RA (2015) Trace eyeblink conditioning in mice is dependent upon the dorsal medial prefrontal cortex, cerebellum, and amygdala: behavioral characterization and functional circuitry. *eNeuro* 2:ENEURO.0051-14.2015.
- Sofroniew NJ, Flickinger D, King J, Svoboda K (2016) A large field of view two-photon mesoscope with subcellular resolution for in vivo imaging. *Elife* 5:e14472.
- Souza BC, Pavão R, Belchior H, Tort ABL (2018) On information metrics for spatial coding. *Neuroscience* 375:62–73.
- Steinbuss G, Bohm K (2020) Generating artificial outliers in the absence of genuine ones—a survey. *arXiv*. <https://doi.org/10.48550/arXiv.2006.03646>.
- Tseng W, Guan R, Disterhoft JF, Weiss C (2004) Trace eyeblink conditioning is hippocampally dependent in mice. *Hippocampus* 14:58–65.
- Villette V, Malvache A, Tressard T, Dupuy N, Cossart R (2015) Internally recurring hippocampal sequences as a population template of spatiotemporal information. *Neuron* 88:357–366.
- Wilson MA, McNaughton BL (1993) Dynamics of the hippocampal ensemble code for space. *Science* 261:1055–1058.
- Wu CT, Haggerty D, Kemere C, Ji D (2017) Hippocampal awake replay in fear memory retrieval. *Nat Neurosci* 20:571–580.

## **Extended Data Figures (Supplementary)**

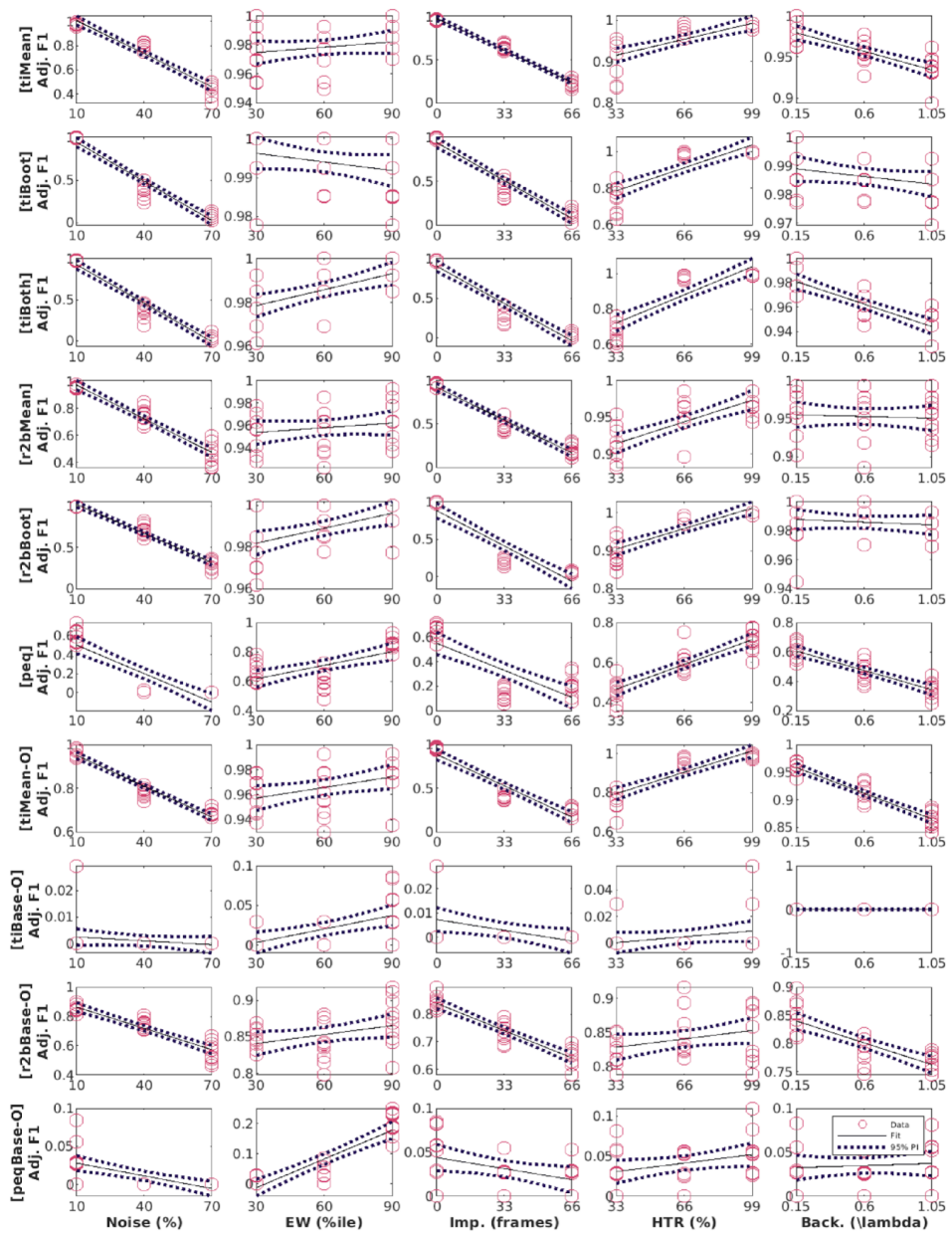
**Extended Figure 1-1.** Modulation profile along with the False Positive and False Negative rates per dataset, for important parameters configured in each of the 567 synthetic datasets generated. A-C: “Unphysiological Regime”, D-F: “Canonical Regime”, G-I: “Physiological Regime”.



**Extended Figure 6-1.** A: Equivalence by XNOR matching the prediction lists from the top six detection algorithms (Blue: Time Cells; Red: Other Cells). B-F: Dependence of the predictive performance (F1 Score) on the various important synthetic dataset configuration parameters, B: Noise (%), C: Event Width (%ile), D: Imprecision (frames), E: Hit Trial Ratio (%), and F: Background Activity ( $\lambda$ ).



**Extended Figure 6-2:** Linear Regression fits for all algorithm parameter dependence curves with data points (red circles), best fit line (black), and the 95% prediction interval (PI; dotted black lines). The columns represent the physiology regime modulation parameter (out of the 5 main parameters tested), and the rows represent the various implemented algorithms for time cell detection.



# **Chapter 5 – Discussion**

## **The study of hippocampal CA1 sequences**

The standardized protocols described in the thesis are expected to aid in future experiments studying hippocampal CA1 sequences. Our simultaneous 2-photon calcium imaging recordings and behavioural training provided us the platform to study neural activity from ~100-150 cells/animal at behaviourally relevant timescales (~70 ms per frame).

We standardized a multi-day Trace Eye-Blink Conditioning or TEC (“Chapter 2 - Behaviour”) training system for mice based on previous literature (Siegel et al., 2015) and could demonstrate several types of behavioural adaptations that experimental animals could learn under a variety of experiment conditions and modulations. Notably,

1. The animals typically learnt the tasks quickly, within 1-2 weeks of training.
2. Modulating the inter-stimulus interval (ISI) between the CS and US results affected the expression of the conditioned response (CR).
3. A wide palette of stimuli may now be incorporated into existing protocols as either of the presented stimuli (data not shown). TEC experiments with multiple CS, viz., blue LED and Tone, have been tried in the lab. They form the primary behavioural modulation being investigated by a lab colleague. These experiments are now directly possible due to the standardization efforts.
4. In our experiments where we extended the Trace Duration, animals show retention of previously learnt CR times (Figures 19-21), showcase complex blinks (Figure 19) without change to CR onset (Figure 20).

5. We could also train animals on very long Trace durations (550 ms, and 750 ms), which have previously not been reported for head-fixed mice.
6. Across all the single interval training experiments, the animals only produce one conditioned response, with time of peak adjusted relative to the timing of the US.
7. Complex blinks were only observed in animals trained to more than one trace interval.

Simultaneous large-scale recordings have been fundamental to the discovery of long spatiotemporal activity patterns with several participant CA1 neurons (Davidson et al., 2009; Foster, 2017). Electrical recordings provide many orders of magnitude better temporal resolution, not to mention being a direct readout of action potentials. However at the time of the design of the thesis, imaging based approaches could yield more recorded neurons per experiment animal. We standardized 2-photon fluorescence based chronic imaging of hippocampal CA1 neurons to allow calcium imaging based recording of the spatiotemporal sequences across multiple days ("Chapter 3 - Imaging"). This gave us the ability to

1. Record neurophysiology over a large population of neurons (~100), in conjunction with temporally relevant behavioural contexts and modulations, albeit at ~100 ms temporal resolution.
2. Chronically track cells across various behaviour sessions without ambiguity.
3. Allow for scalability in the per animal yield of recording neurons with the use of faster and modern 2-photon microscope hardware utilizing Resonant Scanning instead of galvo-scanning, as well as multi-channel imaging.

We could identify time cells with the ability to retain, de-tune, or even re-tune, over the course of multiple sessions. Given no change in the behaviour protocol variables, it is unlikely we would have found such adaptations without scaling up the yield of cells or improving our temporal resolution while recording each individual session. Since the behaviour task is typically learnt to ~70-80% performance levels over the course of multiple sessions, our methodology gives us the ability to look into learning mechanisms utilized by the CA1 in the interim. Production quality datasets were quickly obtained by colleagues in the lab, following the protocols standardized and described here.

From our preliminary data, the largest proportion of re-tuned cells had tuning peaks shift to earlier time points (Chapter 3 – “Imaging”, Figure 37), with subsequent sessions. Early in training, the timing of tuning peaks would typically occur near the time of the Unconditioned Stimulus (US; air-puff to eye). Our experiments presenting stimuli to naive animals (in accordance with Dhawale, 2013) suggested that somatosensory stimuli may be able to modulate CA1 responses, while many neutral stimuli may not (Chapter 3 – “Imaging”, Figure 29), without training. These results do allow for speculation on how initially neutral Conditioned Stimuli (CS; Light LED pulse) could develop behavioural valence for the animal, viz., the selective suppression of Response Inhibition to the previously neutral CS. An as yet unknown fraction of time cells may initially be triggered by the Unconditioned Stimulus (US; air-puff), but over the course of multiple training sessions, shift tuning fields to respond to the CS at the level of the CA1 network. However, many more datasets would be required to firmly establish any mechanistic insight into the phenomenon.

## **Standardizing combined behaviour and recording experiments**

Hippocampal CA1 time cells had been previously described to fire in reliable sequences, as observed in animals that learnt a single-session version of the TEC paradigm (Modi et al., 2014). We wished to further develop the paradigm and more fully study time cells, especially during the early or acquisition phase of training (sessions 1-7). It was not considered trivial to bundle behaviour and recording in a non-interfering way. For instance, we needed to study time cells longitudinally or chronically, and this is likely achieved by ensuring that the experimental animals were not overtly stressed, but rather, were reasonably compliant to the experiment in terms of motivation.

Towards this,

- 1) We focused on performing only one surgery, viz., head-bar implant and hippocampus to minimize surgery-induced trauma, rather than multiple surgery strategies.
- 2) We incorporated a treadmill for the animals to run on during the experiments, at the potential cost of observing z-axis drift in the imaging.
- 3) Imaging requires that the sample (experimental animals) be illuminated only by the excitation laser and that the sensor systems for the emitted photons receive only the photons from the excited sample. We considered and designed the filter sets before our photomultiplier tube (PMT) in the emission path, to reject all IR and partially red frequencies, not just to protect the sensor from the excitation 2-photon

laser, but also the red/short IR illumination on the animal's eye for the behaviour camera.

Through our experiments, we were able to provide some evidence that somatosensory stimuli, but not other neutral stimuli, could trigger CA1 responses but the effect of behavioural training results in the development of CA1 responses to the CS, now triggering a whole spatiotemporal sequence of activation. Altogether, we were able to observe preliminary results regarding the tuning, de-tuning, and re-tuning of time cells to temporal fields during learning, as described in Chapter 3 – “Imaging”.

## **Mapping sequences to abstract variables**

Visual cues are typically considered important to place cell activity and tuning. The specific requirement of vision, however, was tested in a study published in 2015. Experimenters switched off the lights as their animals navigated a maze. The animals were provided only olfactory cues at specific locations in the maze, yet place cell activity and tuning could be recorded. This suggested that the hippocampus could use non-visuospatial resources to generate spatial representations, when vision was compromised (Zhang & Manahan-Vaughan, 2015).

In a sound manipulation task (SMT) rats changed the frequency of auditory tones in their environment, by self-initiated joystick control, ramping logarithmic sweeps of frequency space. The rate of change in frequency could be manipulated either by the animal or pseudorandomly by the experimenter. This study describes neural

activity recorded from the medial entorhinal cortex (MEC) as well as the hippocampal CA1 with sub-populations that were found tuned to specific frequency “landmarks” during the auditory sequence (Aronov et al., 2017). The CA1 were, thus, argued to be capable of tuning to abstract variables and were designed to map out sequences of events/stimuli in their own spatiotemporal patterns of activity.

The ubiquity of neural sequences in a wide variety of systems has been discussed previously (Bhalla, 2019; Conen & Desrochers, 2022; S. Zhou et al., 2020) and over a century of research has discovered remarkable physiological features that may be used to identify neurons that participate in these sequences. However, research is still required to carefully dissect out the contribution that each participant neuron has to behaviour, an important goal in neuroscience (Ranck, 1973, 1975).

The use of user-configurable, categorically labeled synthetic calcium activity profiles allowed us to probe and compare a range of different time cell detection algorithms, identifying strategies to best classify time cells. We were able to identify Temporal Information as a strong contender for the choice of algorithm for such classification (Ananthamurthy & Bhalla, 2023). The algorithms developed along the way were tested within the time scales of ~100 ms, that correspond to Replay Sequences or other behaviour timescale sequences. We expect the analysis routines to be useful in a variety of different experiments that could potentially help describe the neural code in more detail.

## Better temporal resolution requires new techniques

There are many other techniques that experimenters in the field have employed to record activity. Many of these techniques do, in fact, achieve much better temporal resolution. Here are some examples:

- 1) Resonant Scanning based 2p calcium imaging can achieve even up to 30 Hz for 4x larger fields of view, or more frame rates for smaller fields of view (Bonin et al., 2011; Leybaert et al., 2005; Nguyen et al., 2001; Rochefort et al., 2009). At the time when we started the experiments for the thesis, Resonant scanning microscopes required a lot of additional, expensive components to be purchased. Towards this, we co-wrote a sanctioned DBT grant application (BT/PR12255/MED/122/8/2016) and began setting up the new microscope. However, we did not have this technology available for experiments before 2020.
- 2) High-density tetrodes can be used to perform electrical recordings at  $\geq 20$  kHz, as compared to  $\sim 14.5$  Hz for our galvo-scanning 2p calcium imaging experiments. This technique typically achieves yields of  $\sim 40$  cells for hippocampal recordings, and we argued that we could achieve a higher yield ( $> 100$  cells) with galvo-scanning 2p calcium imaging. The relative sparsity of the hippocampal neural code in terms of cells participating in any engram, mandates high-yield recordings to identify the full temporal sequence of CA1 activations (Foster, 2017).
- 3) Neuropixels (Jun et al., 2017) can be used to perform electrical recordings at  $\geq 20$  kHz. At the time when we started the experiments for the thesis, these sorts of electrical probes had yet to be successfully deployed in published literature.

We discuss all these techniques while comparing electrical- vs. imaging-based recording strategies in Chapter 1 – “Introduction”. Fundamentally, given the technological constraints at the time, we had devised combined behaviour with galvo-scanning 2p calcium imaging as the principle for the experiments described in this thesis.

## **Does the brain create or predict?**

An important direction to neuroscience research is to understand the brain and nervous system, in how these structures allow animals to interact meaningfully with their environment. More conservatively, however, the goal of this thesis was to help provide a multi-disciplinary toolkit to study time cells in the hippocampus. Predictive coding has been considered as a way for the brain to ultimately use external sensory information to minimize prediction errors during tasks (Doya et al., 2007; Rao & Ballard, 1999). One of the core ideas of Bayesian approaches to neurophysiology and behaviour is that the brain could be modeled as a prediction machine that is constantly modeling the change of variables. These variables may be external or internal yet salient concepts to any experimental animal, arguably expressed in neurophysiology as the dynamics of engrams. The ability of the mammalian hippocampus to bind both information streams to create new, more elaborate engrams, is likely crucial to the learning of new concepts behaviourally (N. J. Cohen & Eichenbaum, 1993; Eichenbaum, 2017).

Attentional states have been shown to have a bidirectional relationship with the expression of memory and learning (Chun & Johnson, 2011;

Hutchinson & Turk-Browne, 2012; Uncapher et al., 2011). Specifically, Trace Eye-Blink Conditioning (TEC) performance has been suggested to be positively correlated with attention (Manns et al., 2000). The question of the effect of attentional states on the dynamics of the associated engram motivated an important milestone for the Thesis, *viz.*, to combine stable, adaptable behaviour studies with large-scale neurophysiology.

We were able to train head-fixed mice to TEC and confirm adaptable conditioned responses to task variables. We were also able to simultaneous record from ~100 hippocampal CA1 cell bodies as the animals acquired top behavioural performance. We observed in our preliminary results that many identified time cells showcased the ability to tune to different time points across sessions or days, as has been previously reported (Mau et al., 2018). This standardization of simultaneous behaviour and imaging ensured that colleagues from our lab were able to generate production quality data, quickly.

Several more high quality recordings and behaviour modulations would be required to conclusively describe time cells physiology and engram dynamics, at least at the level of a sub-population of hippocampal CA1. However, progress has been made to suggest the best time cell detection algorithm(s) based on their sensitivity to different recording parameters (Ananthamurthy & Bhalla, 2023). We hope that the Thesis is of aid to future research on the neural mechanisms of Learning and Memory by the nervous system.

## Bibliography

- Ananthamurthy, K. G., & Bhalla, U. S. (2023). Synthetic Data Resource and Benchmarks for Time Cell Analysis and Detection Algorithms. *ENeuro*, ENEURO.0007-22.2023.  
<https://doi.org/10.1523/ENEURO.0007-22.2023>
- Aronov, D., Nevers, R., & Tank, D. W. (2017). Mapping of a non-spatial dimension by the hippocampal-entorhinal circuit. *Nature*, 543(7647), 719–722. <https://doi.org/10.1038/nature21692>
- Bhalla, U. S. (2019). Dendrites, deep learning, and sequences in the hippocampus. *Hippocampus*, 29(3), 239–251.  
<https://doi.org/https://doi.org/10.1002/hipo.22806>
- Bonin, V., Histed, M. H., Yurgenson, S., & Reid, R. C. (2011). Local Diversity and Fine-Scale Organization of Receptive Fields in Mouse Visual Cortex. *The Journal of Neuroscience*, 31(50), 18506. <https://doi.org/10.1523/JNEUROSCI.2974-11.2011>
- Chun, M. M., & Johnson, M. K. (2011). Memory: enduring traces of perceptual and reflective attention. *Neuron*, 72(4), 520–535.  
<https://doi.org/10.1016/j.neuron.2011.10.026>
- Cohen, N. J., & Eichenbaum, H. (1993). *Memory, amnesia, and the hippocampal system*.
- Conen, K. E., & Desrochers, T. M. (2022). *The Neural Basis of Behavioral Sequences in Cortical and Subcortical Circuits*. Oxford University Press.  
<https://doi.org/10.1093/acrefore/9780190264086.013.421>
- Davidson, T. J., Kloosterman, F., & Wilson, M. A. (2009). Hippocampal replay of extended experience. *Neuron*, 63(4), 497–507.  
<https://doi.org/10.1016/j.neuron.2009.07.027>
- Dhawale, A. K. (2013). *Temporal and spatial features of sensory coding in the olfactory bulb and hippocampus*. Tata Institute of Fundamental Research.
- Doya, K., Ishii, S., Pouget, A., & Rao, R. P. N. (2007). Bayesian brain: Probabilistic approaches to neural coding. In K. Doya, S. Ishii, A. Pouget, & R. P. N. Rao (Eds.), *Bayesian brain: Probabilistic approaches to neural coding*. MIT Press.
- Eichenbaum, H. (2017). On the Integration of Space, Time, and Memory. *Neuron*, 95(5), 1007–1018.  
<https://doi.org/10.1016/j.neuron.2017.06.036>
- Foster, D. J. (2017). Replay Comes of Age. *Annual Review of Neuroscience*, 40, 581–602. <https://doi.org/10.1146/annurev-neuro-072116-031538>
- Hutchinson, J. B., & Turk-Browne, N. B. (2012). Memory-guided attention: control from multiple memory systems. *Trends in*

- Cognitive Sciences*, 16(12), 576–579.  
<https://doi.org/10.1016/j.tics.2012.10.003>
- Jun, J. J., Steinmetz, N. A., Siegle, J. H., Denman, D. J., Bauza, M., Barbarits, B., Lee, A. K., Anastassiou, C. A., Andrei, A., Aydin, Ç., Barbic, M., Blanche, T. J., Bonin, V., Couto, J., Dutta, B., Gratiy, S. L., Gutnisky, D. A., Häusser, M., Karsh, B., ... Harris, T. D. (2017). Fully integrated silicon probes for high-density recording of neural activity. *Nature*, 551(7679), 232–236.  
<https://doi.org/10.1038/nature24636>
- Leybaert, L., de Meyer, A., Mabilde, C., & Sanderson, M. J. (2005). A simple and practical method to acquire geometrically correct images with resonant scanning-based line scanning in a custom-built video-rate laser scanning microscope. *Journal of Microscopy*, 219(3), 133–140. <https://doi.org/https://doi.org/10.1111/j.1365-2818.2005.01502.x>
- Manns, J. R., Clark, R. E., & Squire, L. R. (2000). Parallel acquisition of awareness and trace eyeblink classical conditioning. *Learning & Memory (Cold Spring Harbor, N.Y.)*, 7(5), 267–272.  
<https://doi.org/10.1101/lm.33400>
- Mau, W., Sullivan, D. W., Kinsky, N. R., Hasselmo, M. E., Howard, M. W., & Eichenbaum, H. (2018). The Same Hippocampal CA1 Population Simultaneously Codes Temporal Information over Multiple Timescales. *Current Biology*, 28(10), 1499-1508.e4.  
<https://doi.org/10.1016/j.cub.2018.03.051>
- Modi, M. N., Dhawale, A. K., & Bhalla, U. S. (2014). CA1 cell activity sequences emerge after reorganization of network correlation structure during associative learning. *eLife*, 3, e01982–e01982.  
<https://doi.org/10.7554/eLife.01982>
- Nguyen, Q.-T., Callamaras, N., Hsieh, C., & Parker, I. (2001). Construction of a two-photon microscope for video-rate Ca<sup>2+</sup> imaging. *Cell Calcium*, 30(6), 383–393.  
<https://doi.org/https://doi.org/10.1054/ceca.2001.0246>
- Ranck, J. B. (1973). Studies on single neurons in dorsal hippocampal formation and septum in unrestrained rats: Part I. Behavioral correlates and firing repertoires. *Experimental Neurology*, 41(2), 462–531. [https://doi.org/https://doi.org/10.1016/0014-4886\(73\)90290-2](https://doi.org/https://doi.org/10.1016/0014-4886(73)90290-2)
- Ranck, J. B. (1975). *Behavioral Correlates and Firing Repertoires of Neurons in the Dorsal Hippocampal Formation and Septum of Unrestrained Rats BT - The Hippocampus: Volume 2: Neurophysiology and Behavior* (R. L. Isaacson & K. H. Pribram, Eds.; pp. 207–244). Springer US. [https://doi.org/10.1007/978-1-4684-2979-4\\_7](https://doi.org/10.1007/978-1-4684-2979-4_7)

- Rao, R. P. N., & Ballard, D. H. (1999). Predictive coding in the visual cortex: a functional interpretation of some extra-classical receptive-field effects. *Nature Neuroscience*, 2(1), 79–87. <https://doi.org/10.1038/4580>
- Rochefort, N. L., Garaschuk, O., Milos, R.-I., Narushima, M., Marandi, N., Pichler, B., Kovalchuk, Y., & Konnerth, A. (2009). Sparsification of neuronal activity in the visual cortex at eye-opening. *Proceedings of the National Academy of Sciences of the United States of America*, 106(35), 15049–15054. <https://doi.org/10.1073/pnas.0907660106>
- Siegel, J. J., Taylor, W., Gray, R., Kalmbach, B., Zemelman, B. V., Desai, N. S., Johnston, D., & Chitwood, R. A. (2015). Trace Eyeblink Conditioning in Mice Is Dependent upon the Dorsal Medial Prefrontal Cortex, Cerebellum, and Amygdala: Behavioral Characterization and Functional Circuitry. *ENeuro*, 2(4), ENEURO.0051-14.2015. <https://doi.org/10.1523/ENEURO.0051-14.2015>
- Uncapher, M. R., Hutchinson, J. B., & Wagner, A. D. (2011). Dissociable effects of top-down and bottom-up attention during episodic encoding. *The Journal of Neuroscience : The Official Journal of the Society for Neuroscience*, 31(35), 12613–12628. <https://doi.org/10.1523/JNEUROSCI.0152-11.2011>
- Zhang, S., & Manahan-Vaughan, D. (2015). Spatial olfactory learning contributes to place field formation in the hippocampus. *Cerebral Cortex (New York, N.Y. : 1991)*, 25(2), 423–432. <https://doi.org/10.1093/cercor/bht239>
- Zhou, S., Masmanidis, S. C., & Buonomano, D. V. (2020). Neural Sequences as an Optimal Dynamical Regime for the Readout of Time. *Neuron*, 108(4), 651-658.e5. <https://doi.org/https://doi.org/10.1016/j.neuron.2020.08.020>

## All Bibliography

- Abe, R., Sakaguchi, T., Matsumoto, N., Matsuki, N., & Ikegaya, Y. (2014). Sound-induced hyperpolarization of hippocampal neurons. *Neuroreport*, 25(13), 1013–1017. <https://doi.org/10.1097/WNR.0000000000000206>
- Abeles, M. (1982). *Local Cortical Circuits: An Electrophysiological Study*. Springer-Verlag.
- <https://books.google.co.in/books?id=s25lwwEACAAJ>
- Abeles, M. (1991). *Corticonics: Neural Circuits of the Cerebral Cortex*. Cambridge University Press. <https://doi.org/DOI:10.1017/CBO9780511574566>
- Abeles, M. (2004). Time Is Precious. *Science*, 304(5670), 523–524. <https://doi.org/10.1126/science.1097725>
- Abeles, M. (2009). *Synfire Chains* (L. R. B. T.-E. of N. Squire, Ed.; pp. 829–832). Academic Press.
- <https://doi.org/https://doi.org/10.1016/B978-008045046-9.01437-6>
- Abeles, M., Hayon, G., & Lehmann, D. (2004). Modeling compositionality by dynamic binding of synfire chains. *Journal of Computational Neuroscience*, 17(2), 179–201. <https://doi.org/10.1023/B:JCNS.0000037682.18051.5f>
- Ananthamurthy, K. G., & Bhalla, U. S. (2023). Synthetic Data Resource and Benchmarks for Time Cell Analysis and Detection Algorithms. *ENeuro*, ENEURO.0007-22.2023. <https://doi.org/10.1523/ENEURO.0007-22.2023>
- Andermann, M. L., Gilfoy, N. B., Goldey, G. J., Sachdev, R. N. S., Wölfel, M., McCormick, D. A., Reid, R. C., & Levene, M. J. (2013). Chronic Cellular Imaging of Entire Cortical Columns in Awake Mice Using Microprisms. *Neuron*, 80(4), 900–913. <https://doi.org/10.1016/j.neuron.2013.07.052>
- Andersen, P., Morris, R., Amaral, D., Bliss, T., & O’Keefe, J. (Eds.). (2006). *The Hippocampus Book*. Oxford University Press. <https://doi.org/10.1093/acprof:oso/9780195100273.001.0001>
- Andersen, R. A., Snyder, L. H., Li, C.-S., & Stricanne, B. (1993). Coordinate transformations in the representation of spatial information. *Current Opinion in Neurobiology*, 3(2), 171–176. [https://doi.org/https://doi.org/10.1016/0959-4388\(93\)90206-E](https://doi.org/https://doi.org/10.1016/0959-4388(93)90206-E)
- Aronov, D., Nevers, R., & Tank, D. W. (2017). Mapping of a non-spatial dimension by the hippocampal-entorhinal circuit. *Nature*, 543(7647), 719–722. <https://doi.org/10.1038/nature21692>
- Attardo, A., Fitzgerald, J. E., & Schnitzer, M. J. (2015). Impermanence of dendritic spines in live adult CA1 hippocampus. *Nature*, 523(7562), 592–596. <https://doi.org/10.1038/nature14467>

- Ballard, I. C., Wagner, A. D., & McClure, S. M. (2019). Hippocampal pattern separation supports reinforcement learning. *Nature Communications*, 10(1), 1073. <https://doi.org/10.1038/s41467-019-08998-1>
- Barreto, R. P. J., Messerschmidt, B., & Schnitzer, M. J. (2009). In vivo fluorescence imaging with high-resolution microlenses. *Nature Methods*, 6(7), 511–512. <https://doi.org/10.1038/nmeth.1339>
- Barreto, R. P. J., & Schnitzer, M. J. (2012). In vivo optical microendoscopy for imaging cells lying deep within live tissue. *Cold Spring Harbor Protocols*, 2012(10), 1029–1034. <https://doi.org/10.1101/pdb.top071464>
- Baudry, M., & Lynch, G. (1981). Hippocampal glutamate receptors. *Molecular and Cellular Biochemistry*, 38(1), 5–18. <https://doi.org/10.1007/BF00235685>
- Bellistri, E., Aguilar, J., Brotons-Mas, J. R., Foffani, G., & de la Prida, L. M. (2013). Basic properties of somatosensory-evoked responses in the dorsal hippocampus of the rat. *The Journal of Physiology*, 591(10), 2667–2686. <https://doi.org/10.1113/jphysiol.2013.251892>
- Bhalla, U. S. (2019). Dendrites, deep learning, and sequences in the hippocampus. *Hippocampus*, 29(3), 239–251. <https://doi.org/https://doi.org/10.1002/hipo.22806>
- Bialek, W., Callan, C. G., & Strong, S. P. (1996). Field Theories for Learning Probability Distributions. *Physical Review Letters*, 77(23), 4693–4697. <https://doi.org/10.1103/physrevlett.77.4693>
- Bialek, W., Nemenman, I., & Tishby, N. (2001). Predictability, Complexity, and Learning. *Neural Comput.*, 13(11), 2409–2463. <https://doi.org/10.1162/089976601753195969>
- Bienenstock, E. (1995). A model of neocortex. *Network: Computation in Neural Systems*, 6(2), 179–224. [https://doi.org/10.1088/0954-898X\\_6\\_2\\_004](https://doi.org/10.1088/0954-898X_6_2_004)
- Bjerknes, T. L., Moser, E. I., & Moser, M.-B. (2014). Representation of Geometric Borders in the Developing Rat. *Neuron*, 82(1), 71–78. <https://doi.org/10.1016/j.neuron.2014.02.014>
- Bonin, V., Histed, M. H., Yurgenson, S., & Reid, R. C. (2011). Local Diversity and Fine-Scale Organization of Receptive Fields in Mouse Visual Cortex. *The Journal of Neuroscience*, 31(50), 18506. <https://doi.org/10.1523/JNEUROSCI.2974-11.2011>
- Brown, G. D. (1998). Nonassociative learning processes affecting swimming probability in the seashell Tritonia diomedea: habituation, sensitization and inhibition. *Behavioural Brain Research*, 95(2), 151–165. [https://doi.org/https://doi.org/10.1016/S0166-4328\(98\)00072-2](https://doi.org/https://doi.org/10.1016/S0166-4328(98)00072-2)
- Buccino, A. P., Garcia, S., & Yger, P. (2022). Spike sorting: new trends

- and challenges of the era of high-density probes. *Progress in Biomedical Engineering*, 4(2), 022005.  
<https://doi.org/10.1088/2516-1091/ac6b96>
- Burgess, N. (2008). Spatial Cognition and the Brain. *Annals of the New York Academy of Sciences*, 1124(1), 77–97.  
<https://doi.org/https://doi.org/10.1196/annals.1440.002>
- Buzsáki, G., & Llinás, R. (2017). Space and time in the brain. *Science (New York, N.Y.)*, 358(6362), 482–485.  
<https://doi.org/10.1126/science.aan8869>
- Cai, D. J., Aharoni, D., Shuman, T., Shobe, J., Biane, J., Song, W., Wei, B., Veshkini, M., La-Vu, M., Lou, J., Flores, S. E., Kim, I., Sano, Y., Zhou, M., Baumgaertel, K., Lavi, A., Kamata, M., Tuszyński, M., Mayford, M., ... Silva, A. J. (2016). A shared neural ensemble links distinct contextual memories encoded close in time. *Nature*, 534(7605), 115–118.  
<https://doi.org/10.1038/nature17955>
- Caporale, N., & Dan, Y. (2008). Spike timing-dependent plasticity: a Hebbian learning rule. *Annual Review of Neuroscience*, 31, 25–46. <https://doi.org/10.1146/annurev.neuro.31.060407.125639>
- Carew, T. J., Castellucci, V. F., & Kandel, E. R. (1971). An Analysis of Dishabituation and Sensitization of The Gill-Withdrawal Reflex In Aplysia. *International Journal of Neuroscience*, 2(2), 79–98.  
<https://doi.org/10.3109/00207457109146995>
- Chen, T.-W., Wardill, T. J., Sun, Y., Pulver, S. R., Renninger, S. L., Baohan, A., Schreiter, E. R., Kerr, R. A., Orger, M. B., Jayaraman, V., Looger, L. L., Svoboda, K., & Kim, D. S. (2013). Ultrasensitive fluorescent proteins for imaging neuronal activity. *Nature*, 499(7458), 295–300. <https://doi.org/10.1038/nature12354>
- Chigirev, D., & Bialek, W. (2004, January). Optimal manifold representation of data: An information theoretic approach. *Advances in Neural Information Processing Systems 16 - Proceedings of the 2003 Conference, NIPS 2003*.
- Chudasama, Y. (2010). Delayed (Non)Match-to-Sample Task. In I. P. Stolerman (Ed.), *Encyclopedia of Psychopharmacology* (p. 372). Springer Berlin Heidelberg. [https://doi.org/10.1007/978-3-540-68706-1\\_1619](https://doi.org/10.1007/978-3-540-68706-1_1619)
- Chun, M. M., & Johnson, M. K. (2011). Memory: enduring traces of perceptual and reflective attention. *Neuron*, 72(4), 520–535.  
<https://doi.org/10.1016/j.neuron.2011.10.026>
- Clayton, N. S., Salwiczek, L. H., & Dickinson, A. (2007). Episodic memory. *Current Biology*, 17(6), R189–R191.  
<https://doi.org/10.1016/j.cub.2007.01.011>
- Cohen, M. R., & Kohn, A. (2011). Measuring and interpreting neuronal

- correlations. *Nature Neuroscience*, 14(7), 811–819.  
<https://doi.org/10.1038/nn.2842>
- Cohen, N. J., & Eichenbaum, H. (1993). *Memory, amnesia, and the hippocampal system*.
- Conen, K. E., & Desrochers, T. M. (2022). *The Neural Basis of Behavioral Sequences in Cortical and Subcortical Circuits*. Oxford University Press.  
<https://doi.org/10.1093/acrefore/9780190264086.013.421>
- Conway, M. A. (2009). Episodic memories. *Neuropsychologia*, 47(11), 2305–2313.  
<https://doi.org/https://doi.org/10.1016/j.neuropsychologia.2009.02.003>
- Csicsvari, J., O'Neill, J., Allen, K., & Senior, T. (2007). Place-selective firing contributes to the reverse-order reactivation of CA1 pyramidal cells during sharp waves in open-field exploration. *The European Journal of Neuroscience*, 26(3), 704–716.  
<https://doi.org/10.1111/j.1460-9568.2007.05684.x>
- Davidson, T. J., Kloosterman, F., & Wilson, M. A. (2009). Hippocampal replay of extended experience. *Neuron*, 63(4), 497–507.  
<https://doi.org/10.1016/j.neuron.2009.07.027>
- Denk, W., Strickler, J. H., & Webb, W. W. (1990). Two-photon laser scanning fluorescence microscopy. *Science (New York, N.Y.)*, 248(4951), 73–76. <https://doi.org/10.1126/science.2321027>
- Deshmukh, S. S., & Bhalla, U. S. (2003). Representation of odor habituation and timing in the hippocampus. *The Journal of Neuroscience : The Official Journal of the Society for Neuroscience*, 23(5), 1903–1915.  
<https://doi.org/10.1523/JNEUROSCI.23-05-01903.2003>
- Dhawale, A. K. (2013). *Temporal and spatial features of sensory coding in the olfactory bulb and hippocampus*. Tata Institute of Fundamental Research.
- Dhawale, A. K., Poddar, R., Wolff, S. B. E., Normand, V. A., Kopelowitz, E., & Ölveczky, B. P. (2017). Automated long-term recording and analysis of neural activity in behaving animals. *eLife*, 6, e27702. <https://doi.org/10.7554/eLife.27702>
- Diamond, A. (2013). Executive Functions. *Annual Review of Psychology*, 64(1), 135–168. <https://doi.org/10.1146/annurev-psych-113011-143750>
- Diba, K., & Buzsáki, G. (2007). Forward and reverse hippocampal place-cell sequences during ripples. *Nature Neuroscience*, 10(10), 1241–1242. <https://doi.org/10.1038/nn1961>
- Dickinson, A., Nicholas, D. J., & Mackintosh, N. J. (1983). A re-examination of one-trial blocking in conditioned suppression. *The*

- Quarterly Journal of Experimental Psychology B: Comparative and Physiological Psychology*, 35, 67–79.  
<https://doi.org/10.1080/14640748308400914>
- Disterhoft, J. F., & Weiss, C. (2017). Eyeblink Conditioning – A Behavioral Model of Procedural and Declarative Learning. In J. H. Byrne (Ed.), *Learning and Memory: A Comprehensive Reference (Second Edition)* (pp. 327–355). Academic Press.  
<https://doi.org/https://doi.org/10.1016/B978-0-12-809324-5.21087-0>
- Dombeck, D. A., Graziano, M. S., & Tank, D. W. (2009). Functional Clustering of Neurons in Motor Cortex Determined by Cellular Resolution Imaging in Awake Behaving Mice. *The Journal of Neuroscience*, 29(44), 13751 LP – 13760.  
<https://doi.org/10.1523/JNEUROSCI.2985-09.2009>
- Dombeck, D. A., Harvey, C. D., Tian, L., Looger, L. L., & Tank, D. W. (2010). Functional imaging of hippocampal place cells at cellular resolution during virtual navigation. *Nature Neuroscience*, 13(11), 1433–1440. <https://doi.org/10.1038/nn.2648>
- Doya, K., Ishii, S., Pouget, A., & Rao, R. P. N. (2007). Bayesian brain: Probabilistic approaches to neural coding. In K. Doya, S. Ishii, A. Pouget, & R. P. N. Rao (Eds.), *Bayesian brain: Probabilistic approaches to neural coding*. MIT Press.
- Dragoi, G. (2013). Internal operations in the hippocampus: single cell and ensemble temporal coding. *Frontiers in Systems Neuroscience*, 7, 46. <https://doi.org/10.3389/fnsys.2013.00046>
- Dragoi, G., & Buzsáki, G. (2006). Temporal encoding of place sequences by hippocampal cell assemblies. *Neuron*, 50(1), 145–157. <https://doi.org/10.1016/j.neuron.2006.02.023>
- Dragoi, G., Carpi, D., Recce, M., Csicsvari, J., & Buzsáki, G. (1999). Interactions between hippocampus and medial septum during sharp waves and theta oscillation in the behaving rat. *The Journal of Neuroscience : The Official Journal of the Society for Neuroscience*, 19(14), 6191–6199.  
<http://www.ncbi.nlm.nih.gov/pubmed/10407055>
- Dragoi, G., & Tonegawa, S. (2011). Preplay of future place cell sequences by hippocampal cellular assemblies. *Nature*, 469(7330), 397–401. <https://doi.org/10.1038/nature09633>
- Eichenbaum, H. (2004). Hippocampus: Cognitive processes and neural representations that underlie declarative memory. *Neuron*, 44(1), 109–120. <https://doi.org/10.1016/j.neuron.2004.08.028>
- Eichenbaum, H. (2017). On the Integration of Space, Time, and Memory. *Neuron*, 95(5), 1007–1018.  
<https://doi.org/10.1016/j.neuron.2017.06.036>

- Ekstrom, A. D., & Ranganath, C. (2018). Space, time, and episodic memory: The hippocampus is all over the cognitive map. *Hippocampus*, 28(9), 680–687.  
<https://doi.org/https://doi.org/10.1002/hipo.22750>
- Fanselow, M. S., & Dong, H.-W. (2010). Are the dorsal and ventral hippocampus functionally distinct structures? *Neuron*, 65(1), 7–19.  
<https://doi.org/10.1016/j.neuron.2009.11.031>
- Fassihi, A., Akrami, A., Pulecchi, F., Schönfelder, V., & Diamond, M. E. (2017). Transformation of Perception from Sensory to Motor Cortex. *Current Biology : CB*, 27(11), 1585-1596.e6.  
<https://doi.org/10.1016/j.cub.2017.05.011>
- Ferbinteanu, J., & Shapiro, M. L. (2003). Prospective and retrospective memory coding in the hippocampus. *Neuron*, 40(6), 1227–1239.  
[https://doi.org/10.1016/s0896-6273\(03\)00752-9](https://doi.org/10.1016/s0896-6273(03)00752-9)
- Ferbinteanu, J., Shirvalkar, P., & Shapiro, M. L. (2011). Memory Modulates Journey-Dependent Coding in the Rat Hippocampus. *The Journal of Neuroscience*, 31(25), 9135 LP – 9146.  
<https://doi.org/10.1523/JNEUROSCI.1241-11.2011>
- Focus on spatial cognition. (2017). *Nature Neuroscience*, 20(11), 1431.  
<https://doi.org/10.1038/nn.4666>
- Foster, D. J. (2017). Replay Comes of Age. *Annual Review of Neuroscience*, 40, 581–602. <https://doi.org/10.1146/annurev-neuro-072116-031538>
- Foster, D. J., & Wilson, M. A. (2006). Reverse replay of behavioural sequences in hippocampal place cells during the awake state. *Nature*, 440(7084), 680–683. <https://doi.org/10.1038/nature04587>
- Foster, D. J., & Wilson, M. A. (2007). Hippocampal theta sequences. *Hippocampus*, 17(11), 1093–1099.  
<https://doi.org/10.1002/hipo.20345>
- Francis, M., Qian, X., Charbel, C., Ledoux, J., Parker, J. C., & Taylor, M. S. (2012). Automated region of interest analysis of dynamic Ca<sup>2+</sup> signals in image sequences. *American Journal of Physiology. Cell Physiology*, 303(3), C236-43.  
<https://doi.org/10.1152/ajpcell.00016.2012>
- Frank, L. M., Brown, E. N., & Wilson, M. (2000). Trajectory encoding in the hippocampus and entorhinal cortex. *Neuron*, 27(1), 169–178.  
[https://doi.org/10.1016/s0896-6273\(00\)00018-0](https://doi.org/10.1016/s0896-6273(00)00018-0)
- Fyhn, M., Molden, S., Witter, M. P., Moser, E. I., & Moser, M.-B. (2004). Spatial representation in the entorhinal cortex. *Science (New York, N.Y.)*, 305(5688), 1258–1264.  
<https://doi.org/10.1126/science.1099901>
- Giovannucci, A., Badura, A., Deverett, B., Najafi, F., Pereira, T. D., Gao, Z., Ozden, I., Kloth, A. D., Pnevmatikakis, E., Paninski, L.,

- De Zeeuw, C. I., Medina, J. F., & Wang, S. S.-H. (2017). Cerebellar granule cells acquire a widespread predictive feedback signal during motor learning. *Nature Neuroscience*, 20(5), 727–734. <https://doi.org/10.1038/nn.4531>
- Grün, S. (2009). Data-Driven Significance Estimation for Precise Spike Correlation. *Journal of Neurophysiology*, 101(3), 1126–1140. <https://doi.org/10.1152/jn.00093.2008>
- Guo, Z. V., Hires, S. A., Li, N., O'Connor, D. H., Komiyama, T., Ophir, E., Huber, D., Bonardi, C., Morandell, K., Gutinsky, D., Peron, S., Xu, N., Cox, J., & Svoboda, K. (2014). Procedures for Behavioral Experiments in Head-Fixed Mice. *PLOS ONE*, 9(2), e88678. <https://doi.org/10.1371/journal.pone.0088678>
- Gupta, A. S., van der Meer, M. A. A., Touretzky, D. S., & Redish, A. D. (2010). Hippocampal Replay Is Not a Simple Function of Experience. *Neuron*, 65(5), 695–705. <https://doi.org/https://doi.org/10.1016/j.neuron.2010.01.034>
- Hafting, T., Fyhn, M., Molden, S., Moser, M.-B., & Moser, E. I. (2005). Microstructure of a spatial map in the entorhinal cortex. *Nature*, 436(7052), 801–806. <https://doi.org/10.1038/nature03721>
- Hamme, L. J. Van, & Wasserman, E. A. (1993). Cue Competition in Causality Judgments: The Role of Manner of Information Presentation. *Bulletin of the Psychonomic Society*, 31(5), 457–460. <https://doi.org/10.3758/bf03334962>
- Han, J.-H., Kushner, S. A., Yiu, A. P., Hsiang, H.-L. L., Buch, T., Waisman, A., Bontempi, B., Neve, R. L., Frankland, P. W., & Josselyn, S. A. (2009). Selective erasure of a fear memory. *Science (New York, N.Y.)*, 323(5920), 1492–1496. <https://doi.org/10.1126/science.1164139>
- Hartley, T., Lever, C., Burgess, N., & O'Keefe, J. (2014). Space in the brain: how the hippocampal formation supports spatial cognition. *Philosophical Transactions of the Royal Society B: Biological Sciences*, 369(1635), 20120510. <https://doi.org/10.1098/rstb.2012.0510>
- Harvey, C. D., Collman, F., Dombeck, D. A., & Tank, D. W. (2009). Intracellular dynamics of hippocampal place cells during virtual navigation. *Nature*, 461(7266), 941–946. <https://doi.org/10.1038/nature08499>
- Hebb, D. O. (1949). The organization of behavior; a neuropsychological theory. In *The organization of behavior; a neuropsychological theory*. Wiley.
- Helmchen, F., & Denk, W. (2005). Deep tissue two-photon microscopy. *2(12)*, 9. <https://doi.org/10.1038/nmeth818>
- Heys, J. G., Rangarajan, K. V., & Dombeck, D. A. (2014). The

- Functional Micro-organization of Grid Cells Revealed by Cellular-Resolution Imaging. *Neuron*, 84(5), 1079–1090.  
<https://doi.org/10.1016/j.neuron.2014.10.048>
- Hjorth-Simonsen, A., & Jeune, B. (1972). Origin and termination of the hippocampal perforant path in the rat studied by silver impregnation. *The Journal of Comparative Neurology*, 144(2), 215–232. <https://doi.org/10.1002/cne.901440206>
- Hubel, D. H., & Wiesel, T. N. (1962). Receptive fields, binocular interaction and functional architecture in the cat's visual cortex. *The Journal of Physiology*, 160(1), 106–154.  
<https://doi.org/10.1113/jphysiol.1962.sp006837>
- Hutchinson, J. B., & Turk-Browne, N. B. (2012). Memory-guided attention: control from multiple memory systems. *Trends in Cognitive Sciences*, 16(12), 576–579.  
<https://doi.org/10.1016/j.tics.2012.10.003>
- Hyde, R. A., & Strowbridge, B. W. (2012). Mnemonic representations of transient stimuli and temporal sequences in the rodent hippocampus in vitro. *Nature Neuroscience*, 15(10), 1430–1438.  
<https://doi.org/10.1038/nn.3208>
- Ikegaya, Y., Aaron, G., Cossart, R., Aronov, D., Lampl, I., Ferster, D., & Yuste, R. (2004). Synfire chains and cortical songs: temporal modules of cortical activity. *Science (New York, N.Y.)*, 304(5670), 559–564. <https://doi.org/10.1126/science.1093173>
- Itskov, P. M., Vinnik, E., & Diamond, M. E. (2011). Hippocampal representation of touch-guided behavior in rats: persistent and independent traces of stimulus and reward location. *PloS One*, 6(1), e16462. <https://doi.org/10.1371/journal.pone.0016462>
- Itskov, V., Pastalkova, E., Mizuseki, K., Buzsaki, G., & Harris, K. D. (2008). Theta-mediated dynamics of spatial information in hippocampus. *The Journal of Neuroscience : The Official Journal of the Society for Neuroscience*, 28(23), 5959–5964.  
<https://doi.org/10.1523/JNEUROSCI.5262-07.2008>
- Jadhav, S. P., Kemere, C., German, P. W., & Frank, L. M. (2012). Awake hippocampal sharp-wave ripples support spatial memory. *Science (New York, N.Y.)*, 336(6087), 1454–1458.  
<https://doi.org/10.1126/science.1217230>
- Jaramillo, S., & Zador, A. M. (2014). Mice and rats achieve similar levels of performance in an adaptive decision-making task . In *Frontiers in Systems Neuroscience* (Vol. 8).  
<https://www.frontiersin.org/articles/10.3389/fnsys.2014.00173>
- Josselyn, S. A., & Tonegawa, S. (2020). Memory engrams: Recalling the past and imagining the future. *Science (New York, N.Y.)*, 367(6473). <https://doi.org/10.1126/science.aaw4325>

- Jun, J. J., Steinmetz, N. A., Siegle, J. H., Denman, D. J., Bauza, M., Barbarits, B., Lee, A. K., Anastassiou, C. A., Andrei, A., Aydin, Ç., Barbic, M., Blanche, T. J., Bonin, V., Couto, J., Dutta, B., Gratiy, S. L., Gutnisky, D. A., Häusser, M., Karsh, B., ... Harris, T. D. (2017). Fully integrated silicon probes for high-density recording of neural activity. *Nature*, 551(7679), 232–236. <https://doi.org/10.1038/nature24636>
- Kaifosh, P., Lovett-Barron, M., Turi, G. F., Reardon, T. R., & Losonczy, A. (2013). Septo-hippocampal GABAergic signaling across multiple modalities in awake mice. *Nature Neuroscience*, 16(9), 1182–1184. <https://doi.org/10.1038/nn.3482>
- Kalmbach, B. E., Davis, T., Ohyama, T., Riusech, F., Nores, W. L., & Mauk, M. D. (2010). Cerebellar Cortex Contributions to the Expression and Timing of Conditioned Eyelid Responses. *Journal of Neurophysiology*, 103(4), 2039–2049. <https://doi.org/10.1152/jn.00033.2010>
- Kalmbach, B. E., Ohyama, T., & Mauk, M. D. (2010). Temporal Patterns of Inputs to Cerebellum Necessary and Sufficient for Trace Eyelid Conditioning. *Journal of Neurophysiology*, 104(2), 627–640. <https://doi.org/10.1152/jn.00169.2010>
- Kamondi, A. (1998). *Theta Oscillations in Somata and Dendrites of Hippocampal Pyramidal Cells In Vivo: Activity-Dependent Phase-Precession of Action Potentials*. 261(March), 244–261.
- Khan, A. G., Parthasarathy, K., & Bhalla, U. S. (2010). Odor representations in the mammalian olfactory bulb. *Wiley Interdisciplinary Reviews. Systems Biology and Medicine*, 2(5), 603–611. <https://doi.org/10.1002/wsbm.85>
- Kim, S., & Lee, I. (2012). The hippocampus is required for visually cued contextual response selection, but not for visual discrimination of contexts. *Frontiers in Behavioral Neuroscience*, 6. <https://doi.org/10.3389/fnbeh.2012.00066>
- Kraus, B. J., Brandon, M. P., Robinson, R. J., Connerney, M. A., Hasselmo, M. E., & Eichenbaum, H. (2015). During Running in Place, Grid Cells Integrate Elapsed Time and Distance Run. *Neuron*, 88(3), 578–589. <https://doi.org/10.1016/j.neuron.2015.09.031>
- Kraus, B., Robinson, R., White, J., Eichenbaum, H., & Hasselmo, M. (2013). Hippocampal “Time Cells”: Time versus Path Integration. *Neuron*, 78(6), 1090–1101. <https://doi.org/10.1016/j.neuron.2013.04.015>
- Kropff, E., Carmichael, J. E., Moser, M.-B., & Moser, E. I. (2015). Speed cells in the medial entorhinal cortex. *Nature*, 523(7561), 419–424. <https://doi.org/10.1038/nature14622>

- Krupa, D., & Thompson, R. (2003). Inhibiting the Expression of a Classically Conditioned Behavior Prevents Its Extinction. *The Journal of Neuroscience : The Official Journal of the Society for Neuroscience*, 23, 10577–10584.  
<https://doi.org/10.1523/JNEUROSCI.23-33-10577.2003>
- Lever, C., Burton, S., Jeewajee, A., O'Keefe, J., & Burgess, N. (2009). Boundary Vector Cells in the Subiculum of the Hippocampal Formation. *The Journal of Neuroscience*, 29(31), 9771 LP – 9777. <https://doi.org/10.1523/JNEUROSCI.1319-09.2009>
- Leybaert, L., de Meyer, A., Mabilde, C., & Sanderson, M. J. (2005). A simple and practical method to acquire geometrically correct images with resonant scanning-based line scanning in a custom-built video-rate laser scanning microscope. *Journal of Microscopy*, 219(3), 133–140. <https://doi.org/https://doi.org/10.1111/j.1365-2818.2005.01502.x>
- Lovett-Barron, M., Kaifosh, P., Kheirbek, M. A., Danielson, N., Zaremba, J. D., Reardon, T. R., Turi, G. F., Hen, R., Zemelman, B. V., & Losonczy, A. (2014). Dendritic inhibition in the hippocampus supports fear learning. *Science (New York, N.Y.)*, 343(6173), 857–863. <https://doi.org/10.1126/science.1247485>
- Luo, L., Callaway, E. M., & Svoboda, K. (2018). Genetic Dissection of Neural Circuits: A Decade of Progress. *Neuron*, 98(2), 256–281. <https://doi.org/https://doi.org/10.1016/j.neuron.2018.03.040>
- MacDonald, C. J., Carrow, S., Place, R., & Eichenbaum, H. (2013). Distinct hippocampal time cell sequences represent odor memories in immobilized rats. *The Journal of Neuroscience : The Official Journal of the Society for Neuroscience*, 33(36), 14607–14616. <https://doi.org/10.1523/JNEUROSCI.1537-13.2013>
- MacDonald, C. J., Lepage, K. Q., Eden, U. T., & Eichenbaum, H. (2011). Hippocampal “time cells” bridge the gap in memory for discontiguous events. *Neuron*, 71(4), 737–749. <https://doi.org/10.1016/j.neuron.2011.07.012>
- Manns, J. R., Clark, R. E., & Squire, L. R. (2000). Parallel acquisition of awareness and trace eyeblink classical conditioning. *Learning & Memory (Cold Spring Harbor, N.Y.)*, 7(5), 267–272. <https://doi.org/10.1101/lm.33400>
- Maruyama, R., Maeda, K., Moroda, H., Kato, I., Inoue, M., Miyakawa, H., & Aonishi, T. (2014). Detecting cells using non-negative matrix factorization on calcium imaging data. *Neural Networks : The Official Journal of the International Neural Network Society*, 55, 11–19. <https://doi.org/10.1016/j.neunet.2014.03.007>
- Mau, W., Sullivan, D. W., Kinsky, N. R., Hasselmo, M. E., Howard, M.

- W., & Eichenbaum, H. (2018). The Same Hippocampal CA1 Population Simultaneously Codes Temporal Information over Multiple Timescales. *Current Biology*, 28(10), 1499–1508.e4. <https://doi.org/10.1016/j.cub.2018.03.051>
- McLelland, D., & Paulsen, O. (2007). Cortical Songs Revisited: A Lesson in Statistics. *Neuron*, 53(3), 319–321. <https://doi.org/https://doi.org/10.1016/j.neuron.2007.01.020>
- McNaughton, N., & Gray, J. A. (2000). Anxiolytic action on the behavioural inhibition system implies multiple types of arousal contribute to anxiety. *Journal of Affective Disorders*, 61(3), 161–176. [https://doi.org/10.1016/s0165-0327\(00\)00344-x](https://doi.org/10.1016/s0165-0327(00)00344-x)
- Medina, J. F., Garcia, K. S., Nores, W. L., Taylor, N. M., & Mauk, M. D. (2000). Timing mechanisms in the cerebellum: testing predictions of a large-scale computer simulation. *The Journal of Neuroscience : The Official Journal of the Society for Neuroscience*, 20(14), 5516–5525. <https://doi.org/10.1523/JNEUROSCI.20-14-05516.2000>
- Meeks, J. P., Arnson, H. A., & Holy, T. E. (2010). Representation and transformation of sensory information in the mouse accessory olfactory system. *Nature Neuroscience*, 13(6), 723–730. <https://doi.org/10.1038/nn.2546>
- Miller, A. M. P., Jacob, A. D., Ramsaran, A. I., De Snoo, M. L., Josselyn, S. A., & Frankland, P. W. (2023). Emergence of a predictive model in the hippocampus. *Neuron*. <https://doi.org/10.1016/j.neuron.2023.03.011>
- Modi, M. N., Dhawale, A. K., & Bhalla, U. S. (2014). CA1 cell activity sequences emerge after reorganization of network correlation structure during associative learning. *eLife*, 3, e01982–e01982. <https://doi.org/10.7554/eLife.01982>
- Mokeichev, A., Okun, M., Barak, O., Katz, Y., Ben-Shahar, O., & Lampl, I. (2007). Stochastic Emergence of Repeating Cortical Motifs in Spontaneous Membrane Potential Fluctuations In Vivo. *Neuron*, 53, 413–425. <https://doi.org/10.1016/j.neuron.2007.01.017>
- Mollinedo-Gajate, I., Song, C., & Knöpfel, T. (2021). Genetically Encoded Voltage Indicators. *Advances in Experimental Medicine and Biology*, 1293, 209–224. [https://doi.org/10.1007/978-981-15-8763-4\\_12](https://doi.org/10.1007/978-981-15-8763-4_12)
- Morris, R. G. M., Garrud, P., Rawlins, J. N. P., & O'Keefe, J. (1982). Place navigation impaired in rats with hippocampal lesions. *Nature*, 297(5868), 681–683. <https://doi.org/10.1038/297681a0>
- Moscovitch, M., Cabeza, R., Winocur, G., & Nadel, L. (2016). Episodic Memory and Beyond: The Hippocampus and Neocortex in

- Transformation. *Annual Review of Psychology*, 67(1), 105–134.  
<https://doi.org/10.1146/annurev-psych-113011-143733>
- Moser, M.-B., & Moser, E. I. (1998). Distributed encoding and retrieval of spatial memory in the hippocampus. In *The Journal of Neuroscience* (Vol. 18, pp. 7535–7542). Society for Neuroscience.
- Moyer, J. R. J., Thompson, L. T., & Disterhoft, J. F. (1996). Trace eyeblink conditioning increases CA1 excitability in a transient and learning-specific manner. *The Journal of Neuroscience : The Official Journal of the Society for Neuroscience*, 16(17), 5536–5546. <https://doi.org/10.1523/JNEUROSCI.16-17-05536.1996>
- Mukamel, E. A., Nimmerjahn, A., & Schnitzer, M. J. (2009). Automated analysis of cellular signals from large-scale calcium imaging data. *Neuron*, 63(6), 747–760.  
<https://doi.org/10.1016/j.neuron.2009.08.009>
- Muller, R. U., & Kubie, J. L. (1989). The firing of hippocampal place cells predicts the future position of freely moving rats. *The Journal of Neuroscience : The Official Journal of the Society for Neuroscience*, 9(12), 4101–4110.  
<https://doi.org/10.1523/JNEUROSCI.09-12-04101.1989>
- Murray, T. A., & Levene, M. J. (2012). Singlet gradient index lens for deep in vivo multiphoton microscopy. *Journal of Biomedical Optics*, 17(2), 021106. <https://doi.org/10.1117/1.JBO.17.2.021106>
- Nakashiba, T., Young, J. Z., McHugh, T. J., Buhl, D. L., & Tonegawa, S. (2008). Transgenic inhibition of synaptic transmission reveals role of CA3 output in hippocampal learning. *Science (New York, N.Y.)*, 319(5867), 1260–1264.  
<https://doi.org/10.1126/science.1151120>
- Nestler, E. J., Hyman, S. E., Holtzman, D. M., & Malenka, R. C. (2015). Higher Cognitive Function and Behavioral Control. In *Molecular Neuropharmacology: A Foundation for Clinical Neuroscience*, 3e. McGraw-Hill Education.  
[neurology.mhmedical.com/content.aspx?aid=1105916482](http://neurology.mhmedical.com/content.aspx?aid=1105916482)
- Nguyen, Q.-T., Callamaras, N., Hsieh, C., & Parker, I. (2001). Construction of a two-photon microscope for video-rate Ca<sup>2+</sup> imaging. *Cell Calcium*, 30(6), 383–393.  
<https://doi.org/https://doi.org/10.1054/ceca.2001.0246>
- Ohyama, T., Nores, W. L., Murphy, M., & Mauk, M. D. (2003). What the cerebellum computes. *Trends in Neurosciences*, 26(4), 222–227. [https://doi.org/10.1016/S0166-2236\(03\)00054-7](https://doi.org/10.1016/S0166-2236(03)00054-7)
- O'Keefe, J., & Burgess, N. (1996). Geometric determinants of the place fields of hippocampal neurons. *Nature*, 381(6581), 425–428.  
<https://doi.org/10.1038/381425a0>
- O'Keefe, J., & Dostrovsky, J. (1971). The hippocampus as a spatial

- map. Preliminary evidence from unit activity in the freely-moving rat. *Brain Research*, 34(1), 171–175. [https://doi.org/10.1016/0006-8993\(71\)90358-1](https://doi.org/10.1016/0006-8993(71)90358-1)
- O'Keefe, J., & Nadel, L. (1978). The Hippocampus as a Cognitive Map. In *Philosophical Studies* (Vol. 27).  
<https://doi.org/10.5840/philstudies19802725>
- O'Keefe, J., & Recce, M. L. (1993). Phase relationship between hippocampal place units and the EEG theta rhythm. *Hippocampus*, 3(3), 317–330.  
<https://doi.org/10.1002/hipo.450030307>
- Ozden, I., Lee, H. M., Sullivan, M. R., & Wang, S. S.-H. (2008). Identification and Clustering of Event Patterns From In Vivo Multiphoton Optical Recordings of Neuronal Ensembles. *Journal of Neurophysiology*, 100(1), 495–503.  
<https://doi.org/10.1152/jn.01310.2007>
- Pachitariu, M., Stringer, C., Dipoppa, M., Schröder, S., Rossi, L. F., Dalgleish, H., Carandini, M., & Harris, K. D. (2017). Suite2p: beyond 10,000 neurons with standard two-photon microscopy. *BioRxiv*, 61507. <https://doi.org/10.1101/061507>
- Paredes, R. M., Etzler, J. C., Watts, L. T., Zheng, W., & Lechleiter, J. D. (2008). Chemical calcium indicators. *Methods (San Diego, Calif.)*, 46(3), 143–151.  
<https://doi.org/10.1016/j.ymeth.2008.09.025>
- Pastalkova, E., Itskov, V., Amarasingham, A., & Buzsaki, G. (2008). Internally Generated Cell Assembly Sequences in the Rat Hippocampus. *Science*, 321(5894), 1322–1327.  
<https://doi.org/10.1126/science.1159775>
- Pavlov, I. P. (1927). Conditioned reflexes: an investigation of the physiological activity of the cerebral cortex. In *Conditioned reflexes: an investigation of the physiological activity of the cerebral cortex*. Oxford Univ. Press.
- Peron, S. P., Freeman, J., Iyer, V., Guo, C., & Svoboda, K. (2015). A Cellular Resolution Map of Barrel Cortex Activity during Tactile Behavior. *Neuron*, 86(3), 783–799.  
<https://doi.org/10.1016/j.neuron.2015.03.027>
- Petersen, C. C. H. (2019). Sensorimotor processing in the rodent barrel cortex. *Nature Reviews Neuroscience*, 20(9), 533–546.  
<https://doi.org/10.1038/s41583-019-0200-y>
- Pfeiffer, B. E., & Foster, D. J. (2013). Hippocampal place-cell sequences depict future paths to remembered goals. *Nature*, 497(7447), 74–79. <https://doi.org/10.1038/nature12112>
- Pnevmatikakis, E. A., Soudry, D., Gao, Y., Machado, T. A., Merel, J., Pfau, D., Reardon, T., Mu, Y., Lacefield, C., Yang, W., Ahrens, M.,

- Bruno, R., Jessell, T. M., Peterka, D. S., Yuste, R., & Paninski, L. (2016). Simultaneous Denoising, Deconvolution, and Demixing of Calcium Imaging Data. *Neuron*, 89(2), 285–299.  
<https://doi.org/https://doi.org/10.1016/j.neuron.2015.11.037>
- Poort, J., Khan, A. G., Pachitariu, M., Nemri, A., Orsolic, I., Krupic, J., Bauza, M., Sahani, M., Keller, G. B., Mrsic-Flogel, T. D., & Hofer, S. B. (2015). Learning Enhances Sensory and Multiple Non-sensory Representations in Primary Visual Cortex. *Neuron*, 86(6), 1478–1490. <https://doi.org/10.1016/j.neuron.2015.05.037>
- Poppenk, J., Evensmoen, H. R., Moscovitch, M., & Nadel, L. (2013). Long-axis specialization of the human hippocampus. *Trends in Cognitive Sciences*, 17(5), 230–240.  
<https://doi.org/10.1016/j.tics.2013.03.005>
- Pudil, P., & Novovičová, J. (1998). Novel Methods for Feature Subset Selection with Respect to Problem Knowledge. In H. Liu & H. Motoda (Eds.), *Feature Extraction, Construction and Selection: A Data Mining Perspective* (pp. 101–116). Springer US.  
[https://doi.org/10.1007/978-1-4615-5725-8\\_7](https://doi.org/10.1007/978-1-4615-5725-8_7)
- Ranck, J. B. (1973). Studies on single neurons in dorsal hippocampal formation and septum in unrestrained rats: Part I. Behavioral correlates and firing repertoires. *Experimental Neurology*, 41(2), 462–531. [https://doi.org/https://doi.org/10.1016/0014-4886\(73\)90290-2](https://doi.org/https://doi.org/10.1016/0014-4886(73)90290-2)
- Ranck, J. B. (1975). *Behavioral Correlates and Firing Repertoires of Neurons in the Dorsal Hippocampal Formation and Septum of Unrestrained Rats BT - The Hippocampus: Volume 2: Neurophysiology and Behavior* (R. L. Isaacson & K. H. Pribram, Eds.; pp. 207–244). Springer US. [https://doi.org/10.1007/978-1-4684-2979-4\\_7](https://doi.org/10.1007/978-1-4684-2979-4_7)
- Rao, R. P. N., & Ballard, D. H. (1999). Predictive coding in the visual cortex: a functional interpretation of some extra-classical receptive-field effects. *Nature Neuroscience*, 2(1), 79–87.  
<https://doi.org/10.1038/4580>
- Rescorla, R. A., & Wagner, A. (1972). A theory of Pavlovian conditioning: Variations in the effectiveness of reinforcement and nonreinforcement. In *Classical Conditioning II: Current Research and Theory: Vol. Vol. 2*.
- Reyes, A. D. (2003). Synchrony-dependent propagation of firing rate in iteratively constructed networks in vitro. *Nature Neuroscience*, 6(6), 593–599. <https://doi.org/10.1038/nn1056>
- Robbins, M., Christensen, C. N., Kaminski, C. F., & Zlatic, M. (2021). Calcium imaging analysis - how far have we come? *F1000Research*, 10, 258.

- Rochefort, N. L., Garaschuk, O., Milos, R.-I., Narushima, M., Marandi, N., Pichler, B., Kovalchuk, Y., & Konnerth, A. (2009). Sparsification of neuronal activity in the visual cortex at eye-opening. *Proceedings of the National Academy of Sciences of the United States of America*, 106(35), 15049–15054. <https://doi.org/10.1073/pnas.0907660106>
- Rogerson, T., Cai, D. J., Frank, A., Sano, Y., Shobe, J., Lopez-Aranda, M. F., & Silva, A. J. (2014). Synaptic tagging during memory allocation. *Nature Reviews Neuroscience*, 15(3), 157–169. <https://doi.org/10.1038/nrn3667>
- Savelli, F., Yoganarasimha, D., & Knierim, J. J. (2008). Influence of boundary removal on the spatial representations of the medial entorhinal cortex. *Hippocampus*, 18(12), 1270–1282. <https://doi.org/10.1002/hipo.20511>
- Schreurs, B. G. (1989). Classical conditioning of model systems: A behavioral review. *Psychobiology*, 17(2), 145–155. <https://doi.org/10.3758/BF03337830>
- Scoville, W. B., & Milner, B. (1957). Loss of recent memory after bilateral hippocampal lesions. In *Journal of Neurology, Neurosurgery & Psychiatry* (Vol. 20, pp. 11–21). BMJ Publishing Group. <https://doi.org/10.1136/jnnp.20.1.11>
- Shadlen, M. N., & Shohamy, D. (2016). Decision making and sequential sampling from memory. *Neuron*, 90(5), 927–939.
- Shannon, C. E. (1948). A Mathematical Theory of Communication. *Bell System Technical Journal*, 27(3), 379–423. <https://doi.org/https://doi.org/10.1002/j.1538-7305.1948.tb01338.x>
- Siegel, J. J., & Mauk, M. D. (2013). Persistent Activity in Prefrontal Cortex during Trace Eyelid Conditioning: Dissociating Responses That Reflect Cerebellar Output from Those That Do Not. *The Journal of Neuroscience*, 33(38), 15272 LP – 15284. <https://doi.org/10.1523/JNEUROSCI.1238-13.2013>
- Siegel, J. J., Taylor, W., Gray, R., Kalmbach, B., Zemelman, B. V., Desai, N. S., Johnston, D., & Chitwood, R. A. (2015). Trace Eyeblink Conditioning in Mice Is Dependent upon the Dorsal Medial Prefrontal Cortex, Cerebellum, and Amygdala: Behavioral Characterization and Functional Circuitry. *ENeuro*, 2(4), ENEURO.0051-14.2015. <https://doi.org/10.1523/ENEURO.0051-14.2015>
- Silva, A. J., Zhou, Y., Rogerson, T., Shobe, J., & Balaji, J. (2009). Molecular and cellular approaches to memory allocation in neural circuits. *Science (New York, N.Y.)*, 326(5951), 391–395. <https://doi.org/10.1126/science.1174519>
- Skaggs, W., McNaughton, B., Gothard, K., & Markus, E. (1996). An

- Information-Theoretic Approach to Deciphering the Hippocampal Code. *Neural Inf. Process Syst.*, 5.
- Sofroniew, N. J., Flickinger, D., King, J., & Svoboda, K. (2016). A large field of view two-photon mesoscope with subcellular resolution for in vivo imaging. *ELife*, 5(JUN2016), 1–20.  
<https://doi.org/10.7554/eLife.14472>
- Solstad, T., Boccara, C. N., Kropff, E., Moser, M.-B., & Moser, E. I. (2008). Representation of Geometric Borders in the Entorhinal Cortex. *Science*, 322(5909), 1865–1868.  
<https://doi.org/10.1126/science.1166466>
- Souza, B. C., Pavão, R., Belchior, H., & Tort, A. B. L. (2018). On Information Metrics for Spatial Coding. *Neuroscience*, 375, 62–73.  
<https://doi.org/10.1016/j.neuroscience.2018.01.066>
- Stosiek, C., Garaschuk, O., Holthoff, K., & Konnerth, A. (2003). In vivo two-photon calcium imaging of neuronal networks. *Proceedings of the National Academy of Sciences of the United States of America*, 100(12), 7319–7324.  
<https://doi.org/10.1073/pnas.1232232100>
- Suh, J., Rivest, A. J., Nakashiba, T., Tominaga, T., & Tonegawa, S. (2011). Entorhinal cortex layer III input to the hippocampus is crucial for temporal association memory. *Science (New York, N.Y.)*, 334(6061), 1415–1420.  
<https://doi.org/10.1126/science.1210125>
- Takehara, K., Kawahara, S., Takatsuki, K., & Kirino, Y. (2002). Time-limited role of the hippocampus in the memory for trace eyeblink conditioning in mice. *Brain Research*, 951(2), 183–190.  
[https://doi.org/10.1016/s0006-8993\(02\)03159-1](https://doi.org/10.1016/s0006-8993(02)03159-1)
- Tao, S., Wang, Y., Peng, J., Zhao, Y., He, X., Yu, X., Liu, Q., Jin, S., & Xu, F. (2021). Whole-Brain Mapping the Direct Inputs of Dorsal and Ventral CA1 Projection Neurons. *Frontiers in Neural Circuits*, 15. <https://doi.org/10.3389/fncir.2021.643230>
- Taube, J. S., Muller, R. U., & Ranck, J. B. J. (1990). Head-direction cells recorded from the postsubiculum in freely moving rats. I. Description and quantitative analysis. *The Journal of Neuroscience : The Official Journal of the Society for Neuroscience*, 10(2), 420–435.  
<https://doi.org/10.1523/JNEUROSCI.10-02-00420.1990>
- Thompson, R. F. (2004). In Search of Memory Traces. *Annual Review of Psychology*, 56(1), 1–23.  
<https://doi.org/10.1146/annurev.psych.56.091103.070239>
- Tishby, N., Pereira, F. C., & Bialek, W. (1999). The information bottleneck method. *Proc. of the 37-Th Annual Allerton Conference on Communication, Control and Computing*, 368–377.

- <https://arxiv.org/abs/physics/0004057>
- Tseng, W., Guan, R., Disterhoft, J. F., & Weiss, C. (2004). Trace eyeblink conditioning is hippocampally dependent in mice. *Hippocampus*, 14(1), 58–65. <https://doi.org/10.1002/hipo.10157>
- Uncapher, M. R., Hutchinson, J. B., & Wagner, A. D. (2011). Dissociable effects of top-down and bottom-up attention during episodic encoding. *The Journal of Neuroscience : The Official Journal of the Society for Neuroscience*, 31(35), 12613–12628. <https://doi.org/10.1523/JNEUROSCI.0152-11.2011>
- Vaidya, A. R., Pujara, M. S., Petrides, M., Murray, E. A., & Fellows, L. K. (2019). Lesion Studies in Contemporary Neuroscience. *Trends in Cognitive Sciences*, 23(8), 653–671. <https://doi.org/https://doi.org/10.1016/j.tics.2019.05.009>
- Valero, M., Cid, E., Averkin, R. G., Aguilar, J., Sanchez-Aguilera, A., Viney, T. J., Gomez-Dominguez, D., Bellistri, E., & de la Prida, L. M. (2015). Determinants of different deep and superficial CA1 pyramidal cell dynamics during sharp-wave ripples. *Nature Neuroscience*. <https://doi.org/10.1038/nn.4074>
- van der Maaten, L., Postma, E., & van den Herik, H. (2009). Dimensionality reduction: a comparative review. *Journal of Machine Learning Research*, 66–71.
- Velasco, M. G. M., & Levene, M. J. (2014). In vivo two-photon microscopy of the hippocampus using glass plugs. *Biomedical Optics Express*, 5(6), 1700–1708. <https://doi.org/10.1364/BOE.5.001700>
- Vinogradova, O. S. (2001). Hippocampus as comparator: Role of the two input and two output systems of the hippocampus in selection and registration of information. *Hippocampus*, 11(5), 578–598. <https://doi.org/https://doi.org/10.1002/hipo.1073>
- Voelcker, B., Pancholi, R., & Peron, S. (2022). Transformation of primary sensory cortical representations from layer 4 to layer 2. *Nature Communications*, 13(1), 5484. <https://doi.org/10.1038/s41467-022-33249-1>
- Wood, E. R., Dudchenko, P. A., Robitsek, R. J., & Eichenbaum, H. (2000). Hippocampal Neurons Encode Information about Different Types of Memory Episodes Occurring in the Same Location. *Neuron*, 27(3), 623–633. [https://doi.org/https://doi.org/10.1016/S0896-6273\(00\)00071-4](https://doi.org/https://doi.org/10.1016/S0896-6273(00)00071-4)
- Yiu, A. P., Mercaldo, V., Yan, C., Richards, B., Rashid, A. J., Hsiang, H.-L. L., Pressey, J., Mahadevan, V., Tran, M. M., Kushner, S. A., Woodin, M. A., Frankland, P. W., & Josselyn, S. A. (2014). Neurons are recruited to a memory trace based on relative neuronal excitability immediately before training. *Neuron*, 83(3),

- 722–735. <https://doi.org/10.1016/j.neuron.2014.07.017>
- Zhang, S., & Manahan-Vaughan, D. (2015). Spatial olfactory learning contributes to place field formation in the hippocampus. *Cerebral Cortex (New York, N.Y.: 1991)*, 25(2), 423–432.  
<https://doi.org/10.1093/cercor/bht239>
- Zhou, S., Masmanidis, S. C., & Buonomano, D. V. (2020). Neural Sequences as an Optimal Dynamical Regime for the Readout of Time. *Neuron*, 108(4), 651-658.e5.  
<https://doi.org/https://doi.org/10.1016/j.neuron.2020.08.020>
- Zhou, Y., Won, J., Karlsson, M. G., Zhou, M., Rogerson, T., Balaji, J., Neve, R., Poirazi, P., & Silva, A. J. (2009). CREB regulates excitability and the allocation of memory to subsets of neurons in the amygdala. *Nature Neuroscience*, 12(11), 1438–1443.  
<https://doi.org/10.1038/nn.2405>
- Ziv, Y., Burns, L. D., Cocker, E. D., Hamel, E. O., Ghosh, K. K., Kitch, L. J., El Gamal, A., & Schnitzer, M. J. (2013). Long-term dynamics of CA1 hippocampal place codes. *Nature Neuroscience*, 16(3), 264–266. <https://doi.org/10.1038/nn.3329>